Clay surface reactivity and its interaction with trace elements

by

Weiduo Hao

A thesis submitted in partial fulfillment of the requirements for the degree of

Doctor of Philosophy

Department of Earth and Atmospheric Sciences
University of Alberta

Abstract

Clay minerals are ubiquitous at the Earth's surface and they impart a significant influence on numerous geochemical cycles due to their high surface reactivity. Aqueous pH and ionic strength (hereafter IS) are two major factors that affect clay surface reactivity and subsequently govern trace elemental behavior on clay surfaces. In environmental settings with dynamic pH and IS (such as estuaries), the variation of clay surface reactivity significantly controls the fate and transport of trace elements. In this regard, this work explores the variation of clay surface properties under various aqueous conditions, and how this impacts their ability to accumulate trace metals.

Chapter 1 is an introductory chapter, where I briefly outline some background information about clay surface reactivity, solution pH and ionic strength, and trace elemental behavior on clay surfaces.

In chapter 2, the net surface proton charge of three clays (kaolinite, illite and montmorillonite) under a range of pH and IS was evaluated through acid-base titration. The observation that the point of zero net proton charge (pH_{PZNPC}) varies with IS for the three clay minerals implies that the variation of clay surface reactivities with IS differs from simple oxides minerals (such as Fe-oxides, Al-oxides). A mathematical relationship was established between the charge property of clay minerals and solution IS which can be used to predict the clay surface proton charge.

In chapter 3, the proton interaction constants on clay surfaces and their variation with IS was further elucidated within a surface complexation modeling framework. Previous studies are still unclear on whether solution IS affects clay surface reactivities through attenuation of clay surface electrostatic field or saturation of surface adsorption sites by electrolytes. The application of models to investigate Na competitive adsorption onto surface active adsorption sites failed to

match the experimental results and theoretical assumptions, thus indicating that attenuation of the clay surface electrostatic field better explains the experimental behavior.

In chapter 4, I described how solution pH influences clay surface functional group protonation and deprotonation. Interestingly, under extremely low pH, structural elements of clay minerals can be released and lead to differences in surface reactivity compared to normal clays. To determine this differences, variable degrees of acidic treatment were applied, and the results reveal an increase in surface area but decrease in Cd adsorption capacity after acidic treatment despite a lack of morphological and crystal structure changes.

In chapter 5, once the clay surface properties as a function of solution pH and IS were characterized, Cd behavior onto the clay surfaces was evaluated under simulated estuary conditions with dynamic changes in pH and IS. Coupled with Cd adsorption isotherms, surface complexation modeling and Extended X-ray Adsorption Fine Structure (EXAFS), I demonstrated that Cd mainly forms outer-sphere complex onto clay surfaces under freshwater conditions, while inner-sphere adsorption was observed under marine conditions. My results show that once clays are transported from rivers to the oceans, Cd will be released from clay surfaces to water column in estuaries.

In chapter 6, experimental results show that phosphate, as a bio-limiting nutrient, is readily shuttled by kaolinite from land to the oceans. The “kaolinite-shuttle” mechanism is subsequently used to explain the transport of nutrients to the Paleoproterozoic oceans following the Great Oxidation Event at ~2.5 Ga when intense continental weathering generated kaolinite on the paleo-Earth surfaces. I hypothesized that the transport of kaolinite from the paleosol to seawater at that period of time delivered nutrients to the ocean, thus facilitating enhanced primary productivity in

marginal marine settings. These events ultimately contributed to the largest carbon burial event in Earth's history, the so-called Lomagundi Event between 2.20 to 2.06 Ga.

In chapter 7, I summarize our current state of knowledge about clay surface reactivity and propose future avenues of research.

Preface

This papers-based thesis consisted of 5 original research articles is the cumulative effort of several collaborative projects focused on the clay surface reactivity and its implication to Earth surface geochemistry. All of the research works involved in this thesis are supervised by Dr. Kurt Konhauser and Dr. Daniel Alessi at the University of Alberta, and I was intensively involved in all aspects of the research from designing of the project to data collection, analysis and interpretation, as well as manuscript drafting. To be explicit, my contribution to each chapter is outlined below.

Chapter 2 has been published in *Chemical Geology* as: Hao, W.; Flynn, S.L.; Alessi, D.S.; Konhauser, K.O., 2018. Change of the point of zero net proton charge (pH_{PZNPC}) of clay minerals with ionic strength, Chemical Geology, 493, 458-467. I was responsible for designing the experiments, collecting data, calculating pH_{PZNPC} through literature methods, and executing the surface complexation modeling. The initial formulation of the manuscript was performed by me with all authors' contributions.

Chapter 3 has been accepted by *Chemical Geology* as: Hao, W.; Flynn, S.L.; Kashiwabara, T.; Alam, M.S.; Bandara, S.; Swaren, L.; Robbins, L.J.; Alessi, D.S.; Konhauser, K.O., 2019. The impact of ionic strength on the proton reactivity of clay minerals, 529, 119294. I was responsible for the conception of the idea, experimental design, and data processing. S. Bandara and I conducted the freeze-dry of the studied clays. L. Swaren performed the size-fraction titration of clays. The manuscript was written by me with input from all authors.

Chapter 4 has been published by *ACS Earth and Space Chemistry* as: Hao, W.; Pudasainee, D.; Gupta, R.; Kashiwabara, T.; Alessi, D.S.; Konhauser, K.O., 2019. Effect of acidic conditions on surface properties and metal binding capacity of clay minerals, 3, 2421-2429. I was responsible for the experimental design, analyses using XRD and SEM, and Cd adsorption experiments. D. Pudasainee and I performed the BET surface area measurements. The manuscript was written by me with input from all authors.

Chapter 5 has been prepared as a manuscript for submission as: Hao, W.; Kashiwabara, T.; Jin, R.; Takahashi, Y.; Gingras, M.; Alessi, D.S.; Konhauser, K.O. Transport of Cd by clay minerals from land to the oceans. I conducted the Cd adsorption experiments, data analysis for the isotherms, and the surface complexation modeling. T. Kashiwabara, Y. Takahashi and I performed the EXAFS analysis and fitting of spectra. The manuscript was written by me with input from all authors.

Chapter 6 has been prepared as a manuscript for submission as: Hao, W.; Mand, K.; Li Y.; Alessi, D.S.; Konhauser, K.O. The kaolinite shuttle: A mechanistic link between the Great Oxidation Event and Earth's largest carbon burial event. K.O. Konhauser, D.S. Alessi and I initiated the concept and idea. I conducted the P adsorption experiments onto three clay minerals, surface complexation modeling, and the compilation of P database for river suspended sediments. Y. Li conducted bacterial culture experiments. I summarized the initial manuscript and all authors contributed to the writing of the manuscript.

To people I love and people who love me.

Acknowledgements

I express sincere gratitude to my supervisor Dr. Kurt Konhauser for his help on every steps of my PhD period. His patience, guidance, support on my academic activities are great treasure for my future. Special thanks to my co-supervisor Dr. Daniel Alessi, who played a major role in my research conduction and initiation. The skills and scientific altitude taught by him will benefit me throughout my career. Also, I would like to extend my thanks to all my co-authors who made great contribution to my research work. Especially, I would like to acknowledge Dr. Ning Chen at Canadian Light Source for his assist on EXAFS analysis, Dr. Teruhiko Kashiwabara at Japan Agency for Marine-Earth Science and Technology for providing me opportunity of Synchrotron work, and Dr. Murray Gingras at University of Alberta for his inspiration in sedimentology.

The friendship from geobiology group members is my good fortune. Here, I would thank to Yuhao Li, Rong Jin, Kaarel Mänd, Logan Swaren, Konstantin von Guten, Cheng Zhong, Leslie Jamie Robbins, Md. Samrat Alam and all the students/professors who have ever been to our group for the time we spent together and their experimental help.

My doctoral research would not have been possible without the support of a scholarship from the China Scholarship Council, and several scholarships from the University of Alberta. Additionally, my trip to Japan for synchrotron work was supported by the Japan Society for the Promotion of Science.

Ultimately, my parents and friends are always with me and I won't achieve anything without the unwavering support from them.

Table of Contents

Chapter 1. General introduction 1

References 4

Chapter 2. Change of the point of zero net proton charge (pH_{PZNPC}) of clay minerals with ionic strength 6

2.1 Introduction 6

2.2 Materials and experimental procedures 8

2.3 Data treatment 9

2.4 Results 12

2.4.1 Titration curves as a function of ionic strength 12

2.4.2 Variation of pH_{PZNPC} with ionic strength 13

2.5 Discussion 14

2.5.1 Differences in the proton interactions between clays and simple oxides 14

2.5.2 The pH_{PZNPC} of clay minerals 16

2.5.3 Surface complexation modeling 18

2.6 Conclusions and environmental implications 21

2.7 References 22

Chapter 3. The impact of ionic strength on the proton reactivity of clay minerals 42

3.1 Introduction 42

3.2 Background theory 44

3.3 Methods 46

3.4 Results 49
3.4.1 Surface complexation modeling 49
3.4.2 Proton interaction constants as a function of ionic strength 50
3.4.3 Chromium adsorption onto three clay minerals 51
3.5 Discussion 51
3.5.1 The comparison of surface proton reactivity among clay minerals 51
3.5.2 The competitive adsorption of solution electrolytes 53
3.5.3 Attenuation of the surface electrostatic field by increasing ionic strength 55
3.5.4 The inability of SCMs to produce an ionic strength independent proton interaction constant for clay minerals 57
3.6 Conclusions 59
3.7 References 60
Chapter 4. Effect of acidic conditions on surface properties and metal binding capacity of clay minerals 80
4.1 Introduction 80
4.2 Materials and experimental procedures 81
4.3 Results and discussion 84
4.3.1 Release of elements during neutral and acidic treatment 84
4.3.2 Changes in morphology and crystal structures of the studied clay minerals 86
4.3.3 Variations in surface area of the studied clay minerals 88

4.3.4 Cd^{2+} adsorption capacity 89

4.4 Conclusions and Implications 90

4.5 References 91

Chapter 5. Transport of Cd by clay minerals from land to the oceans 107

5.1 Introduction 107

5.2 Materials, experiments and methods 109

5.2.1 Clay minerals preparation 109

5.2.2 Adsorption isotherms 110

5.2.3 The Cd behaviour under simulated estuary environments 110

5.2.4 pH edge experiments 111

5.2.5 Surface complexation modelling 112

5.2.6 Synchrotron X-ray adsorption spectroscopy 113

5.3 Results and discussion 114

5.3.1 Cd behavior on clay surfaces from river to ocean 114

5.3.2 Surface complexation modelling 116

5.3.4 Coordination of Cd at clay mineral surfaces 117

5.4 Conclusions 119

5.5 References 121

Chapter 6. The kaolinite shuttle: A mechanistic link between the Great Oxidation Event and Earth's largest carbon burial event 139

6.1 Introduction 139
6.2 Methods 141
6.2.1 P adsorption isotherm 141
6.2.2 P desorption experiments 141
6.2.3 Cyanobacterium growth curve 142
6.3 Results and Discussion 143
6.4 References 146
Chapter 7. Conclusions 154
7.1 The shale record and its interpretation 155
7.2 Future work 157
7.3 References 159
Bibliography 161
Appendix 1. Supplementary information for Chapter 2 179
Appendix 2. Supplementary information for Chapter 3 181
Appendix 3. Supplementary information for Chapter 5 202
Appendix 4. Supplementary information for Chapter 6 206

List of Tables

Table 2.1: PZNPC values calculated using Method 1. 29

Table 2.2: PZNPC values calculated using Method 2. 31

Table 2.3: PZNPC values calculated using the SCM method. 33

Table 3.1: Results of surface complexation modeling summary for kaolinite 68

Table 3.2: Results of surface complexation modeling summary for illite 69

Table 3.3: Results of surface complexation modeling summary for montmorillonite 70

Table 3.4: Mathematical relationship between K values and ionic strength (IS). 71

Table 3.5: Degree of chromium adsorption onto three clay minerals at two IS conditions 72

Table 3.6: Na^+ binding constants on the two surface functional groups of the three clay minerals 73

Table 4.1: Elements released from the three studied clay minerals during acidic and neutral treatment (units: ppm) 99

Table 4.2: Surface area summary of the three studied clay minerals 101

Table 5.1: Maximum Cd adsorption onto three clay minerals at freshwater and marine conditions. 130

Table 5.2: Structural parameters of Cd adsorption onto three clay minerals at river and marine conditions. 131

Table 5.3: A compilation of Cd concentration in suspended sediments (μg/g). 132

List of Figures

Figure 2.1 Potentiometric titration curves for (a) kaolinite, (b) illite, and (c) montmorillonite. .. 35

Figure 2.2 Changes in the PZNPC using Method 1, as a function of ionic strength (inset plots), and the logarithm of ionic strength, for (a) kaolinite, (b) illite and (c) montmorillonite. 36

Figure 2.3 Changes in the PZNPC using Method 2, as a function of ionic strength (inset plots), and the logarithm of ionic strength, for (a) kaolinite, (b) illite and (c) montmorillonite. 37

Figure 2.4 Speciation diagrams for kaolinite surface sites at the seven IS values tested. 38

Figure 2.5 Speciation diagrams for illite surface sites at the seven IS values tested. 39

Figure 2.6 Speciation diagrams for montmorillonite surface sites at the seven IS values tested. 40

Figure 2.7 Changes in the PZNPC using the SCM method as a function of ionic strength (inset plots), and the logarithm of ionic strength, for (a) kaolinite, (b) illite and (c) montmorillonite... 41

Figure 3.1 Proton interaction constants of kaolinite and their relationship with ionic strength. (a) $\log K_a$ change with solution IS; (b) $\log K_{a-}$ variation with solution IS; and (c) the relationship between $\log K_{a+}$ and solution IS. 75

Figure 3.2 Proton interaction constants of illite and their relationship with ionic strength. (a) $\log K_a$ change with solution IS; (b) $\log K_{a-}$ variation with solution IS; and (c) the relationship between $\log K_{a+}$ and solution IS. 76

Figure 3.3 Proton interaction constants of montmorillonite and their relationship with ionic strength. (a) $\log K_a$ change with solution IS; (b) $\log K_{a-}$ variation with solution IS; and (c) the relationship between $\log K_{a+}$ and solution IS. 77

Figure 3.4 The change in the Na^+ binding constant ($\log K_a$) with changing IS for all three clay minerals: (a) kaolinite; (b) montmorillonite and (c) illite. 78

Figure 3.5 Change in the Cd binding constant ($logK_{LCd}$) of the permanently charged site ($logK_{LCd}$) with IS for three clay minerals: (a) kaolinite; (b) illite; and (c) montmorillonite. 79

Figure 4.1 Scanning electron microscopy (SEM) images of neutral and acid treated clay minerals (A: Kao-N; B: Kao-A; C: Illite-N; D: Illite-A; E: Mont-N; F: Mont-A). 102

Figure 4.2 X-ray diffraction data of the three studied clays under acidic and neutral treatments of acid-treated (A; red) and neutral-treated (N, black) diffraction patterns. 103

Figure 4.3 Adsorption isotherms of Cd^{2+} onto kaolinite..... 104

Figure 4.4 Adsorption isotherms of Cd^{2+} onto illite 105

Figure 4.5 Adsorption isotherms of Cd^{2+} onto montmorillonite..... 106

Figure 5.1 Comparison of Cd adsorption onto three tested clay minerals at freshwater (green) and marine (black) conditions. Filled circles are experimental adsorption data; curves are Langmuir model fits. 133

Figure 5.2 Adsorption of Cd onto three tested clay minerals as a function of changing aqueous conditions from freshwater to seawater. 134

Figure 5.3 Cd pH adsorption edge and the fitting of experimental data by non-electrostatic and constant capacitance surface complexation models. 135

Figure 5.4 Cd speciation diagram as a function of pH under freshwater and marine conditions 136

Figure 5.5 EXAFS analyses of Cd adsorption onto three clay minerals under freshwater and marine conditions. 137

Figure 5.6 Molecular model of Cd adsorption onto clay minerals. 138

Figure 6.1 The adsorption of P onto kaolinite under three conditions: (1) pH=4, ionic strength=0.01M; (2) pH=6, ionic strength=0.01M; (3) pH=8, ionic strength=0.56M..... 151

Figure 6.2 Desorption of P from kaolinite surfaces when transiting from freshwater conditions to marine conditions..... 152

Figure 6.3 Growth curves of cyanobacterium Synechococcus PCC7002 cultures..... 153

Chapter 1. General introduction

Clay minerals are products of continental weathering, which are mainly derived from water-rock interaction at the rock-atmosphere interface (Velde, 2013). The transportation of clay minerals from land to the oceans through river delivery provides the bulk of clay minerals needed for shale deposition (Eisma et al., 1978; Ongley et al., 1981; Walling and Moorehead, 1989; Feng et al., 2014; Zhao et al., 2018). However, the geochemical impacts of this clay delivery process, especially regarding trace elemental behavior on clay surfaces, are still not well understood. Their potential impacts on trace metal cycling stem are from the fact that clay minerals have a high affinity to trace elements in aqueous environments, and such affinity is highly influenced by solution pH and ionic strength (Baeyens and Bradbury, 1997; Sinitsyn et al., 2000; Bradbury and Baeyens, 2002; Bradbury and Baeyens, 2009; Landry et al., 2009; Schaller et al., 2009; Reich et al., 2010). When clay minerals are transported from river to the oceans where the aqueous environments experience increase in both pH and ionic strength, the trace elemental behavior on clay surfaces is still understudied. Therefore, my research summarized in this dissertation addressed several important questions that related to the impact of solution pH and ionic strength to clay surface reactivities, and the impact on trace elemental adsorption behaviors:

(1) The binding of trace metals on clay surfaces is dependent on electrostatic attraction and, therefore, clay surface change – but how does solution ionic strength influence the surface proton charge property of clay minerals? In contrast to simple oxide minerals that have a constant point of zero net proton charge (pH_{PZNPC}; the pH at which the net surface proton charge is zero) at various ionic strengths, the pH_{PZNPC} of clay minerals varies as a function of solution pH. This indicates that solution ionic strength impacts on the surface proton charge of clay minerals. In Chapter 1, I report results from acid-base titration experiments that enabled us to calculate the pH_{PZNPC} of three

clay minerals: kaolinite, illite and montmorillonite. We successfully quantified the relationship between pH_{PZNPC} of clay minerals and solution ionic strength. Our results provide an important framework between the clay surface proton charge and solution ionic strengths, which can be applied under various ionic strength aqueous conditions.

(2) Does solution ionic strength impact clay surface reactivity through the competitive adsorption of solution electrolytes on functional groups or the attenuation of the surface electrostatic field? Debates on these mechanisms still persist due to the complexity of the clay surface and its adsorption pathways. In Chapter 2, I calculated the acidity constants of three different clay minerals (kaolinite, illite, and montmorillonite) and developed a relationship between acidity constants and solution ionic strength. I concluded that the competitive adsorption of solution electrolytes cannot explain the decrease of proton adsorption capacity with increasing solution ionic strength. Instead, this effect is better explained through the attenuation of the clay surface electrostatic field. We provided a database relating the acidity constants of clay minerals with solution ionic strengths, which can be applied for further clay surface reactivity modeling.

(3) Can extremely low pH modify the clay surface and change the surface reactivity of clay minerals? Previous studies have shown that under low pH conditions (pH<0), clay surface structural elements (e.g. Si, Al, Fe, and, Mg) can be leached out. In Chapter 3, I treated three clay minerals: kaolinite, illite, and montmorillonite under various acidic conditions (pH=0, 2, 4). Through comparing morphology, crystal structure, surface area, and Cd adsorption capacity, we came to the conclusion that acidic treatment cannot significantly modify the morphology and crystal structure of clay minerals, but it can increase clay surface area and decrease Cd adsorption capacity. Our conclusions provide a new insight for studying clay minerals that have been exposed

to acidic conditions in natural environments, which is common in mining sites that acidic rock drainages are pervasive.

(4) Cadmium is a major environmental pollutant in riverine systems, yet the effects of clays on its transport and distribution are poorly understood – are clay minerals a source or sink of Cd under estuary conditions? It has previously been proven that Cd adsorption onto clay minerals increases with pH but decreases with ionic strength. When clay minerals are transported to estuarine environment where there is increase in both pH and ionic strength, it is still unclear whether clay minerals will release Cd or re-adsorb Cd. In Chapter 4, I conducted Cd adsorption isotherm, pH edge, and synchrotron extended X-ray absorption fine structure (EXAFS) experiments and demonstrated that illite and montmorillonite can release 20-30% of bound Cd into estuarine environments. EXAFS spectra show that the local structure of adsorbed Cd changes from outer-sphere complex to inner-sphere complex, when Cd-bearing clays are transported from freshwater environments to the ocean. The collective results of this study emphasize the importance of the estuarine environment for the global trace elemental cycle and provide a methodology for studying trace elemental cycling under estuarine conditions.

(5) Given the ability of clays to adsorb, transport, and release trace metals depending on pH and ionic strength, what effect did clays have on nutrient delivery after the Great Oxidation Event (GOE)? The increase in atmospheric oxygen concentration at around ~2.5 Ga (the GOE) leads to intense pyrite oxidation and the generation of acidic rock drainage that increased clay production in weathering environments. It has been postulated that the increase of continental weathering enhanced the nutrient flux from land to the oceans and increased near-shore bio-productivity. However, it is still unclear how nutrients, such as P, were delivered into the oceans, since P is scarcely soluble under modern aqueous environments. In Chapter 5, I present a kaolinite

shuttle mechanism that could effectively deliver P from land to the oceans, as we show that the P adsorption capacity of kaolinite is very high in freshwater conditions, but quickly drops in marine environments, leading to P release. It is also demonstrated that the delivery of P by kaolinite from freshwater environments to the oceans can effectively promote plankton growth and increase bio-productivity. This study provides critical information linking the GOE and the Lomagundi Event and a nutrient delivery mechanism from land to the oceans.

Overall, my dissertation highlights the impact of aqueous solution on the surface reactivity of clay minerals and establishes a framework between clay surface reactivities and aqueous environmental parameters. We also emphasize the trace elemental behavior on clay minerals under the estuarine environment with increases in both solution pH and ionic strength, which is critical for the global and local geochemical cycle.

References

Baeyens, B., Bradbury, M.H., 1997. A mechanistic description of Ni and Zn sorption on Na-montmorillonite .1. Titration and sorption measurements. Journal of Contaminant Hydrology, 27(3-4): 199-222.

Bradbury, M.H., Baeyens, B., 2002. Sorption of Eu on Na- and Ca-montmorillonites: Experimental investigations and modelling with cation exchange and surface complexation. Geochimica et Cosmochimica Acta, 66(13): 2325-2334.

Bradbury, M.H., Baeyens, B., 2009. Sorption modelling on illite Part I: Titration measurements and the sorption of Ni, Co, Eu and Sn. Geochimica et Cosmochimica Acta, 73(4): 990-1003.

Eisma, D., Van Der Gaast, S.J., Martin, J.M., Thomas, A.J., 1978. Suspended matter and bottom deposits of the Orinoco delta: Turbidity, mineralogy and elementary composition. Netherlands Journal of Sea Research, 12(2): 224-251.

Feng, H. et al., 2014. Distribution characteristic of clay minerals contents in Minjiang River and its environmental significance. Journal of Applied Oceanography, 33(3): 418-424.

Landry, C.J., Koretsky, C.M., Lund, T.J., Schaller, M., Das, S., 2009. Surface complexation modeling of Co(II) adsorption on mixtures of hydrous ferric oxide, quartz and kaolinite. Geochimica et Cosmochimica Acta, 73(13): 3723-3737.

Ongley, E., Bynoe, M., Percival, J., 1981. Physical and geochemical characteristics of suspended solids, Wilton Creek, Ontario. Canadian Journal of Earth Sciences, 18(8): 1365-1379.

Reich, T.J., Das, S., Koretsky, C.M., Lund, T.J., Landry, C.J., 2010. Surface complexation modeling of Pb(II) adsorption on mixtures of hydrous ferric oxide, quartz and kaolinite.

Chemical Geology, 275(3): 262-271.
Schaller, M.S., Koretsky, C.M., Lund, T.J., Landry, C.J., 2009. Surface complexation modeling of Cd(II) adsorption on mixtures of hydrous ferric oxide, quartz and kaolinite. Journal of Colloid and Interface Science, 339(2): 302-309.
Sinitsyn, V.A., Aja, S.U., Kulik, D.A., Wood, S.A., 2000. Acid-base surface chemistry and sorption of some lanthanides on K+-saturated marblehead illite: I. Results of an experimental investigation. Geochimica et Cosmochimica Acta, 64(2): 185-194.
Velde, B., 2013. Origin and mineralogy of clays: clays and the environment. Springer Science & Business Media.
Walling, D.E., Moorehead, P.W., 1989. The particle size characteristics of fluvial suspended sediment: an overview. In: Sly, P.G., Hart, B.T. (Editors), Sediment/Water Interactions. Springer Netherlands, Dordrecht, pp. 125-149.
Zhao, Y. et al., 2018. Clay mineralogy and source-to-sink transport processes of Changjiang River sediments in the estuarine and inner shelf areas of the East China Sea. Journal of Asian Earth Sciences, 152: 91-102.

Chapter 2. Change of the point of zero net proton charge (pH_{PZNPC}) of clay minerals with ionic strength[1]

2.1 Introduction

Over the past decade, our understanding of the mechanisms underpinning the adsorption of ions to geologic media has considerably improved through the use of sorption isotherms and experimentally-derived surface complexation modeling (e.g., Borrok and Fein, 2005; Alessi and Fein, 2010; Wang et al., 2010; Komárek et al., 2015; Liu et al., 2015; Alam et al., 2018; Liu et al., 2018;). Adsorption is generally governed by two parameters: the surface charge properties of the adsorbent and the chemical complexation of aqueous adsorbates onto specific surface functional groups (Dzombak and Morel, 1990). The point of zero net proton charge (pH_{PZNPC}) is one parameter used to assess the surface charge; by definition, it is the pH at which the surface proton charge of a mineral is zero (Drever, 1997).

The pH_{PZNPC} is often calculated using potentiometric acid-base titration data (Zhao et al., 2011; Ahmady-Asbchin and Jafari, 2012; Lützenkirchen et al., 2012a), although it has been argued that what is actually measured is the apparent net proton charge because the initial protonation condition of the surface at the start of the titration is unknown (Sposito, 1998; Hou and Song, 2004). Using this approach, titrations of the adsorbent of interest are conducted at several ionic strength values (IS), and the common intersection point (CIP) of the titration curves is assumed to be the pH_{PZNPC} (Kraepiel et al., 1998; Appel et al., 2003; Lützenkirchen et al., 2012a). It has been shown that for minerals without structural charge (e.g., metal oxides) that a CIP exists, but for

[1] This chapter has been published in *Chemical Geology* as: Hao, W.; Flynn, S.L.; Alessi, D.S.; Konhauser, K.O.

those with structural charge (e.g. clay minerals) there is no CIP (Kraepiel et al., 1998; Zarzycki and Thomas, 2006; Rozalén et al., 2009; Lützenkirchen et al., 2012b). The veracity of this argument has been demonstrated by several previous experimental studies. For instance, Avena and Pauli (1998) titrated Na-montmorillonite at three IS values (0.006 M, 0.014 M, and 0.088 M) and the resulting titration curves were essentially parallel to one another (Avena and Pauli, 1998); Consistent with this, titration curves for both Na-montmorillonite and Na-kaolinite at ionic strength values of 0.01 M, 0.1 M and 1.0 M also failed to intersect (Tombácz et al., 2004; Tombácz and Szekeres, 2006); while simple oxides minerals, such as ferrihydrite, hematite, and goethite, all have the CIP for titrations conducted at different IS values (Dyer et al., 2003; Peacock and Sherman, 2004a).

Nonetheless, despite the existence of these previous studies, the underlying reason and mathematic relationship between ionic strength and pH_{PZNPC} have not been addressed. Moreover, debate remains as to whether a CIP exists for minerals having structural charges. For example, several studies on kaolinite and montmorillonite have found that a CIP does exists for titration curves measured at different IS values (Helmy et al., 1994; Kriaa et al., 2007; Kriaa et al., 2008; Ijagbemi et al., 2009), and a theoretical derivation also proves that a CIP can exist for minerals with structural charge (Hou and Song, 2004). If there is CIP for minerals with structural charge, then the pH_{PZNPC} of clay minerals is constant and independent of IS. However, if a CIP does not exist, determination of clay pH_{PZNPC} values must be determined using another method and the pH_{PZNPC} is variable with IS.

Resolving the above discrepancy is important, because it influences the way in which we study the surface charge of minerals, and thus it directly impacts the predictive accuracy of clay surface properties in systems that have varying IS. Accordingly, this study performed acid-base

titrations on three common clay minerals (kaolinite, illite, and montmorillonite) at seven IS values. Kaolinite [$Al_2Si_2O_5(OH)_4$] results from bonding of a silica tetrahedron to an aluminum/magnesium octahedron to form what is known as a 1:1 type (TO type) of clay mineral. The 1:1 clays are then constructed via hydrogen bonding between the O atoms of the tetrahedron of one layer with the OH groups of the octahedron of a different layer. Both montmorillonite [$(Na,Ca)_{0.33}(Al,Mg)_2(Si_4O_{10})(OH)_2 \cdot nH_2O$] and illite [$(Al_2)(Si_{4-x}Al_x)O_{10}(OH)_2 \cdot K_{1-x}$] are 2:1 type clays (TOT type), in which the octahedron is situated between two tetrahedra. Given that the outer tetrahedron of one layer faces the tetrahedron of another layer, the natural repulsive forces of the outer O atoms require interlayer cations to bridge the layers together. Importantly, all three clay minerals have structural charges resulting from the isomorphic substitution of higher valence cations by lower valence cations (Hower and Mowatt, 1966; Chiou and Rutherford, 1997; Schroth and Sposito, 1997) and the SSA, CEC and Ca/Na data can be referred to Appendix 1 SI Table 1.1.

2.2 Materials and experimental procedures

Samples of kaolinite (KGa-2), montmorillonite (SWy-2), and illite (IMt-2) were obtained from the Clay Mineral Society, Source Clays Repository (Purdue University, West Lafayette, USA). All clays were grounded to pass a 100-mesh sieve. They were then washed three times by suspending 0.5 g of clay in 50 ml of 0.1 M sodium nitrate solution (ACS certified, Fisher Scientific) for 3 h and then centrifuged at 10,000 g for 20 min. After washing, clays were frozen to -20℃ for 12 h and then freeze dried.

Potentiometric titrations of clay minerals were conducted using an automated continuous titrator (Metrohm Titrando 905). Before each titration, the pH electrode was calibrated using commercial pH buffers (Thermo Fisher Scientific; pH 4.0, 7.0, 10.0). For each titration, 0.05 g of

clay was suspended into 50 mL of $NaNO_3$ solution (concentration from 0.001 M to 0.1 M), and the suspension was then bubbled for 30 min with N_2(g) to ensure the solution was devoid of CO_2. During titrations, the experimental apparatus remained sealed and was continually bubbled with N_2 to prevent CO_2 from entering the system.

Seven concentrations of $NaNO_3$ electrolyte solution (0.001 M, 0.005 M, 0.01 M, 0.025 M, 0.05 M, 0.075 M, and 0.1 M) were used for the titrations, and each clay was titrated in triplicate at each IS. A previous study showed that clays may partially dissolve at pH < 4 (Bibi et al., 2014); accordingly, all clays were titrated over a pH range of 4 to 10.5. Initially, a small volume of 0.1 M nitric acid (HNO_3, ACS certified, Fisher Scientific) was added to bring pH to 4, and then 0.1 M sodium hydroxide (NaOH, ACS certified, Fisher Scientific) solution was incrementally added to bring the pH up to 10.5. The volume of acid and base added, and corresponding pH changes, were recorded at each titration step. The pH was considered stable and recorded only after an electrode stability of 12 mV/min was achieved. A blank titration, without addition of clay minerals, was performed for electrolyte solutions at each of the seven IS considered.

2.3 Data treatment

If a CIP does not exist for acid-base titrations of clay minerals conducted at various IS values, the pH_{PZNPC} must be calculated from titration data by determining the pH condition at which the net surface proton charge is equal to zero (Tschapek et al., 1974; Drever, 1997). This condition can be calculated using the following equation:

$$\delta_p = F^*(\Gamma_{H^+} - \Gamma_{OH^-}) \quad \text{(eq. 1.1)}$$

where, F is faraday constant, Γ_{H+} is the surface concentration of H^+, and Γ_{OH-} is the surface concentration of OH^-. It should be noted that the surface proton charges calculated are actually

"apparent" charges because the impact of structural charge is not explicitly established. Two calculation methods have been previously described in the literature to determine (Γ_{H+}-Γ_{OH-}).

Method 1: The proton budget in a titration system is comprised of proton consumption at the solid surface and water hydrolysis. In a system where no mineral exists, the titration (blank titration) represents the proton budget of the hydrolysis of water. Thus, the difference between the amount of base and acid added to solid suspension (electrolyte + clay) and to a blank solution (only electrolyte) is used to determine the net consumption of H^+ by surfaces (Tschapek et al., 1974; Yates and Healy, 1980; Schroth and Sposito, 1997; Gu and Evans, 2008; Lützenkirchen et al., 2012a). With this, eq. (1.1) can be expanded to:

$$\delta_p = F*(\Gamma_{H+}-\Gamma_{OH-}) = \frac{F}{A}*((n(H^+)_{ads} - n(OH^-)_{ads}) = (\frac{F}{s*\gamma m})*(c(H^+)_{ads} - c(OH^-)_{ads})$$

$$= (\frac{F*V}{s*m}) *(c(H^+)_{ads} - c(OH^-)_{ads}) \text{ (eq. 1.2)}$$

where, A is the surface area, s is the specific surface area of the solid, γ_m is the mass concentration of the solid, m is the mass of the solid, V is the volume of solution, and $c(H^+)_{ads}$ and $c(OH^-)_{ads}$ are concentrations of adsorbed H^+ and OH^- ions, respectively. $c(H^+)_{ads}$ and $c(OH^-)_{ads}$ are related to differences between the blank (b) and clay dispersion titration (d) (Lützenkirchen et al., 2012a):

$$\delta_p = (\frac{F*V}{s*m})*[(c(H^+)_d - c(H^+)_b) - (c(OH^-)_d - c(OH^-)_b)] \text{ or}$$

$$\delta_p = (\frac{F*V}{s*m})*[(c(H^+)_d - c(OH^-)_d) - (c(H^+)_b - c(OH^-)_b)] = \frac{F*V*\Delta c_d}{s*m} - \frac{F*V*\Delta c_b}{s*m} \text{ (eq. 1.3)}$$

where, Δc_d is the difference in the amount of acid and base added into the dispersion titration (in concentration units) and Δc_d is the same for the blank titration. However, since the blank titration generally has little influence on the proton budget at surfaces especially at neutral pH, the term is often ignored (Lützenkirchen et al., 2012a).

Method 2: The surface proton charge is considered equal to the difference between the amount of acid and base added into solution and the number of protons and hydroxyl groups remaining in the solution (see e.g., Huertas et al., 1998; Rabung et al., 1998; Missana et al., 2003; Rozalén et al., 2009; Liu et al., 2015), which is described by the following equation:

$$\delta_p=[C_a-C_b]-([H^+]_{meas}-[OH^-])_{meas} \text{ (eq. 1.4)}$$

where, C_a and C_b are the amounts of acid or base titrant added (mol/L), and $[H^+]_{meas}$ and $[OH^-]_{meas}$ are the concentration of protons and hydroxides left in solution (obtained from pH measurements), respectively.

The range of IS values considered here is purposely broad, and as such, the change in the activities of aqueous species must be considered. For the calculation of pH_{PZNPC} through Method 2, because the pH probe measures proton activity, the Debye-Hückel equation (eq. 1.5, 1.6) is required to translate the proton activity to the proton concentration (Langmuir, 1997):

$$\log\gamma=-AZ_i^2\sqrt{I}/(1+Ba_i\sqrt{I}) \text{ (eq. 1.5)}$$

$$a=\gamma*C \text{ (eq. 1.6)}$$

Both methods were used to model our titration data, as well as estimate the pH_{PZNPC} values for kaolinite, illite and montmorillonite.

To calculate pH_{PZNPC}, the pH value where $\delta_p=0$ must be identified. In this regard, we selected the positive and negative values that were closest to zero, and then regressed them linearly. The equation of the regression line was subsequently used to extrapolate the pH at which δ_p becomes zero. The extrapolated pH_{PZNPC} values were then averaged based on the triplicate results and standard deviations were calculated to estimate the error.

2.4 Results

2.4.1 Titration curves as a function of ionic strength

The titration curves calculated using Method 1 for each of the three clays are shown in Figure 2.1. With increasing pH, the surface proton charge of clays decreases due to the progressive deprotonation of surface sites, consistent with previous studies (Avena and Pauli, 1998; Tombácz et al., 2004; Arda et al., 2006; Tertre et al., 2006; Tombácz and Szekeres, 2006; Gu and Evans, 2007, 2008; Gu et al., 2010;). However, our data show no CIP for the titration curves measured at varying solution IS values. As discussed above, previous research has shown that clay minerals have a CIP; however, some of those studies only performed titrations at two ionic strengths (Helmy et al., 1994; Ijagbemi et al., 2009). In our opinion, to better ascertain whether a CIP exists, titrations at more IS values are required. Furthermore, some of the titrations were performed in CO_2 containing systems (Kriaa et al., 2007), in which the influence of aqueous carbonate species on water hydrolysis is taken into consideration for the proton budget of the surface. Although the authors claimed that there is a CIP for kaolinite (Kriaa et al., 2008), the titration curves at varying IS sometimes overlapped with one other, thereby increasing the difficulty in determining the intersection point.

The proton buffering capacity is greater for montmorillonite than illite and kaolinite (in the order of montmorillonite>illite>kaolinite). As shown in Figure 2.1, montmorillonite has the highest surface proton charge amongst these three clays while kaolinite has the lowest. For montmorillonite, the titration curves (Figure 2.1c) distort at pH 5.0-6.5, while for kaolinite and illite, such behavior does not exist. This may be attributed to the well-known swelling property of montmorillonite, which increases its surface area and thus increases the degree of proton interaction. We also found that this effect is reduced as a function of increasing IS, which probably

indicates that a high electrolyte concentration can inhibit the swelling process or proton adsorption onto the swelled surfaces. Moreover, the titration curves (Figure 2.1) for all three clays show a direct relationship with increasing IS, as clays titrated in high IS electrolyte position at the bottom, with lower IS titration curves progressively lying above them. This indicates that at the same pH, the clay in the highest IS solution has the lowest surface proton charge.

2.4.2 Variation of pH_{PZNPC} with ionic strength

The pH_{PZNPC} values calculated using the two methods are generally the same for kaolinite (Table 1.1, 1.2), increasing from 5.6 to 6.6 as solution IS increases from 0.001 M to 0.1 M. However, more variation is observed between the methods for illite and montmorillonite, with the estimated pH_{PZNPC} values from Method 2 being 0.4 to 0.5 pH units higher than from Method 1. Illite has an average pH_{PZNPC} of between 8.8 to 9.2 using Method 1, but between 9.1 to 9.7 for Method 2, while the pH_{PZNPC} of montmorillonite is calculated to be between 9.6 to 9.8 by Method 1 and between 10.0 to 10.1 using Method 2. Similar to kaolinite, there is a trend of decreasing calculated pH_{PZNPC} with increasing IS. Comparison amongst the three clay minerals shows that the variation among the triplicates (standard deviation) for montmorillonite is much larger than that for kaolinite and illite. As mentioned above, the swelling property of montmorillonite likely causes variations in the experimental results.

The variation in calculated pH_{PZNPC} values as a function of ionic strength are illustrated in Figure 2.2 for Method 1, and Figure 2.3 for Method 2. For all three clay minerals and for both methods, the pH_{PZNPC} values initially decrease sharply with increasing IS at low IS range (0.001 M to 0.025 M). However, with IS increasing (0.025 to 0.1M), the pH_{PZNPC} changes more slowly. When the pH_{PZNPC} values for all three clays are plotted as a function of log (IS), a negative linear

relationship is observed. The regressed linear relationships for kaolinite (eq. 1.7), illite (eq. 1.8) and montmorillonite (eq. 1.9) are best fit by the following three equations:

$$pH_{PZNPCkao} = -0.5084*\log(IS)+5.142 \text{ (eq. 1.7)}$$

$$pH_{PZNPCillite} = -0.1872*\log(IS)+8.697 \text{ (eq. 1.8)}$$

$$pH_{PZNPCmont} = -0.07386*\log(IS)+9.531 \text{ (eq. 1.9)}$$

Using Method 2 results in similar linearly decreasing relationships for each clay with log(IS), which are expressed as:

$$pH_{PZNPCkao} = -0.5744*\log(IS)+4.942 \text{ (eq. 1.10)}$$

$$pH_{PZNPCillite} = -0.2956*\log(IS)+8.968 \text{ (eq. 1.11)}$$

$$pH_{PZNPCmont} = -0.06572*\log(IS)+9.945 \text{ (eq. 1.12)}$$

The two methods of calculating pH_{PZNPC} produce similar linear relationships between the pH_{PZNPC} and log(IS), with only small differences in the slope and intercept values of the linear equations for each clay.

2.5 Discussion

2.5.1 Differences in the proton interactions between clays and simple oxides

For simple oxides and hydroxides, such as goethite, magnetite, ferrihydrite, gibbsite, and quartz, surface binding sites are amphoteric and can be represented by a generalized surface functional group ≡MOH, where M represents the metal or metalloid that hosts the proton-active hydroxyl moiety. A characteristic feature of titration curves for simple oxides and hydroxides is that at various IS values, the titration curves tend to intersect at one point (CIP), the pH_{PZNPC} (Appendix 1 SI Figure 1.1), and at that point, the concentration of species $\equiv MOH_2^+$ is, by definition, equal to that of $\equiv MO^-$. At the pH_{PZNPC}, the net surface charge is zero, indicating that the surface electric

field is zero. Therefore, the solution IS has no impact on the surface electric field. This leads to a common intersection point of titration curves at varying IS (Kraepiel et al., 1998; Lützenkirchen et al., 2012a). Experimental data show this phenomenon: for instance, Peacock and Sherman (2004a, b) performed titrations on goethite at three different IS values (0.1 M, 0.01 M, and 0.003 M), and the curves intersect at pH 8.5 (Peacock and Sherman, 2004a, b), while titration curves for hematite at IS of 0.1 M, 0.01 M, and 0.001 M intersect at approximately pH 6.1 (Rabung et al., 1998). Similar trends have been found for magnetite, ferrihydrite and titanium oxide (Yates and Healy, 1980; Kuo and Hst, 1985; Missana et al., 2003). Collectively, previous studies have demonstrated that at pH values below the pH_{PZNPC}, the surfaces of minerals in higher IS solutions have a higher net proton charge than those in lower IS solutions, while at pH values above the pH_{PZNPC}, the opposite is true (Figure 2.4). This pattern can be explained by the impact of IS on the mineral's surface electric field. When $pH<pH_{PZNPC}$, the solid surfaces have a net positive charge, which reduces further adsorption of protons onto the surfaces. However, increasing IS at this pH condition will weaken the positive electrostatic field at the mineral surface and thereby reduce the repulsive force to protons. This effect allows more protons to adsorb onto the surface at high IS conditions as compared to low IS conditions; this likely explains why oxide mineral surfaces have higher surface proton charges at high IS solution conditions when $pH<pH_{PZNPC}$ (Appendix 1 SI Figure 1.1). Conversely, when $pH>pH_{PZNPC}$, the surfaces of simple oxides are negatively charged favoring proton adsorption. Thus, the weakening of the net negative electrical field above the pH_{PZNPC} and at high IS causes the mineral surfaces to have less proton charge than they would at lower IS conditions.

Unlike the metal oxides and hydroxides, clay minerals have no CIP as a function of IS. In a pristine system without adsorption of other aqueous ions, clays have two types of surface charge:

surface proton charge and permanent structural charge. The surface proton charge of a clay can be described in the same way as above for metal oxides and hydroxides, while permanent charge is mainly due to the isomorphic substitution of higher valent ions by lower valent ions; the latter is a characteristic feature of clay minerals. Generally, trivalent ions (Al^{3+}) in octahedral sheets can be replaced by divalent ions (Mg^{2+}), resulting in one negative charge at the clay surface. This also applies for tetravalent ions (Si^{4+}) in tetrahedral sheets where some are substituted by trivalent ions (Al^{3+}). The permanent charge of clay minerals can only be partially offset by surface protonation/deprotonation reactions, as evident from the observation that the zeta-potentials of kaolinite, montmorillonite and illite increase slightly with decreasing pH, but remain overall negative even at pH=2 (Chorom and Rengasamy, 1995; Vane and Zang, 1997; Kaya and Yukselen, 2005). Therefore, the increase of solution IS for clay systems results in the shielding of the net negatively-charged surface electric field, and thereby lowers proton binding onto the surface across the entire pH range tested (4.0 to 10.5). This explains why the pH_{PZNPC} values for clay minerals decrease systematically with increasing IS (Figure 2.2, 2.3) and why the curves never cross (Figure 2.1).

2.5.2 The pH_{PZNPC} of clay minerals

Both of our methods show that the pH_{PZNPC} of clay minerals changes linearly with logarithm of solution IS, which is in accordance with a previous study by Cao et al. (2016). This relationship may be related to the dynamics of the ion cloud at the mineral surface. According to electric double layer theory, electrolyte ions form a diffuse layer around charged surfaces. This effect will neutralize surface charge and lead to surface potential decrease as a function of distance from surface. The distribution of the surface ion cloud can then be affected by solution ionic strength

which results in a decrease of electric double layer thickness with increasing IS (Bohn et al., 2002). Since pH_{PZNPC} is the zero-proton adsorption condition at the surface, its decreasing trend may indicate the thickness of surface electric field varies linearly with the logarithm of IS, with the assumption that the thickness of this double layer is proportional to ion adsorption. Detailed information on this aspect needs further theoretical derivation and experimental evidence.

For the three clays studied here, the pH_{PZNPC} determined for montmorillonite and illite over the seven IS values tested is generally between 9 to 10, while the pH_{PZNPC} for kaolinite is between 5 to 6. Natural water has a pH range between 5-8, which is lower than the pH_{PZNPC} of illite and montmorillonite. Thus, under most natural conditions, clay surfaces have a net positive proton charge, i.e., the surfaces are protonated. The structural negative charge of kaolinite is relatively low compared to illite and montmorillonite, which leads to less affinity to protons and a lower pH_{PZNPC} value.

Based on our two methods for calculating pH_{PZNPC}, kaolinite shows the greatest sensitivity to changes in IS (from Figure 2.2a and 2.3a, note that the slope for kaolinite is -0.5 to -0.6), while montmorillonite is the least sensitive (Figure 2.2c and 2.3c shows that the slope for montmorillonite is -0.06 to -0.07). The following reasons may explain the phenomenon above mentioned. Kaolinite's pH_{PZNPC} is at a neutral pH—where there are equal and modest concentrations of H^+ and OH^- ions in solution—making it susceptible to change when modifying the solution proton concentration. This is in contrast to illite and montmorillonite, which have pH_{PZNPC} values at higher pH. Additionally, the tendency for montmorillonite to swell in the presence of water could act as a potential buffer against changes in ionic strength (i.e., $NaNO_3$ and protons can enter into the interlayers during swelling), and thus impact the change of pH_{PZNPC} with solution IS.

Our pH_{PZNPC} values are slightly higher compared to those in the literature (Kosmulski, 2011) and we believe experimental conditions can account for this discrepancy. The pH_{PZNPC} values of these clays from literature compilation are between 7 to 9 for both illite and montmorillonite (Kosmulski, 2011). The clay pretreatment methods, the source of the clay used and the removal of CO_2 from titration cells may lead to the differences of results. For instance, titration of montmorillonite with an elevated Zn concentration gives pH_{PZNPC} values around 8.8 (Stathi et al., 2009); without pre-bubbling of experimental cell, the pH_{PZNPC} values of montmorillonite are from 8.1 to 7.6 for an IS range between 0.001M to 0.1M (Rozalén et al., 2009). It has also been reported that kaolinite pretreated with H_2O_2 at 60 ^oC with no CO_2 removal procedure has a measured pH_{PZNPC} value of 3.7 (Zhuang and Yu, 2002). Thus, the presence of CO_2 during the titration process is a critical factor in lowering the determined pH_{PZNPC} value. Atmospheric CO_2 can result in a lower pH_{PZNPC} value by forming carbonic acid in water. To prevent this effect, our experimental cell was well sealed to avoid influx of atmospheric CO_2 and bubbled for 30 min with N_2 to ensure that CO_2 initially dissolved into the system was removed, a treatment critical to ensure measurement of a valid pH_{PZNPC} value.

2.5.3 Surface complexation modeling

Surface complexation modeling (SCM) is a tool that has been used to assess the adsorption capacity of protons and metals onto heterogeneous surfaces in aqueous solution. SCM attributes surface proton charge to proton interactions on discrete surface functional groups, and treats these interactions using balanced chemical reactions. For clay minerals with amphoteric sites (≡MOH) and permanently charged sites (≡LH), the key protonation and deprotonation reactions can be written as:

$$\equiv LH \rightleftharpoons H^+ + \equiv L^- \text{ (eq. 1.13)}$$

$$\equiv XOH \rightleftharpoons H^+ + \equiv XO^- \text{ (eq. 1.14)}$$

$$\equiv XOH + H^+ \rightleftharpoons \equiv XOH_2^+ \text{ (eq. 1.15)}$$

It should be noted that the permanently charged sites in clay minerals cannot be satisfied by proton adsorption because they are inherent. Mechanically, they can provide a negative electrostatic field at the mineral surface, which facilitates proton adsorption. However, this "facilitation" effect is hard to represent in a SCM model. Accordingly, we applied a protonated site ≡LH to simulate the promotion effect of the surface electrostatic field on proton adsorption. Choosing between an electrostatic model (EM) and a non-electrostatic model (NEM) is also a critical consideration. Electrostatic models distinguish the electrostatic term from bulk adsorption through applying various theories of how surface charge develops (for example, Helmholtz, Gouy-Chapman, Stern theories), in order to derive an intrinsic chemical affinity for the binding of protons or other aqueous species. However, the electrostatic factor is not separated in NEMs, and thus, the result of a NEM is not the intrinsic chemical affinity but can be influenced by changes in the surface electrostatic field. The presence of solution electrolytes may either impact the mineral surface electric field or the affinity of aqueous species for surface functional groups (or both). The purpose of this paper is to investigate the impact of IS on the proton adsorption process; thus, we chose to apply a non-electrostatic model instead in order to explicitly quantify the impact of changes in IS on proton adsorption, and ultimately the pH_{PZNPC}.

Using potentiometric titration data for each of the three clay minerals, the protonation constants and corresponding site concentrations of surface functional groups (≡LH, ≡XOH) can be calculated using the software program FITEQL 4.0 (Westall, 1982). The concentrations of surface species (≡LH, $\equiv L^-$, ≡XOH, $\equiv XO^-$, and $\equiv XOH_2^+$) at each pH point are also listed in the

output file and are plotted as a function of pH in Figure 2.4, 2.5, 2.6. Because ≡LH and ≡XOH groups are uncharged, we can then plot the concentration of $\equiv L^-$, $\equiv XO^-$, and $\equiv XOH_2^+$ with pH and IS to observe how the pH_{PZNPC} value changes with IS.

The ≡LH group of kaolinite only begins to deprotonate significantly at pH > 8.5, while for the ≡XOH group, the concentration of two species $\equiv XO^-$ and $\equiv XOH_2^+$ intersects at approximately pH 6. Since at pH 6 the ≡LH group is mainly in a neutral, protonated state (as ≡LH, with a considerably lower concentration of $\equiv L^-$ species), the pH at the intersection point of the ≡XOH species is nearly equivalent to the value of the pH_{PZNPC} for this clay. We found that the intersection point moves toward lower pH, with increasing IS (Figure 2.4), indicating that the pH_{PZNPC} decreases with IS. This is in accordance with the trend uncovered by the two pH_{PZNPC} calculation methods. Illite and montmorillonite behaved differently than kaolinite. For those minerals, the following trends were observed: (1) the species $\equiv L^-$ and $\equiv XOH_2^+$ intersect between pH 9 to 10; (2) at the intersection point, the concentration of species $\equiv XO^-$ is considerably lower than the other two surface species, and thus is not important in determining the overall pH_{PZNPC}; and (3) the intersection point of species $\equiv L^-$ and $\equiv XOH_2^+$, which is nearly equivalent to the pH_{PZNPC}, moves toward lower pH with increasing IS.

Surface species concentrations from the speciation diagrams (Figures 2.4-2.6) were used to calculate pH_{PZNPC} values, using the following equation:

$$\delta_p=[\equiv XOH_2^+]-[\equiv L^-]-[\equiv XO^-] \text{ (eq. 1.16)}$$

The pH_{PZNPC} of kaolinite calculated with the SCM method is generally similar to the previous two methods, ranging from 5.6 to 6.7 across the range of IS tested (Table 1.3). Similar linear trends of the pH_{PZNPC} as a function of the logarithm of IS were observed for each clay using the SCM method (Figure 2.7), according to the following relationships:

$$pH_{PZNPCkao}=-0.5605*\log(IS)+5.073 \quad \text{(eq. 1.17)}$$

$$pH_{PZNPCillite}=-0.2344*\log(IS)+8.934 \quad \text{(eq. 1.18)}$$

$$pH_{PZNPCmont}=-0.09864*\log(IS)+9.773 \quad \text{(eq. 1.19)}$$

However, the SCM-calculated pH_{PZNPC} values for illite and montmorillonite are between 0.3 to 0.4 pH units higher than those calculated with Method 1, but nearly identical using Method 2. One possible reason for the discrepancy between Method 1 and the latter two methods could be the initial protonation state of the clay minerals. Theoretically, both Method 1 and Method 2 are valid for the calculation of surface proton budget. However, the subtraction between the amount of protons added in a real titration versus the blank titration ignores the fact that the surface could be initially protonated, and that protons pre-existing on the surface can be released into solution. The result is that the calculation of protons adsorbed on surface by Method 1 is likely lower than it is in actuality. This is perhaps the reason why pH_{PZNPC} calculated by Method 1 is lower than the actual conditions. But this cannot be applied to Method 2, because Method 2 calculates the difference between protons added and protons remaining in solution, and in this way the desorption of pre-existing protons is considered in the surface proton budget.

2.6 Conclusions and environmental implications

Our work demonstrates that acid-base titration curves for kaolinite, montmorillonite and illite at different IS have no CIPs. This indicates that the change of clay surface reactivity and pH_{PZNPC} is a function of solution IS. By then using three different methods to calculate the pH_{PZNPC} of three clay minerals, we additionally observed that pH_{PZNPC} decreases linearly with increasing solution IS. The pH_{PZNPC} values calculated by the SCM method are around 0.3 to 0.4 pH units higher than those calculated with Method 1 but are generally in accordance with Method 2 for montmorillonite

and illite. For kaolinite, SCM-calculated pH_{PZNPC} values are approximately the same as those calculated using the above two methods.

The study of changes in the pH_{PZNPC} of clay minerals with ionic strength has important environmental implications. Clay particles originally released to streams characterized by low IS and slightly acidic waters may eventually be discharged into estuaries with more alkaline pH and higher IS. One of the goals of our future research is to then ascertain whether clay minerals deposited in estuaries serve as trace metal sinks or sources to the overlying water column. Although this work is currently being conducted, there are existing data available that consider clay mineral reactivity in such settings. For instance, experimental results of Cd adsorption onto montmorillonite showed that almost 90% of Cd adsorbed onto montmorillonite at pH=6 and at 0.001 M ionic strength (Gu et al., 2010), while this number decreased to only 10% if ionic strength was increased to mimic seawater (0.56 M) (Liu et al., 2018). The increase of pH has inverse effect with IS, where the increase of pH from 6 to 8 results in an additional 40% of Cd adsorption (Liu et al., 2018). The overall budget of Cd in estuary environment could be more complicated when considering activity of Cd and its aqueous complexation with carbonate and hydroxide groups. Future work could specific this problem, but the empirical relationships we have developed here can be used in consort with surface complexation models to quantitatively account for changing proton binding behavior as pH and solution IS conditions change.

2.7 References

Ahmady-Asbchin, S., Jafari, N., 2012. Physicochemical Studies of Copper (II) Biosorption from Wastewater by Marine Brown Algae Sargassum angustifolium C. Agardh (Fucales, Phaeophyceae). International Journal on Algae, 14(4): 367-379.

Alam, M.S., Swaren, L., von Guten, K., Cossio, M., Bishop, B., Robbins, L.J., Hou, D., Flynn, S.L., Ok, Y.S., Konhauser, K.O., Alessi, D.S., 2018. Application of surface complexation modeling to trace metals uptake by biochar-amended agricultural soils. Applied Geochemistry, 88: 103-112.

Alessi, D.S., Fein, J.B., 2010. Cadmium adsorption to mixtures of soil components: Testing the component additivity approach. Chemical Geology, 270(1): 186-195.

Appel, C., Ma, L.Q., Dean, R.R., Kennelley, E., 2003. Point of zero charge determination in soils and minerals via traditional methods and detection of electroacoustic mobility. Geoderma, 113(1): 77-93.

Arda, D., Hizal, J., Apak, R., 2006. Surface complexation modelling of uranyl adsorption onto kaolinite based clay minerals using FITEQL 3.2. Radiochim. Acta, 94: 835- 844.

Avena, J.M., Pauli, P.D.C., 1998. Proton Adsorption and Electrokinetics of an Argentinean Montmorillonite. Journal of Colloid and Interface Science, 202: 195-204.

Bibi, I., Singh, B., Silvester, E., 2014. Dissolution kinetics of soil clays in sulfuric acid solutions: Ionic strength and temperature effects. Applied Geochemistry, 51: 170-183.

Bohn, H.L., Myer, R.A., O'Connor, G.A., 2002. Soil chemistry. Chapter 8 Cation Retention (Exchange) in Soils. John Wiley & Sons.

Borrok, D.M., Fein, J.B., 2005. The impact of ionic strength on the adsorption of protons, Pb, Cd, and Sr onto the surfaces of Gram negative bacteria: testing non-electrostatic, diffuse, and triple-layer models. Journal of Colloid and Interface Science, 286(1): 110-126.

Cao, X., Chen, Y., Zhang, Y., Qiu, J., Li, L., Lv, X., Zhao, X., 2016. Study and modeling surface charge characteristics of montmorillonite. Functional Material, 4(47): 4152-4156 (in Chinese).

Chiou, C.T., Rutherford, D.W., 1997. Effects of exchanged cation and layer charge on the sorption of water and EGME vapors on montmorillonite clays. Clays and Clay Minerals, 45(6): 867-880.

Chorom, M., Rengasamy, P., 1995. Dispersion and zeta potential of pure clays as related to net particle charge under varying pH, electrolyte concentration and cation type. European Journal of Soil Science, 46(4): 657-665.

Drever, J.I., 1997. The geochemistry of natural waters: surface and groundwater environments, Prentice-Hall, Inc., Upper Saddle River, NJ.

Dyer, J.A., Trivedi, P., Scrivner, N.C., Sparks, D.L., 2003. Lead sorption onto ferrihydrite. 2. Surface complexation modeling. Environmental Science and Technology, 37(5): 915-922.

Dzombak, D.A., Morel, F.M., 1990. Surface complexation modeling: hydrous ferric oxide. John Wiley & Sons.

Gu, X., Evans, L.J., 2007. Modelling the adsorption of Cd(II), Cu(II), Ni(II), Pb(II), and Zn(II) onto Fithian illite. Journal of colloid and interface science, 307(2): 317-25.

Gu, X., Evans, L.J., 2008. Surface complexation modelling of Cd(II), Cu(II), Ni(II), Pb(II) and Zn(II) adsorption onto kaolinite. Geochimica et Cosmochimica Acta, 72(2): 267-276.

Gu, X., Evans, L.J., Barabash, S.J., 2010. Modeling the adsorption of Cd (II), Cu (II), Ni (II), Pb (II) and Zn (II) onto montmorillonite. Geochimica et Cosmochimica Acta, 74(20): 5718-5728.

Helmy, A.K., Ferreiro, E.A., Debussetti, S.G., 1994. Cation-exchange capacity and condition of zero charge of hydroxy-Al montmorillonite. Clays and Clay Minerals, 42(4): 444-450.

Hou, W., Song, S., 2004. Intrinsic surface reaction equilibrium constants of structurally charged amphoteric hydrotalcite-like compounds. Journal of Colloid and Interface Science, 269(2):

381-387.

Hower, J., Mowatt, C.T., 1966. The mineralogy of illite and mixed-layer illite/montmorillonites. The American Mineralogist, 51: 825-854.

Huertas, F.J., Chou, L., Wollast, R., 1998. Mechanism of kaolinite dissolution at room temperature and pressure: Part 1. Surface speciation. Geochimica et Cosmochimica Acta, 62(3): 417-431.

Ijagbemi, C.O., Baek, M.H., Kim, D.S., 2009. Montmorillonite surface properties and sorption characteristics for heavy metal removal from aqueous solutions. Journal of Hazardous Materials, 166(1): 538-546.

Kaya, A., Yukselen, Y., 2005. Zeta potential of clay minerals and quartz contaminated by heavy metals. Canadian Geotechnical Journal, 42(5): 1280-1289.

Komárek, M., Koretsky, C.M., Stephen, K.J., Alessi, D.S., Chrastný, V., 2015. Competitive Adsorption of Cd(II), Cr(VI), and Pb(II) onto Nanomaghemite: A Spectroscopic and Modeling Approach. Environmental Science and Technology, 49(21): 12851-12859.

Kosmulski, M., 2011. The pH-dependent surface charging and points of zero charge: V. Update. Journal of Colloid and Interface Science, 353(1): 1-15.

Kraepiel, A.M.L., Keller, K., Morel, F.M.M., 1998. On the acid-base chemistry of permanently charged minerals. Environmental Science and Technology, 32(19): 2829-2838.

Kriaa, A., Hamdi, N., Srasra, E., 2007. Acid-base chemistry of montmorillonitic and beidellitic-montmorillonitic smectite. Russian Journal of Electrochemistry, 43(2): 167-177.

Kriaa, A., Hamdi, N., Srasra, E., 2008. Determination of Point of Zero Charge of Tunisian Kaolinites by Potentiometric and Mass Titration Methods. Journal of the Chinese Chemical Society, 55(1): 53-61.

Kuo, C., Hst, D., 1985. Adsorption of uranyl onto ferric oxyhydroxides: Application of the surface complexation site-binding model. Geochimica et Cosmochimica Acta, 49: 1931-1941.

Lützenkirchen, J., Preočanin, T., Kovačević, D., Tomišić, V., Lövgren, L., Kallay, N., 2012a. Potentiometric Titrations as a Tool for Surface Charge Determination. Croatica Chemica Acta, 85(4): 391-417.

Lützenkirchen, J., Preočanin, T., Bauer, A., Metz, V., Sjöberg, S., 2012b. Net surface proton excess of smectites obtained from a combination of potentiometric acid–base, mass and electrolyte titrations. Colloids and Surfaces A: Physicochemical and Engineering Aspects, 412(Supplement C): 11-19.

Langmuir, D., 1997. Aqueous Environmental Geochemistry. Prentice-Hall, Inc.

Liu, Y., Alessi, D.S., Flynn, S.L., Alam, M.S., Hao, W., Gingras, M., Zhao, H., Konhauser, K.O., 2018. Acid-base properties of kaolinite, montmorillonite and illite at marine ionic strength. Chemical Geology, 483: 191-200.

Liu, Y., Alessi, D.S., Owttrim, G.W., Petrash, D.A., Mloszewska, A.M., Lalonde, S.V., Martinez, R.E., Zhou, Q.X., Konhauser, K.O., 2015. Cell surface reactivity of Synechococcus sp PCC 7002: Implications for metal sorption from seawater. Geochimica et Cosmochimica Acta, 169: 30-44.

Missana, T., García-Gutiérrez, M., Fernńdez, V., 2003. Uranium (VI) sorption on colloidal magnetite under anoxic environment: experimental study and surface complexation modelling. Geochimica et Cosmochimica Acta, 67(14): 2543-2550.

Peacock, C.L., Sherman, D.M., 2004a. Copper(II) sorption onto goethite, hematite and lepidocrocite: a surface complexation model based on ab initio molecular geometries and EXAFS spectroscopy. Geochimica et Cosmochimica Acta, 68(12): 2623-2637.

Peacock, C.L., Sherman, D.M., 2004b. Vanadium(V) adsorption onto goethite (α-FeOOH) at pH 1.5 to 12: a surface complexation model based on ab initio molecular geometries and EXAFS spectroscopy. Geochimica et Cosmochimica Acta, 68(8): 1723-1733.

Rabung, T., Geckeis, H., Kim, J., Beck, P.H., 1998. Sorption of Eu(III) on a natural hematite application of a surface complexation model. Journal of Colloid and Interface Science, 208: 153-161.

Rozalén, M., Brady, P.V., Huertas, F.J., 2009. Surface chemistry of K-montmorillonite: Ionic strength, temperature dependence and dissolution kinetics. Journal of Colloid and Interface Science, 333(2): 474-484.

Schroth, B.K., Sposito, G., 1997. Surface charge properties of kaolinite. Clays and Clay Minerals, 45(1): 85-91.

Sposito, G., 1998. On points of zero charge. Environmental Science and Technology, 32(19): 2815-2819.

Stathi, P., Papadas, I.T., Enotiadis, A., Gengler, R.Y.N., Gournis, D., Rudolf, P., Deligiannakis, Y., 2009. Effects of acetate on cation exchange capacity of a Zn-containing montmorillonite: Physicochemical significance and metal uptake. Langmuir, 25(12): 6825-6833.

Tertre, E., Castet, S., Berger, G., Loubet, M., Giffaut, E., 2006. Surface chemistry of kaolinite and Na-montmorillonite in aqueous electrolyte solutions at 25 and 60°C: Experimental and modeling study. Geochimica et Cosmochimica Acta, 70(18): 4579-4599.

Tombácz, E., Nyilas, T., Libor, Z., Csanaki, C., 2004. Surface charge heterogeneity and aggregation of clay lamellae in aqueous suspensions. Progress in Colloid and Polym Science, 125: 206-215.

Tombácz, E., Szekeres, M., 2006. Surface charge heterogeneity of kaolinite in aqueous suspension in comparison with montmorillonite. Applied Clay Science, 34(1-4): 105-124.

Tschapek, M., Tcheichvili, L., Wasowski, C., 1974. The point of zero charge (pzc) of kaolinite and SiO_2+Al_2O_3 mixtures. Clay Minerals, 10: 219-229.

Vane, L.M., Zang, G.M., 1997. Effect of aqueous phase properties on clay particle zeta potential and electro-osmotic permeability: Implications for electro-kinetic soil remediation processes. Journal of Hazardous Materials, 55(1): 1-22.

Wang, G.H., Wang, X.G., Chai, X.J., Liu, J.S., Deng, N.S., 2010. Adsorption of uranium (VI) from aqueous solution on calcined and acid-activated kaolin. Applied Clay Science, 47(3-4): 448-451.

Westall, J.C., 1982. FITEQL: A Computer Program for Determination of Chemical Equilibrium Constants from Experimental Data. Department of Chemistry, Oregon State University.

Yates, D.E., Healy, T.W., 1980. Titanium dioxide-electrolyte interface. Part 2.-Surface charge (titration) studies. Journal of the Chemical Society, Faraday Transactions 1: Physical Chemistry in Condensed Phases, 76(0): 9-18.

Zarzycki, P., Thomas, F., 2006. Theoretical study of the acid–base properties of the montmorillonite/electrolyte interface: Influence of the surface heterogeneity and ionic strength on the potentiometric titration curves. Journal of Colloid and Interface Science, 302(2): 547-559.

Zhao, Z., Jia, Y., Xu, L., Zhao, S., 2011. Adsorption and heterogeneous oxidation of As(III) on ferrihydrite. Water Research, 45(19): 6496-6504.

Zhuang, J., Yu, G., 2002. Effects of surface coatings on electrochemical properties and contaminant sorption of clay minerals. Chemosphere, 49(6): 619-628.

Table 2.1: PZNPC values calculated using Method 1.

Kao		1	2	3		
Log(IS)	IS	PZNPC	PZNPC	PZNPC	Ave	Std
-3.000	0.001	6.697	6.700	6.623	6.673	0.043
-2.301	0.005	6.128	6.380	6.370	6.293	0.143
-2.000	0.01	6.313	6.148	6.163	6.208	0.091
-1.602	0.025	5.817	6.024	5.934	5.925	0.104
-1.301	0.05	5.747	5.772	5.679	5.733	0.048
-1.125	0.075	5.708	5.772	5.798	5.759	0.046
-1.000	0.1	5.639	5.696	5.687	5.674	0.030
Illite		1	2	3		
Log(IS)	IS	PZNPC	PZNPC	PZNPC	Ave	Std
-3.000	0.001	9.204	9.290	9.205	9.233	0.050
-2.301	0.005	9.121	9.175	9.148	9.148	0.027
-2.000	0.01	9.084	9.063	9.043	9.063	0.021
-1.602	0.025	9.041	9.049	9.059	9.050	0.009
-1.301	0.05	8.942	8.984	8.944	8.956	0.024
-1.125	0.075	8.834	8.915	8.943	8.897	0.057
-1.000	0.1	8.801	8.830	8.894	8.842	0.048
Mont		1	2	3		
Log(IS)	IS	PZNPC	PZNPC	PZNPC	Ave	Std
-3.000	0.001	9.790	9.834	9.678	9.767	0.080
-2.301	0.005	9.714	9.591	9.739	9.681	0.079

-2.000	0.01	9.699	9.612	9.718	9.676	0.056
-1.602	0.025	9.674	9.636	9.604	9.638	0.035
-1.301	0.05	9.623	9.536	9.742	9.634	0.103
-1.125	0.075	9.616	9.663	9.603	9.627	0.032
-1.000	0.1	9.597	9.637	9.571	9.601	0.033

Numbers 1, 2, and 3 indicate triplicate titrations; IS means ionic strength; Kao means kaolinite; Mont means montmorillonite; Ave stands for average value of the three sets of PZNPC value; Std stands for the standard deviation of the average value.

Table 2.2: PZNPC values calculated using Method 2.

Kao		1	2	3		
Log(IS)	IS	PZNPC	PZNPC	PZNPC	Ave	Std
-3.000	0.001	6.684	6.682	6.603	6.657	0.046
-2.301	0.005	6.089	6.345	6.327	6.254	0.143
-2.000	0.01	6.275	6.071	6.118	6.154	0.107
-1.602	0.025	5.711	5.957	5.831	5.833	0.123
-1.301	0.05	5.622	5.658	5.601	5.627	0.029
-1.125	0.075	5.573	5.621	5.655	5.616	0.041
-1.000	0.1	5.500	5.571	5.537	5.536	0.036
Illite		1	2	3		
Log(IS)	IS	PZNPC	PZNPC	PZNPC	Ave	Std
-3.000	0.001	9.689	9.892	9.792	9.791	0.102
-2.301	0.005	9.513	9.642	9.806	9.653	0.147
-2.000	0.01	9.589	9.607	9.539	9.578	0.035
-1.602	0.025	9.681	9.715	9.518	9.638	0.106
-1.301	0.05	9.246	9.415	9.306	9.322	0.085
-1.125	0.075	9.144	9.246	9.295	9.229	0.077
-1.000	0.1	9.127	9.214	9.279	9.207	0.076
Mont		1	2	3		
Log(IS)	IS	PZNPC	PZNPC	PZNPC	Ave	Std
-3.000	0.001	10.24	10.25	9.949	10.14	0.170
-2.301	0.005	10.16	10.17	10.01	10.11	0.086

-2.000	0.01	10.16	9.890	10.08	10.04	0.137
-1.602	0.025	10.05	10.21	9.941	10.06	0.135
-1.301	0.05	10.06	9.875	10.12	10.02	0.128
-1.125	0.075	10.09	10.03	10.00	10.04	0.046
-1.000	0.1	10.08	9.968	9.954	10.00	0.066

Numbers 1, 2, and 3 indicate triplicate titrations; IS means ionic strength; Kao means kaolinite; Mont means montmorillonite; Ave stands for average value of the three sets of PZNPC value; Std stands for the standard deviation of the average value.

Table 2.3: PZNPC values calculated using the SCM method.

Kao		1	2	3		
Log(IS)	IS	PZNPC	PZNPC	PZNPC	Ave	Std
-3.000	0.001	nd	6.743	6.699	6.721	0.031
-2.301	0.005	6.111	6.453	6.452	6.339	0.197
-2.000	0.01	6.480	6.229	6.215	6.308	0.149
-1.602	0.025	5.828	6.128	5.987	5.981	0.150
-1.301	0.05	5.709	5.815	5.638	5.721	0.089
-1.125	0.075	5.706	5.780	5.706	5.731	0.042
-1.000	0.1	5.558	5.666	5.642	5.622	0.056
Illite		1	2	3		
Log(IS)	IS	PZNPC	PZNPC	PZNPC	Ave	Std
-3.000	0.001	9.584	9.725	9.650	9.653	0.070
-2.301	0.005	9.438	9.532	9.477	9.483	0.047
-2.000	0.01	9.316	9.317	9.302	9.311	0.008
-1.602	0.025	9.354	9.363	9.428	9.382	0.040
-1.301	0.05	9.222	9.267	9.263	9.251	0.025
-1.125	0.075	9.134	9.199	9.240	9.191	0.053
-1.000	0.1	9.133	9.184	9.149	9.155	0.026
Mont		1	2	3		
Log(IS)	IS	PZNPC	PZNPC	PZNPC	Ave	Std
-3.000	0.001	10.19	10.18	9.848	10.07	0.195
-2.301	0.005	10.07	10.10	9.934	10.04	0.089

-2.000	0.01	10.06	9.809	9.958	9.941	0.124
-1.602	0.025	9.915	9.892	9.842	9.883	0.037
-1.301	0.05	9.944	9.768	10.01	9.907	0.125
-1.125	0.075	9.949	9.906	9.852	9.902	0.049
-1.000	0.1	9.928	9.906	9.826	9.886	0.054

Numbers 1, 2, and 3 indicate triplicate titrations; IS means ionic strength; nd means no data, this is because the first titration data did not converge with the SCM method; Kao means kaolinite; Mont means montmorillonite; Ave stands for average value of the three sets of PZNPC value; Std stands for the standard deviation of the average value.

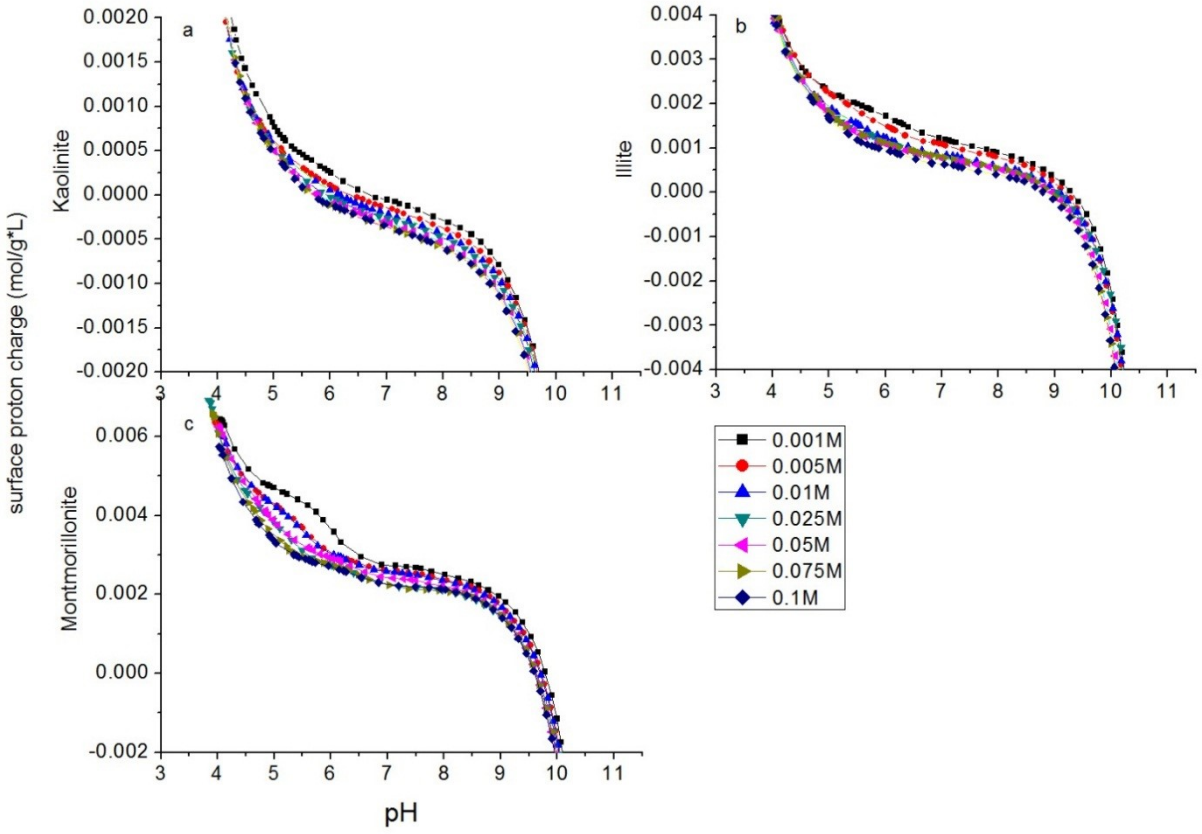

Figure 2.1 Potentiometric titration curves for (a) kaolinite, (b) illite, and (c) montmorillonite.

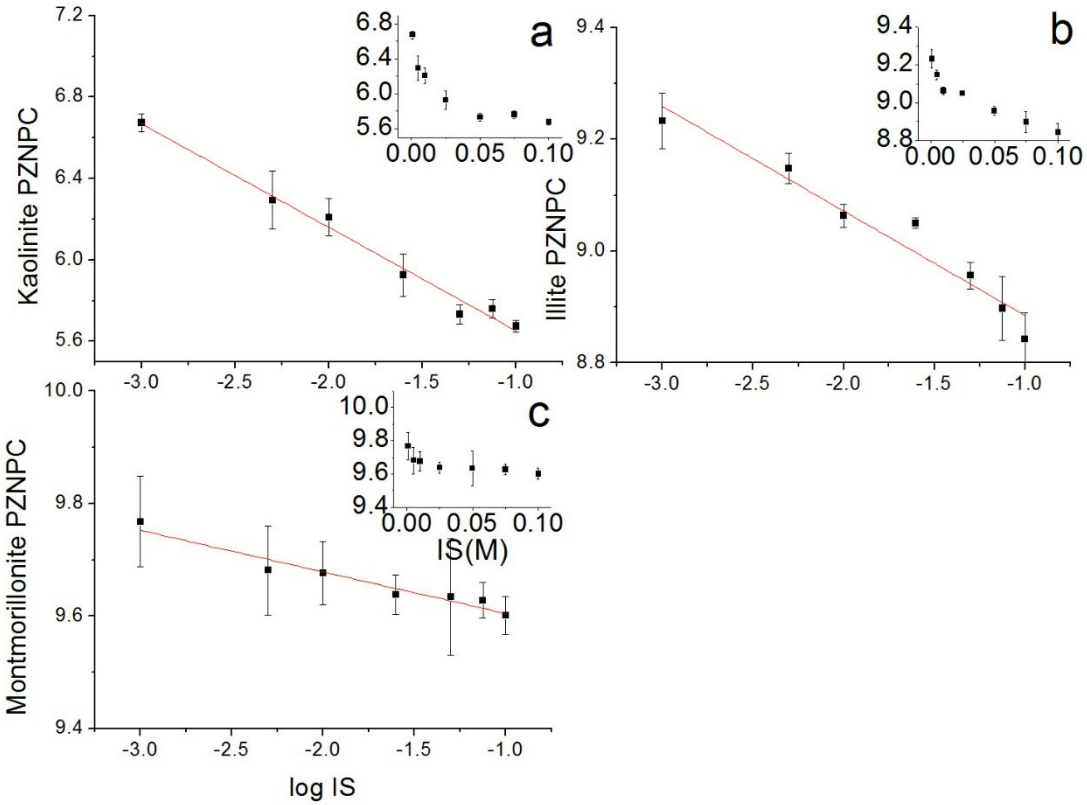

Figure 2.2 Changes in the PZNPC using Method 1, as a function of ionic strength (inset plots), and the logarithm of ionic strength, for (a) kaolinite, (b) illite and (c) montmorillonite.

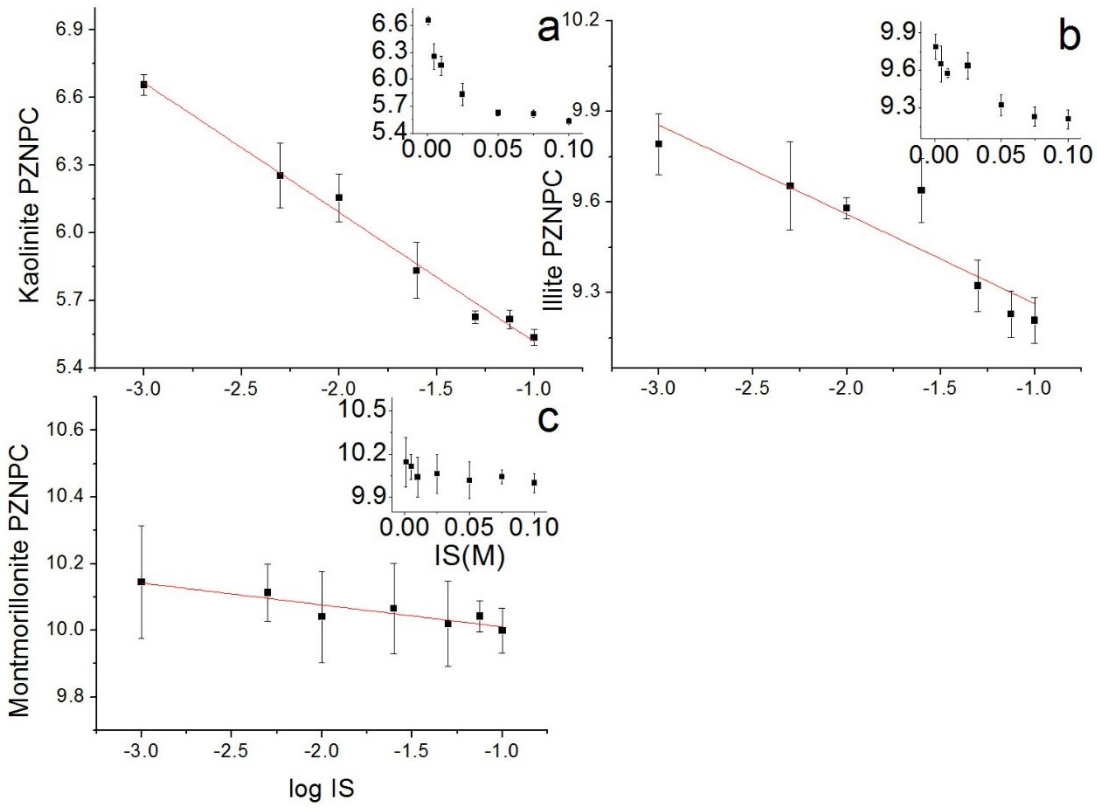

Figure 2.3 Changes in the PZNPC using Method 2, as a function of ionic strength (inset plots), and the logarithm of ionic strength, for (a) kaolinite, (b) illite and (c) montmorillonite.

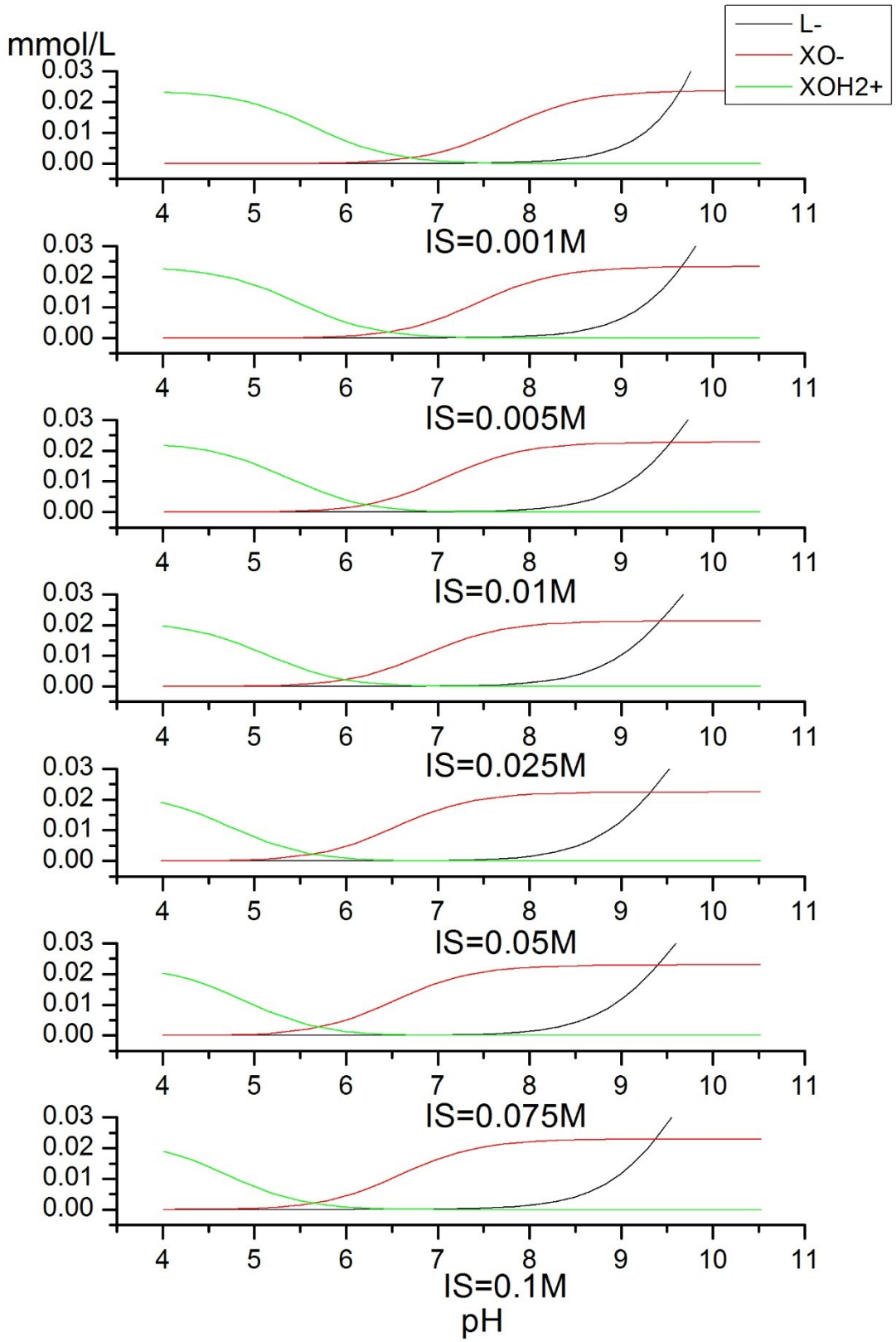

Figure 2.4 Speciation diagrams for kaolinite surface sites at the seven IS values tested.

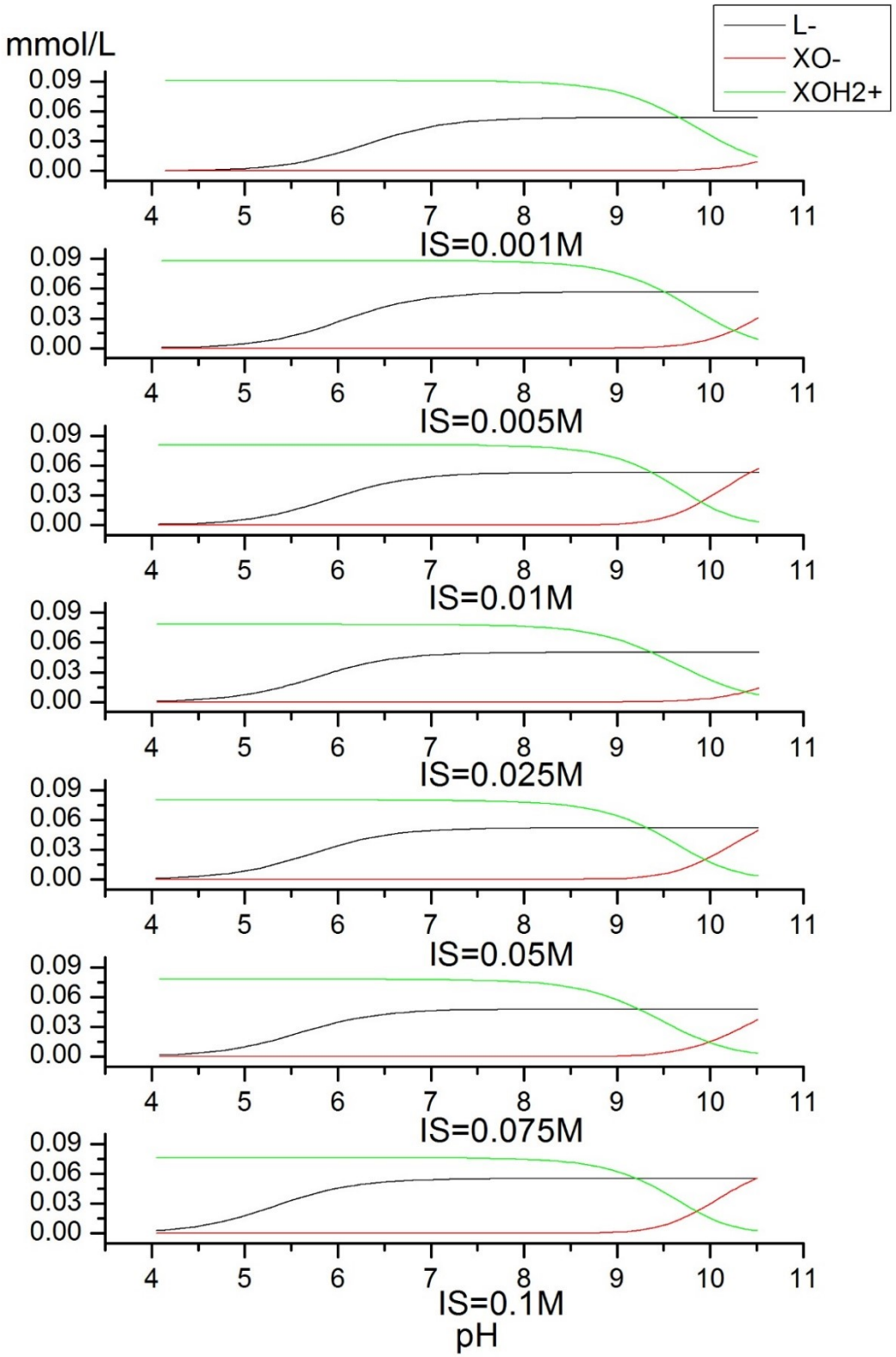

Figure 2.5 Speciation diagrams for illite surface sites at the seven IS values tested.

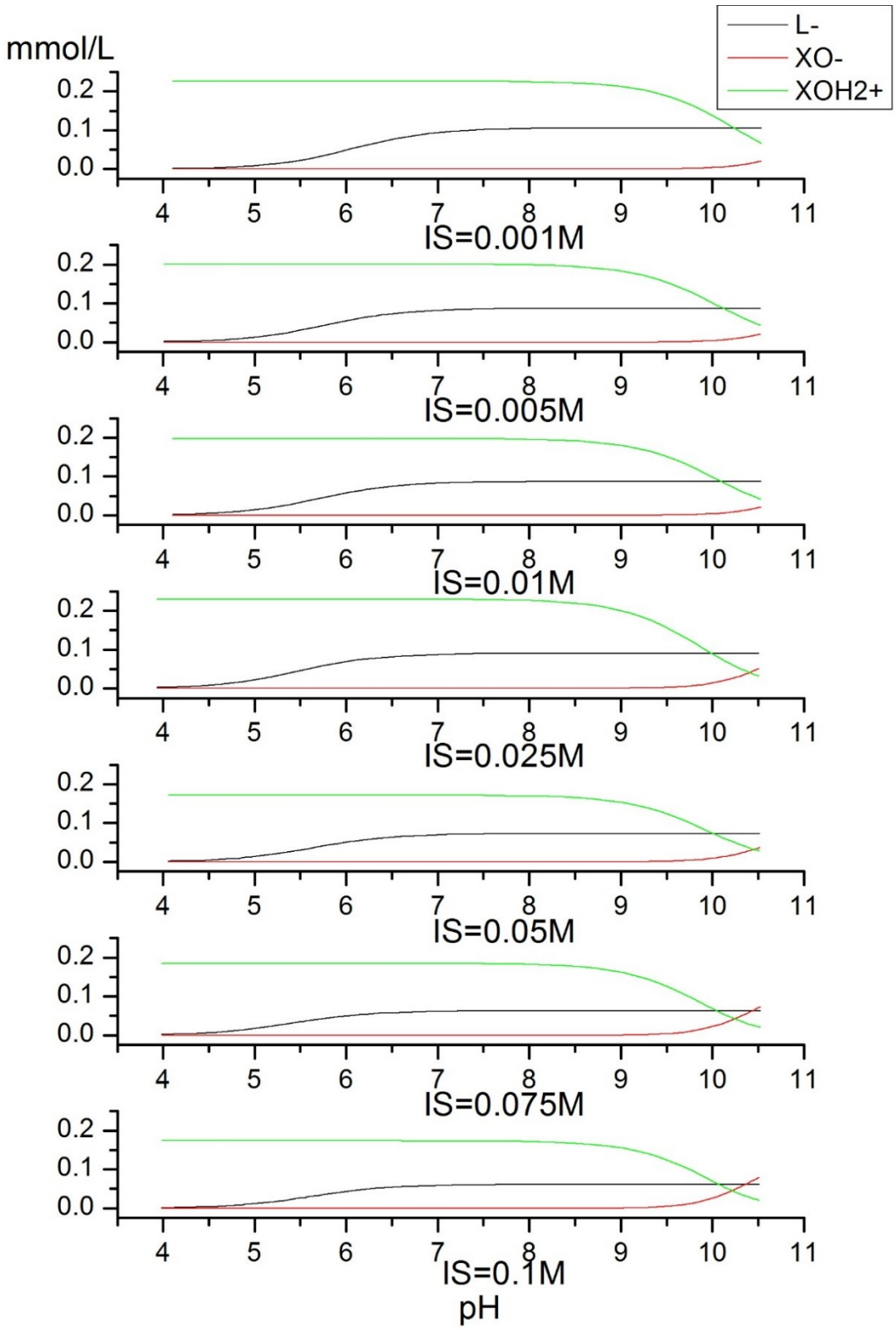

Figure 2.6 Speciation diagrams for montmorillonite surface sites at the seven IS values tested.

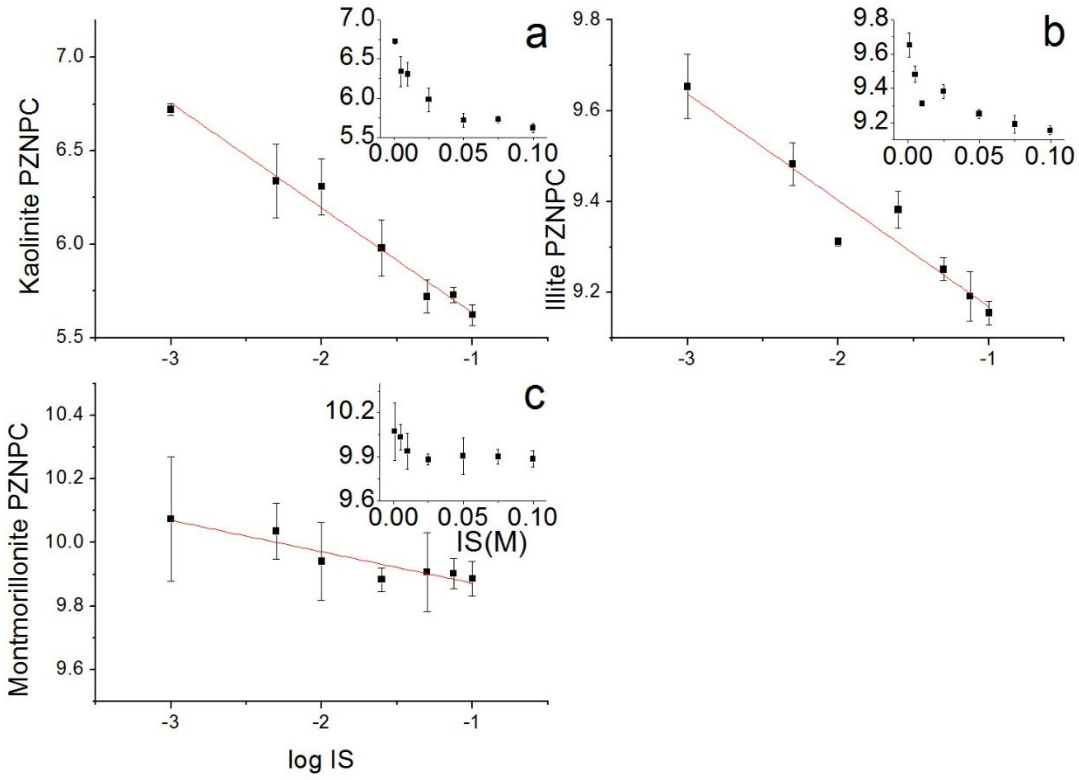

Figure 2.7 Changes in the PZNPC using the SCM method as a function of ionic strength (inset plots), and the logarithm of ionic strength, for (a) kaolinite, (b) illite and (c) montmorillonite.

Chapter 3. The impact of ionic strength on the proton reactivity of clay minerals[2]

3.1 Introduction

As ubiquitous components at Earth's surface, clay minerals play a crucial role in the adsorption of protons and trace metals from solution. Potentiometric titrations coupled with surface complexation modeling (SCM) have increasingly been used to determine clay surface reactivity and quantify proton and metal adsorption onto clay mineral surfaces (Sverjensky and Sahai, 1996; Schroth and Sposito, 1998; Arda et al., 2006; Hizal and Apak, 2006; Tertre et al., 2006; Gu and Evans, 2007, 2008; Liu et al., 2018; Hao et al., 2018). In short, these studies have demonstrated that clay minerals have high surface reactivities and a strong affinity for trace metal adsorption.

However, considerably less work has been directed at determining how variations in solution ionic strength (IS) affect clay surface reactivity and, in turn, impact trace metal adsorption. One such study, by Sinitsyn et al. (2000), investigated the acid-base properties of illite and the sorption of Nd and Eu at 0.01, 0.1, and 1 M ionic strength and demonstrated that the amount of Nd adsorbed was inversely related to IS. Bradbury and Baeyens (2002, 2009) subsequently applied a 2-site, non-electrostatic surface complexation and cation exchange model to describe the protonation, as well as Ni, Co, Eu, and Sn sorption edges, of Na-montmorillonite and illite over a wide range of pH and ionic strength conditions. Alternatively, Gu et al. (2008, 2010) applied a constant capacitance surface complexation model (CCM) to potentiometric titration and trace metal (Cd, Cu, Ni, Pb, and Zn) adsorption data for kaolinite and montmorillonite, and similarly demonstrated

[2] This chapter has been accepted by *Chemical Geology* as: Hao, W.; Flynn, S.L.; Kashiwabara, T.; Alam, M.S.; Bandara, S.; Swaren, L.; Robbins, L.J.; Alessi, D.S.; Konhauser, K.O.

that the amount of trace metal adsorbed decreases with increasing IS. Other studies have also shown that clay surface reactivity varies as a function of solution IS (Xu et al., 2008; El-Bayaa et al., 2009; Wu et al., 2011). The collective results of these earlier studies on the effects of solution IS on clay reactivity suggest that IS dependent changes can be explained in one of two ways: (1) the competitive adsorption of solution electrolytes (e.g., Na^+, Cl^-) with trace elements for adsorption to clay surface sites (McBride, 1989; Sahai and Sverjensky, 1997; Coppin et al., 2002; Bradl, 2004), or (2) the weakening of the clay mineral's surface electrostatic field, which, in turn, leads to a reduction in the capacity for trace metal adsorption (Kraepiel et al., 1998; Bohn et al., 2002). Distinguishing which of these two mechanisms is responsible for observed changes in clay mineral surface reactivity as a function of IS is, therefore, essential to understanding how trace metals interact with clay surfaces in environments where stark contrasts in environmental conditions may occur, such as the transition from riverine to estuarine systems.

In theory, the successful prediction of how IS impacts clay surface reactivity and metal adsorption can be evaluated using electrostatic surface complexation models. For example, the diffuse layer model (DLM) and triple layer model (TLM) both incorporate IS as an adjustable parameter for derivation of chemical equilibrium constants (K values) and site concentrations. Although the objective of those models is to derive "intrinsic" chemical equilibrium constants that are independent of solution IS, previous work has highlighted the difficulty in generating IS independent chemical equilibrium constants even when electrostatic models are used (Goldberg, 2005; Landry et al., 2009; Schaller et al., 2009; Reich et al., 2010). A non-electrostatic SCM approach cannot quantify the impact of IS, but it can generate apparent chemical equilibrium constants for metals and/or proton binding at the IS condition being considered. The shortcoming of IS-dependent K values could be alleviated by either developing more mechanistic electrostatic

models that properly parameterize the impact of IS or by establishing empirical relationships between IS and chemical equilibrium constants for incorporation into non-electrostatic models.

In this study, three common clay minerals (kaolinite, illite, and montmorillonite) were selected for potentiometric titration to evaluate the impact of IS on their surface reactivity. A non-electrostatic SCM approach was applied to potentiometric titration data to develop a basic framework that considers chemical equilibrium constants and solution IS. The SCM was complimented by metal adsorption experiments to distinguish whether solution electrolyte competition or an attenuation of the electric field strength accounts for the observed changes in clay surface reactivity resulting as a function of changes in solution IS. Unlike purely theoretical and structural models of clay chemistry, the purpose of this paper is to derive applicable knowledge on natural clay materials, and describe how clay surface properties change as a function of fluctuations in the aqueous environment, specifically in regard to changes in IS.

3.2 Background theory

Surface complexation models based on potentiometric titrations are practical for determining discrete proton exchanging surface ligands. Various models, including both non-electrostatic models (NEM) and electrostatic models (EM), offer a range of mathematical approaches and assumptions regarding electrostatic phenomena. Such models are, however, unified by the ultimate parameterization of chemical equilibrium constants (K values) for proton surface interactions and the concentrations of surface functional groups (site concentrations) (Lalonde et al., 2007; Alessi and Fein, 2010). In general, the adsorption process as described by SCM can be broken down into a system of equations:

$$\equiv XO^- + M^{n+} \leftrightarrow \equiv XO\text{-}(M)^{(n-1)+} \qquad \text{(R2.1)}$$

$$K = \frac{[\equiv XO-(M)^{(n-1)+}]}{[\equiv XO^{-}]\bullet\alpha_{M^{n+}}} \quad \text{(eq. 2.1)}$$

where $\equiv XO^-$ is the negatively charged surface functional group, M^{n+} is the metal cation or proton of interest, and K is the chemical equilibrium constant for the adsorption reaction. In this notation, the square brackets represent molar concentration and $\alpha_{M^{n+}}$ indicates the activity of an aqueous cation. The mass action equation of the NEM is represented by eq. 2.1, where the impact of the surface electric field and the IS of solution are not explicitly described. The derived K values from NEM are, therefore, "apparent" and may be represented by K_{app}. Conversely, an EM aims to generate "intrinsic" chemical equilibrium constants (K_{int}) that are independent of aqueous conditions during adsorption (e.g., IS and pH) by separating the electrostatic effect from K_{app} (Hao et al., 2018). In doing so, the Gibbs free energy of ion adsorption onto mineral surfaces is divided into two components: (i) the Gibbs free energy for the reaction of ions binding onto surface functional groups, and (ii) the Gibbs free energy for the work done to move ions from their initial position to the mineral surface(s) by the surface electrostatic field (Sverjensky and Sahai, 1996). With regard to K values, the relationship between EM and NEM, may be represented by the Gouy-Chapman model, where:

$$K_{app} = K_{int} * 10^{\frac{-\Delta Z * F * \Psi}{2.303 * R * T}} \quad \text{(eq. 2.2)}$$

where F is the Faraday constant, R is the ideal gas constant, T is temperature in Kelvin, and ΔZ is the change in surface charge. A detailed derivation of this equation is presented in Severjensky and Sahai (1996).

There are three kinds of EMs, each of which is based on different assumptions regarding the relationship between surface charge (δ) and the potential of the surface electric field (Ψ) (Davis and Kent, 1990). The constant capacitance model (CCM), based on Helmholz theory, assumes a constant electrostatic capacitance at clay surfaces, and that the electrostatic potential decreases

linearly with increasing distance away from surface. The DLM is designed according to the Gouy-Chapman theory and assumes that there is an accumulation of diffused ions at the surface and that the surface potential decreases exponentially with increasing distance from surface. Finally, the TLM is a combination of the CCM and DLM models. In the TLM, the electrostatic field is divided into three separate layers: two Helmholz layers, and one Gouy-Chapman layer that extends from the solid surface outwards to infinity (Hohl and Stumm, 1976; Davis et al., 1978; Dzombak and Morel, 1990; Kallay et al., 2006). Each of these three EMs is elaborated on in Section 5.4.

3.3 Methods

Automated titrations of kaolinite (KGa-2), illite (IMt-2), and montmorillonite (SWy-2) were performed at seven IS conditions, spanning two orders of magnitude, using a potentiometric titrator (Metrohm Titrando 905) at the University of Alberta. Sodium nitrate solutions (ACS certified, Fisher Scientific) of 0.001 M, 0.005 M, 0.01 M, 0.025 M, 0.05 M, 0.075 M, and 0.1 M were prepared and used as the background electrolyte in titrations, and each titration was performed in triplicate. Acids and bases (0.1 M HCl and 0.1 M NaOH) were used to adjust pH during each titration. Each of the three clay minerals used in titrations were sodium saturated, and therefore contain little surface-bound or interlayer calcium. The source and pretreatment of clay minerals, and specific experimental conditions are detailed in Hao et al. (2018), and the physical and chemical properties of each of the three clay minerals are provided in the Appendix 2 SI Table 2.1. Briefly, all clay minerals were washed in 0.1 M $NaNO_3$ solution for 3 h and freeze-dried before experiments. All titrations were conducted in sealed reaction vessels in which the electrolyte solutions were bubbled with $N_{2(g)}$ for 30 minutes prior to the initiation of titrations, to avoid contamination with atmospheric $CO_{2(g)}$. Size-fractionation experiments were also performed on

three clay minerals to make comparison with raw clay samples, and the experimental methods and results are provided in the Appendix 2 SI Table 2.6.

Surface complexation modeling was performed using the resultant data from 63 titration curves spanning the seven IS conditions. Surface functional groups for the clays were assigned to one of two types: ≡LH or ≡XOH, which represent a permanently charged (i.e. structural) surface functional group (one that can only deprotonate) and an amphoteric surface functional group (representing Si-O and Al-OH groups), respectively (Barbier et al., 2000; Peacock and Sherman, 2005; Gu et al., 2010). The protonation behaviors of the permanently charged and amphoteric sites are described as follows:

$$\equiv LH \leftrightarrow H^+ + \equiv L^- \quad \text{(R2.2)}$$

$$K_a = \frac{[\equiv L^-] \bullet \alpha_{H^+}}{[\equiv LH]} \quad \text{(eq. 2.3)}$$

$$\equiv XOH \leftrightarrow H^+ + \equiv XO^- \quad \text{(R2.3)}$$

$$K_{a-} = \frac{[\equiv XO^-] \bullet \alpha_{H^+}}{[\equiv XOH]} \quad \text{(eq. 2.4)}$$

$$\equiv XOH + H^+ \leftrightarrow \equiv XOH_2^+ \quad \text{(R2.4)}$$

$$K_{a+} = \frac{[\equiv XOH_2^+]}{[\equiv XOH] \bullet \alpha_{H^+}} \quad \text{(eq. 2.5)}$$

where, square brackets denote the concentration of surface functional groups and α_{H^+} the activity of protons in solution; K values derived by equations 3, 4 and 5 are proton interaction constants that govern the adsorption and desorption of protons from the clay surface. To examine the impact of changing IS on the surface electrostatic field, a NEM at each of the seven IS conditions was generated using the titration data and the modeling software FITEQL 4.0 (Westall, 1982) in order to calculate K_{app} for each of the three clay minerals at the given IS.

The range of IS conditions investigated spans two orders of magnitude, and the activity of aqueous species was accounted for in the SCM using the Debye-Huckel equation (eq. 2.6) through which activity coefficients (γ) were calculated. The corresponding activity for H^+ (α_{H+}) (eq. 2.7) was then used in the SCM (Langmuir, 1997).

$$\log \gamma = -Az_i^2\sqrt{I}/(1+Ba_i\sqrt{I}) \quad \text{(eq. 2.6)}$$

$$\alpha_{H+} = \gamma * [H^+] \quad \text{(eq. 2.7)}$$

where A and B are empirical constants that are a function of the density, dielectric constant, and temperature of water, z_i is the charge of the ion, a_i is a size parameter, I is the ionic strength, and $[H^+]$ is the molar concentration of protons (see Ref. Langmuir (1997) for a detailed description).

Anion adsorption experiments can be applied to test whether the impact of ionic strength on clay surface reactivity is due to a weakening surface electrostatic field or competitive adsorption. Here, we performed chromate, Cr(VI), adsorption experiments at 0.001 M and 0.1 M $NaNO_3$ for each of the three clay minerals to examine the impact of IS on Cr(VI) adsorption. A 0.001 M stock solution was made by first adding 0.017 g of $NaNO_3$ (ACS grade) to a 200 mL volumetric flask, and then 2 mL of a 2 mM Cr(VI) stock solution was added, followed by dilution with DI water to a final volume of 200 mL. The resulting solution contained 0.001 M $NaNO_3$ and 1 mg/kg Cr(VI). The 0.1 M IS solution was made in a similar manner, but 1.7 g of $NaNO_3$ was added. For adsorption experiments, 25 mL of each the above solution was mixed with 0.25 g of each clay to achieve a clay concentration of 10 g/L. The adsorption experiments were then allowed to equilibrate for 48 h and the pH of each tube was adjusted to pH 5 because a considerable amount of negatively-charged chromate (CrO_4^{2-}) would be adsorbed to the clays due to a lesser overall net-negative charge of the clays versus at higher pH values (Liu et al., 2018; Veselska et al., 2016). The pH was continuously adjusted through the addition of small aliquots of either 0.1 M HNO_3 and NaOH

(ACS grade) until a stable pH was achieved. Once equilibrium was reached, 5 mL of each solution was taken by pipet and filtered through a 0.2 μm membrane for measurement on an Agilent 8800 ICP-MS/MS at the Environmental Geochemistry Lab at the University of Alberta. All samples for ICP-MS analysis were diluted 50 times to avoid matrix effects. An internal standard of 1 mg/kg Indium was added to all samples and used to monitor instrumental drift during analysis. The standard deviation of ICP-MS measurement was less than 3%, as calculated by the triplicate analysis of each sample.

3.4 Results

3.4.1 Surface complexation modeling

Our modeling results are in excellent agreement with experimental results, validating of our modeling procedure (Appendix 2 SI Figures 2.1-2.4). K values for the surface reactions calculated through the SCM approach are listed in Tables 2.1, 2.2, and 2.3 for kaolinite, illite, and montmorillonite, respectively (details of the triplicates are provided in Appendix 2 SI Tables 2.2-2.4). For kaolinite, the $\log K_{a}$, $\log K_{a-}$ and $\log K_{a+}$ values vary from -9.6 to -10.6, -6.5 to -7.8, and 4.7 to 5.7, respectively, as IS increases. Compared to kaolinite, illite has higher $\log K_{a}$ and $\log K_{a+}$ values which range from -6.3 to -5.5, and 9.8 to 9.5, respectively, but a lower K_{a-} (-11.4 to -10.4) (Table 2.2). The $\log K_{a}$ and $\log K_{a-}$ of montmorillonite are similar to those of illite, but the $\log K_{a+}$ of montmorillonite is higher and ranges from 9.8 to 10.1. (Table 2.3). For all three clay minerals, the standard deviation is generally small compared to the K values. Illite and montmorillonite's proton reaction constants are very similar. In contrast, kaolinite's proton reaction constants differ from those of illite and montmorillonite's $\log K_{a}$, $\log K_{a-}$ and $\log K_{a+}$.

Previous studies have applied the cation exchange reaction ($\equiv LH+Na^{+}\leftrightarrow H^{+}+\equiv LNa$) for ≡LH sites (e.g. Gu and Evans, 2007, 2008). In this manuscript, the primary purpose is to investigate the impact of solution electrolyte on clay surface reactivity, that is, whether competitive adsorption or a weakening surface electrostatic field best explains sorption behavior. In previous studies the approach taken has led to competitive adsorption being assumed in the first place, without knowing if it is actually the case. Nonetheless, for the sake of comparison with previous data and to demonstrate our linear trend is robust, we provide modeling results applying cation exchange reaction as described above in the Appendix 2.

3.4.2 Proton interaction constants as a function of ionic strength

Our modeling results show an increase in $logK_a$ and $logK_{a-}$ but a decrease in $logK_{a+}$ with increasing IS for all three clay minerals. Figures 3.1, 3.2, and 3.3 show the empirical relationship between solution IS and the proton interaction constants for each of the three clay minerals. When plotted as a function of log(IS), a linear relationship with the $logK_{app}$ becomes apparent. The linear equations were fitted in Origin 9.1 and are defined as:

$$logK_{app}=m*log(IS)+b \qquad \text{(eq. 2.8)}$$

The specific values for m and b for each of the three clay minerals are provided in Table 2.4. The intercept of this equation (b) represents the presumed logK value of the clay at highly saline conditions (1 M) where log(IS)=0, while the slope (m) quantifies how the clay surface reactivity varies with ionic strength. Most of the proton interaction values are highly correlated with solution IS (Table 2.4), with the exception of the $logK_{a-}$ of illite (R^2= 0.3516), which may be the result of an anomalous point in the 0.01M titration. Additionally, montmorillonite has a higher variability

between triplicates than kaolinite or illite; this may be attributed to the swelling nature of montmorillonite.

3.4.3 Chromium adsorption onto three clay minerals

The results of Cr(VI) adsorption experiments are listed in Table 2.5. The amount of Cr adsorbed onto three clay minerals was generally low (< 1 mg/kg), likely the result of Cr(VI) being present as an oxyanion (CrO_4^{2-}) and, therefore, subject to a repulsive force at the negatively charged clay surfaces. At the low IS condition (0.001 M), kaolinite can adsorb more Cr(VI) compared to the high IS condition (0.1 M), while for montmorillonite and illite, the amount of Cr(VI) adsorbed at 0.1 M is higher than that at 0.001 M.

3.5 Discussion

3.5.1 The comparison of surface proton reactivity among clay minerals

Illite and montmorillonite have $\log K_{a+}$, $\log K_{a-}$ values between 9.5 to 9.8 and -10.4 to -11.4, respectively. This means that the illite and montmorillonite ≡XOH groups are largely protonated at neutral pH conditions, while the range of $\log K_a$ values from -6.3 to -5.5 indicates that the ≡LH groups may become either deprotonated or protonated at a pH near 6, as pH is increased or decreased, respectively. In contrast, kaolinite's $\log K_a$ values indicate that the ≡LH site is protonated until around pH 10, while the ≡XOH site can be protonated and deprotonated between pH 5 and 6.

The titration results for size-fractionation clay shows that the <2 μm clay fraction has lower $\log K_a$ values for montmorillonite and illite, but $\log K_{a-}$ and $\log K_{a+}$ values are nearly identical to those of the raw clay. Size fractionated kaolinite cannot be modeled with the current modeling

method, which can only be modeled through either one amphoteric site model or two sites deprotonation model. The decreasing in $\log K_a$ indicates that the < 2 μm clay fraction has stronger proton binding on the ≡LH site than does the bulk clay.

Previously published proton interaction constants for clay minerals vary significantly. For example, the $\log K_a$ value for the ≡XOH site of montmorillonite is -10.5 according to Bradbury and Baeyens (1997), while Barbier et al. (2000) derived a value of -5.26 for the same site. A detailed compilation of literature K values for clay adsorption sites is provided by Gu and Evans (2007, 2008) and Gu et al. (2010). Differences in values reported in the literature may be attributed to heterogeneity in natural samples that result in differing values between batches, additionally, varied modeling assumptions and experimental conditions likely also contribute to these differences. For example, some literature K values for the permanently charged site have modeled it as an ion exchange site ($\equiv LNa \leftrightarrow Na^+ + \equiv L^-$) (Lackovic et al., 2003; Ikhsan et al., 2005), which leads to K values that differ than those derived here. Moreover, EMs will have lower absolute logK values compared to NEMs, as EMs separate the electrostatic effect from the constant, while the logK derived from NEMs represents a combination of the chemical affinity and electrostatic effect. This may explain why our data has higher absolute values compared to the existing literature values. Other factors influencing the calculation of K values may include contamination by atmospheric $CO_{2(g)}$ during the titration process (see Hao et al. (2018)) as well as the method of clay pretreatment. In the latter case, work by Liu et al. (2018), using the same three clay minerals, resulted in lower absolute K values, but in this case the clays were pretreated with acid. The acid treatment increases the surface area of the clay particles by partially solubilizing Al and Si. The structural charge of the acidic treated clay increases due to the loss of octahedral and tetrahedral elements like Al and Si (Hao et al. 2019, in review).

3.5.2 The competitive adsorption of solution electrolytes

With increasing IS, both the K_a and K_{a-} values for each of the three studied clay minerals increase, while the K_{a+} value decreases (Figures 3.1-3.3). This pattern indicates a clear decrease in the proton binding ability at higher IS, as the requisite pH for ≡LH deprotonation and ≡XOH site deprotonation/protonation decreases with increasing IS. One possibility is that the change in K_{app} that accompanies increasing IS can be explained by the competitive adsorption of solution electrolytes onto the clay surface. To test this possibility, the Na^+ adsorption constant (K_{Na}) can be modeled. By incorporating K_{Na} into our SCM models at various IS titration data, IS-independent chemical equilibrium constants should be derived if the competitive adsorption of solution electrolytes is responsible for the observed trend.

To model K_{Na}, the clay minerals were titrated in ultrapure water with the same method used in the titration experiments and the same SCM approach for the calculation of K values was applied. This ultrapure titration data was then considered to represent the same system of equations without a Na^+ binding reaction being included (the pre-existing Na^+ concentration on the surface was analyzed; detailed information can be seen in Appendix 2 SI Figure 2.5). An iterative approach (see Alessi et al. (2010)) was applied to the titration data from the seven IS experiments for three clay minerals to calculate K_{Na}:

$$\equiv LH + Na^+ \leftrightarrow \equiv LNa + H^+ \quad \text{(R2.5)}$$

$$K_{LNa} = \frac{[\equiv LNa] \bullet \alpha_{H^+}}{[\equiv LH] \bullet \alpha_{Na^+}} \quad \text{(eq. 2.9)}$$

$$\equiv XOH + Na^+ \leftrightarrow \equiv XONa + H^+ \quad \text{(R2.6)}$$

$$K_{XONa} = \frac{[\equiv XONa] \bullet \alpha_{H^+}}{[\equiv XOH] \bullet \alpha_{Na^+}} \quad \text{(eq. 2.10)}$$

To be specific, the K values of surface protonation/deprotonation reactions in pure water titration were input into the SCM model for parameterizing $\log K_{LNa}$ and $\log K_{XONa}$ with the known initial Na^+ concentrations for each titration. The $\log K_{Na}$ values for each of the clay minerals are provided in Table 2.6. For all three clays, the $\log K_{XONa}$ values are exceedingly low (approaching -170), indicating that Na^+ binding on the amphoteric site is effectively negligible. The $\log K_{LNa}$ for kaolinite is lower than that of illite and montmorillonite, indicating that the Na^+ binding capacity of kaolinite is less than that of illite and montmorillonite. A plot of $\log K_{LNa}$ versus IS shows a relatively constant K_{LNa} across the range of IS conditions considered here (Figure 3.4).

Most SCM models of titration with K_{Na} incorporated fail to converge (detailed systematic equations are provided in the Appendix 2), indicating that the adsorption of Na^+ is unlikely to explain the change in K_{app} values for proton interactions observed with increasing IS. To further test the effect of competitive Na^+ adsorption, the corresponding binding constants were incorporated into a NEM for Cd adsorption onto clay minerals at varied IS using literature Cd adsorption data (Gu and Evans, 2007, 2008; Gu et al., 2010). The Cd adsorption model is detailed below, and the results summarized in Appendix 2 SI Table 2.5.

$$\equiv LH + Cd^{2+} \leftrightarrow \equiv LCd^{+} + H^{+} \quad \text{(R2.7)}$$

$$K_{LCd} = \frac{[\equiv LCd^{+}] \bullet \alpha_{H^{+}}}{[\equiv LH] \bullet \alpha_{Cd^{2+}}} \quad \text{(eq. 2.11)}$$

$$\equiv XOH + Cd^{2+} \leftrightarrow \equiv XOCd^{+} + H^{+} \quad \text{(R2.8)}$$

$$K_{XOCd} = \frac{[\equiv XOCd^{+}] \bullet \alpha_{H^{+}}}{[\equiv XOH] \bullet \alpha_{Cd^{2+}}} \quad \text{(eq. 2.12)}$$

After including Na^+ binding, the results still produce IS dependent values for both K_{LCd} and K_{XOCd} (Appendix 2 SI Table 2.5), where K_{LCd} shows a decreasing trend with increasing IS for all three clays, and K_{XOCd} increases with IS, except for kaolinite. This is consistent with previous research that has shown trace metals tend to adsorb primarily to permanently charged sites via

cation exchange at low IS condition, and mainly onto amphoteric sites at high IS condition (Morton et al., 2001). The exception of kaolinite may be attributed to its lower permanent charge (Sposito et al., 1999). The plot of K_{LCd} values versus log(IS) produces a linear relationship which is similar to the relationship observed between log(IS) and $logK_a$, $logK_{a+}$, $logK_{a-}$ (Figure 3.5), suggesting that, despite incorporating K_{Na} into our NEM, the SCM approach still fails to capture the inherent variability of K_{app} values as a function of IS.

Our results indicate that the sorption of monovalent electrolyte ions, such as Na^+, cannot account for the IS dependent nature of the K values for clay minerals as calculated by SCM. For inorganic clay surfaces, H^+ preferentially adsorbs, while other ions, such as K^+, Na^+, NO_3^-, and Cl^-, only weakly adsorb to the surface (Davis et al., 1978).

3.5.3 Attenuation of the surface electrostatic field by increasing ionic strength

The change in K_{app} with solution IS may also be attributed to the attenuation of the surface electrostatic field as IS increases. However, there is no direct method to quantify the surface electric field and only a theoretical estimation can be made. Sverjensky and Sahai (1996) demonstrated that K_{int} values for surface protonation reactions are solely influenced by the surface properties of the solid and the specific surface reaction. Therefore, for a surface reaction, K_{int} is independent of solution IS, while K_{app} shows a direct relationship with IS as indicated by our experimental results (eq. 2.8). The relationship between surface electric field and solution IS can be derived by substituting eq. 2.8 into eq. 2.2:

$$\Psi=\frac{2.303RT}{\Delta ZF}*(\log K_{int}-[m*\log(IS)+b]) \qquad \text{(eq. 2.13)}$$

where, m and b are the slope and intercept generated from our experimental results, respectively. By simplifying all the constants eq. 2.13 can be written as:

$$\Psi = N_1 - N_2[m*\log(IS)+b] \quad \text{(eq. 2.14)}$$

where, m, b, are the slope and intercept of eq. 2.8; N_1, N_2 are all constants, representing $\frac{2.303RT}{\Delta ZF}\log K_{int}$ and $\frac{2.303RT}{\Delta ZF}$, respectively. As is evident from eq. 2.14, surface potential is inversely related to the IS of the solution, indicating the electrostatic field becomes weaker at higher IS.

Negatively-charged clay surfaces promote cation adsorption and tend to limit the degree of anion adsorption. If attenuation of the surface electric field is the mechanism by which solution IS influences the adsorption process, an increase in IS will lead to a decrease in trace metal cation adsorption and a corresponding increase in trace anion adsorption. However, if the competitive adsorption of solution electrolytes is the mechanism, the result would be a decrease of both cation and anion adsorption as IS increases. The decrease in cation adsorption that accompanies an increase in IS has been well documented (Gu and Evans, 2007, 2008; Gu et al., 2010). A direct way to distinguish which of these two mechanisms is operative is to observe the anion adsorption behavior at different IS. To this end, we conducted Cr(VI) adsorption experiments onto the three clay minerals at different IS (Table 2.5). Results showed that for illite and montmorillonite, which have a higher structural charge (Sposito et al., 1999), the amount of CrO_4^{2-} adsorbed onto clay surfaces at IS=0.1 M is higher than that at IS=0.001 M. This is because the increased IS led to a weakening of the negative surface electric field, which subsequently promoted the increased adsorption of CrO_4^{2-}.

Interestingly, the above trend is not observed for kaolinite, probably because kaolinite has a lower structural charge compared to illite and montmorillonite (Sposito et al., 1999). In this regard, previous studies have shown that more B(III) (speciated as the ion borate, $B(OH)_4^-$, at neutral to alkaline pH) can adsorb onto montmorillonite at greater concentrations at high IS (Goldberg, 2005), while As(V), which forms the oxyanion arsenate (AsO_4^{3-}), shows higher affinity to soil

samples dominated by clay minerals at higher IS when pH is above 5 (Xu et al., 2009). An exception to this general trend, is U. At pH conditions below 6, the adsorption of U(VI) onto kaolinite and montmorillonite is inhibited by increasing IS, while the adsorption is enhanced at pH conditions above 6 (Bachmaf and Merkel, 2011). This occurs because at around pH 6, U(VI) aqueous species shift from the positive uranyl ion (UO_2^{2+}) to negative charged uranyl carbonate ion ($UO_2(CO_3)_3^{4-}$).

It should be noted that while electrostatic field effects influence the amount of metal/proton adsorption onto clay surfaces, there are other considerations. For instance, detailed molecular information regarding the formation of inner-sphere versus outer-sphere complexes can be accessed through spectroscopic methods and may provide useful information for predicting differences in the adsorptive behavior of trace metals at varied IS (Kashiwabara et al., 2011; Gu et al., 2016; Wang et al., 2018).

3.5.4 The inability of SCMs to produce an ionic strength independent proton interaction constant for clay minerals

The K_{app} derived from NEMs should have an IS dependent signature because K_{app} does not separate the electrostatic factor, and IS has been shown to be capable of influencing the surface electric field. The CCM incorporates an electrostatic term by assuming the surface electrical capacitance (C) is a constant at the mineral-water interface, where the relationship between plane charge (δ) and surface potential (Ψ) is defined as:

$$\Psi = \frac{\delta}{C} \qquad \text{(eq. 2.15)}$$

Since the CCM fails to consider the impact that varied IS may have, it is not surprising that the CCM derived K values display an IS dependent character (Gu and Evans, 2007, 2008; Gu et al.,

2010). The DLM assumes that the electrolyte ions diffuse around the mineral surface, and that the surface potential is related to the plane charge (δ), solution IS (I), and dielectric constant (ε):

$$\Psi=\frac{2RT}{F}*\text{arsinh}(-\delta/\sqrt{8RT\varepsilon IS}) \quad \text{(eq. 2.16)}$$

Finally, the TLM divides the electric field into three layers: the first two are CCM-type layers that have different capacitances, and the third is a diffuse layer. Both the DLM and TLM incorporate IS into the modeling procedure, and thus theoretically the K values derived from both models should display an IS independent character. Yet, previous experimental results and arguments contradict this notion (Goldberg, 2005; Landry et al., 2009; Schaller et al., 2009; Reich et al., 2010), which indicates that K values derived from both electrostatic models are not constant with varying ionic strength. In our titration modeling, CCM can successfully simulate experimental data, but produces IS dependent K values as well. Both DLM and TLM iterations fail to converge, indicating that when IS is included as an input parameter, these electrostatic models fail to provide a satisfactory fit for the observed proton interaction behavior.

The IS dependent results of EMs may be the result of our SCM approaches failing to properly account for the inherent structural charge of clay minerals. The surface charge calculation for titration data in the SCM methodology is based on the net surface protonation and deprotonation reactions. However, for clay minerals, surface charge includes both the charge produced by proton interactions and the inherent permanent charge imparted to the clay by isomorphic substitution. This permanent charge cannot be accounted for through SCM simulations when applying EMs. This is particularly true for three-layer clays, such as illite and montmorillonite, that have a tetrahedral-octahedral-tetrahedral sheet structure (TOT type clays) in which isomorphic substitution on the octahedral and tetrahedral sheets leads to the development of a permanent surface charge within the clay structure. Nonetheless, the shielding effect of solution electrolytes

with regards to the surface electrostatic field can be significant, especially when one considers the existence of a strong negative surface field at clay mineral surfaces as indicated by the zeta potential (Chorom and Rengasamy, 1995; Vane and Zang, 1997; Kaya and Yukselen, 2005). This defect in accurately simulating the permanent surface charge of clay minerals may be the reason why electrostatic SCMs are unable to generate IS independent K values for these surfaces. It is worth noting that this shielding effect may be assessed through running NEMs at different IS values. The linear relationship between log(IS) and the $\log K_{app}$ determined by NEMs thereby provides an alternative empirical way for assessing clay surface reactivity at various IS conditions and offers a simpler approach than the development of complicated electrostatic models.

3.6 Conclusions

Variations in solution IS lead to changes in the derived K_{app} values for the clay minerals, kaolinite, illite, and montmorillonite. The relationship between K_{app} and IS was found to have a linear correlation when plotted in log-log space, and indicates that there is a decrease in the proton adsorption ability of clay minerals with increasing IS. A detailed discussion of our experimental data reveals that the mechanism underlying the impact of changing IS on adsorptive process at the clay mineral surface is the attenuation of the surface electrostatic field. To this end, an empirical equation relating surface potential and environmental IS was derived that potentially can be used to better model and predict the contribution of clay minerals to trace element sequestration in environments with dynamic, changing IS conditions. Indeed, understanding the influence that IS has on the adsorption of trace metals to clay surfaces is an underexplored aspect of interpreting the geological past, such as the record of trace metal availability through time as recorded by the shale record. Shales have been used to track changes in paleomarine chemistry based on a first-order

relationship that exists between trace metal concentrations in shale and in seawater from which they were deposited (Tribovillard et al., 2006; Scott et al., 2008; Lyons et al., 2009; Scott et al., 2013; Partin et al., 2013; Reinhard et al., 2013; Reinhard et al., 2017). Natural environments, however, such as estuaries are subject to strong changes in the IS. It is possible that when low IS rivers transport clay minerals sourced from the continents into the high IS ocean, the increase in environmental IS could lead to the release of cations that were adsorbed onto the surface of clay minerals, while at the same time promoting an increase in the adsorption and removal of anions. There is of course a caveat to this simplifying statement because metal behavior in estuaries is influenced by several factors that may include, but are by no means limited to, competitive adsorption, co-precipitation, and the prevailing redox conditions, the variation of clay surface reactivity may also be a significant factor that requires further evaluation. In this regard, future work is needed to assess the trace metal behavior, for both cations and anions, in an estuarine environment to better understand how changes in environmental IS may affect the interpretation of the shale record.

3.7 References

Alessi, D.S., Fein, J.B., 2010. Cadmium adsorption to mixtures of soil components: Testing the component additivity approach. Chemical Geology, 270: 186-195.

Alessi, D.S., Henderson, J.M., Fein, J.B., 2010. Experimental Measurement of Monovalent Cation Adsorption onto Bacillus subtilis Cells. Geomicrobiology Journal, 27: 464-472.

Arda, D., Hizal, J., Apak, R., 2006. Surface complexation modelling of uranyl adsorption onto kaolinite based clay minerals using FITEQL 3.2. Radiochimica Acta, 94: 835- 844.

Bachmaf, S., Merkel, B.J., 2011. Sorption of uranium(VI) at the clay mineral-water interface.

Environmental Earth Science, 63: 925-934.

Baeyens, B., Bradbury, M.H., 1997. A mechanistic description of Ni and Zn sorption on Na-montmorillonite .1. Titration and sorption measurements. Journal of Contaminant Hydrology, 27: 199-222.

Barbier, F., Duc, G., Petit-Ramel, M., 2000. Adsorption of lead and cadmium ions from aqueous solution to the montmorillonite/water interface. Colloids and Surfaces A, 166: 153-159.

Bohn, H.L., Myer, R.A., O'Connor, G.A., 2002. Soil chemistry. John Wiley & Sons.

Bradbury, M.H., Baeyens, B., 2002. Sorption of Eu on Na- and Ca-montmorillonites: Experimental investigations and modelling with cation exchange and surface complexation. Geochimica Cosmochimica Acta, 66: 2325-2334.

Bradbury, M.H., Baeyens, B., 2009. Sorption modelling on illite Part I: Titration measurements and the sorption of Ni, Co, Eu and Sn. Geochimica Cosmochimica Acta, 73: 990-1003.

Bradl, H.B., 2004. Adsorption of heavy metal ions on soils and soils constituents. Journal of Colloid and Interface Science, 277: 1-18.

Chorom, M., Rengasamy, P., 1995. Dispersion and zeta potential of pure clays as related to net particle charge under varying pH, electrolyte concentration and cation type. European Journal of Soil Science, 46: 657-665.

Coppin, F., Berger, G., Bauer, A., Castet, S., Loubet, M., 2002. Sorption of lanthanides on smectite and kaolinite. Chemical Geology, 182: 57-68.

Davis, J.A., James, R.O., Leckie, J.O., 1978. Surface ionization and complexation at the oxide/water interface: I. Computation of electrical double layer properties in simple electrolytes. Journal of Colloid and Interface Science, 63: 480-499.

Davis, J.A., Kent, D.B., 1990. Surface complexation modeling in aqueous geochemistry. Reviews

Mineralogy and Geochemistry, 23: 177-260.

Dzombak, D.A., Morel, F.M., 1990. Surface complexation modeling: hydrous ferric oxide. John Wiley & Sons.

El-Bayaa, A.A., Badawy, N.A., AlKhalik, E.A., 2009. Effect of ionic strength on the adsorption of copper and chromium ions by vermiculite pure clay mineral. Journal of Hazardous Materials, 170: 1204-1209.

Goldberg, S., 2005. Inconsistency in the triple layer model description of ionic strength dependent boron adsorption. Journal of Colloid and Interface Science, 285: 509-517.

Gu, C., Wang, Z., Kubicki, J.D., Wang, X., Zhu, M., 2016. X-ray adsorption spectroscopic quantification and speciation modeling of sulfate adsorption on ferrihydrite surfaces. Environmental Science and Technology, 50: 8067-8076.

Gu, X., Evans, L.J., 2007. Modelling the adsorption of Cd(II), Cu(II), Ni(II), Pb(II), and Zn(II) onto Fithian illite. Journal of Colloid and Interface Science, 307: 317-325.

Gu, X., Evans, L.J., 2008. Surface complexation modelling of Cd(II), Cu(II), Ni(II), Pb(II) and Zn(II) adsorption onto kaolinite. Geochimica Cosmochimica Acta, 72: 267-276.

Gu, X., Evans, L.J., Barabash, S.J., 2010. Modeling the adsorption of Cd (II), Cu (II), Ni (II), Pb (II) and Zn (II) onto montmorillonite. Geochimica Cosmochimica Acta, 74: 5718-5728.

Hao, W., Pudasainee, D., Gupta, R., Kashiwabara, T., Alessi, D.S., Konhauser, K.O. Effect of acidic conditions on surface properties and metal binding capacity of clay minerals. ACS Earth and Space Chemistry, in review.

Hao, W., Flynn, S.L., Alessi, D.S., Konhauser, K.O., 2018. Change of the point of zero net proton charge (pHPZNPC) of clay minerals with ionic strength. Chemical Geology, 493: 458-467.

Hizal, J., Apak, R., 2006. Modeling of copper(II) and lead(II) adsorption on kaolinite-based clay

minerals individually and in the presence of humic acid. Journal of Colloid and Interface Science, 295: 1-13.

Hohl, H., Stumm, W., 1976. Interaction of Pb2+ with hydrous γ-Al2O3. Journal of Colloid and Interface Science, 55: 281-288.

Ikhsan, J., Wells, J.D., Johnson, B.B., Angove, M.J., 2005. Surface complexation modeling of the sorption of Zn(II) by montmorillonite. Colloids and Surfaces A, 252: 33-41.

Kallay, N., Kovačević, D., Žalac, S., 2006. Chapter 6 - Thermodynamics of the solid/liquid interface - its application to adsorption and colloid stability, in: Johannes, L. (Ed.), Interface Science and Technology. Elsevier, pp. 133-170.

Kashiwabara, T., Takahashi, Y., Tanimizu, M., Usui, A., 2011. Molecular-scale mechanisms of distribution and isotopic fractionation of molybdenum between seawater and ferromanganese oxides. Geochimica Cosmochimica Acta, 75: 5762-5784.

Kaya, A., Yukselen, Y., 2005. Zeta potential of clay minerals and quartz contaminated by heavy metals. Canadian Geotechnical Journal, 42: 1280-1289.

Kraepiel, A.M.L., Keller, K., Morel, F.M.M., 1998. On the acid-base chemistry of permanently charged minerals. Environmental Science and Technology, 32: 2829-2838.

Lackovic, K., Angove, M.J., Wells, J.D., Johnson, B.B., 2003. Modeling the adsorption of Cd(II) onto Muloorina illite and related clay minerals. Journal of Colloid and Interface Science, 257: 31-40.

Lalonde, S.V., Amskold, L.A., Warren, L.A., Konhauser, K.O., 2007. Surface chemical reactivity and metal adsorptive properties of natural cyanobacterial mats from an alkaline hydrothermal spring, Yellostone National Park. Chemical Geology, 243: 36-52.

Landry, C.J., Koretsky, C.M., Lund, T.J., Schaller, M., Das, S., 2009. Surface complexation

modeling of Co(II) adsorption on mixtures of hydrous ferric oxide, quartz and kaolinite. Geochimica Cosmochimica Acta, 73: 3723-3737.

Langmuir, D., 1997. Aqueous Environmental Geochemistry. Prentice-Hall, Inc.

Liu, Y., Alessi, D.S., Flynn, S.L., Alam, M.S., Hao, W., Gingras, M., Zhao, H., Konhauser, K.O., 2018. Acid-base properties of kaolinite, montmorillonite and illite at marine ionic strength. Chemical Geology, 483: 191-200.

Lyons, T.W., Anbar, A.D., Severmann, S., Scott, C., Gill, B.C., 2009. Tracking euxinia in the ancient ocean: a multiproxy perspective and Proterozoic case study. Annual Review of Earth and Planetary Sciences, 37: 507-534.

McBride, M., 1989. Reactions controlling heavy metal solubility in soils, Advances in soil science. Springer, pp. 1-56.

Morton, J.D., Semrau, J.D., Hayes, K.F., 2001. An X-ray absorption spectroscopy study of the structure and reversibility of copper adsorbed to montmorillonite clay. Geochimica Cosmochimica Acta, 65: 2709-2722.

Partin, C.A., Bekker, A., Planavsky, N.J., Scott, C.T., Gill, B.C., Li, C., Podkovyrov, V., Maslov, A., Konhauser, K.O., Lalonde, S.V., Love, G.D., Poulton, S.W., Lyons, T.W., 2013. Large-scale fluctuations in Precambrian atmospheric and oceanic oxygen levels from the record of U in shales. Earth and Planetary Science Letters, 369-370: 284-293.

Peacock, C.L., Sherman, D.M., 2005. Surface complexation model for multisite adsorption of copper(II) onto kaolinite. Geochimica Cosmochimica Acta, 69: 3733-3745.

Reich, T.J., Das, S., Koretsky, C.M., Lund, T.J., Landry, C.J., 2010. Surface complexation modeling of Pb(II) adsorption on mixtures of hydrous ferric oxide, quartz and kaolinite. Chemical Geology, 275: 262-271.

Reinhard, C.T., Planavsky, N.J., Gill, B.C., Ozaki, K., Robbins, L.J., Lyons, T.W., Fischer, W.W., Wang, C.J., Cole, D.B., Konhauser, K.O., 2017. Evolution of the global phosphorus cycle. Nature, 541: 386-389.

Reinhard, C.T., Planavsky, N.J., Robbins, L.J., Partin, C.A., Gill, B.C., Lalonde, S.V., Bekker, A., Konhauser, K.O., Lyons, T.W., 2013. Proterozoic ocean redox and biogeochemical stasis. Proceedings of the National Academy of Sciences, 110: 5357-5362.

Sahai, N., Sverjensky, D.A., 1997. Solvation and electrostatic model for specific electrolyte adsorption. Geochimica Cosmochimica Acta, 61: 2827-2848.

Schaller, M.S., Koretsky, C.M., Lund, T.J., Landry, C.J., 2009. Surface complexation modeling of Cd(II) adsorption on mixtures of hydrous ferric oxide, quartz and kaolinite. Journal of Colloid and Interface Science, 339: 302-309.

Schroth, B.K., Sposito, G., 1998. Effect of landfill leachate organic acids on trace metal adsorption by kaolinite. Environmental Science and Technology, 32: 1404-1408.

Scott, C., Lyons, T., Bekker, A., Shen, Y.-a., Poulton, S., Chu, X.-l., Anbar, A., 2008. Tracing the stepwise oxygenation of the Proterozoic ocean. Nature, 452: 456.

Scott, C., Planavsky, N.J., Dupont, C.L., Kendall, B., Gill, B.C., Robbins, L.J., Husband, K.F., Arnold, G.L., Wing, B.A., Poulton, S.W., 2013. Bioavailability of zinc in marine systems through time. Nature Geoscience, 6: 125-128.

Sinitsyn, V.A., Aja, S.U., Kulik, D.A., Wood, S.A., 2000. Acid-base surface chemistry and sorption of some lanthanides on K+-saturated marblehead illite: I. Results of an experimental investigation. Geochimica Cosmochimica Acta, 64: 185-194.

Sposito, G., Skipper, N.T., Sutton, R., Park, S.-h., Soper, A.K., Greathouse, J.A., 1999. Surface geochemistry of the clay minerals. Proceedings of the National Academy of Sciences, 96:

3358-3364.

Sverjensky, D.A., Sahai, N., 1996. Theoretical prediction of single-site surface-protonation equilibrium constants for oxides and silicates in water. Geochimica Cosmochimica Acta, 60: 3773-3797.

Tertre, E., Castet, S., Berger, G., Loubet, M., Giffaut, E., 2006. Surface chemistry of kaolinite and Na-montmorillonite in aqueous electrolyte solutions at 25 and 60°C: Experimental and modeling study. Geochimica Cosmochimica Acta, 70: 4579-4599.

Tribovillard, N., Algeo, T.J., Lyons, T., Riboulleau, A., 2006. Trace metals as paleoredox and paleoproductivity proxies: An update. Chemical Geology, 232: 12-32.

Vane, L.M., Zang, G.M., 1997. Effect of aqueous phase properties on clay particle zeta potential and electro-osmotic permeability: Implications for electro-kinetic soil remediation processes. Journal of Hazardous Materials, 55: 1-22.

Veselska, V., Fajgar, R., Cihalova, S. Bolanz, R., Gottlicher, J. Steininger, R., Siddique, J., Komarek, M., 2016. Chromate adsorption on selected soil minerals: Surface complexation modeling coupled with spectroscopic investigation. Journal of Hazardous Materials, 318: 433-442.

Wang, X., Wang, Z., Peak, D., Tang, Y., Feng, X., Zhu, M., 2018. Quantification of coexisting inner- and outer-sphere complexation of sulfate on hematite surfaces. ACS Earth and Space Chemistry, 2: 387-398.

Westall, J.C., 1982. FITEQL: A computer program for determination of chemical equilibrium constants form experimental data. Department of chemistry. In: Oregon State University.

Wu, X.L., Zhao, D., Yang, S.T., 2011. Impact of solution chemistry conditions on the sorption behavior of Cu(II) on Lin'an montmorillonite. Desalination, 269: 84-91.

Xu, D., Zhou, X., Wang, X., 2008. Adsorption and desorption of Ni2+ on Na-montmorillonite: Effect of pH, ionic strength, fulvic acid, humic acid and addition sequences. Applied Clay Science, 39: 133-141.

Xu, R., Wang, Y., Tiwari, D., Wang, H., 2009. Effect of ionic strength on adsorption of As(III) and As(V) on variable charge soils. Journal of Environmental Sciences, 21: 927-932.

Table 3.1: Results of surface complexation modeling summary for kaolinite

IS	0.001	0.005	0.01	0.025	0.05	0.075	0.1
Log(IS)	-3	-2.301	-2	-1.602	-1.301	-1.125	-1
$LogK_a$	-10.584	-9.785	-10.026	-9.622	-9.299	-9.495	-9.625
STD	0.168	0.699	0.133	0.447	0.556	0.263	0.227
$LogK_{a-}$	-7.765	-7.176	-7.274	-6.785	-6.515	-6.552	-6.539
STD	0.030	0.462	0.266	0.334	0.199	0.242	0.132
$LogK_{a+}$	5.682	5.385	5.346	5.179	4.933	4.877	4.707
STD	0.036	0.139	0.048	0.067	0.197	0.118	0.020

Note: STD means standard deviation, IS means ionic strength.

Table 3.2: Results of surface complexation modeling summary for illite

IS	0.001	0.005	0.01	0.025	0.05	0.075	0.1
Log(IS)	-3	-2.301	-2	-1.602	-1.301	-1.125	-1
$LogK_{a}$	-6.288	-5.995	-5.917	-5.793	-5.670	-5.556	-5.488
STD	0.017	0.053	0.055	0.029	0.045	0.062	0.148
$LogK_{a-}$	-11.419	-11.118	-10.119	-11.166	-10.611	-10.671	-10.408
STD	0.401	0.452	0.038	0.130	0.312	0.146	0.388
$LogK_{a+}$	9.825	9.715	9.734	9.629	9.554	9.473	9.579
STD	0.034	0.075	0.008	0.022	0.077	0.033	0.103

Table 3.3: Results of surface complexation modeling summary for montmorillonite

IS	0.001	0.005	0.01	0.025	0.05	0.075	0.1
Log(IS)	-3	-2.301	-2	-1.602	-1.301	-1.125	-1
$LogK_a$	-5.997	-5.759	-5.661	-5.560	-5.567	-5.478	-5.699
STD	0.062	0.051	0.041	0.061	0.062	0.054	0.131
$LogK_{a-}$	-11.126	-10.990	-10.850	-10.884	-10.818	-10.715	-10.566
STD	0.643	0.341	0.488	0.146	0.143	0.283	0.149
$LogK_{a+}$	10.133	10.060	9.988	9.875	9.871	9.858	9.833
STD	0.094	0.036	0.050	0.041	0.141	0.017	0.153

Table 3.4: Mathematical relationship between K values and ionic strength (IS).

		m	b	R^2
Kaolinite	$logK_a$	0.485	-8.944	0.675
	$logK_{a-}$	0.631	-5.842	0.928
	$logK_{a+}$	-0.471	4.325	0.953
Illite	$logK_a$	0.384	-5.139	0.990
	$logK_{a-}$	0.382	-10.120	0.352
	$logK_{a+}$	-0.157	9.368	0.868
Montmorillonite	$logK_a$	0.199	-5.324	0.698
	$logK_{a-}$	0.235	-10.440	0.869
	$logK_{a+}$	-0.158	9.667	0.960

Note: m and b are slope and intercept, respectively, of the linear relationship between proton interaction constants and IS (in eq. 2.7), and R^2 is the correlation coefficient of the linear relationship.

Table 3.5: Degree of chromium adsorption onto three clay minerals at two IS conditions

		Adsorbed (mg/kg)	STD
Kaolinite	IS=0.001 M	0.403	0.016
	IS=0.1 M	0.247	0.018
Montmorillonite	IS=0.001 M	0.190	0.011
	IS=0.1 M	0.206	0.015
Illite	IS=0.001 M	0.084	0.005
	IS=0.1 M	0.152	0.012

Table 3.6: Na^+ binding constants on the two surface functional groups of the three clay minerals

Kaolinite					
Log(IS)	IS	$logK_{LNa}$	STD	$logK_{XONa}$	STD
-3	0.001	-6.981	0.231	-169	0
-2.301	0.005	-8.410	0.106	-3.237	0.413
-2	0.01	-7.606	0.114	-170	0
-1.602	0.025	-8.125	0.018	-170	0
-1.301	0.05	-8.587	0.263	-59.071	96.934
-1.125	0.075	-8.062	0.110	-115.222	96.610
-1	0.1	-8.266	0.040	-171	0
Illite					
Log(IS)	IS	$logK_{LNa}$	STD	$logK_{XONa}$	STD
-3	0.001	-3.362	0.360	-169	0
-2.301	0.005	-3.635	0.258	-170	0
-2	0.01	-3.256	0.104	-170	0
-1.602	0.025	-3.398	0.124	-171	0
-1.301	0.05	-3.559	0.060	-171	0
-1.125	0.075	-3.570	0.087	-171	0
-1	0.1	-3.355	0.119	-170.965	0.061
Montmorillonite					
Log(IS)	IS	$logK_{LNa}$	STD	$logK_{XONa}$	STD
-3	0.001	-3.111	0.424	-8.144	1.244

-2.301	0.005	-3.355	0.955	-8.885	0.003
-2	0.01	-3.201	0.511	-8.709	0.430
-1.602	0.025	-3.263	0.612	-9.234	0.454
-1.301	0.05	-3.322	0.518	-9.388	0.231
-1.125	0.075	-3.032	0.351	-9.529	0.177
-1	0.1	-2.959	0.852	-9.476	0.337

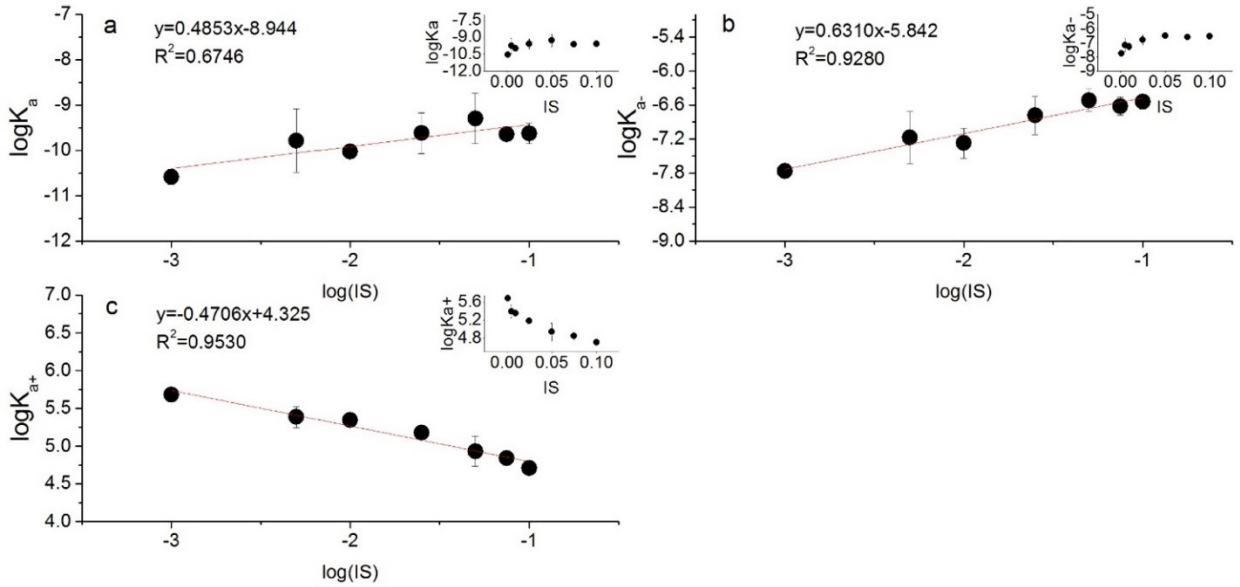

Figure 3.1 Proton interaction constants of kaolinite and their relationship with ionic strength. (a) $logK_a$ change with solution IS; (b) $logK_{a-}$ variation with solution IS; and (c) the relationship between $logK_{a+}$ and solution IS.

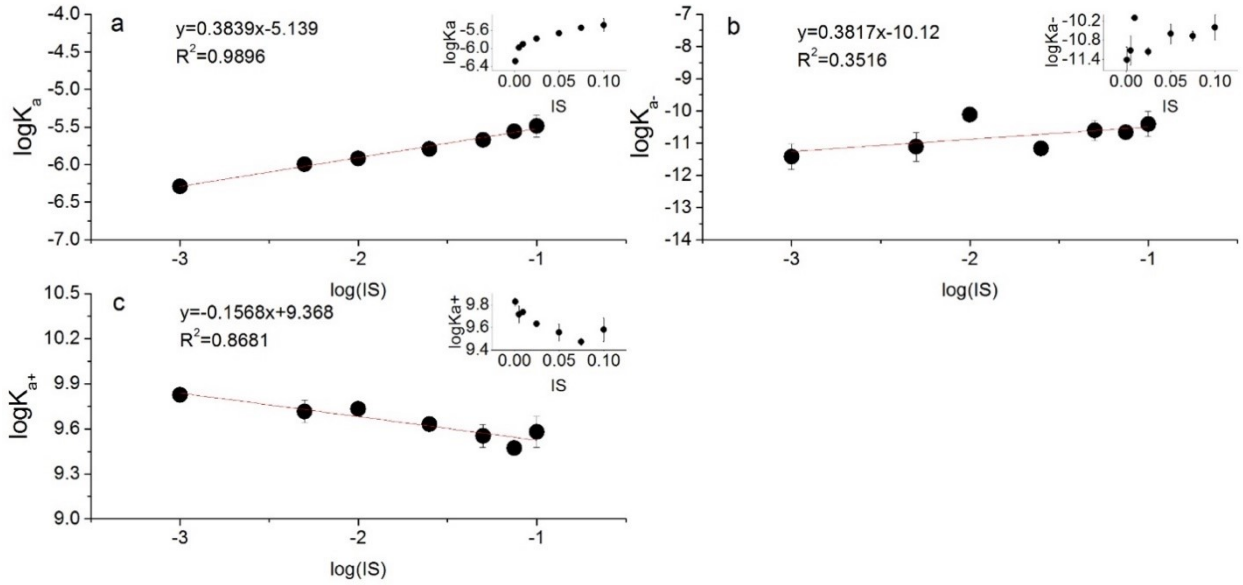

Figure 3.2 Proton interaction constants of illite and their relationship with ionic strength. (a) $logK_a$ change with solution IS; (b) $logK_{a-}$ variation with solution IS; and (c) the relationship between $logK_{a+}$ and solution IS.

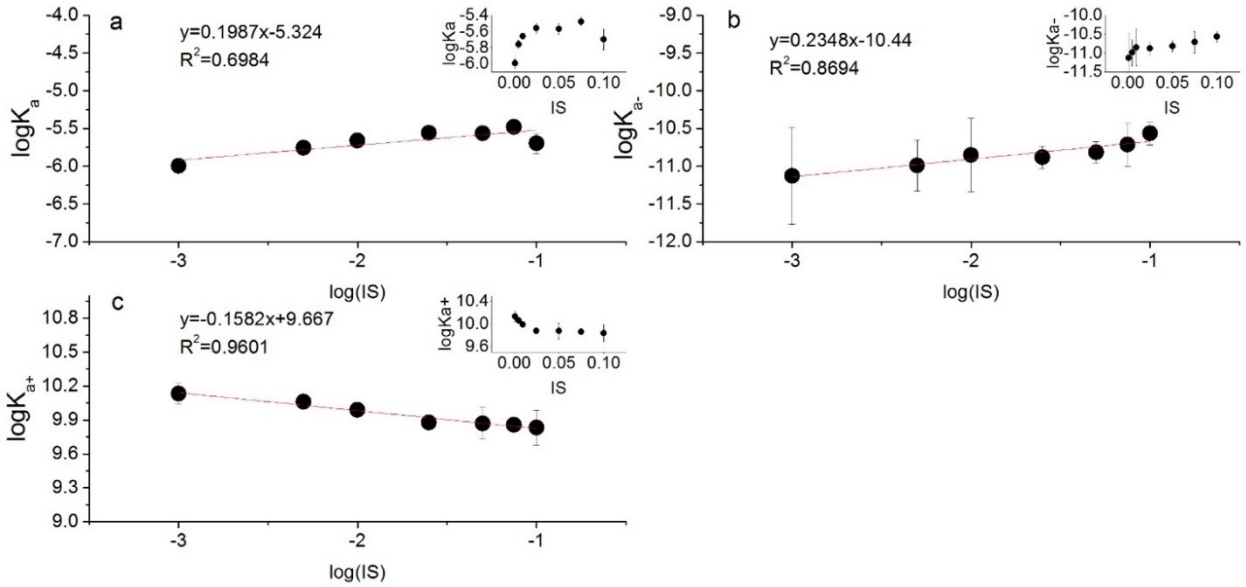

Figure 3.3 Proton interaction constants of montmorillonite and their relationship with ionic strength. (a) $logK_a$ change with solution IS; (b) $logK_{a-}$ variation with solution IS; and (c) the relationship between $logK_{a+}$ and solution IS.

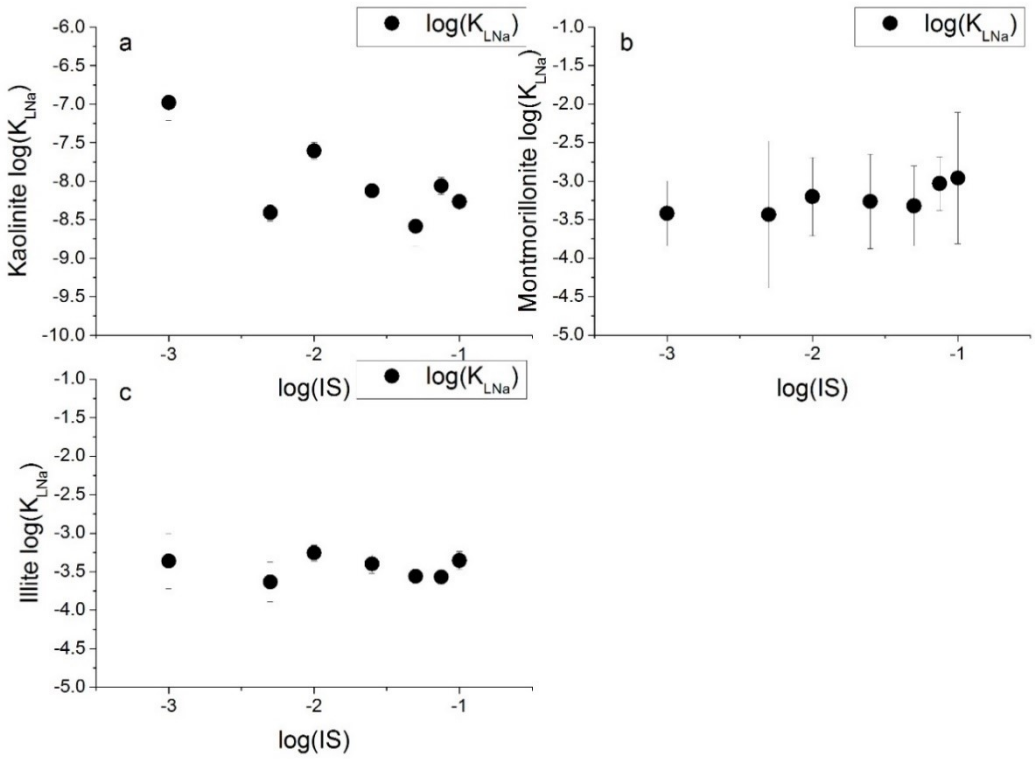

Figure 3.4 The change in the Na^+ binding constant ($logK_a$) with changing IS for all three clay minerals: (a) kaolinite; (b) montmorillonite and (c) illite.

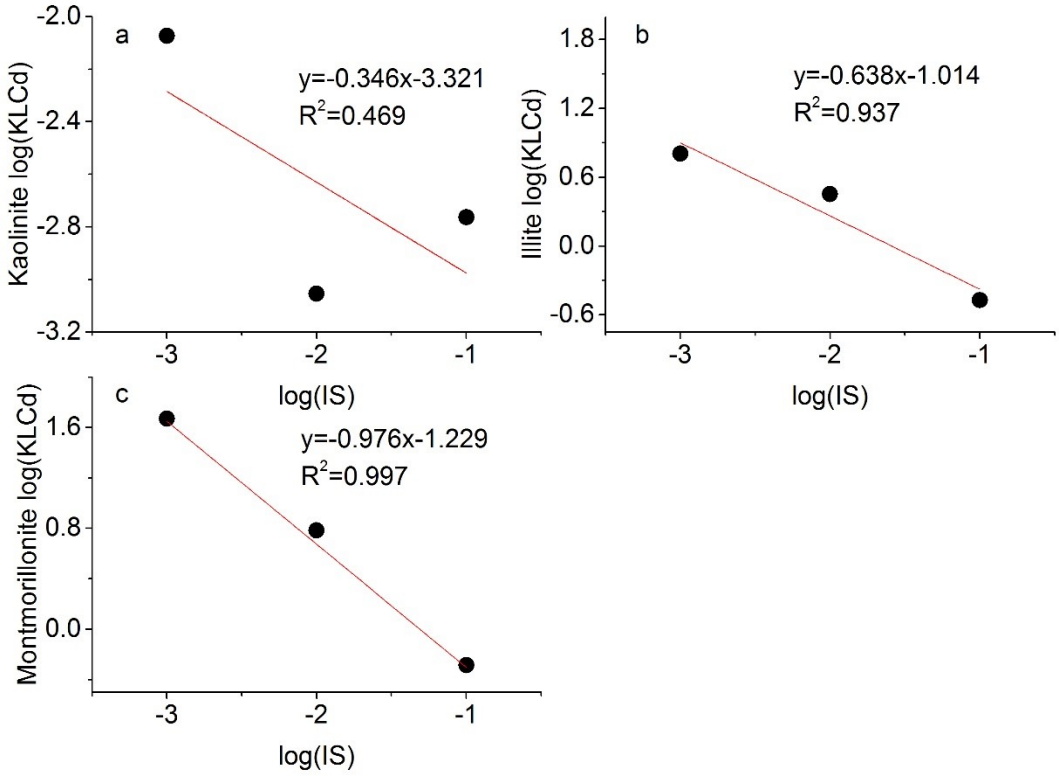

Figure 3.5 Change in the Cd binding constant ($logK_{LCd}$) of the permanently charged site ($logK_{LCd}$) with IS for three clay minerals: (a) kaolinite; (b) illite; and (c) montmorillonite.

Chapter 4. Effect of acidic conditions on surface properties and metal binding capacity of clay minerals[3]

4.1 Introduction

Clay minerals are layered aluminosilicates that are ubiquitous in soils and sediments, making them an important component of ancient sedimentary rocks (Griffin et al., 1968; Sposito et al., 1999; Gingele et al., 2001). The fine-grain size of clay minerals enables them high chemical reactivity, and as a consequence, they exert a considerable impact on global trace element cycling (Manning and Goldberg, 1997; Konhauser et al., 1998; Yariv and Cross, 2002; Bergaya and Lagaly, 2006; Bhattacharyya and Sen Gupta, 2006; Sen and Ling, 2009; Wang et al., 2010; Bachmaf and Merkel, 2011; Ghayaza et al., 2011; Ozdes et al., 2011; Sdiri et al., 2012; Anna et al., 2015; Veselská et al., 2016; Hao et al., 2018). However, one aspect of clay reactivity that has received less attention is changes in the surface reactivity during variations in solution pH. For instance, at local or regional scales the environment can receive significant acid input, as might be expected from metal and coal mine abandonment (e.g., acid mine drainage) or acidic rain caused by industrial activities.

Solution pH influences the protonation behavior of adsorbents and the aqueous speciation of trace elements (Zhao et al., 2011; Yang et al., 2015; Yang et al., 2018; Hao et al., 2019; Qin et al., 2019). However, in highly acidic environments, clay minerals undergo partial dissolution, during which structural elements such as Si and Al leach into solution (Huertas et al., 1998; Bibi et al., 2011; Khawmee et al., 2013; Bibi et al., 2014). The loss of structural elements changes the surface properties of clay minerals, leading to, for example, variations in crystal structure, morphology

[3] This chapter has been accepted by *ACS Earth and Space Chemistry* as: Hao, W.; Pudasainee, D.; Gupta, R.; Kashiwabara, T.; Alessi, D.S.; Konhauser, K.O.

and the surface electrostatic field, and thus may influence their metal binding capacity. Indeed, clay acidification has been widely used in industrial applications, for example the removal of dyes, trace metals and catalyst of chemical synthesis (Adams et al., 1982; Chitnis and Mohan Sharma, 1997; Vaccari, 1999; Espantaleon et al., 2003; Bhattacharyya and Gupta, 2008b).

Although clay minerals are widely reported to undergo acidic leaching (Johnson and Hallberg, 2005; Agboola et al., 2017; Peng et al., 2017a), it is still not clear to what extent clay surface reactivity can be modified through this process. Moreover, previous studies focused on the pH impact on metal adsorption onto clay minerals, (Schroth and Sposito, 1998; Lackovic et al., 2003; Gu and Evans, 2007; Gu and Evans, 2008; Gu et al., 2010; Liu et al., 2018) but there are few studies that have focused on acidification and the structural changes to the clay minerals reactivity. In this regard, our work aimed to assess the surface properties and metal binding capacity of three common clay minerals (kaolinite, illite and montmorillonite) under acid-washed (hereafter named as "acid-treated clay") and neutral washed (hereafter named as "neutral clay") conditions to mimic conditions that clay minerals experience when exposed to acidic fluids (e.g., acid mine drainage) at the Earth's surface. We used Cd^{2+} as a model divalent cation for the following reasons: (1) the aqueous speciation is relatively simple and it does not precipitate at our experimental conditions until pH>8; (2) its use in laboratory settings is not complicated by the precipitation of cadmium carbonate or hydroxide solids; (3) many previous researchers study Cd^{2+} adsorption, so we can compare our results with those of previous studies.

4.2 Materials and experimental procedures

Samples of kaolinite (KGa-2), montmorillonite (SWy-2), and illite (IMt-2) were obtained from the Clay Mineral Society, Source Clays Repository (Purdue University, West Lafayette, USA). All

three clays were ground by an agate mortar and pestle to pass through a 100-mesh sieve. A 0.1 M $NaNO_3$ (ACS certified, Fisher Scientific) solution was prepared in advance of the clay mineral washing. For all treatments (pH 0, 2, 4, and 7), 4 g of each of the three clays were washed with 30 mL of 0.1 M $NaNO_3$ solution. The pH of the 0.1 M $NaNO_3$ solution was adjusted with aliquots of 70% HNO_3 (ACS certified, Fisher Scientific) to pH 0, 2 and 4 for acidic leaching (hereafter 'acidic treatment' refers to the pH 0-4 range). We use this range because it encompasses the effluent pH from most acidic mine drainage environments (Edwards et al., 2000; Johnson and Hallberg, 2005; Agboola et al., 2017; Peng et al., 2017b). For the pH 7 treatment (hereafter referred to as "neutral treatment"), the same amount of all three clays were washed with 30 mL of 0.1M $NaNO_3$ without adjusting pH (at pH around 7). For both methods, clays were washed three times, at time intervals of 1, 2 and 4 hours. Between washes, the solid and liquid were separated by centrifugation at 10,000 *xg* for 10 minutes. The liquid was collected for ICP analysis and the solid was resuspended, as described above. Total elemental release due to washing was calculated by summing the elemental release from all three washes.

Following washing, the pelleted clay samples were stored at -20°C for 24 h. Once frozen, each clay sample was freeze-dried (Thermo Savant MicroModulyo-115) to remove water molecules from their surface and interlayers. Hereafter, Kao-N is used to indicate neutral kaolinite, while Kao-A0, Kao-A2, and Kao-A4 indicate acidic kaolinite at pH=0, 2 and 4, respectively. The same nomenclature is applied to illite and montmorillonite.

To quantify how acidic treatment changes the surface of each clay, morphological analyses of the clays were conducted using a Zeiss Sigma 300 VP-FESEM scanning electron microscopy (SEM). Before SEM imaging, samples were carbon coated via a Leica EM SCD005 evaporative carbon coater. Crystal structure changes after acidic treatment were determined by X-ray

diffraction (XRD) analysis using a Rigaku Powder X-Ray diffractometer. XRD data were collected over a 2θ range of 5° to 90° with a scanning speed of 2° per minute in a continuous mode. The Brunauer–Emmett–Teller (BET) surface areas were determined for raw and treated kaolinite, illite and montmorillonite samples (Autosorb iQ, Quantachrome Instruments, USA). All samples were degassed at 250°C for 4 hours before analysis. The BET surface area was calculated using multipoint N_2 BET by tagging a P/P_0 range of 0.05–0.30. Triplication analysis was performed on samples to confirm the surface area values of all clay samples.

The supernatants of both acidic and neutral treatments were analyzed for Al, Mg, Si, and Fe concentrations by inductively coupled plasma mass spectrometry (ICP-MS; Agilent 8800). An internal indium standard (20 ppb) was employed to quantify instrumental drift during measurements. The standard deviation for each element analyzed was less than 3%.

Cadmium adsorption onto both acidic clay and neutral clay was studied as a function of Cd^{2+} concentration. Batch experiments were performed in a reciprocating shaker with a speed of 200 rpm. In each experiment, 40 mg of clay minerals were suspended in 40 mL of Milli-Q water to make a 1 g/L clay suspension at Cd^{2+} concentrations of 1 ppm, 10 ppm, 20 ppm, 30 ppm, and 40 ppm. Sodium nitrate, at a concentration of 0.01M, was used to buffer the ionic strength of the solution. After 12 hours, 5 mL of the suspension was taken out, filtered through 0.2 μm nylon membranes, and the supernatant analyzed by ICP-MS to determine the Cd^{2+} concentration in solution. The Cd^{2+} adsorption experiments were confirmed by duplication and the analytical uncertainty is < 5%.

4.3 Results and discussion

4.3.1 Release of elements during neutral and acidic treatment

The major elements released into solution during neutral and acidic treatments of kaolinite are Al and Si, with lesser amounts of Mg and Fe (Table 3.1). This is possibly because kaolinite [$Al_2Si_2O_5(OH)_4$)] has less isomorphic substitution by Mg and Fe in its structure (Sposito et al., 1999). Compared with the Kao-N, Kao-A2 released approximately 10 times more Al and 4 times more Si into solution, and the elemental release of Kao-A4 and Kao-N shows little difference with less than 10 ppm of each element released. Interestingly, Al and Si release from Kao-A0 is less than that of Kao-A2, which could be attributed to the generation of a leached layer and secondary precipitation of the released elements (Weissbart and Rimstidt, 2000; Ruiz-Agudo et al., 2012).

The neutral wash of illite [$(Al,Mg,Fe)_2(Si,Al)_4O_{10}(OH)_2$•K] released considerable Mg and smaller amounts of Si, while Al and Fe were also leached at acidic conditions (Table 3.1). Magnesium in the structure of illite mainly exists due to isomorphic substitution on the octahedral sheet, and the release of Mg at neutral pH indicating the instability of it which could easily be released into solution. Acidic treatment (pH=0, 2, 4) of illite releases more ions than the neutral treatment and decreasing pH leads to the release of higher elemental concentrations. At pH=0 treatment, illite released more than 1000 times Al, 2 times Mg, 20 times Si and 1000 times Fe than the neutral treatment. The treatment of illite at pH=4 resulted in only slight increases in elemental release as compared to pH=7, while significant amounts of Al release were observed for pH<2 treatment. Compared to kaolinite, illite has more isomorphic substitution in both the tetrahedral Si sheets and octahedral Al sheets (Sposito et al., 1999; González Sánchez et al., 2008), and as a consequence, these substituted elements (for example, Al, Mg, Fe) are more easily extracted during acidic treatment.

Magnesium and Si are the main elements mobilized during both acidic and neutral treatment of montmorillonite [$(Al,Mg)_2(Si,Al)_4O_{10}(OH)_2 \bullet nH_2O(Na)_{0.33}$], while the release of Al under pH>2 treatment was negligible (Table 3.1). This may be because the substituted ions (Al and Mg replace Si and Al in tetrahedral layer and octahedral layer, respectively) in the clay structure are more liable to be leached during acidic exposure. Aluminum substitution of Si in the tetrahedral layer of montmorillonite is minor (0.025%) compared to illite (15.38%), which explains why illite releases more Al compared to montmorillonite during acidic treatment. However, the pH=0 treatment of montmorillonite releases a greater amount of Al (344.8 ppm in total) which could be explained as stoichiometric dissolution since the elemental release ratio is around 1.5:1:1.5:1 for Al:Mg:Si:Fe (Weissbart and Rimstidt, 2000; Ruiz-Agudo et al., 2012). This result is also consistent with Si release (tetrahedral layer dissolution), which is significant for the pH=0 treatment. Interestingly, Mg release from montmorillonite shows little difference for the pH=2, 4, 7 treatment (approximately 100 ppm released in total), indicating that isomorphically substituted ions are more liable to release, a result also observed for illite.

Once structural elements, such as Si, Mg, Fe and Al, are released from a clay mineral into solution post acidification, the resulting vacancy in the octahedral or tetrahedral sheet can be replaced by dissolved cations from the external milieu. In natural environments, the most abundant cations (e.g., Ca^{2+}, Na^{+}) could potentially replace these structural cations. This process is similar to isomorphic substitution of higher valent cations (for example Al^{3+}, Si^{4+}) by lower valent cations (Mg^{2+}, Fe^{2+}) that occur extensively in clay structures (Hower and Mowatt, 1966; Chiou and Rutherford, 1997; Schroth and Sposito, 1997). Consequently, excess structural charge will be generated which leads to a greater negatively-charged surface electric field and increased electrostatic attraction metal cations.

Pentrak et al. (2010) studied the dissolution of 2:1 clay minerals and found that those with higher degrees of isomorphic substitution are more easily dissolved in HCl (Pentrak et al., 2010). Our study shows similar findings, with montmorillonite and illite having more isomorphic substitution than kaolinite and thus the former has a higher degree of elemental release, particularly at lower pH. Interestingly, kaolinite, a 1:1 clay mineral, released more Al than either montmorillonite and illite at pH=2 condition (Suraj et al., 1998). This might be attributed to the property that Al octahedral sheets in 1:1 clay minerals are more exposed to solution (i.e., acid attack) versus 2:1 clays where the Al octahedral are sandwiched between two Si tetrahedral sheets.

4.3.2 Changes in morphology and crystal structures of the studied clay minerals

The changes in clay particle morphology and crystal structure between the acidic and neutral treatments are shown by SEM and XRD (Figure 4.1, 4.2). We chose pH=2 and pH=7 as examples, since pH=2 represents a moderately acidic environment and pH=7 is the lone neutral treatment. All three clay minerals exhibit a planar structure in the SEM images, with clay platelets both stacked on and perpendicular to each other. In all cases, the comparison between acid treated clay and neutral treated clay shows that the acidic treatment had a negligible influence on the morphology of the studied clay minerals. Figure 4.2 shows the comparison of XRD patterns of the three clay minerals after both acidic and neutral treatments. To better visualize the differences, the patterns of Kao-A, Illite-A, and Mont-A were overlapped with Kao-N, Illite-N, and Mont-N, respectively. Acidic treatment changed diffraction peaks between 2θ=5-15° for kaolinite and montmorillonite, while for illite there is no difference across the whole two-theta range. Diffraction peaks in Mont-A have a lower intensity compared to Mont-N, while those in Kao-A have a higher intensity than Kao-N at two-theta values below 10 degrees. The comparison of XRD spectra

between acidic clay and neutral clay indicates that the crystal structure of clay minerals displays little difference after acidic treatment.

Although the acidic modification of clay minerals leads to the release of structural elements into solution, this influence cannot be detected by traditional mineral characterization methods, such as SEM and XRD (Figs. 1 and 2). A simple calculation was done, summing all of the elements that were lost during washing (the total elemental loss) to estimate the total mass of elemental release, which is 0.80 mg, 5.49 mg, 3.39 mg, 4.32 mg, 1.74 mg, 5.08 mg for Kao-N, Kao-A2, Mont-N, Mont-A2, Illite-N, and Illite-A2, respectively. This accounts for only 0.02%, 0.14%, 0.08%, 0.11%, 0.04%, and 0.13% of the total clay mass, respectively. It is also possible that secondary precipitation could occur on the clay surfaces that may not be detected by XRD and SEM, since the amount of elemental release is negligible compared to the mass of clay. Kumar et al (1995) and Jozefaciuk and Bowanko (2002) treated montmorillonite and kaolinite using various concentrations of acid and found that the XRD spectra of acid-activated montmorillonite varies primarily between 2θ of 0-20°(Kumar et al., 1995; Jozefaciuk and Bowanko, 2002). These findings correlate well with our clay XRD spectra that show the major peak differences are within $2\theta < 20°$. Collectively, acid-treated clays show little difference in crystal structure compared to neutral-treated clays.

Wang et al. (2016) studied morphological modifications of kaolinite after both alkali and acid leaching.(Wang et al., 2016) Their results showed significant changes in morphology between untreated kaolinite, alkali-leached kaolinite and acid-leached kaolinite. The authors found that following an initial alkali leaching of the kaolinite, most of the Si in the mineral was released into solution (more than 60%), and this led to the morphological changes observed. Although our results also indicate that Si is leached, the amount of Si released is negligible relative to that

observed by Wang et al. (2016) in their alkali treatment. This likely explains why the morphology change in our samples is undetectable.

4.3.3 Variations in surface area of the studied clay minerals

The surface area of kaolinite shows no difference for the pH>2 treatment (within the analysis uncertainty of ±2 m^2/g), except for Kao-A0 which has a surface area of 25 m^2/g indicating that strong acidic treatment can increase its surface area (Table 3.2). The same trend is found for illite which shows little variation in surface area for the pH=2, 4, 7 treatments. Montmorillonite experienced a significant surface area increase for pH=0 (115 m^2/g), and 2 (24 m^2/g) treatment compared to pH=4, and 7 treatment, indicating that the montmorillonite surface area is significantly affected by acidic treatment as compared to illite and kaolinite. It should be noted that the surface areas of Mont-N, Mont-A4, and Mont-A2 are lower than for raw montmorillonite which has a surface area of 32 m^2/g (data from Clay Minerals Society). This could be attributed to the flocculation of clay montmorillonite at the higher solution electrolyte concentration (0.1M $NaNO_3$).

At our experimental conditions, insignificant changes in the surface areas of kaolinite and illite were observed after acidic treatment (Table 3.2, except for montmorillonite). This contradicts previous studies showing that the surface area of clay minerals increased dramatically after acidic activation (Barrios et al., 1995; Kumar et al., 1995; Christidis et al., 1997; Dekany et al., 1999; Bhattacharyya and Gupta, 2008b). One clear difference between those studies and ours is that the former applied intensive acid attack to clay minerals, with acid concentrations up to 8 M, at temperatures over 70°C, and with extended reaction times of as much as 71 hours. These experiments aim to modify clay minerals through acidic treatment but, in our opinion, are not

relevant to natural conditions. Thus, although structural elements were leached out during the acidic treatment, we observed that there is no significant change in the surface area of kaolinite and illite, especially at conditions that simulate short-term Earth surface acidic drainage exposure (less than 7h, pH=0, 2, 4). However, after decades to centuries of exposure to acidic weathering, large degrees of alteration might be expected (Jackson et al., 1948).

4.3.4 Cd^{2+} adsorption capacity

The Cd^{2+} adsorption isotherms for the three studied clay minerals are shown in Figures 4.3-4.5. Kaolinite basically shows no difference in Cd^{2+} adsorption capacity for the pH=2, 4, 7 treatments. However, Cd^{2+} adsorption for the pH=0 treatment of kaolinite markedly decreases compared with the other treatments (around 0.5-1 mg/g difference). The pH=0 treatment of illite decreased its Cd^{2+} adsorption capacity by approximately 4-5 mg/g, more than for kaolinite. The acidic treatment of montmorillonite illustrates a steadily decrease of Cd^{2+} adsorption with increasing acidity, with around 2 mg/g maximum adsorption for Mont-A0 compared to approximately 17 mg/g for Mont-7.

While it is generally accepted that acidic clay minerals have higher metal adsorption capacity than do neutral clays (Bhattacharyya and Gupta, 2008a; Gupta and Bhattacharyya, 2012), our experimental results show that the Cd^{2+} adsorption capacity variation is little for treatments of pH 2 and above, while decreased significantly for the pH=0 treatment (Figures 4.1-4.3). This result is different with a previous study that considered Cu(II) and Ni(II) adsorption onto acid treated clays by applying 0.25M H_2SO_4 at 110 °C, which results in a higher Cu(II) and Ni(II) adsorption capacity after acidification (Bhattacharyya and Gupta, 2008b). The high temperature treatment likely activated the clays, creating surface sites for metal adsorption. In our study, the acidic

treatment increases surface area of the three clay minerals but decreases the Cd^{2+} adsorption. This is possibly because strong acidic treatment leads to the dissolution of clay, which creates a leached layer that is enriched in certain elements, ultimately leading to the formation of secondary precipitates on the clay mineral surfaces (Weissbart and Rimstidt, 2000; Ruiz-Agudo et al., 2012). The precipitation of secondary minerals, most likely amorphous silica, could explain the increase of BET surface area. However, it could simultaneously cover the exposed clay surface functional groups and inhibit Cd^{2+} adsorption (Weissbart and Rimstidt, 2000). Also, the adsorption of Cd^{2+} onto amorphous Si is significantly lower than that onto clay minerals (Pivovarov, 2008). Secondary precipitation of amorphous silica could scarcely form under high temperature since its solubility increases with temperature (Fournier and Rowe, 1977), which could explain the literature results that clays treated by acid under high temperature have higher metal adsorption capacity than normal clays (Bhattacharyya and Gupta, 2008b).

Our results show that the variation of Cd^{2+} adsorption capacity and surface area of the clays is negligible for pH 2, 4, 7, which represents a wide range of environments at the Earth's surface. However, we found that highly acidic conditions (pH=0) may result in a considerable decline in Cd^{2+} adsorption capacity. Our experimental results demonstrate conclusively that acidic treatment has little impact on the morphology and crystal structure of clay minerals but could lead to the release of structural elements and changes in surface area, and thus influence the overall Cd^{2+} adsorption capacity.

4.4 Conclusions and Implications

Our results indicated that the exposure of clay minerals to acidic conditions will extract structural elements, which leads to a measurable variation of Cd^{2+} binding capacity and surface area,

although this effect showed no discernible variation in terms of clay morphology and crystal structure. The partial dissolution of clay minerals by acid has several implications for their surface reactivity and potential transport from land to the oceans. For instance, in mining operations, the oxidation of pyrite – a mineral constituent of both metal ores and coal bodies – can lead to the acidification of the proximal environment (Konhauser et al., 2011). When clay minerals that are present in the soils become eroded by the AMD or acidic rain (pH=0), their surface properties change, and according to our results, they should be a variation of trace metals adsorption compared to the natural clays. This could be of environmental concern because AMD also carries with it a number of toxic metals in solution, and thus the soils surrounding the mine might become metal-enriched.

4.5 References

Adams, J.M., Davies, S.E., Graham, S.H., Thomas, J.M., 1982. Catalyzed reactions of organic molecules at clay surfaces: Ester breakdown, dimerizations, and lactonizations. Journal of Catalysis, 78(1): 197-208.

Agboola, O., Mokrani, T., Sadiku, E.R., Kolesnikov, A., Olukunle, O.I., Maree, J.P., 2017. Characterization of Two Nanofiltration Membranes for the Separation of Ions from Acid Mine Water. Mine Water and the Environment, 36(3): 401-408.

Anna, B., Kleopas, M., Constantine, S., Anestis, F., Maria, B., 2015. Adsorption of Cd(II), Cu(II), Ni(II) and Pb(II) onto natural bentonite: study in mono- and multi-metal systems. Environmental Earth Sciences, 73(9): 5435-5444.

Bachmaf, S., Merkel, B.J., 2011. Sorption of uranium(VI) at the clay mineral-water interface. Environmental Earth Sciences, 63(5): 925-934.

Barrios, M.S., Gonzalez, L.V.F., Rodriguez, M.A.V., Pozas, J.M.M., 1995. Acid Activation of a Palygorskite with Hcl - Development of Physicochemical, Textural and Surface-Properties. Applied Clay Science, 10(3): 247-258.

Bergaya, F., Lagaly, G., 2006. General introduction: clays, clay minerals, and clay science. Developments in clay science, 1: 1-18.

Bhattacharyya, K.G., Sen Gupta, S., 2006. Adsorption of chromium (VI) from water by clays. Industrial & engineering chemistry research, 45(21): 7232-7240.

Bhattacharyya, K.G., Gupta, S.S., 2008a. Adsorption of a few heavy metals on natural and modified kaolinite and montmorillonite: a review. Adv Colloid Interface Sci, 140(2): 114-31.

Bhattacharyya, K.G., Gupta, S.S., 2008b. Influence of acid activation on adsorption of Ni(II) and Cu(II) on kaolinite and montmorillonite: Kinetic and thermodynamic study. Chemical Engineering Journal, 136(1): 1-13.

Bibi, I., Singh, B., Silvester, E., 2011. Dissolution of illite in saline-acidic solutions at 25 degrees C. Geochimica et Cosmochimica Acta, 75(11): 3237-3249.

Bibi, I., Singh, B., Silvester, E., 2014. Dissolution kinetics of soil clays in sulfuric acid solutions: Ionic strength and temperature effects. Applied Geochemistry, 51: 170-183.

Chiou, C.T., Rutherford, D.W., 1997. Effects of exchanged cation and layer charge on the sorption of water and EGME vapors on montmorillonite clays. Clays and Clay Minerals, 45(6): 867-880.

Chitnis, S.R., Mohan Sharma, M., 1997. Industrial applications of acid-treated clays as catalysts. Reactive and Functional Polymers, 32(1): 93-115.

Christidis, G.E., Scott, P.W., Dunham, A.C., 1997. Acid activation and bleaching capacity of

bentonites from the islands of Milos and Chios, Aegean, Greece. Applied Clay Science, 12(4): 329-347.

Dekany, I., Turi, L., Fonseca, A., Nagy, J.B., 1999. The structure of acid treated sepiolites: small-angle X-ray scattering and multi MAS-NMR investigations. Applied Clay Science, 14(1-3): 141-160.

Edwards, K.J., Bond, P.L., Gihring, T.M., Banfield, J.F., 2000. An archaeal iron-oxidizing extreme acidophile important in acid mine drainage. Science, 287(5459): 1796-1799.

Espantaleon, A.G., Nieto, J.A., Fernandez, M., Marsal, A., 2003. Use of activated clays in the removal of dyes and surfactants from tannery waste waters. Applied Clay Science, 24(1-2): 105-110.

Fournier, R.O., Rowe, J.J., 1977. The solubility of amorphous silica in water at high temperatures and high pressures. American Mineralogist, 62(9-10): 1052-1056.

Ghayaza, M., Le Forestier, L., Muller, F., Tournassat, C., Beny, J.M., 2011. Pb(II) and Zn(II) adsorption onto Na- and Ca-montmorillonites in acetic acid/acetate medium: Experimental approach and geochemical modeling. Journal of Colloid and Interface Science, 361(1): 238-246.

Gingele, F.X., De Deckker, P., Hillenbrand, C.-D., 2001. Clay mineral distribution in surface sediments between Indonesia and NW Australia - source and transport by ocean currents. Marine Geology, 179(3–4): 135-146.

González Sánchez, F., Van Loon, L.R., Gimmi, T., Jakob, A., Glaus, M.A., Diamond, L.W., 2008. Self-diffusion of water and its dependence on temperature and ionic strength in highly compacted montmorillonite, illite and kaolinite. Applied Geochemistry, 23(12): 3840-3851.

Griffin, J.J., Windom, H., Goldberg, D.E., 1968. The distribution of clay minerals in the World

Ocean. Deep-Sea Research, 15: 433-459.

Gu, X., Evans, L.J., 2007. Modelling the adsorption of Cd(II), Cu(II), Ni(II), Pb(II), and Zn(II) onto Fithian illite. Journal of colloid and interface science, 307(2): 317-25.

Gu, X., Evans, L.J., 2008. Surface complexation modelling of Cd(II), Cu(II), Ni(II), Pb(II) and Zn(II) adsorption onto kaolinite. Geochimica et Cosmochimica Acta, 72(2): 267-276.

Gu, X., Evans, L.J., Barabash, S.J., 2010. Modeling the adsorption of Cd (II), Cu (II), Ni (II), Pb (II) and Zn (II) onto montmorillonite. Geochimica et Cosmochimica Acta, 74(20): 5718-5728.

Gupta, S.S., Bhattacharyya, K.G., 2012. Adsorption of heavy metals on kaolinite and montmorillonite: a review. Physical Chemistry Chemical Physics, 14(19): 6698-6723.

Hao, W., Flynn, S.L., Alessi, D.S., Konhauser, K.O., 2018. Change of the point of zero net proton charge (pHPZNPC) of clay minerals with ionic strength. Chemical Geology, 493: 458-467.

Hao, W., Flynn, S.L., Kashiwabara, T., Alam, M.S., Bandara, S., Swaren, L. et al., 2019. The impact of ionic strength on the proton reactivity of clay minerals. Chemical Geology: 119294.

Hower, J., Mowatt, C.T., 1966. The mineralogy of illite and mixed-layer illite/montmorillonites. The American Mineralogist, 51: 825-854.

Huertas, F.J., Chou, L., Wollast, R., 1998. Mechanism of kaolinite dissolution at room temperature and pressure: Part 1. Surface speciation. Geochimica Et Cosmochimica Acta, 62(3): 417-431.

Jackson, M., Tyler, S., Willis, A., Bourbeau, G., Pennington, R., 1948. Weathering sequence of clay-size minerals in soils and sediments. I. Fundamental generalizations. The Journal of Physical Chemistry, 52(7): 1237-1260.

Johnson, D.B., Hallberg, K.B., 2005. Acid mine drainage remediation options: a review. Science of the total environment, 338(1-2): 3-14.

Jozefaciuk, G., Bowanko, G., 2002. Effect of acid and alkali treatments on surface areas and adsorption energies of selected minerals. Clays and Clay Minerals, 50(6): 771-783.

Khawmee, K., Suddhiprakarn, A., Kheoruenromne, I., Bibi, I., Singh, B., 2013. Dissolution behaviour of soil kaolinites in acidic solutions. Clay Minerals, 48(3): 447-461.

Konhauser, K.O., Fisher, Q.J., Fyfe, W.S., Longstaffe, F.J., Powell, M.A., 1998. Authigenic mineralization and detrital clay binding by freshwater biofilms: The Brahmani River, India. Geomicrobiology Journal, 15(3): 209-222.

Konhauser, K.O., Lalonde, S.V., Planavsky, N.J., Pecoits, E., Lyons, T.W., Mojzsis, S.J. et al., 2011. Aerobic bacterial pyrite oxidation and acid rock drainage during the Great Oxidation Event. Nature, 478(7369): 369-373.

Kumar, P., Jasra, R.V., Bhat, T.S.G., 1995. Evolution of Porosity and Surface Acidity in Montmorillonite Clay on Acid Activation. Industrial & Engineering Chemistry Research, 34(4): 1440-1448.

Lackovic, K., Angove, M.J., Wells, J.D., Johnson, B.B., 2003. Modeling the adsorption of Cd(II) onto Muloorina illite and related clay minerals. Journal of Colloid and Interface Science, 257(1): 31-40.

Liu, Y., Alessi, D.S., Flynn, S.L., Alam, M.S., Hao, W., Gingras, M. et al., 2018. Acid-base properties of kaolinite, montmorillonite and illite at marine ionic strength. Chemical Geology, 483: 191-200.

Manning, B.A., Goldberg, S., 1997. Adsorption and stability of arsenic (III) at the clay mineral−water interface. Environmental Science & Technology, 31(7): 2005-2011.

Ozdes, D., Duran, C., Senturk, H.B., 2011. Adsorptive removal of Cd(II) and Pb(II) ions from aqueous solutions by using Turkish illitic clay. Journal of Environmental Management, 92(12): 3082-3090.

Peng, X., Tang, T., Zhu, X., Jia, G., Ding, Y., Chen, Y. et al., 2017a. Remediation of acid mine drainage using microbial fuel cell based on sludge anaerobic fermentation. Environmental Technology (United Kingdom), 38(19): 2400-2409.

Peng, X., Tang, T., Zhu, X., Jia, G., Ding, Y., Chen, Y. et al., 2017b. Remediation of acid mine drainage using microbial fuel cell based on sludge anaerobic fermentation. Environmental technology, 38(19): 2400-2409.

Pentrak, M., Madejova, J., Komadel, P., 2010. Effect of chemical composition and swelling on acid dissolution of 2: 1 clay minerals. Philosophical Magazine, 90(17-18): 2387-2397.

Pivovarov, S., 2008. Adsorption of ions onto amorphous silica: ion exchange model. Journal of colloid and interface science, 319(1): 374-376.

Qin, H.-B., Uesugi, S., Yang, S., Tanaka, M., Kashiwabara, T., Itai, T. et al., 2019. Enrichment mechanisms of antimony and arsenic in marine ferromanganese oxides: Insights from the structural similarity. Geochimica et Cosmochimica Acta, 257: 110-130.

Ruiz-Agudo, E., Putnis, C.V., Rodriguez-Navarro, C., Putnis, A., 2012. Mechanism of leached layer formation during chemical weathering of silicate minerals. Geology, 40(10): 947-950.

Schroth, B.K., Sposito, G., 1997. Surface charge properties of kaolinite. Clays and Clay Minerals, 45(1): 85-91.

Schroth, B.K., Sposito, G., 1998. Effect of landfill leachate organic acids on trace metal adsorption by kaolinite. Environmental science & technology, 32(10): 1404-1408.

Sdiri, A., Higashi, T., Chaabouni, R., Jamoussi, F., 2012. Competitive Removal of Heavy Metals

from Aqueous Solutions by Montmorillonitic and Calcareous Clays. Water, Air, & Soil Pollution, 223(3): 1191-1204.

Sen, T.K., Ling, H.K., 2009. Removal of cadmium (Cd2+) metal ion from its aqueous solution by kaolin clay minerals: A kinetic and equilibrium study. Journal of the Institution of Engineers (India): Chemical Engineering Division, 89(MAR): 26-30.

Sposito, G., Skipper, N.T., Sutton, R., Park, S.-h., Soper, A.K., Greathouse, J.A., 1999. Surface geochemistry of the clay minerals. Proceedings of the National Academy of Sciences, 96(7): 3358-3364.

Suraj, G., Iyer, C.S.P., Lalithambika, M., 1998. Adsorption of cadmium and copper by modified kaolinite. Applied Clay Science, 13(4): 293-306.

Vaccari, A., 1999. Clays and catalysis: a promising future. Applied Clay Science, 14(4): 161-198.

Veselská, V., Fajgar, R., Číhalová, S., Bolanz, R.M., Göttlicher, J., Steininger, R. et al., 2016. Chromate adsorption on selected soil minerals: Surface complexation modeling coupled with spectroscopic investigation. Journal of Hazardous Materials, 318: 433-442.

Wang, G.H., Wang, X.G., Chai, X.J., Liu, J.S., Deng, N.S., 2010. Adsorption of uranium (VI) from aqueous solution on calcined and acid-activated kaolin. Applied Clay Science, 47(3-4): 448-451.

Wang, H., Feng, Q., Liu, K., 2016. The dissolution behavior and mechanism of kaolinite in alkali-acid leaching process. Applied Clay Science, 132–133: 273-280.

Weissbart, E.J., Rimstidt, J.D., 2000. Wollastonite: Incongruent dissolution and leached layer formation. Geochimica et Cosmochimica Acta, 64(23): 4007-4016.

Yang, S., Ren, X., Zhao, G., Shi, W., Montavon, G., Grambow, B. et al., 2015. Competitive sorption and selective sequence of Cu (II) and Ni (II) on montmorillonite: batch, modeling,

EPR and XAS studies. Geochimica et cosmochimica Acta, 166: 129-145.

Yang, S., Uesugi, S., Qin, H., Tanaka, M., Kurisu, M., Miyamoto, C. et al., 2018. Comparison of arsenate and molybdate speciation in hydrogenetic ferromanganese nodules. ACS Earth and Space Chemistry, 3(1): 29-38.

Yariv, S., Cross, H., 2002. Organo-clay complexes and interactions. Marcel Dekker, 270 Madison Avenue, New York.

Zhao, D., Chen, S., Yang, S., Yang, X., Yang, S., 2011. Investigation of the sorption behavior of Cd (II) on GMZ bentonite as affected by solution chemistry. Chemical Engineering Journal, 166(3): 1010-1016.

Table 4.1: Elements released from the three studied clay minerals during acidic and neutral treatment (units: ppm)

	1h	3h	7h	Total	% of 1h	% of 3h	% of 7h
				Kao-A0			
Al	20.86	5.68	4.42	30.95	67.39	18.34	14.27
Mg	4.17	0.25	0.07	4.50	92.70	5.65	1.65
Si	6.68	4.51	4.15	15.34	43.55	29.42	27.03
Fe	0.54	0.29	0.22	1.04	51.65	27.52	20.83
				Kao-A2			
Al	66.26	19.68	9.20	95.14	69.64	20.68	9.67
Mg	3.50	0.36	0.06	3.92	89.18	9.26	1.57
Si	30.98	12.60	7.48	51.06	60.68	24.68	14.64
Fe	0.39	0.41	0.29	1.08	35.75	37.66	26.59
				Kao-A4			
Al	2.24	1.47	0.90	4.60	48.59	31.90	19.51
Mg	3.44	0.62	0.20	4.26	80.63	14.61	4.75
Si	1.22	1.78	1.16	4.15	29.35	42.84	27.81
Fe	0.08	0.07	0.04	0.20	42.95	36.05	21.00
				Kao-N			
Al	5.92	2.75	1.71	10.38	56.99	26.52	16.49
Mg	3.10	0.54	0.12	3.76	82.45	14.38	3.17
Si	5.86	5.33	5.12	16.31	35.93	32.70	31.37
Fe	0.12	0.12	0.10	0.34	35.80	34.49	29.71
				Mont-A0			
Al	203.27	88.02	53.51	344.80	58.95	25.53	15.52
Mg	146.92	47.61	20.76	215.29	68.24	22.11	9.64
Si	130.45	92.51	99.27	322.24	40.48	28.71	30.81
Fe	103.14	51.49	36.77	191.41	53.89	26.90	19.21
				Mont-A2			
Al	BD	0.005	BD	0.005	BD	100	BD
Mg	35.75	32.77	32.44	101.0	35.41	32.46	32.13
Si	11.51	15.02	16.29	42.82	26.89	35.07	38.04
Fe	0.036	0.035	0.031	0.102	35.10	34.33	30.57
				Mont-A4			
Al	0.01	BD	BD	0.01	66.32	9.90	23.79
Mg	57.19	30.26	26.35	113.80	50.26	26.59	23.15
Si	4.32	5.71	5.73	15.77	27.43	36.22	36.35
Fe	BD	BD	BD	0.01	32.59	16.98	50.43
				Mont-N			
Al	BD	BD	BD	BD	BD	BD	BD

Mg	40.20	30.46	25.98	96.64	41.59	31.52	26.89
Si	5.171	5.353	5.761	16.28	31.75	32.87	35.38
Fe	0.034	0.034	0.028	0.096	35.38	35.73	28.89
			Illite-A0				
Al	108.07	29.84	22.76	160.67	67.26	18.57	14.17
Mg	104.05	14.31	8.46	126.82	82.05	11.28	6.67
Si	92.55	39.55	39.71	171.81	53.87	23.02	23.11
Fe	51.52	23.91	25.26	100.69	51.17	23.75	25.09
			Illite-A2				
Al	3.940	14.60	14.63	33.18	11.87	44.02	44.11
Mg	48.95	17.47	6.008	72.42	67.59	24.12	8.296
Si	15.37	23.82	11.85	51.03	30.11	46.67	23.21
Fe	0.414	4.488	7.783	12.68	3.263	35.38	61.35
			Illite-A4				
Al	0.01	0.03	0.04	0.08	13.94	37.95	48.12
Mg	40.01	15.34	9.26	64.61	61.92	23.75	14.33
Si	2.90	3.10	3.65	9.65	30.06	32.09	37.86
Fe	BD	BD	BD	0.01	33.43	51.09	15.48
			Illite-N				
Al	0.018	0.066	0.098	0.183	10.10	36.08	53.82
Mg	34.10	10.05	5.848	49.99	68.21	20.10	11.70
Si	2.250	2.596	2.936	7.782	28.91	33.36	37.73
Fe	0.038	0.025	0.021	0.084	44.82	29.95	25.23

Note: A means acidic treatment; N stands for neutral treatment; the number 1, 2, 3 is first time wash, second time wash and third time wash; BD stands for below detection limit and our detection limit for ICP-MS analysis is 0.002 ppm

Table 4.2: Surface area summary of the three studied clay minerals

BET surface area (m^2/g) (uncertainties±2 m^2/g)					
Kao-A0	25	Mont-A0	115	Illite-A0	30
Kao-A2	21	Mont-A2	24	Illite-A2	22
Kao-A4	21	Mont-A4	7	Illite-A4	23
Kao-N	18	Mont-N	5	Illite-N	19

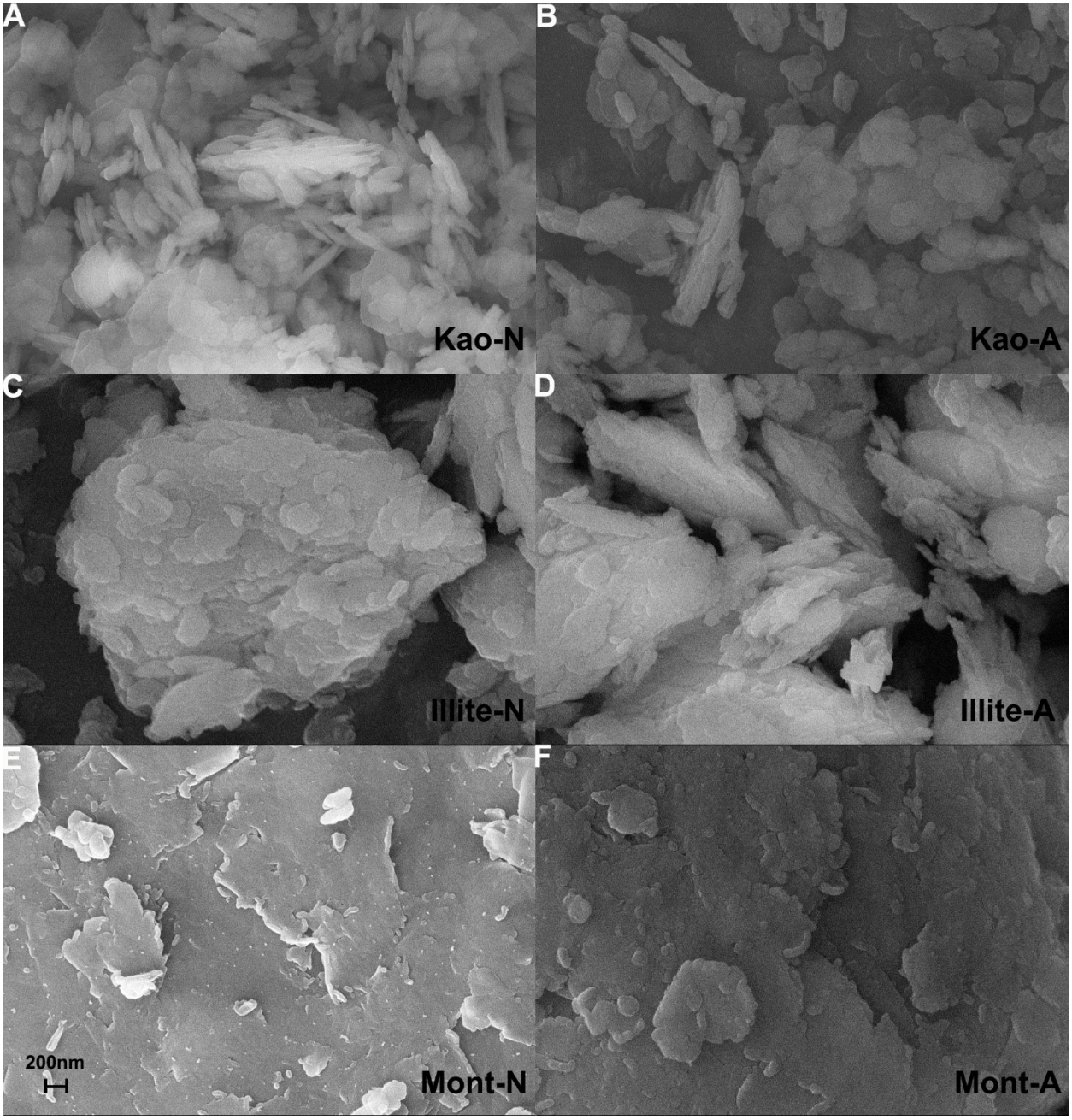

Figure 4.1 Scanning electron microscopy (SEM) images of neutral and acid treated clay minerals (A: Kao-N; B: Kao-A; C: Illite-N; D: Illite-A; E: Mont-N; F: Mont-A).

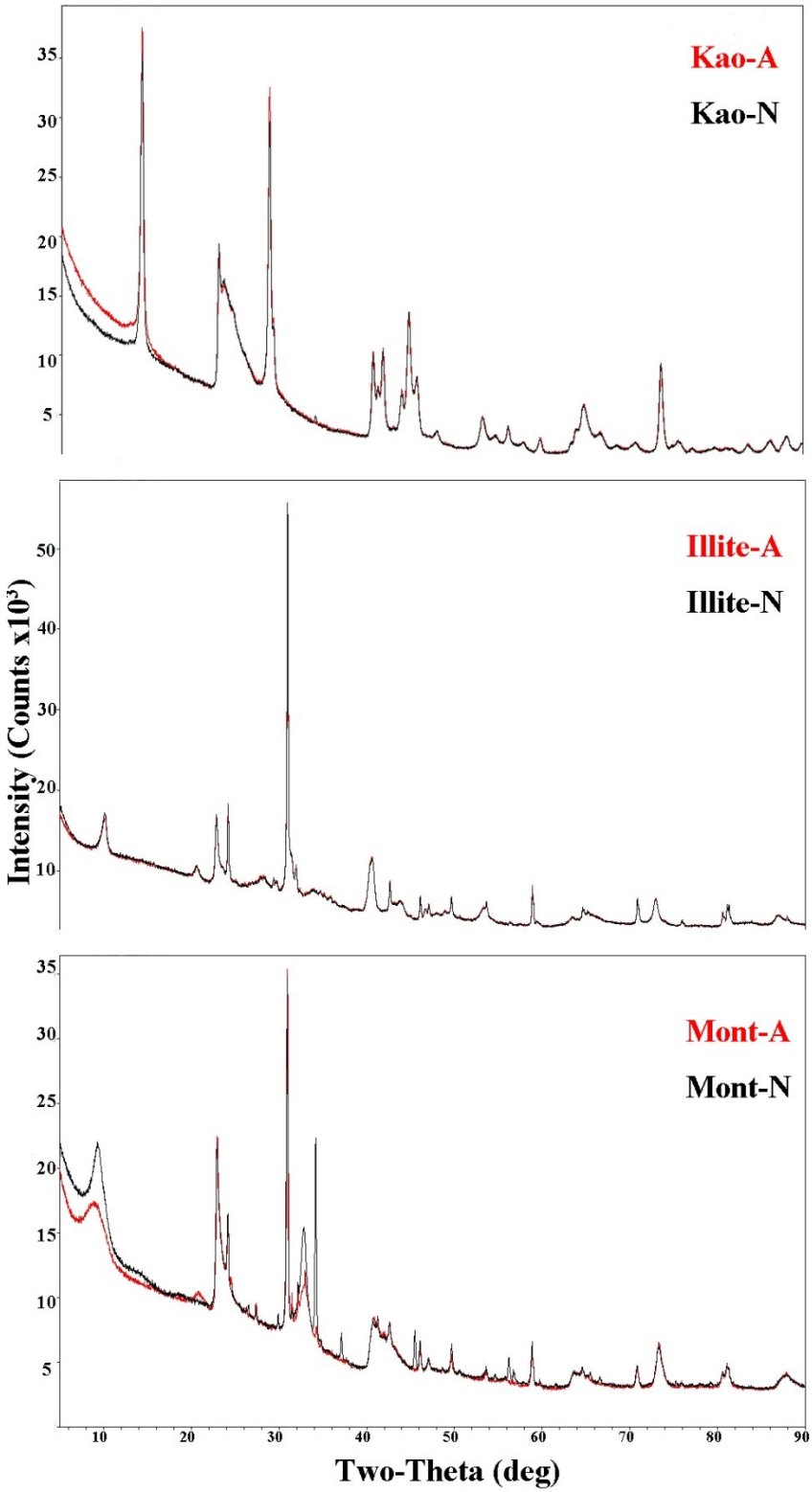

Figure 4.2 X-ray diffraction data of the three studied clays under acidic and neutral treatments of acid-treated (A; red) and neutral-treated (N, black) diffraction patterns.

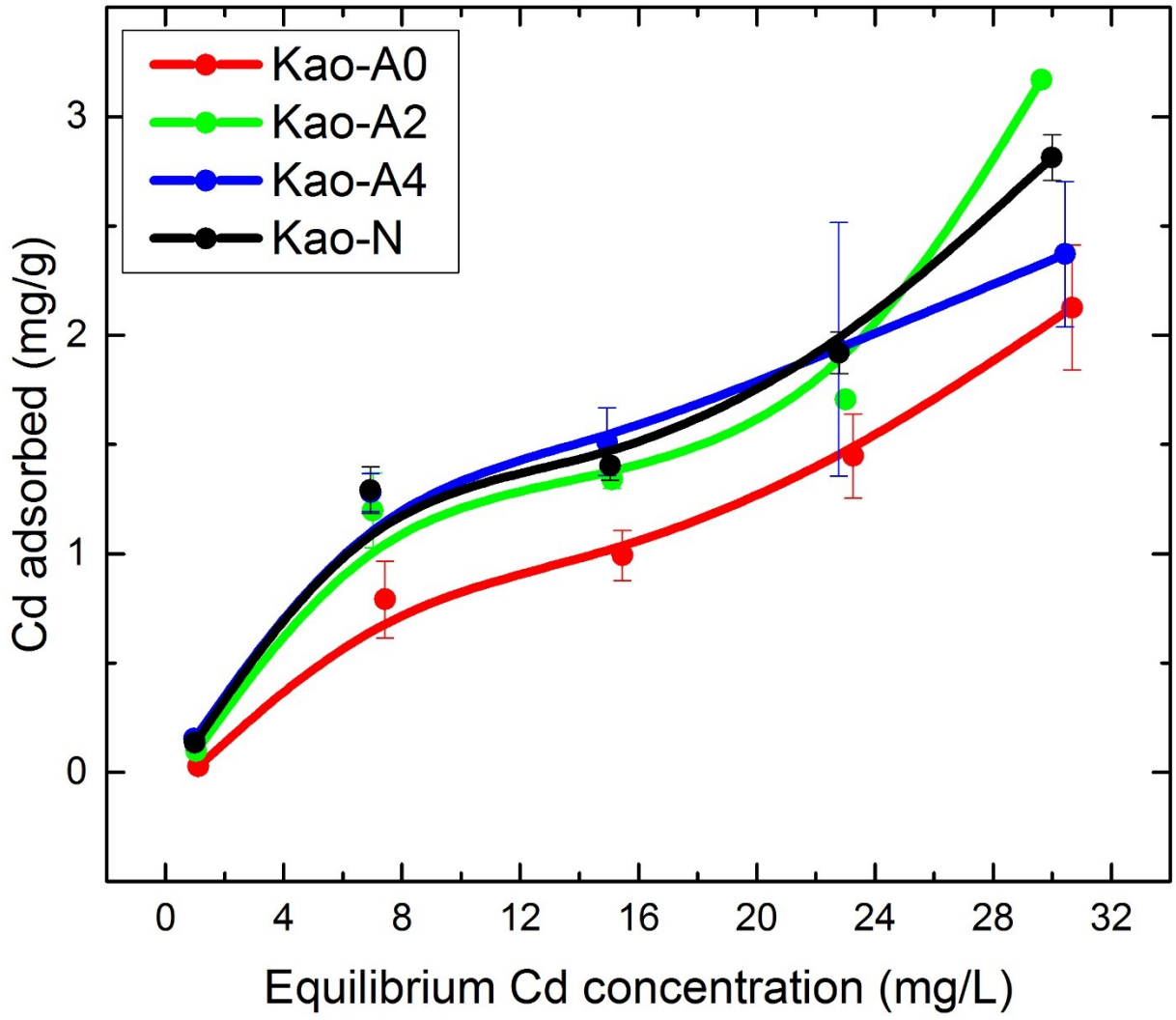

Figure 4.3 Adsorption isotherms of Cd^{2+} onto kaolinite

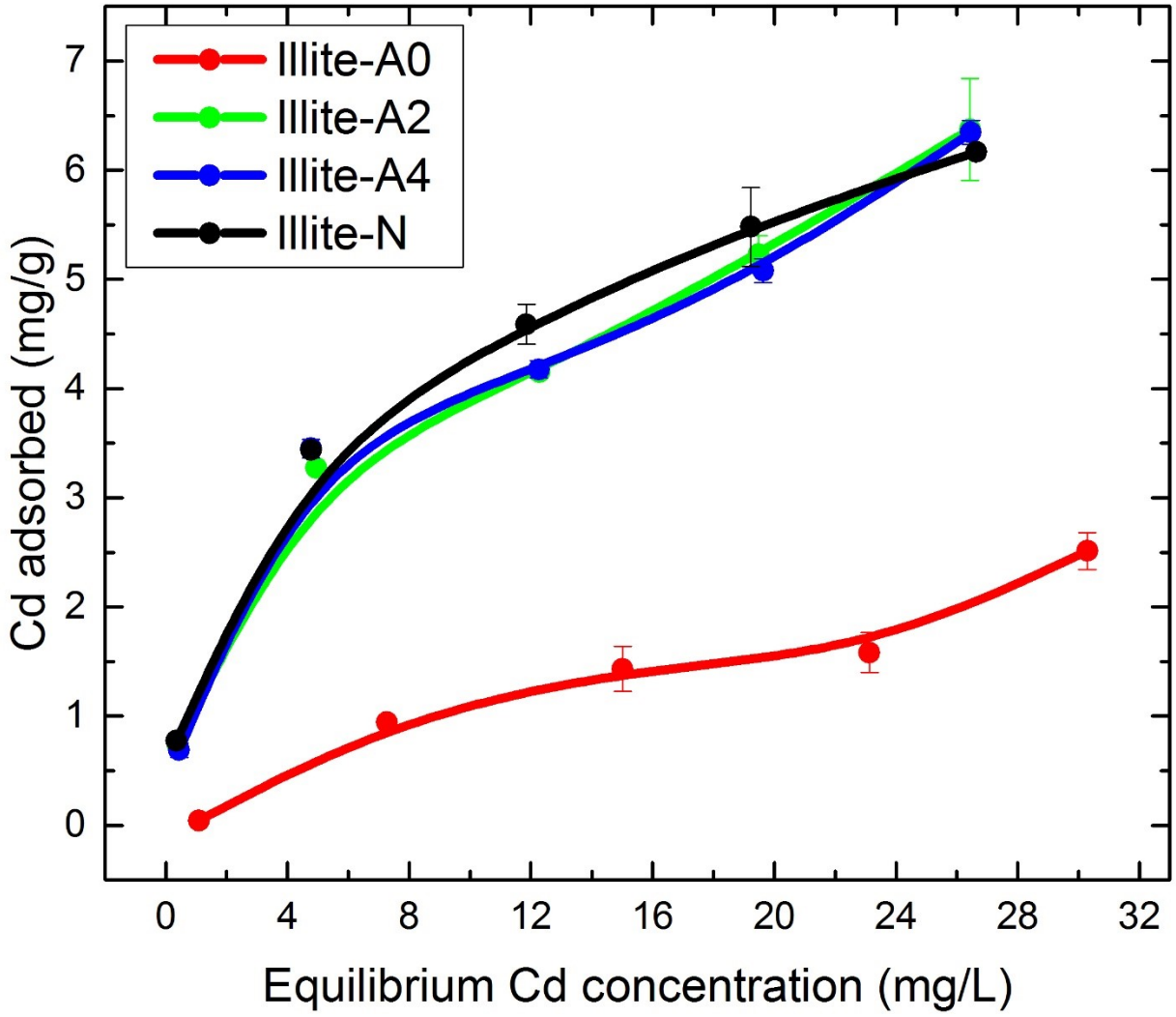

Figure 4.4 Adsorption isotherms of Cd^{2+} onto illite

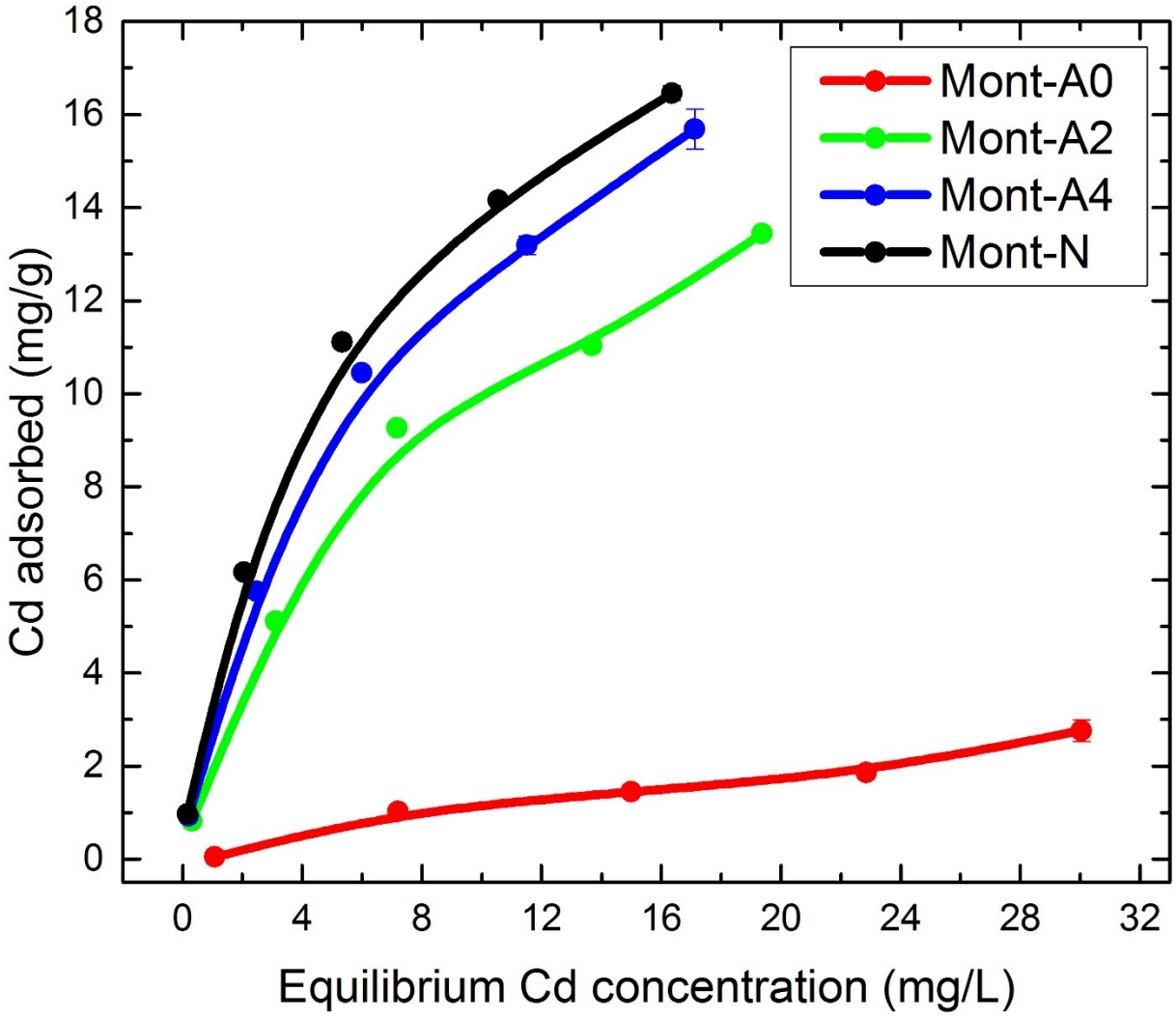

Figure 4.5 Adsorption isotherms of Cd^{2+} onto montmorillonite

Chapter 5. Transport of Cd by clay minerals from land to the oceans[4]

5.1 Introduction

Clay minerals are characterized by their high chemical reactivity (Baeyens and Bradbury, 1997; Bradbury and Baeyens, 2002; Lackovic et al., 2003; Bradbury and Baeyens, 2009), and thus as major components in the suspended sediments of rivers (Gibbs, 1967; Sposito et al., 1999; Viers et al., 2009; Brack, 2013), they have a considerable influence on the transfer of trace metals from land to the oceans (Uncles et al., 2006; Zhao et al., 2018b). Differences between the chemistry of rivers (pH around 6, ionic strength around 0.01 M) and oceans (pH around 8, ionic strength around 0.56 M) result in variations in both the aqueous speciation of trace elements and clay surface properties. This, in turn, affects the capacity with which metals stay bound to clays. For instance, previous studies indicate that increases in solution pH promote the adsorption of trace elements (e.g., Cu, Zn, Ni, Co and Cd) onto clay minerals, while conversely, high ionic strength (hereafter abbreviated as IS) inhibits their adsorption (Gu and Evans, 2007; Gu and Evans, 2008; Gu et al., 2010). These phenomena are explained by the fact that increased pH enhances the deprotonation of surface functional groups, while high ionic strength attenuates the negative electrostatic field at the clay surface (Hao et al., 2018; Hao et al., 2019a). Understanding how changes in aqueous chemistry during the transition from riverine to marine settings (e.g., within estuaries) impact trace metal behaviour on clay surfaces is critical to determining the degree to which they serve as sink for metals to the bottom sediments or a source of metals to the water column.

[4] This chapter has been prepared as a manuscript for submission as: Hao, W.; Kashiwabara, T.; Jin, R.; Takahashi, Y.; Gingras, M.; Alessi, D.S.; Konhauser, K.O.

The interactions between Cd and clay minerals is well studied due to its relatively simple aqueous speciation and potential as an environmental pollutant (Srour and Mcdonald, 2005; da Fonseca et al., 2006; Zhou et al., 2017; Hao et al., 2019b; Johnson et al., 2019). Previous studies indicate that clay minerals are a significant sink for Cd under marine conditions because of elevated pH versus most freshwater environments (Liu et al., 2018). However, the impact of increased IS on clay-Cd interactions could be more significant than the change in pH, especially the attenuation of electrostatic field induced by increasing solution ionic strength (Hao et al., 2019a). The adsorption/desorption behaviour of metals and nutrients, including Cd, on clays as they transit from freshwater to estuarine conditions is still not well-understood, despite potentially critical impacts on the near-shore biosphere.

Despite considerable research on the adsorption behaviour of Cd (Petersen et al., 1998; Yee and Fein, 2001; Alessi and Fein, 2010; Lalonde et al., 2010; Petrash et al., 2011; Liu et al., 2015), molecular-scale mechanistic studies of clay-Cd interactions are limited. The binding structure determines the stability of adsorbed Cd species and regulates the remobilization of the metal from clay surfaces when environmental conditions change (Takamatsu et al., 2006; Grafe et al., 2007; Malferrari et al., 2007; Sajidu et al., 2008; Vasconcelos et al., 2008; Du et al., 2016). Saijdu et al. (2008) studied Cd adsorption onto natural mixed clay minerals, and found that Cd is primarily bound as an outer-sphere complex which is octahedrally-coordinated by O (Sajidu et al., 2008). Grafe et al. (2007) and Du et al. (2017) revealed that Cd binding onto kaolinite and montmorillonite is also an outer-sphere complex coordinated by 6 O (oxygen) at around 2.2 Å from Cd (Grafe et al., 2007; Du et al., 2016). However, Takamatsu et al. (2006) analysed the local structure of the Cd-montmorillonite complex and found that Cd formed outer-sphere complexes in low pH environments, but formed surface precipitates at pH higher than 7.1 (Takamatsu et al., 2006). By

contrast, Vasconcelos et al. (2008) showed that Cd formed inner-sphere complexes with Al or Si on clay surfaces at high pH (Vasconcelos et al., 2008). As such, in this study, we tried to address the question of Cd adsorption behaviour onto clay surfaces and the corresponding local structure variations between freshwater conditions and marine conditions.

In this work, we tested variations in Cd affinity toward three clay minerals – kaolinite, illite and montmorillonite – as a function of increasing pH and ionic strength to determine whether clay minerals release or sequester Cd under marginal marine conditions. Surface complexation modelling (SCM) was conducted to provide a thermodynamic perspective on Cd adsorption under freshwater and marine conditions, while extended X-ray adsorption fine structure (EXAFS) analysis was performed on Cd-bearing-clay samples to constrain the local coordination environment of Cd.

5.2 Materials, experiments and methods

5.2.1 Clay minerals preparation

Samples of kaolinite (KGa-2), montmorillonite (SWy-2), and illite (IMt-2) were obtained from the Clay Mineral Society, Source Clays Repository (Purdue University, West Lafayette, USA). All clays were grounded to pass a 100-mesh sieve and washed by 0.01M HNO_3 to remove impurities. They were then washed three times by suspending 0.5 g of clay in 50 ml of 0.1 M sodium nitrate solution (ACS certified, Fisher Scientific) for 3 h and then centrifuged at 10,000 g for 20 min. After washing, clays were frozen to -20℃ for 12 h and then freeze dried.

5.2.2 Adsorption isotherms

Cadmium (Cd) was adsorbed onto the three clay minerals at different Cd initial concentrations (1 ppm, 5 ppm, 10 ppm, 20 ppm, 40 ppm, 60 ppm, 80 ppm) in order to construct Cd sorption isotherms. A 1000 ppm $CdCl_2$ stock solution was made by dissolving $CdCl_2$ salt (ACS certified, Fisher Scientific), after which Cd solutions of the above concentrations were prepared by diluting the 1000 ppm solution into polypropylene tubes to a total volume of 50 ml. A 0.01M NaCl solution was used during dilutions to buffer solution ionic strength. Inductively coupled plasma – mass spectrometry (ICP-MS; Agilent 8800) was used to precisely determine the initial Cd concentrations in these solutions (5ml of solution was pipetted). Finally, 45 mg of clay was added to each solution to make a 1g/L solid suspension. After agitation, the pH of each solution was adjusted to 6 by adding small aliquots of 0.1 M HCl and 0.1 M NaOH. Another set of adsorption isotherm using the same Cd concentration was performed at pH=8 and ionic strength=0.56M as NaCl. The solution pH was repeatedly adjusted during the adsorption period (24 h). Once equilibrium was reached, 5 ml of clay suspension was pipetted and filtered using a 0.2μm PTFE filter. The filtrate and initial 5 ml solution were acidified by 2% HNO_3 and 0.5% HCl solution for ICP-MS analysis.

5.2.3 The Cd behaviour under simulated estuary environments

To ascertain Cd behavior on clay surfaces when aqueous conditions change from freshwater to seawater (i.e., as clays are transported from land to the oceans), laboratory experiments were performed by simulating this transition between aqueous conditions and taking samples under both freshwater conditions and marine conditions. The entire marine conditions adsorption process took 2 days, with time intervals (at 0h, 1h, 2h, 4h, 8h, 12h, 1d, 2d) and solution pH was maintained at

pH=8. Thus, 400 mL of 0.01M NaCl solution was added into a 500 ml beaker, after which 0.4 mL of 1000 ppm $CdCl_2$ stock solution was added into the reaction beaker to result in a 1 ppm Cd solution. A magnetic stir bar kept the solution mixing at 240 rpm during the experimental period. During the experiments the reaction beaker was covered by Parafilm to prevent possible solution evaporation. Once well mixed, a 5 ml aliquot was taken for initial Cd concentration analysis. After that the solution pH was adjusted to 6 by adding small aliquots of 0.1 M HCl and 0.1 M NaOH to mimic freshwater conditions and 0.395 g of the target clay mineral were added into the beaker to make a 1 g/L clay suspension. The adsorption of Cd onto clays at freshwater conditions lasted 24 hours and the pH was maintained at 6 during this period. After 24 h, a final 5 ml aliquot was taken and filtered through a 0.2 μm PTFE, to determine the degree of Cd adsorption at freshwater conditions. Then, the solution pH was adjusted to 8 using aliquots of a 0.5 M NaOH solution, and 12.87 g of NaCl salt were added into the beaker to increase the IS to 0.56 M, representing marine conditions. Once the pH was stable, a 5 ml aliquot was sampled and filtered for Cd concentration analysis at t=0. All collected samples were acidified by 0.5% HCl and 2% HNO_3 prior to Cd analysis by ICP-MS.

5.2.4 pH edge experiments

Cadmium pH adsorption edge experiments were performed to understand how pH impacts Cd adsorption behavior. Initially 100 mL of 0.56 M NaCl was added to a 150 mL glass beaker and a solution Cd concentration of 1 ppm was achieved by adding a small volume of the 1000 ppm $CdCl_2$ stock solution. The resulting solution was stirred for 5 minutes before a 10 mL initial sample was taken. Then, 90 mg of the target clay was added to the Cd solution to create a 1 g/L slurry. During continuous agitation, 10 mL aliquots of the slurry were transferred to seven 15 mL polypropylene

test tubes. Following transfer, the individual test tubes were pH adjusted using small aliquots of 1 M, 0.1 M, and 0.01 M HCl and NaOH across a pH range of 3 to 9. Freshwater conditions pH edge experiments were performed in the same way, but the IS was instead buffered by a 0.01M NaCl solution.

5.2.5 Surface complexation modelling

Surface complexation modelling of Cd adsorption pH edge data was performed using the software FITEQL (4.0) (Westall, 1982). Surface protonation equations and corresponding constants and site concentrations were utilized from previous studies (Hao et al., 2018; Hao et al., 2019a). The system of equations to represent Cd adsorption include:

$$\equiv LH + Cd^{2+} \leftrightarrow \equiv LCd^{+} + H^{+} \quad \text{(R4.1)}$$

$$K_{LCd} = \frac{[\equiv LCd^{+}] \bullet \alpha_{H^{+}}}{[\equiv LH] \bullet \alpha_{Cd^{2+}}} \quad \text{(eq. 4.1)}$$

$$\equiv XOH + Cd^{2+} \leftrightarrow \equiv XOCd^{+} + H^{+} \quad \text{(R4.2)}$$

$$K_{XOCd} = \frac{[\equiv XOCd^{+}] \bullet \alpha_{H^{+}}}{[\equiv XOH] \bullet \alpha_{Cd^{2+}}} \quad \text{(eq. 4.2)}$$

Surface functional groups for the clays were assigned to one of two types: ≡LH or ≡XOH, which represent a permanently charged (i.e., structural) surface functional group (one that can only deprotonate) and an amphoteric surface functional group (representing Si-O and Al-OH groups), respectively (Barbier et al., 2000; Peacock and Sherman, 2005; Gu et al., 2010). Both non-electrostatic (NEM) and constant capacitance models (CCM) were applied to fit the experimental results. The specific modelling procedure and surface acidity constants of protonation-deprotonation reactions were taken from our previous study (Hao et al., 2019a). A Na exchange reaction was applied to the three clay minerals' ≡LH sites because the clay's interlayer has high

ion exchange capacity. The proton interaction constants of the IS=0.01 M condition and 0.56 M condition were extrapolated from our previous research (Hao et al., 2019a). Aqueous complexation constants for Cd hydrolysis and chlorine complexation were taken from Baes and Mesmer (1977) and then calibrated by the Davies equation and Debye-Hückel equation because of the difference between IS for river and marine conditions (Liu et al., 2018). The detailed input parameters are listed in Appendix 3 SI Table 3.1.

5.2.6 Synchrotron X-ray adsorption spectroscopy

Cadmium K-edge EXAFS spectra were measured at BL01B1 in SPring-8 (Hyogo, Japan). The white beam from a bending magnet was monochromatized by a Si(311) double crystal monochromator. Two Rh coated mirrors, placed above and downstream of the monochromator, were used for collimation and focusing of the X-ray beam. Harmonic rejection was achieved by adjusting the glancing angle of these two mirrors. The beam size was adjusted by slits to *ca.* 1 mm (V) × 6 mm (H) on the sample placed at 45° to the incident X-ray. Intensities of incident and transmission X-rays were monitored with ionization chambers up and downstream of the samples, and fluorescence X-rays were monitored with a 19-element Ge sold-state detector placed at 90° to the incident X-ray. The Cd K-edge EXAFS spectra for all the adsorbed clay samples were measured in fluorescence mode. The X-ray energy was calibrated with the first peak of CdO at 26.7159 keV.

EXAFS analyses were performed using REX2000 ver. 2.5 (Rigaku Co.). The background was removed from the raw spectra by a spline smoothing method, and E_0 was set at the edge inflection point for all of the studied samples. The $\chi(k)$ functions were extracted from the raw spectrum by a spline smoothing method. The Fourier transformation was performed to convert

$k^3\chi(k)$ oscillations from k space to r space in the range from 3.25 to 7.70 Å for all the samples. The inversely Fourier filtered $k^3\chi(k)$ spectra were analyzed with a curve-fitting method, where the theoretical backscattering amplitudes and phase-shift functions were calculated from the structure of $Cd(OH)_2$, $CdCl_2$, and $Cd_4(Al_8Si_8O_{32})(H_2O)_{17.35}$ using FEFF 8.5 (Partin and Okeeffe, 1991; Hemmingsen et al., 1999; Nery et al., 2003).

5.3 Results and discussion

5.3.1 Cd behavior on clay surfaces from river to ocean

The Cd adsorption isotherms show that the freshwater conditions have a higher degree of Cd binding than the marine conditions (Figure 5.1). At the maximum Cd concentrations used (80 ppm), kaolinite shows the smallest difference between the marine and freshwater conditions, with only 1.5 mg/g difference. Illite showed a 2 mg/g difference, while montmorillonite displayed the largest difference with more than 20 mg/g.

A Langmuir adsorption isotherm was applied to derive the maximum Cd adsorption capacity (Table 4.1) for three clay minerals by using the following equation:

$$\frac{C_e}{q_e} = \frac{1}{q_m K_L} + \frac{C_e}{q_m} \qquad \text{(eq. 4.3)}$$

where, C_e is the equilibrium concentration of Cd (mg/L), q_e is the amount of solute adsorbed per unit weight of sorbent (mg/g), q_m is the Langmuir constant which represents the saturated monolayer sorption capacity (mg/g), and K_L is the Langmuir constant. The maximum Cd adsorption capacity experienced a decreasing trend from freshwater to marine conditions (Table 4.1). This is especially significant for montmorillonite which decreased from 36.76 mg/g to 4.73 mg/g, while kaolinite and illite decreased from 2.31 mg/g to 1 mg/g, and 3.59 mg/g to 1.94 mg/g, respectively. In summary, the results of the Cd adsorption isotherms indicate that when clays are

transported from rivers to the ocean, the suppression effect of IS increase is more significant compared to the promotion effect due to the increase of solution pH. This then relates to differences between the 3 clays as follows: Illite has relative stronger surface electrostatic field compared to montmorillonite (Sposito et al., 1999), however, the swelling property of montmorillonite ensures a higher adsorption capacity compared to illite under freshwater. Then, when montmorillonite encounters marine conditions, it flocculates and releases a large portion of Cd from interlayer. We suggest that this may be the reason why Cd desorbed more significantly from montmorillonite surfaces once subjected to seawater conditions relative to illite.

The measured differences in adsorption provide further insights into how adsorbed Cd will behave when it encounters an estuary (Figure 5.2). In freshwater, the amount of Cd removed from solution onto the surfaces of montmorillonite and illite is between 40% to 50%. However, once the solution was changed to marine conditions, Cd adsorption immediately decreased to approximately 20%. Contrastingly, kaolinite shows minimal difference in Cd adsorption (i.e., 25-30% adsorption at both freshwater and marine conditions). This pattern is likely a consequence of the offset effect on Cd adsorption with increases in both pH and solution ionic strength. By comparison with illite and montmorillonite, kaolinite has less isomorphic substitution, thus the effect of suppressing Cd adsorption by attenuation of surface electrostatic field is relatively weaker. This likely explains why kaolinite shows little difference in terms of Cd adsorption via an increase in IS and pH, but illite and montmorillonite surface reactivity to Cd is significantly inhibited. It is worth noting that in our experimental results, the release of Cd at marine conditions is simply due to changes in clay surface reactivity because of variations in pH and IS. In reality, there will be competitive adsorption reactions (such as Pb, Ni, and Cu), dissolved organic matter (DOC) chelation and changes in redox conditions that could also influence Cd behaviour (Jiang et

al., 2010). As such, it is important to note that under marine conditions, the release of Cd from clay surfaces could be more complex due to various aqueous conditions.

5.3.2 Surface complexation modelling

The degree of adsorption of Cd onto the tested clay minerals increased with solution pH (Figure 5.3) as a result of increased deprotonation of functional groups and negative charge at the clay surfaces. Furthermore, the pH edge results show that Cd adsorption under marine conditions is significantly depressed as compared to freshwater conditions (Figure 5.3). Kaolinite shows the least difference amongst the three studied clays in Cd adsorption under marine ionic strength (99% adsorption at pH=9) compared to freshwater ionic strength (70% adsorption at pH=9). Cd adsorption onto illite is strongly suppressed at marine ionic strength, with only 32% adsorbed at marine IS and pH=9 compared to 98% adsorbed at freshwater ionic strength (pH=9). This behaviour is similar to montmorillonite, showing 95% adsorption at pH=9, IS=0.01M and 40% adsorption at pH=9, IS=0.56 M. This Cd behaviour difference between kaolinite and illite, montmorillonite can be explained by multiple impact of pH and IS to surface protonation and electrostatic field that discussed above.

NEM and CCM surface complexation models show little difference for the fitting of Cd adsorption data (Figure 5.3), indicating that both models can successfully predict Cd adsorption behaviour. The modelled montmorillonite adsorption shows minimal deviation compared to experimental data, which may be attributed to the swelling property that can accommodate more Cd in the interlayer. Detailed modelling procedure including input parameters and output results are provided in Appendix 3.

Cd speciation diagrams at freshwater and marine IS were calculated based on the SCM results (Figure 5.4). Compared to freshwater conditions, Cd was significantly mobilized by Cl in seawater, resulting in less Cd adsorption. This is an additional mechanism of Cd release from clay surfaces, although the attenuation of surface electrostatic field influences clay surface reactivity as well. The surface species ≡XOCd is dominant for kaolinite under freshwater conditions, while ≡LCd is the primary species under marine conditions. By contrast, montmorillonite and illite both have ≡LCd as the predominant species at low pH, but this species concentration as both pH and the concentration of ≡XOCd correspondingly increase. In summary, the collective results of modeling indicate Cd adsorption onto illite and montmorillonite is dominated by the ≡LH group under freshwater conditions, while under marine conditions the ≡XOH group becomes the main functional group for Cd adsorption. The distribution of Cd onto kaolinite surfaces shows the opposite trend.

5.3.4 Coordination of Cd at clay mineral surfaces

Figure 5.5A and B show the fitting of k^3-weighted χ(k) spectra of Cd K-edge EXAFS data and their Flourier transformations for a series of the samples, respectively. The first peaks of K-space spectra show that the freshwater conditions samples for all three clays were narrower than the marine conditions samples. This pattern is also evident in the R-space spectra where the first oscillation was broader and more flat in marine samples compared to freshwater samples. This phenomenon may be attributed to the distorted structure when forming inner-sphere complex. We then applied Cd-O, Cd-Cl, Cd-Al, Cd-Si, Cd-Cd distances to the experimental spectra, and the Cd-O and Cd-Al bonds ended up better simulating the sample spectra. The spectra of Cd bound to the three clay minerals under freshwater conditions are dominated by one Cd-O frequency with a

coordination number (CN) around 6 Å at approximately 2.27 Å (Table 4.2). This corresponds to a Cd hydration sphere where 6 water molecules hydrate the Cd^{2+} aqueous ions, indicating that Cd dominantly forms an outer-sphere complex under freshwater conditions. However, under marine conditions, a second shell of Cd-Al appears for all three clay minerals at R+ΔR =3.12-3.35 Å. This can be attributed to the formation of an inner-sphere complex that has a higher affinity to ≡AlOH functional groups at high ionic strength conditions, whereas Cd bound to the surface as outer-sphere complexes desorbs from the clay surfaces. Meanwhile, the collapse of clay interlayer due to increase of IS could decrease the amount of outer-sphere binding of Cd, and then result in the inner-sphere form on Al adsorption sites. In previous studies conducted by Takamatsu et al. (2006) and Vasconcelos et al. (2008), Cd inner-sphere complexes onto clay surfaces were observed at high pH compared to outer-sphere complex at low pH (Takamatsu et al., 2006; Vasconcelos et al., 2008), which corroborates our results of inner-sphere complexes preferentially existing under marine conditions.

In seawater, the coordination number of Cd on Al site is around 1 for illite, with a bonding distance of 3.35 Å. This indicates a monodentate edge sharing coordination environment. The Al-OH bonding distance in Al-octahedron is around 2 Å, while Cd-O is 2.3 Å. Through edge sharing, there might be distortion in the Cd octahedron leading to a longer bonding distance around 3.35 Å. By contrast, kaolinite and montmorillonite have a coordination number around 2, and a distance around 3.1 Å. This corresponds to a bidentate plane sharing where the Cd octahedron shares three oxygens from two Al octahedrons. Each Al-octahedron provides apex oxygen with Cd and the third oxygen is shared between the two Al octahedrons. Our bonding distance corresponds to previous studies of which corresponds to Cd-exchanged zeolites with a distance of approximately 3.1-3.3 Å (Choi et al., 2002; Nery et al., 2003). At present it is unclear to us why illite shows

monodentate bonding environment compared to bidentate bonding on kaolinite and montmorillonite surfaces. Perhaps it is a consequence of illite having more surface charge (relative to kaolinite) and is non-swelling (relative to montmorillonite). Moreover, illite interlayer spaces are saturated by larger cations such as K^+ compared to montmorillonite and kaolinite which both have relatively larger interlayer space.

A proposed molecular model of Cd adsorption is illustrated in Figure 5.6. Edge site adsorption was observed for Cd binding onto clay surfaces under marine conditions based on the EXAFS results. Previous research shows that at high IS and pH conditions, trace elemental adsorption (e.g., Cu and U) tends to transfer from basal sites to edge sites (Morton et al., 2001; Catalano and Brown, 2005) due to their high energy and unsaturated bonding. This is a consequence of greater electrostatic attraction of cations at low IS conditions as compared to high IS where the electric field is attenuated (Hao et al., 2019a). At the same time, elevated pH in the marine experiments promotes edge site deprotonation, which provides more Al sites for Cd adsorption. The preferential adsorption of Cd to Al sites may partially explain why kaolinite shows less Cd desorption from river to marine conditions, since kaolinite, a 1:1 clay with exposed Al-octahedral sheets, provides more Al octahedrons as adsorption sites. It is interesting that Cd-Cl complex adsorption was not detected in our experimental conditions even at the 0.56M Cl^- concentration, indicating that Cd-Cl complexes are not strongly adsorbed to clays under marine conditions.

5.4 Conclusions

The Cd adsorption experimental results indicate that Cd can be released from clay surfaces in estuaries due to higher ionic strength, despite increased pH.. Furthermore, these variations

influence clay surface properties, directly impacting the local binding environment of Cd at the various clay surfaces. For instance, we found that 20-30% of adsorbed Cd can be released as free cations from illite and montmorillonite, while kaolinite shows little Cd release.

A compilation of Cd concentration in suspended sediments is provided for rivers worldwide (Table 4.3). Although the sampling season, method and location varies, there is clear trend that Cd concentration in sediments decreases from rivers to the ocean (an exception for the Seine River which has higher Cd concentration on suspended sediments of estuary). The collective results confirm what we observe in the experimental study, that trace metals such as Cd are liberated from clays as they reach estuaries and the open ocean.

The potential release of Cd from suspended clay minerals during this environmental transition could be significant because the annual discharge of suspended particles to the oceans is around 15 Gt per year (Viers et al., 2009), with the <2μm size fraction accounting for an estimated 10-50 weight % of those suspended particles (Ongley et al., 1981; Walling and Moorehead, 1989); although in some rivers clay minerals contribute more than 90% of the <2 μm size fraction (Zhao et al., 2018b). In terms of clay mineral composition in river suspended sediments, this varies substantially depending on source terrain, with for example the Amazon River and the Minjiang River having clays dominated by kaolinite (Eisma et al., 1978; Feng et al., 2014), while the Yangtze River and the Wadden sea estuary have clays dominated by illite and montmorillonite (Uncles et al., 2006; Griffioen et al., 2016; Zhao et al., 2018b). Even though there is paucity of compositional data for rivers worldwide, clay compositions in suspended sediments of 62% illite, 6% montmorillonite, and 11% kaolinite can be derived. Cadmium concentrations under river or marine are generally in ppb level, based on our SCM results, it is predicted that around 54% , 8%, and 24% of Cd can be released from montmorillonite, kaolinite, and illite surface, respectively, if

we assume 1ppb of total Cd in river reservoir (dissolved as free ions plus adsorbed on suspended sediments). Applying the average suspended clay composition and the smallest of the above mentioned fractions of clay in river suspended sediments (10%), the total discharge of clay into estuaries is 1.35 Gt. This translates into an annual contribution of 256.5t of Cd to the oceans.

It is also worth speculating on the relationship between the release of Cd from clay minerals and flocculation. Although flocculation occurs throughout the range of oligohaline to mixohaline environments (Sutherland et al., 2015). Sutherland et al. (2015) studies in modern estuaries show that Na-facilitated ionic bridging can lead to intense flocculation at salinities as low as 1 ppt and a significant volume of the clay minerals may well be removed before salinities exceed 5 ppt. As such flocculation of clay minerals and the release of Cd are not surprisingly linked. As Cd is outcompeted by Na and released, flocculation rates increase. This relationship suggests that flocculated clays in estuarine muds should predictably increase landwards and seawards from what is commonly referred to as the turbidity maximum. What is unclear is how the competition for clay surface sites for ionic bridging is influenced by the surface chemistry of clays arriving with fluvial waters into estuaries and deltas influences the kinetics of flocculation.

5.5 References

Alessi, D.S., Fein, J.B., 2010. Cadmium adsorption to mixtures of soil components: Testing the component additivity approach. Chemical Geology, 270(1): 186-195.

Baes, C.F., Mesmer, R.S., 1977. The Hydrolysis of Cations. John Wiley & Sons, New York, London, Sydney, Toronto 1976. 489 Seiten, Preis: £ 18.60. Berichte der Bunsengesellschaft für physikalische Chemie, 81(2): 245-246.

Baeyens, B., Bradbury, M.H., 1997. A mechanistic description of Ni and Zn sorption on Na-

montmorillonite .1. Titration and sorption measurements. Journal of Contaminant Hydrology, 27(3-4): 199-222.

Barbier, F., Duc, G., Petit-Ramel, M., 2000. Adsorption of lead and cadmium ions from aqueous solution to the montmorillonite/water interface. Colloids and Surfaces A: Physicochemical and Engineering Aspects, 166(1–3): 153-159.

Brack, A., 2013. Chapter 10.4 - Clay Minerals and the Origin of Life. In: Bergaya, F., Lagaly, G. (Eds.), Developments in Clay Science. Elsevier, pp. 507-521.

Bradbury, M.H., Baeyens, B., 2002. Sorption of Eu on Na- and Ca-montmorillonites: Experimental investigations and modelling with cation exchange and surface complexation. Geochimica et Cosmochimica Acta, 66(13): 2325-2334.

Bradbury, M.H., Baeyens, B., 2009. Sorption modelling on illite Part I: Titration measurements and the sorption of Ni, Co, Eu and Sn. Geochimica et Cosmochimica Acta, 73(4): 990-1003.

Catalano, J.G., Brown, G.E., 2005. Uranyl adsorption onto montmorillonite: Evaluation of binding sites and carbonate complexation. Geochimica et Cosmochimica Acta, 69(12): 2995-3005.

Chiffoleau, J.-F., Cossa, D., Auger, D., Truquet, I., 1994. Trace metal distribution, partition and fluxes in the Seine estuary (France) in low discharge regime. Marine Chemistry, 47(2): 145-158.

Choi, E.Y., Lee, S.H., Kim, Y., Han, Y.W., Seff, K., 2002. Crystal structure of a cadmium sorption complex of dehydrated fully Cd2+-exchanged zeolite X containing Cd2+, Cd+, and Cd-0. Journal of Physical Chemistry B, 106(30): 7569-7573.

da Fonseca, M.G., de Oliveira, M.M., Arakaki, L.N., 2006. Removal of cadmium, zinc, manganese and chromium cations from aqueous solution by a clay mineral. Journal of Hazardous

Materials, 137(1): 288-292.

Du, H.H., Chen, W.L., Cai, P., Rong, X.M., Dai, K., Peacock, C.L. et al., 2016. Cd(II) Sorption on Montmorillonite-Humic acid-Bacteria Composites. Scientific Reports, 6.

Eisma, D., Van Der Gaast, S.J., Martin, J.M., Thomas, A.J., 1978. Suspended matter and bottom deposits of the Orinoco delta: Turbidity, mineralogy and elementary composition. Netherlands Journal of Sea Research, 12(2): 224-251.

El-Bouraie, M., El-Barbary, A., Yehia, M., Motawea, E., 2010. Heavy metal concentrations in surface river water and bed sediments at Nile Delta in Egypt. Suo, 61(1): 1-12.

Elshanawany, R., Ibrahim, M.I., Frihy, O., Abodia, M., 2018. Foraminiferal evidence of anthropogenic pollution along the Nile Delta coast. Environmental earth sciences, 77(12): 444.

Feng, H., Gao, A., Zhu, X., Wang, W., Ni, G., Peng, J., 2014. Distribution characteristic of clay minerals contents in Minjiang River and its environmental significance. Journal of Applied Oceanography, 33(3): 418-424.

Gibbs, R.J., 1967. The geochemistry of the Amazon River system: Part I. The factors that control the salinity and the composition and concentration of the suspended solids. Geological Society of America Bulletin, 78(10): 1203-1232.

Grafe, M., Singh, B., Balasubramanian, M., 2007. Surface speciation of Cd(II) and Pb(II) on kaolinite by XAFS spectroscopy. Journal of Colloid and Interface Science, 315(1): 21-32.

Griffioen, J., Klaver, G., Westerhoff, W., 2016. The mineralogy of suspended matter, fresh and Cenozoic sediments in the fluvio-deltaic Rhine–Meuse–Scheldt–Ems area, the Netherlands: An overview and review. Netherlands Journal of Geosciences, 95(1): 23-107.

Gu, X., Evans, L.J., 2007. Modelling the adsorption of Cd(II), Cu(II), Ni(II), Pb(II), and Zn(II)

onto Fithian illite. Journal of colloid and interface science, 307(2): 317-25.

Gu, X., Evans, L.J., 2008. Surface complexation modelling of Cd(II), Cu(II), Ni(II), Pb(II) and Zn(II) adsorption onto kaolinite. Geochimica et Cosmochimica Acta, 72(2): 267-276.

Gu, X., Evans, L.J., Barabash, S.J., 2010. Modeling the adsorption of Cd (II), Cu (II), Ni (II), Pb (II) and Zn (II) onto montmorillonite. Geochimica et Cosmochimica Acta, 74(20): 5718-5728.

Hao, W., Flynn, S.L., Alessi, D.S., Konhauser, K.O., 2018. Change of the point of zero net proton charge (pHPZNPC) of clay minerals with ionic strength. Chemical Geology, 493: 458-467.

Hao, W., Flynn, S.L., Kashiwabara, T., Alam, M.S., Bandara, S., Swaren, L. et al., 2019a. The impact of ionic strength on the proton reactivity of clay minerals. Chemical Geology: 119294.

Hao, W., Pudasainee, D., Gupta, R., Kashiwabara, T., Alessi, D.S., Konhauser, K.O., 2019b. Effect of acidic conditions on surface properties and metal binding capacity of clay minerals. ACS Earth and Space Chemistry.

Hemmingsen, L., Bauer, R., Bjerrum, M.J., Schwarz, K., Blaha, P., Andersen, P., 1999. Structure, chemical bonding, and nuclear quadrupole interactions of beta-Cd(OH)(2): Experiment and first principles calculations. Inorganic Chemistry, 38(12): 2860-2867.

Hu, G., Bi, S., Xu, G., Zhang, Y., Mei, X., Li, A., 2015. Distribution and assessment of heavy metals off the Changjiang River mouth and adjacent area during the past century and the relationship of the heavy metals with anthropogenic activity. Marine pollution bulletin, 96(1-2): 434-440.

Huang, W., Zhang, J., Zhou, Z., 1992. Particulate element inventory of the Huanghe (Yellow River): A large, high-turbidity river. Geochimica et Cosmochimica Acta, 56(10): 3669-3680.

Jiang, M.-q., Jin, X.-y., Lu, X.-Q., Chen, Z.-l., 2010. Adsorption of Pb(II), Cd(II), Ni(II) and Cu(II) onto natural kaolinite clay. Desalination, 252(1): 33-39.

Johnson, C.R., Hopf, J., Shrout, J.D., Fein, J.B., 2019. Testing the component additivity approach to surface complexation modeling using a novel cadmium-specific fluorescent probe technique. Journal of Colloid and Interface Science, 534: 683-694.

Lackovic, K., Angove, M.J., Wells, J.D., Johnson, B.B., 2003. Modeling the adsorption of Cd(II) onto Muloorina illite and related clay minerals. Journal of Colloid and Interface Science, 257(1): 31-40.

Lalonde, S.V., Dafoe, L.T., Pemberton, S.G., Gingras, M.K., Konhauser, K.O., 2010. Investigating the geochemical impact of burrowing animals: Proton and cadmium adsorption onto the mucus lining of Terebellid polychaete worms. Chemical Geology, 271(1-2): 44-51.

Liu, Y., Alessi, D.S., Flynn, S.L., Alam, M.S., Hao, W., Gingras, M. et al., 2018. Acid-base properties of kaolinite, montmorillonite and illite at marine ionic strength. Chemical Geology, 483: 191-200.

Liu, Y.X., Alessi, D.S., Owttrim, G.W., Petrash, D.A., Mloszewska, A.M., Lalonde, S.V. et al., 2015. Cell surface reactivity of Synechococcus sp PCC 7002: Implications for metal sorption from seawater. Geochimica et Cosmochimica Acta, 169: 30-44.

Malferrari, D., Brigatti, M.F., Laurora, A., Pini, S., Medici, L., 2007. Sorption kinetics and chemical forms of Cd(II) sorbed by thiol-functionalized 2 : 1 clay minerals. Journal of Hazardous Materials, 143(1-2): 73-81.

Morton, J.D., Semrau, J.D., Hayes, K.F., 2001. An X-ray absorption spectroscopy study of the structure and reversibility of copper adsorbed to montmorillonite clay. Geochimica et Cosmochimica Acta, 65(16): 2709-2722.

Nery, J.G., Mascarenhas, Y.P., Cheetham, A.K., 2003. A study of the highly crystalline, low-silica, fully hydrated zeolite P ion exchanged with (Mn2+, Cd2+, Pb2+, Sr2+, Ba2+) cations. Microporous and mesoporous materials, 57(3): 229-248.

Ongley, E., Bynoe, M., Percival, J., 1981. Physical and geochemical characteristics of suspended solids, Wilton Creek, Ontario. Canadian Journal of Earth Sciences, 18(8): 1365-1379.

Osman, A.G., Kloas, W., 2010. Water quality and heavy metal monitoring in water, sediments, and tissues of the African Catfish Clarias gariepinus (Burchell, 1822) from the River Nile, Egypt. Journal of Environmental Protection, 1(4): 389-400.

Partin, D.E., Okeeffe, M., 1991. The Structures and Crystal-Chemistry of Magnesium-Chloride and Cadmium Chloride. Journal of Solid State Chemistry, 95(1): 176-183.

Peacock, C.L., Sherman, D.M., 2005. Surface complexation model for multisite adsorption of copper(II) onto kaolinite. Geochimica et Cosmochimica Acta, 69(15): 3733-3745.

Petersen, K., Kristensen, E., Bjerregaard, P., 1998. Influence of bioturbating animals on flux of cadmium into estuarine sediment. Marine Environmental Research, 45(4): 403-415.

Petrash, D.A., Lalonde, S.V., Raudsepp, M., Konhauser, K.O., 2011. Assessing the Importance of Organic Matrix Materials in Biofilm Chemical Reactivity: Insights from Proton and Cadmium Adsorption onto the Commercially Available Biopolymer Alginate. Geomicrobiology Journal, 28(3): 266-273.

Presley, B., Trefry, J., Shokes, R., 1980. Heavy metal inputs to Mississippi Delta sediments. Water, Air, and Soil Pollution, 13(4): 481-494.

Sajidu, S.M.I., Persson, I., Masamba, W.R.L., Henry, E.M.T., 2008. Mechanisms of heavy metal sorption on alkaline clays from Tundulu in Malawi as determined by EXAFS. Journal of Hazardous Materials, 158(2-3): 401-409.

Sposito, G., Skipper, N.T., Sutton, R., Park, S.-h., Soper, A.K., Greathouse, J.A., 1999. Surface geochemistry of the clay minerals. Proceedings of the National Academy of Sciences, 96(7): 3358.

Srour, R.K., Mcdonald, L.M., 2005. Effect of alcohols on the retention mechanisms of Cd and Zn on Wyoming bentonite and illite. Environmental science & technology, 39(18): 7111-7117.

Sutherland, B.R., Barrett, K.J., Gingras, M.K., 2015. Clay settling in fresh and salt water. Environmental Fluid Mechanics, 15(1): 147-160.

Takamatsu, R., Asakura, K., Chun, W.J., Miyazaki, T., Nakano, M., 2006. EXAFS studies about the sorption of cadmium ions on montmorillonite. Chemistry Letters, 35(2): 224-225.

Trefry, J.H., Presley, B.J., 1976. Heavy metals in sediments from San Antonio Bay and the northwest Gulf of Mexico. Environmental Geology, 1(5): 283-294.

Uncles, R.J., Stephens, J.A., Harris, C., 2006. Properties of suspended sediment in the estuarine turbidity maximum of the highly turbid Humber Estuary system, UK. Ocean Dynamics, 56(3): 235-247.

Vasconcelos, I.F., Haack, E.A., Maurice, P.A., Bunker, B.A., 2008. EXAFS analysis of cadmium(II) adsorption to kaolinite. Chemical Geology, 249(3-4): 237-249.

Viers, J., Dupré, B., Gaillardet, J., 2009. Chemical composition of suspended sediments in World Rivers: New insights from a new database. Science of The Total Environment, 407(2): 853-868.

Walling, D.E., Moorehead, P.W., 1989. The particle size characteristics of fluvial suspended sediment: an overview. In: Sly, P.G., Hart, B.T. (Editors), Sediment/Water Interactions. Springer Netherlands, Dordrecht, pp. 125-149.

Wang, Y., Liu, R.-h., Zhang, Y.-q., Cui, X.-q., Tang, A.-k., Zhang, L.-j., 2016. Transport of heavy

metals in the Huanghe River estuary, China. Environmental Earth Sciences, 75(4): 288.

Westall, J.C., 1982. FITEQL: A Computer Program for Determination of Chemical Equilibrium Constants from Experimental Data. Department of Chemistry, Oregon State University.

Yang, Z., Xia, X., Wang, Y., Ji, J., Wang, D., Hou, Q. et al., 2014. Dissolved and particulate partitioning of trace elements and their spatial–temporal distribution in the Changjiang River. Journal of Geochemical Exploration, 145: 114-123.

Ye, F., Huang, X., Zhang, D., Tian, L., Zeng, Y., 2012. Distribution of heavy metals in sediments of the Pearl River Estuary, Southern China: implications for sources and historical changes. Journal of Environmental sciences, 24(4): 579-588.

Yee, N., Fein, J., 2001. Cd adsorption onto bacterial surfaces: A universal adsorption edge? Geochimica et Cosmochimica Acta, 65(13): 2037-2042.

Yin, S., Wu, Y., Xu, W., Li, Y., Shen, Z., Feng, C., 2016. Contribution of the upper river, the estuarine region, and the adjacent sea to the heavy metal pollution in the Yangtze Estuary. Chemosphere, 155: 564-572.

Zhao, G., Ye, S., Yuan, H., Ding, X., Wang, J., 2017. Surface sediment properties and heavy metal pollution assessment in the Pearl River Estuary, China. Environmental Science and Pollution Research, 24(3): 2966-2979.

Zhao, G., Ye, S., Yuan, H., Ding, X., Wang, J., Laws, E.A., 2018a. Surface sediment properties and heavy metal contamination assessment in river sediments of the Pearl River Delta, China. Marine pollution bulletin, 136: 300-308.

Zhao, Y., Zou, X., Gao, J., Wang, C., Li, Y., Yao, Y. et al., 2018b. Clay mineralogy and source-to-sink transport processes of Changjiang River sediments in the estuarine and inner shelf areas of the East China Sea. Journal of Asian Earth Sciences, 152: 91-102.

Zhou, W., Ren, L., Zhu, L., 2017. Reducement of cadmium adsorption on clay minerals by the presence of dissolved organic matter from animal manure. Environmental Pollution, 223: 247-254.

Table 5.1: Maximum Cd adsorption onto three clay minerals at freshwater and marine conditions.

Unit (mg/g)	Freshwater	Seawater
Kaolinite	2.31	1.00
Illite	3.59	1.94
Montmorillonite	36.76	4.73

Table 5.2: Structural parameters of Cd adsorption onto three clay minerals at river and marine conditions.

	Shell	CN	R (Å)	dE (eV)	δ^2 (Å^2)	R factor (%)
Kao river	Cd-O	6.6	2.28	3.5	0.009	0.63
Illite river	Cd-O	6.0	2.27	3.0	0.008	1.50
Mont river	Cd-O	6.8	2.27	1.6	0.008	0.65
Kao marine	Cd-O	5.5	2.27	4.9	0.010	0.07
	Cd-Al	2.5	3.16	4.9	0.010	
Illite marine	Cd-O	5.6	2.29	5.4	0.010	0.36
	Cd-Al	1.5	3.35	5.4	0.009	
Mont marine	Cd-O	6.0	2.26	4.8	0.010	2.37
	Cd-Al	2.1	3.16	4.8	0.009	

Table 5.3: A compilation of Cd concentration in suspended sediments (μg/g).

	River	Estuary	Ocean	River	Estuary	Ocean
Huanghe	0.39	0.11	0.02	Huang et al., 1992	Wang et al., 2016	Wang et al., 2016
Yangtze River	4.73	0.03	0.09	Yang et al., 2014	Yin et al., 2016	Hu et al., 2015
Pearl River	0.84	0.46	0.29	Zhao et al., 2018a	Zhao et al., 2017	Ye et al., 2012
Mississippi River	1.3	1.5	0.3	Presley et al., 1980	Presley et al., 1980	Trefry and Presley, 1976
Seine River	2.47	6.18	2.25	Chiffoleau et al., 1994	Chiffoleau et al., 1994	Chiffoleau et al., 1994
Neil River	1.17	0.23	0.49	EI-Bouraie et al., 2010	Osman and Kloas, 2010	Elshanawany et al., 2018

Ref: Trefry and Presley, 1976; Presley et al., 1980; Huang et al., 1992; Chiffoleau et al., 1994; El-Bouraie et al., 2010; Osman and Kloas, 2010; Ye et al., 2012; Yang et al., 2014; Hu et al., 2015; Wang et al., 2016; Yin et al., 2016; Zhao et al., 2017; Elshanawany et al., 2018; Zhao et al., 2018a.

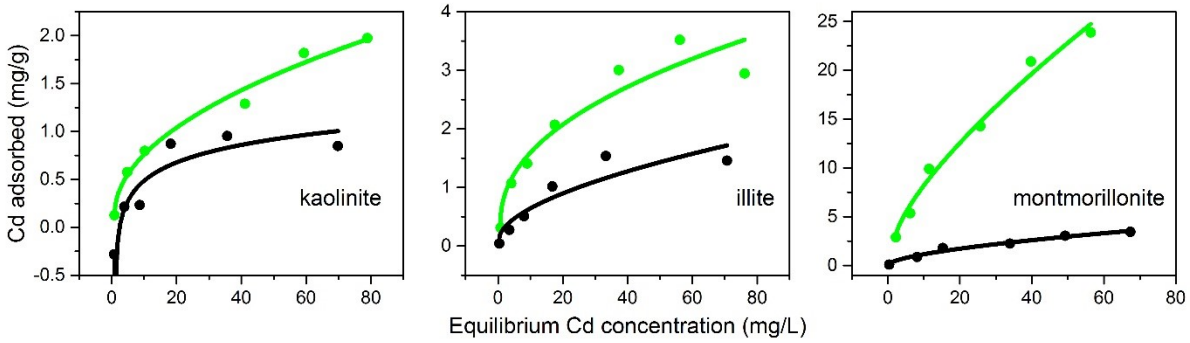

Figure 5.1 Comparison of Cd adsorption onto three tested clay minerals at freshwater (green) and marine (black) conditions. Filled circles are experimental adsorption data; curves are Langmuir model fits.

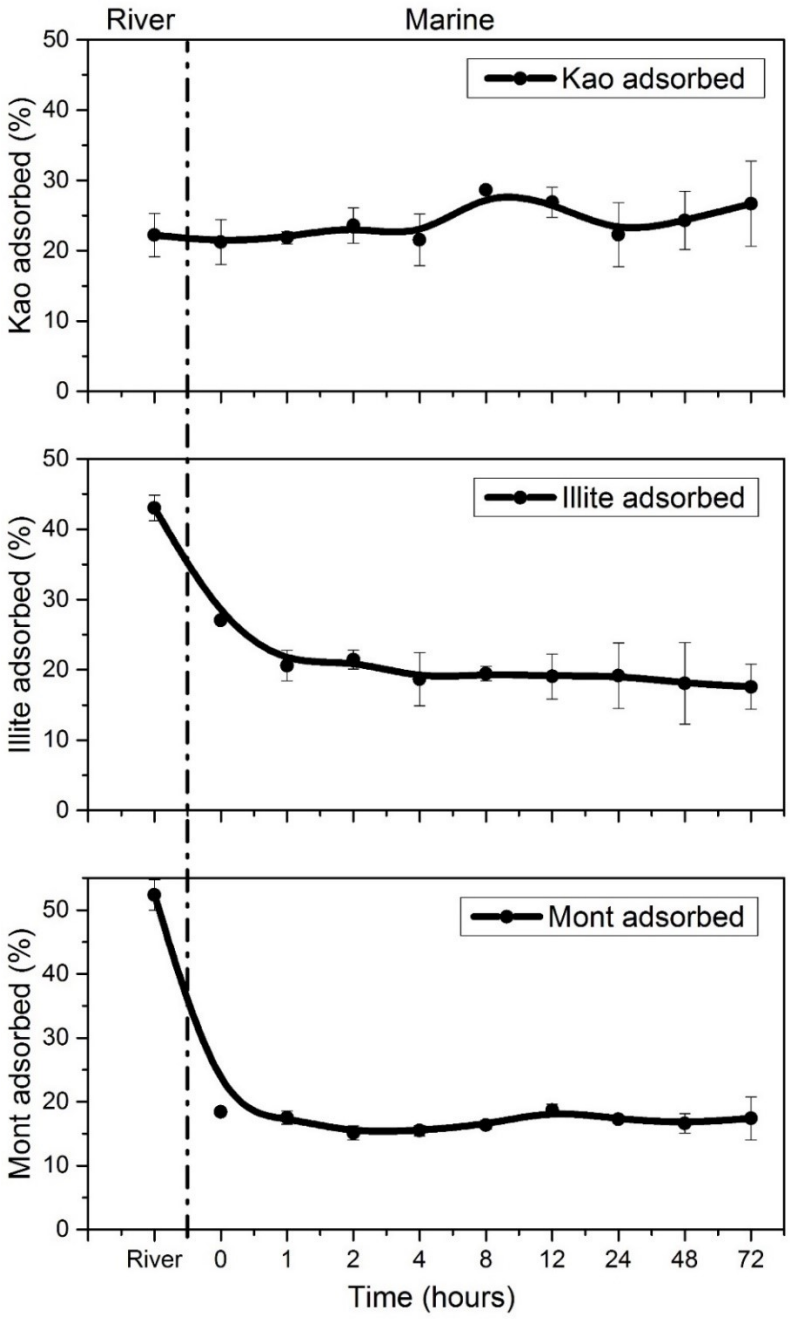

Figure 5.2 Adsorption of Cd onto three tested clay minerals as a function of changing aqueous conditions from freshwater to seawater. The area left of the dashed line represents the amount of Cd adsorbed under freshwater conditions; the area right of the dashed line represents Cd adsorbed at marine condition as a function of time after changing to marine condition (i.e., pH increases to 8 and ionic strength increases to 0.56 M).

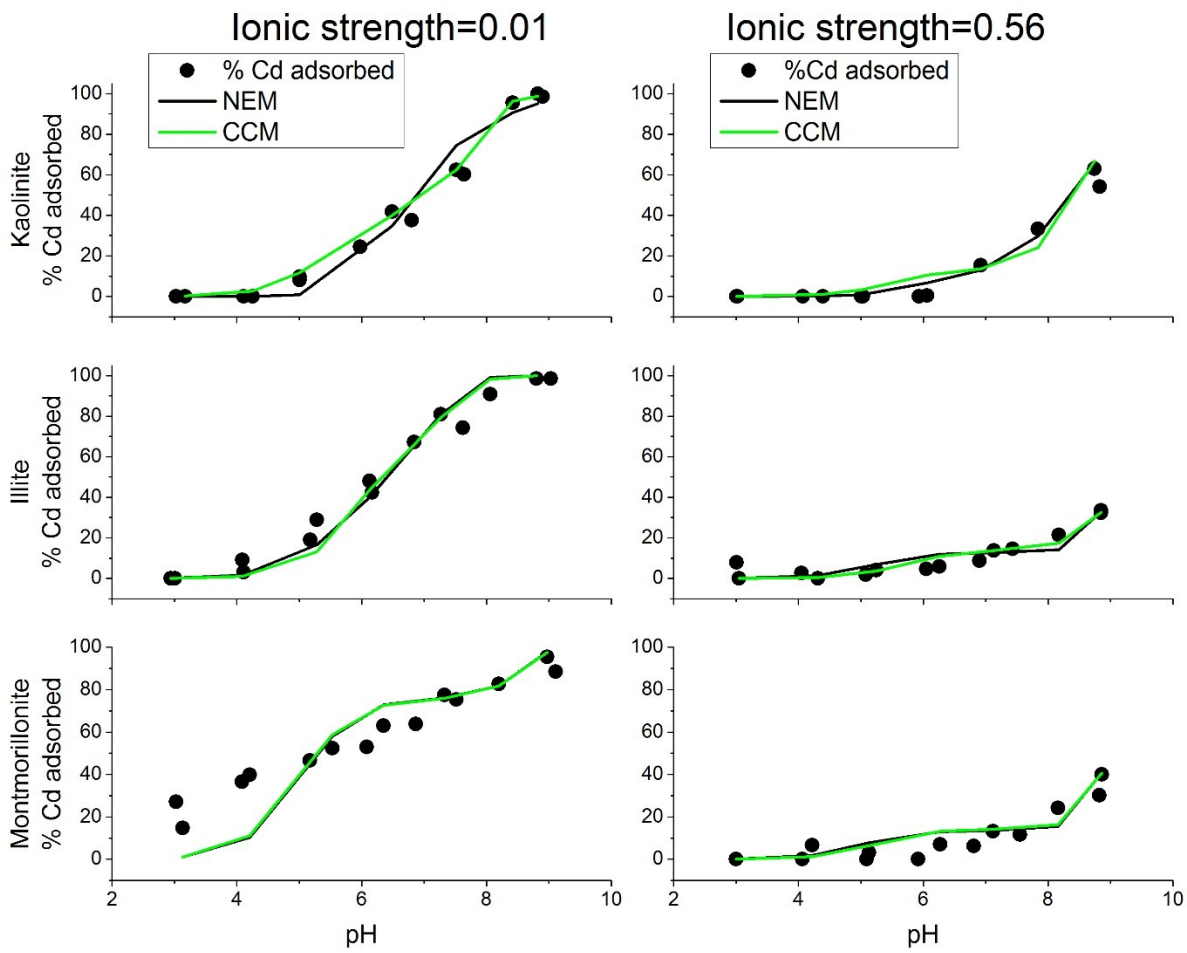

Figure 5.3 Cd pH adsorption edge and the fitting of experimental data by non-electrostatic and constant capacitance surface complexation models.

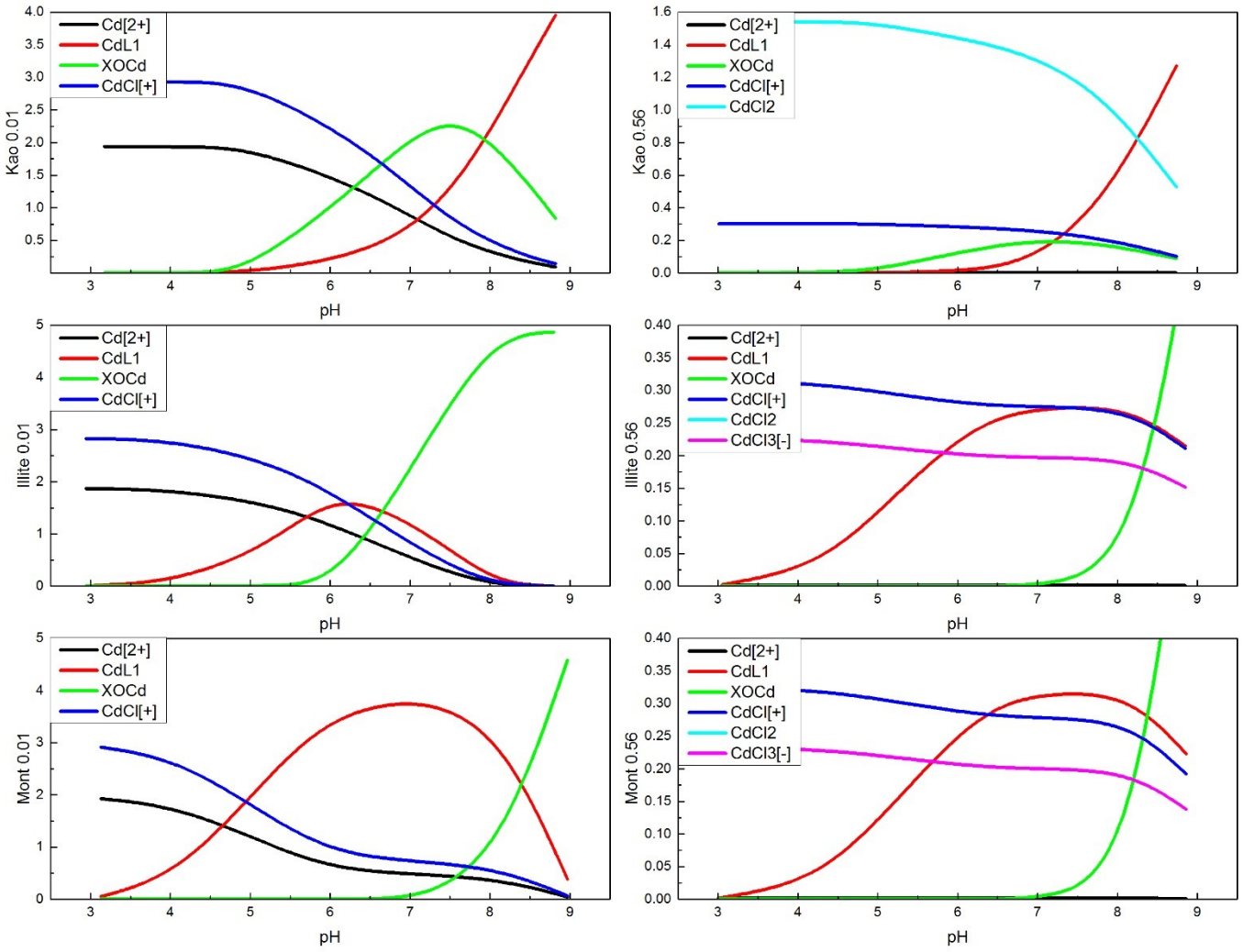

Figure 5.4 Cd speciation diagram as a function of pH under freshwater and marine conditions

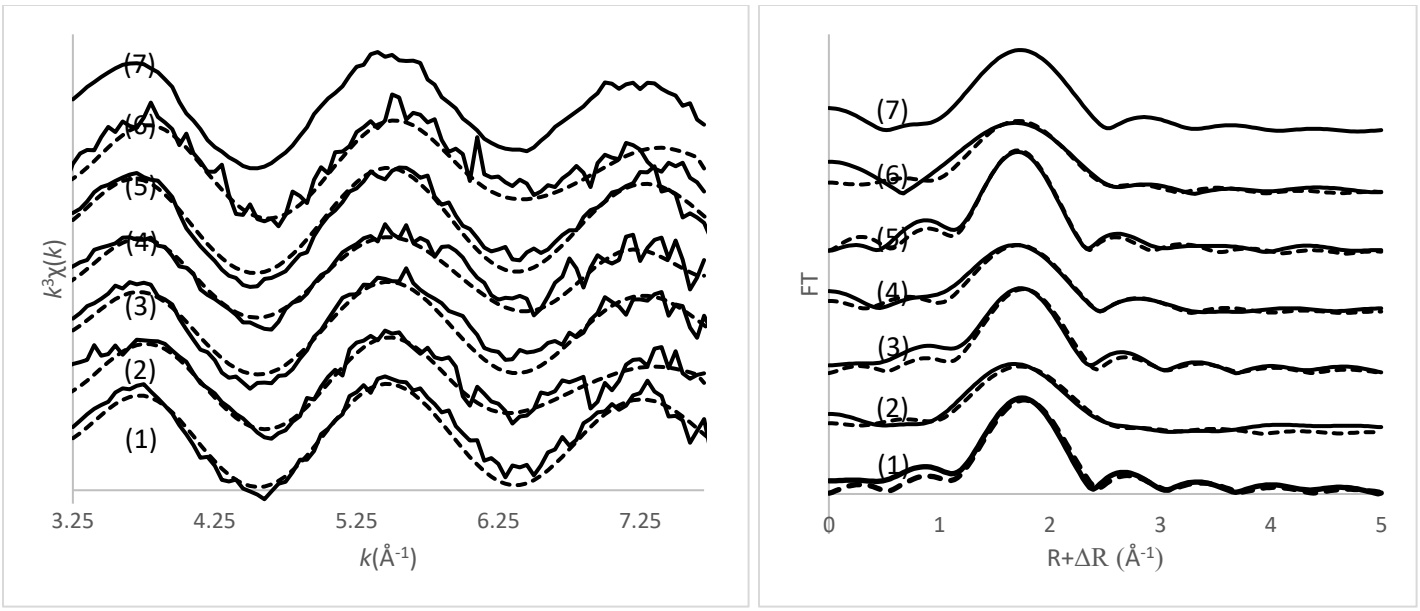

Figure 5.5 EXAFS analyses of Cd adsorption onto three clay minerals under freshwater and marine conditions. The numbers represent: (1) kaolinite in river; (2) kaolinite in seawater; (3) illite in river; (4) illite in seawater; (5) montmorillonite in river; (6) montmorillonite in seawater; (7) $CdCl_2$ aqueous solution.

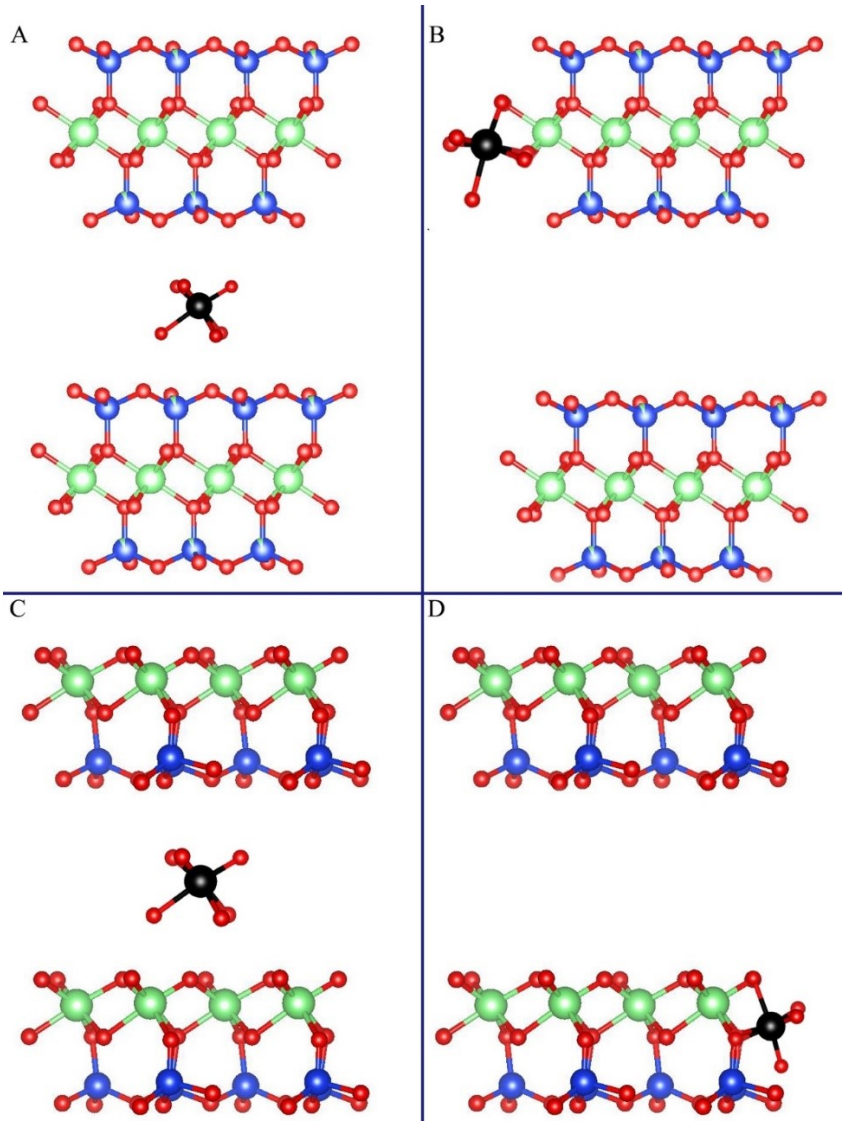

Figure 5.6 Molecular model of Cd adsorption onto clay minerals. (A) outer-sphere complexation of Cd onto 2:1 layer clays (e.g., Cd adsorption onto illite or montmorillonite under riverine conditions); (B) inner-sphere complexation of Cd onto 2:1 layered clays (e.g., Cd adsorption onto illite or montmorillonite under marine conditions); (C) outer-sphere complexation of Cd onto 1:1 layer clays (e.g., Cd adsorption onto kaolinite under riverine conditions); and (D) inner-sphere complexation of Cd onto 1:1 layer clays (e.g., Cd adsorption onto kaolinite under marine conditions). Black, red, blue and green balls represent Cd, O, Si, and Al, respectively.

Chapter 6. The kaolinite shuttle: A mechanistic link between the Great Oxidation Event and Earth's largest carbon burial event[5]

6.1 Introduction

The Lomagundi Event (LE) is the most pronounced and long-lived positive carbon isotope excursion in Earth history. Marine carbonate rocks deposited during the LE, which lasted at least 160 million years, are characterized by $\delta^{13}C_{carb}$ values as high as +10 to +15‰ (Bekker et al., 2003; Karhu and Holland, 1996; Melezhik et al., 1999; Schidlowski et al., 1976). The most widely accepted explanation for the LE relies on significant perturbation in the balance of different C burial fluxes—since organic C (C_{org}) is depleted in ^{13}C, an increase in C_{org} burial compared to carbonate burial will result in the ^{13}C-enrichment of the dissolved marine carbonate pool (Karhu and Holland, 1996). Higher rates of primary productivity in the oceans are implicated in this increase in C_{org} burial, and were likely the result of enhanced nutrient supply resulting from the Great Oxidation Event (GOE) ca. 2.4 – 2.3 Ga. Specifically, the proliferation of aerobic chemolithoautotrophy would have facilitated the weathering of crustal sulfide minerals (e.g., pyrite), leading to an extended episode of acid rock drainage, solubilization of nutrient-bearing minerals (e.g., apatite in rocks and soils), increased P transport to the oceans, and ultimately enhanced marine biomass production (Konhauser et al., 2011). There are multiple lines of evidence for intensified and acidic chemical weathering during the GOE, including elevated chemical alteration indices (CIA) in Precambrian paleosols relative to modern soil; the enrichment of Cr without isotopic fractionation; and the prevalence of highly mature paleosols as indicated by the

[5] This chapter has been prepared as a manuscript for submission as: Hao, W.; Mand, K.; Li Y.; Alessi, D.S.; Konhauser, K.O.

high variability in Ti/Al and Ti/Zr. However, how these profound disturbances to the surface weathering environment influenced the continental supply of biolimiting nutrients during this critical period remains largely unknown.

Despite being essential for life, P is easily precipitated with metal cations in aqueous environments making it a limiting nutrient for marine plankton. Indeed, in the modern, only 0.079-22% of P is transported via rivers as dissolved anions (for detailed discussion, see Appendix 4); most is either organically complexed or adsorbed onto Fe(III)-Al(III)- oxyhydroxides or clay minerals (see Appendix 4 SI Table 4.2). A large portion of sorbed P is flocculated and sedimented in estuaries and marginal marine environments where they remain inaccessible to plankton until diagenetic remobilization (Conley et al., 1995). However, unlike in the modern, the post-GOE acidic rock drainage would have solubilized metal oxyhydroxides, while the absence of plants meant that the only organic compounds delivered to the oceans would have been from degraded microbial mats. Clay minerals, therefore, were likely the main vector by which P was delivered to the oceans.

In highly weathered soils today, kaolinite [$Al_2Si_2O_5(OH)_4$)] clays are often the only remaining mineral phases aside from gibbsite and quartz (Tardy, 1997), and given the post-GOE acidification, it was likely a predominant clay on the Paleoproterozoic Earth surface.

$$2NaAlSi_3O_8 + H_2SO_4 + 9H_2O \rightarrow 2Na^+ + 4H_4SiO_4 + Al_2Si_2O_5(OH)_4 + SO_4^{2-} \quad (R5.1)$$

Moreover, in acidic environments, clay minerals undergo partial dissolution, during which structural elements, such as Si and Al, leach into solution (Bibi et al., 2011; Bibi et al., 2014; Hao et al., 2019b; Huertas et al., 1998; Khawmee et al., 2013). Kaolinite surface reactivity is significantly influenced by solution pH and ionic strength (Hao et al., 2018; Hao et al., 2019a), both of which vary during the transportation from rivers to oceans. Here, we test P sorption to

acidic kaolinite under various aqueous conditions via both static and dynamic adsorption experiments, in order to provide evidence that kaolinite can effectively shuttle P from weathering sites to the oceans, and thus increase bio-productivity in estuary environments.

6.2 Methods

6.2.1 P adsorption isotherm

Phosphate adsorption isotherms onto three clay minerals (kaolinite, illite and montmorillonite) were performed at different phosphate concentrations: 1 μM, 5 μM, 10 μM, 15 μM, 20 μM, 25 μM and 30 μM to represent the natural freshwater range. A 5 mM Na_2HPO_4 stock solution was prepared by dissolving Na_2HPO_4 particles (ACS certified, Fisher Scientific) into MQ water. Phosphate solutions with different concentrations were prepared by diluting stock solution with 0.01 M NaCl and 0.56 M NaCl solution to make a total volume of 50 ml. Then, 5 ml of solution was pipetted to analyze initial phosphate concentration. After that, 45 mg of clay was added into solution to make a 1 g/L solid suspension. After agitation, solution pH of each experiments was adjusted to 4, 6 and 8 separately by 0.1 M HCl and 0.1 M NaOH solution. The solution pH was consistently maintained during adsorption period. Once reach equilibrium, 5 ml of clay suspension was pipetted and filtered by 0.2 μm filter. The filtrate and initial 5 ml solution were acidified for ICP-MS analysis. All the experiments were performed in duplicate.

6.2.2 P desorption experiments

Phosphate desorption experiments were performed in 500 ml beaker. For simulation of freshwater condition, 400 ml of 0.01 M NaCl solution was added into reaction beaker. Then, 0.4 mL of 5 mM Na_2HPO_4 stock solution was added into the reaction beaker to make a 5 μM phosphate solution. A

magnetic stir bar was added into beaker to keep the solution mixing during the whole experimental period. Once well mixed, 5 ml aliquot was taken for initial phosphate concentration analysis. After that, the solution pH was adjusted to 6 mimicking freshwater condition and 0.395 g of kaolinite were added into beaker to make a 1 g/L clay suspension. The adsorption of phosphate onto clays under freshwater condition lasted 24 hours and during this process, the pH was maintained at pH=4 using 0.1M HCl and 0.1M NaOH solution. After 24 hours, 5ml of aliquot was syringed out and filtered through 0.2μm filter for ICP-MS analysis. Then, the solution pH was adjusted to 8 by 0.1M NaOH solution and 12.87g of NaCl solid particle was added into beaker at the same time to change ionic strength to 0.56M, representing marine water condition. Once pH is stable, 5ml of aliquot was syringed out for phosphate concentration analysis at t=0. The whole marine condition adsorption process took 2 days and time interval of sample collecting was t=0, t=1h, t=2h, t=4h, t=8h, t=12h, t=1d, t=2d. During the whole process, reaction beaker was covered by parafilm to prevent possible solution evaporation. The phosphate concentration in these samples were then acidified and analyzed by ICP-MS.

6.2.3 Cyanobacterium growth curve

The cyanobacterium *Synechococcus* sp. PCC7002 was used as an analogue strain in the growth experiment to analyze its response to addition of P-bearing Kaolinite clay. This axenic strain was incubated in a modified A+ growth media with limited phosphate concentration at 5 μM. All cultures were grown on a shaker in a designated growth chamber that was set at 30°C with constant halogen lighting. A sterile 1L Erlenmeyer flask with 550 mL of modified A+ growth media was initially inoculated from an axenic PCC 7002 culture growing on an agar plate. The growth of microbial culture was closely monitored by optical density at 750 nm (OD750 nm) on a daily basis

after inoculation. The growth curve started at day 0 when the OD750 nm adsorbance was above 0.15. A triplicate of 1 mL cultures was extracted sterilely from the flask each day for chlorophyll-*a* concentration as an indicator of cell growth from day 0. When it was certain that the culture reached the stationary phase, at which chlorophyll-*a* concentration stopped increasing at ~ 0.680 µg/mL, the culture was further subdivided into three 150 mL sub-cultures in 500 mL Erlenmeyer flasks. Immediately after sub-culturing, 150 mg and 300 mg of P-bearing kaolinite were added into two of the three sub-cultures to make a 1 g/L and 2 g/L kaolinite suspension, respectively. The last sub-culture was the control without any addition of clay. All three cultures were continuously examined for cell growth using chlorophyll-*a* concentration until day 14, when there was a clear cell density difference among three sub-cultures (Figure 6.3). Both optical density at 750 nm and chlorophyll-*a* concentration were measured on a Beckman Coulter DU®520 UV/VIS spectrophotometer. The chlorophyll-*a* concentration was lastly converted to cell density using a correlation that was established from a standard growth curve, which was systematically quantified by both chlorophyll-*a* concentration and cell density that was performed on an Attune NXT acoustic focusing flow cytometer (Figure 6.3).

6.3 Results and Discussion

To infer the P adsorption capacity of kaolinite, we tested P adsorption under various P concentrations. Since atmospheric CO_2 concentrations are thought to have been relatively high in the Archean and the Proterozoic (von Paris et al., 2008), we chose a pH 4 and ionic strength 0.01 M solution to simulate freshwater conditions and a pH 8 and ionic strength 0.56 M solution for marine conditions. Except at initial P concentrations higher than 400 ppb, the difference between the adsorption isotherms of simulated freshwater (pH=4, IS=0.01 M) and estuary environments

(pH=6, IS=0.01 M) was negligible (Figure 6.1). There was around 100-200 ppb more P adsorbed in the freshwater environment than the estuary environment at an initial P concentration higher than 400 ppb. In contrast, adsorption was significantly suppressed under marine conditions, with >300 ppb less P adsorbed under seawater conditions compared to freshwater conditions for an initial P concentration higher than 400 ppb (Figure 6.1). Surprisingly, ionic strength variations were found to be insignificant factors in modulating P adsorption compared to pH (a similar trendline for IS=0.01 M and 0.56 M under pH=8 condition).

Dynamic adsorption experiments were performed to directly observe P behaviour on kaolinite surfaces under simultaneously changing pH and ionic strength conditions (Figure 6.2). At a P concentration of ~5 μM, around 95% of the P was adsorbed onto kaolinite surfaces under freshwater conditions. After switching to marine conditions, the proportion of adsorbed P experienced a steady decrease throughout our experimental period (3 days). In total, around 20% of pre-adsorbed P was released into the aqueous environment.

To test if the P released into the ocean is significant for facilitating marine productivity, we explored the impact of P bearing kaolinite input to the growth of cyanobacteria (*Synechococcus* sp. PCC 7002) in continuous culture. Without clay input, cell density reached a plateau at the 2nd day and then decreased to 5x10^6 cells/mL at the 14th day, while with 1 g/L of P-bearing clay input, the cell number reached 8x10^6 cells/mL at the end of the growth period. A 2 g/L P-bearing kaolinite input led to a bacterial cell density of 1.2x10^7, more than twice that of the blank (Figure 6.3).

The adsorption properties of kaolinite—a high adsorption capacity under freshwater conditions and a low capacity under marine conditions—results in a shuttling of P from continents to oceans and increases near-shore bio-productivity. In natural conditions, the release of P from kaolinite surfaces can be even higher than in our experiments—whereas both the Na^+ and NO_3^-

ions in our buffering solutions show little preference towards mineral surfaces, various aqueous ions in the marine environment show competitive adsorption capacity with P (e.g., arsenate, organic acids) (Kafkafi et al., 1988; Manning and Goldberg, 1996; Violante and Pigna, 2002).

The surface charge property of kaolinite adsorption sites is pH dependent (Hao et al., 2018). Surface complexation modelling based on acid-base titration of kaolinite shows that the kaolinite surface is highly protonated with a positive charge at pH<4.7 (Hao et al., 2019a). This results in the electrostatic attraction of negatively charged P species (e.g., $H_2PO_4^-$ at pH 2-7). A bidentate surface complexation of P onto positively charged sites is the dominant adsorption mechanism on kaolinite explains the pH-dependency of P adsorption (details see Appendix 4).

Besides kaolinite, illite and montmorillonite also show higher P adsorption capacity in freshwater compared to marine conditions (data shown in Appendix 4). This indicates that, even under lower degrees of weathering characterized by montmorillonite and illite production, the transportation of clays from rivers to oceans can act as a P source simply due to the variation in aqueous conditions.

Aside from phosphate, bioavailable nitrogen is another limiting factor for primary production (Planavsky et al., 2010). Molybdenum, as an essential element of nitrogenase, has been shown as the key element for nitrogen fixation in the Archaean (Stüeken et al., 2015). Our experimental results show that the desorption of Mo from kaolinite surfaces has a similar trend to P (Appendix 4), indicating that kaolinite can similarly carry Mo from the continents to the oceans, further facilitating near-shore productivity. We suggest that a coupled increase in phosphate input and nitrogen fixation due to the kaolinite shuttle could have triggered the Lomagundi Event after the GOE.

Kaolinite is expected to have been prevalent in the acidic weathering environments formed in the aftermath of the GOE, as oxic weathering of crustal pyrite led to a pulse of acid rock drainage (Konhauser et al., 2011). However, kaolinite is not commonly to be preserved over long geologic histories due to the prevalence of K-metasomatism in old terranes (Fedo et al., 1995)—K addition leads to the conversion of kaolinite to illite (Lanson et al., 1996), sericite (Nedachi et al., 2005; Rye and Holland, 1998), or illite-sericite (Teitler et al., 2015), depending on the composition of the altering fluid. Alternatively, under high burial temperatures and pressures, SiO_2-rich fluids can transform kaolinite into pyrophyllite (Marmo, 1992) or kyanite (de Wall et al., 2012). Despite this, the formation of kaolinite is still commonly inferred from many paleosols formed around and following the GOE (Bandopadhyay et al., 2010; de Wall et al., 2012; Gall, 1994; Gutzmer and Beukes, 1998; Marmo, 1992; Nedachi et al., 2005; Retallack and Krinsley, 1993; Rye and Holland, 1998; Soomer et al., 2019; Teitler et al., 2015), demonstrating its prevalence in the weathering environments of the time.

6.4 References

Bandopadhyay, P., Eriksson, P., Roberts, R., 2010. A vertic paleosol at the Archean-Proterozoic contact from the Singhbhum-Orissa craton, eastern India. Precambrian Research, 177(3-4): 277-290.

Bekker, A., Karhu, J.A., Eriksson, K.A., Kaufman, A.J., 2003. Chemostratigraphy of Paleoproterozoic carbonate successions of the Wyoming Craton: tectonic forcing of biogeochemical change? Precambrian Research, 120(3-4): 279-325.

Bekker, A., Holland, H.D., 2012. Oxygen overshoot and recovery during the early Paleoproterozoic. Earth and Planetary Science Letters, 317: 295-304.

Bibi, I., Singh, B., Silvester, E., 2011. Dissolution of illite in saline-acidic solutions at 25 degrees C. Geochimica et Cosmochimica Acta, 75(11): 3237-3249.

Bibi, I., Singh, B., Silvester, E., 2014. Dissolution kinetics of soil clays in sulfuric acid solutions: Ionic strength and temperature effects. Applied Geochemistry, 51: 170-183.

Conley, D.J., Smith, W.M., Cornwell, J.C., Fisher, T.R., 1995. Transformation of particle-bound phosphorus at the land-sea interface. Estuarine, Coastal and Shelf Science, 40(2): 161-176.

de Wall, H., Pandit, M.K., Chauhan, N.K., 2012. Paleosol occurrences along the Archean–Proterozoic contact in the Aravalli craton, NW India. Precambrian Research, 216: 120-131.

Fedo, C.M., Wayne Nesbitt, H., Young, G.M., 1995. Unraveling the effects of potassium metasomatism in sedimentary rocks and paleosols, with implications for paleoweathering conditions and provenance. Geology, 23(10): 921-924.

Follmi, K.B., 1996. The phosphorus cycle, phosphogenesis and marine phosphate-rich deposits. Earth-Science Reviews, 40(1-2): 55-124.

Gall, Q., 1994. The Proterozoic Thelon paleosol, Northwest Territories, Canada. Precambrian Research, 68(1-2): 115-137.

Gutzmer, J., Beukes, N.J., 1998. Earliest laterites and possible evidence for terrestrial vegetation in the Early Proterozoic. Geology, 26(3): 263-266.

Hao, W., Flynn, S.L., Alessi, D.S., Konhauser, K.O., 2018. Change of the point of zero net proton charge (pHPZNPC) of clay minerals with ionic strength. Chemical Geology.

Hao, W. et al., 2019a. The impact of ionic strength on the proton reactivity of clay minerals. Chemical Geology, 529: 119294.

Hao, W. et al., 2019b. Effect of acidic conditions on surface properties and metal binding capacity of clay minerals. ACS Earth and Space Chemistry.

Huertas, F.J., Chou, L., Wollast, R., 1998. Mechanism of kaolinite dissolution at room temperature and pressure: Part 1. Surface speciation. Geochimica Et Cosmochimica Acta, 62(3): 417-431.

Kafkafi, U., Bar-Yosef, B., Rosenberg, R., Sposito, G., 1988. Phosphorus adsorption by kaolinite and montmorillonite: II. Organic anion competition. Soil Science Society of America Journal, 52(6): 1585-1589.

Karhu, J.A., Holland, H.D., 1996. Carbon isotopes and the rise of atmospheric oxygen. Geology, 24(10): 867-870.

Khawmee, K., Suddhiprakarn, A., Kheoruenromne, I., Bibi, I., Singh, B., 2013. Dissolution behaviour of soil kaolinites in acidic solutions. Clay Minerals, 48(3): 447-461.

Konhauser, K.O. et al., 2011. Aerobic bacterial pyrite oxidation and acid rock drainage during the Great Oxidation Event. Nature, 478(7369): 369-373.

Lanson, B., Beaufort, D., Berger, G., Baradat, J., Lacharpagne, J.C., 1996. Illitization of diagenetic kaolinite-to-dickite conversion series: Late-stage diagenesis of the Lower Permian Rotliegend sandstone reservoir, offshore of the Netherlands. Journal of Sedimentary Research, 66(3): 501-518.

Lepland, A. et al., 2014. Potential influence of sulphur bacteria on Palaeoproterozoic phosphogenesis. Nature geoscience, 7(1): 20.

Manning, B.A., Goldberg, S., 1996. Modeling arsenate competitive adsorption on kaolinite, montmorillonite and illite. Clays and clay minerals, 44(5): 609-623.

Marmo, J.S., 1992. The lower Proterozoic Hokkalampi paleosol in north Karelia, eastern Finland, Early Organic Evolution. Springer, pp. 41-66.

Melezhik, V.A., Fallick, A.E., Medvedev, P.V., Makarikhin, V.V., 1999. Extreme C-13(carb)

enrichment in ca, 2.0 Ga magnesite-stromatolite-dolomite- 'red beds' association in a global context: a case for the world-wide signal enhanced by a local environment. Earth-Science Reviews, 48(1-2): 71-120.

Nedachi, Y., Nedachi, M., Bennett, G., Ohmoto, H., 2005. Geochemistry and mineralogy of the 2.45 Ga Pronto paleosols, Ontario, Canada. Chemical Geology, 214(1-2): 21-44.

Papineau, D., 2010. Global Biogeochemical Changes at Both Ends of the Proterozoic: Insights from Phosphorites. Astrobiology, 10(2): 165-181.

Planavsky, N.J. et al., 2010. The evolution of the marine phosphate reservoir. Nature, 467(7319): 1088-1090.

Retallack, G.J., Krinsley, D.H., 1993. Metamorphic alteration of a Precambrian (2.2 Ga) paleosol from South Africa revealed by backscattered electron imaging. Precambrian Research, 63(1): 27-41.

Rye, R., Holland, H.D., 1998. Paleosols and the evolution of atmospheric oxygen: a critical review. American journal of science, 298(8): 621-672.

Schidlowski, M., Eichmann, R., Junge, C.E., 1976. CARBON ISOTOPE GEOCHEMISTRY OF PRECAMBRIAN LOMAGUNDI CARBONATE PROVINCE, RHODESIA. Geochimica Et Cosmochimica Acta, 40(4): 449-455.

Schulz, H.N., Schulz, H.D., 2005. Large sulfur bacteria and the formation of phosphorite. Science, 307(5708): 416-418.

Soomer, S. et al., 2019. High-CO2, acidic and oxygen-starved weathering at the Fennoscandian Shield at the Archean-Proterozoic transition. Precambrian Research, 327: 68-80.

Stüeken, E.E., Buick, R., Guy, B.M., Koehler, M.C., 2015. Isotopic evidence for biological nitrogen fixation by molybdenum-nitrogenase from 3.2 Gyr. Nature, 520: 666.

Tardy, Y., 1997. Petrology of laterites and tropical soils. AA Balkema.

Teitler, Y. et al., 2015. Ubiquitous occurrence of basaltic-derived paleosols in the Late Archean Fortescue Group, Western Australia. Precambrian Research, 267: 1-27.

Violante, A., Pigna, M., 2002. Competitive sorption of arsenate and phosphate on different clay minerals and soils. Soil Science Society of America Journal, 66(6): 1788-1796.

von Paris, P. et al., 2008. Warming the early Earth—CO2 reconsidered. Planetary and Space Science, 56(9): 1244-1259.

Wang, K., Wommack, K.E., Chen, F., 2011. Abundance and distribution of Synechococcus spp. and cyanophages in the Chesapeake Bay. Appl. Environ. Microbiol., 77(21): 7459-7468.

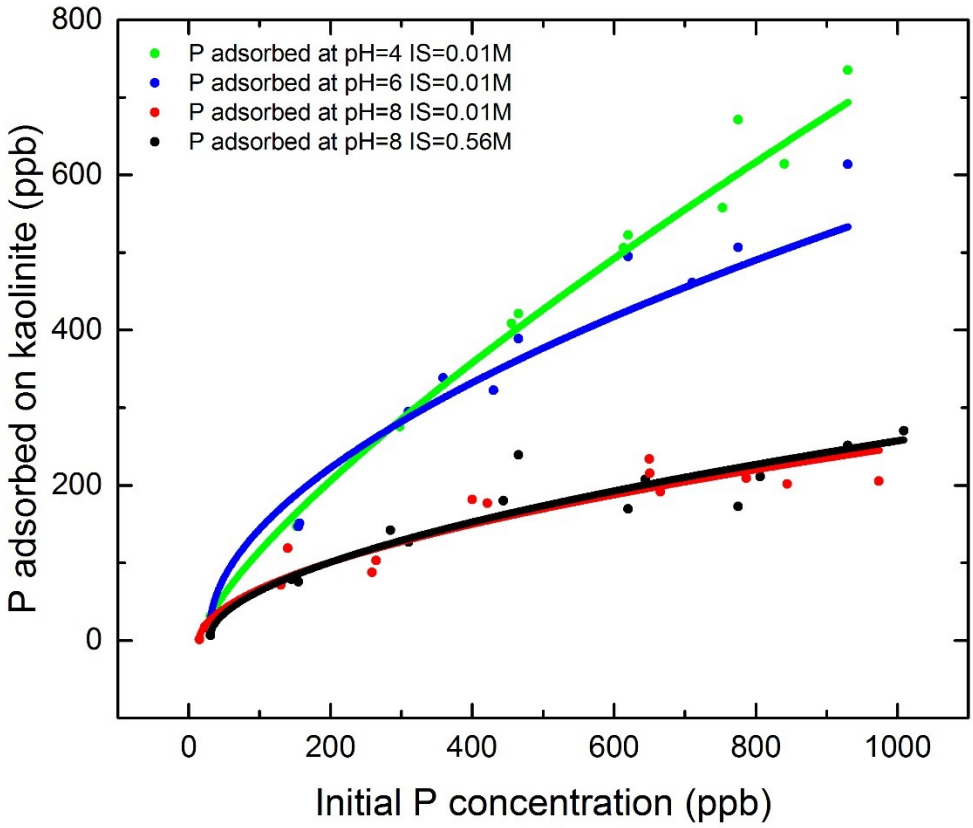

Figure 6.1 The adsorption of P onto kaolinite under three conditions: (1) pH=4, ionic strength=0.01M; (2) pH=6, ionic strength=0.01M; (3) pH=8, ionic strength=0.56M.

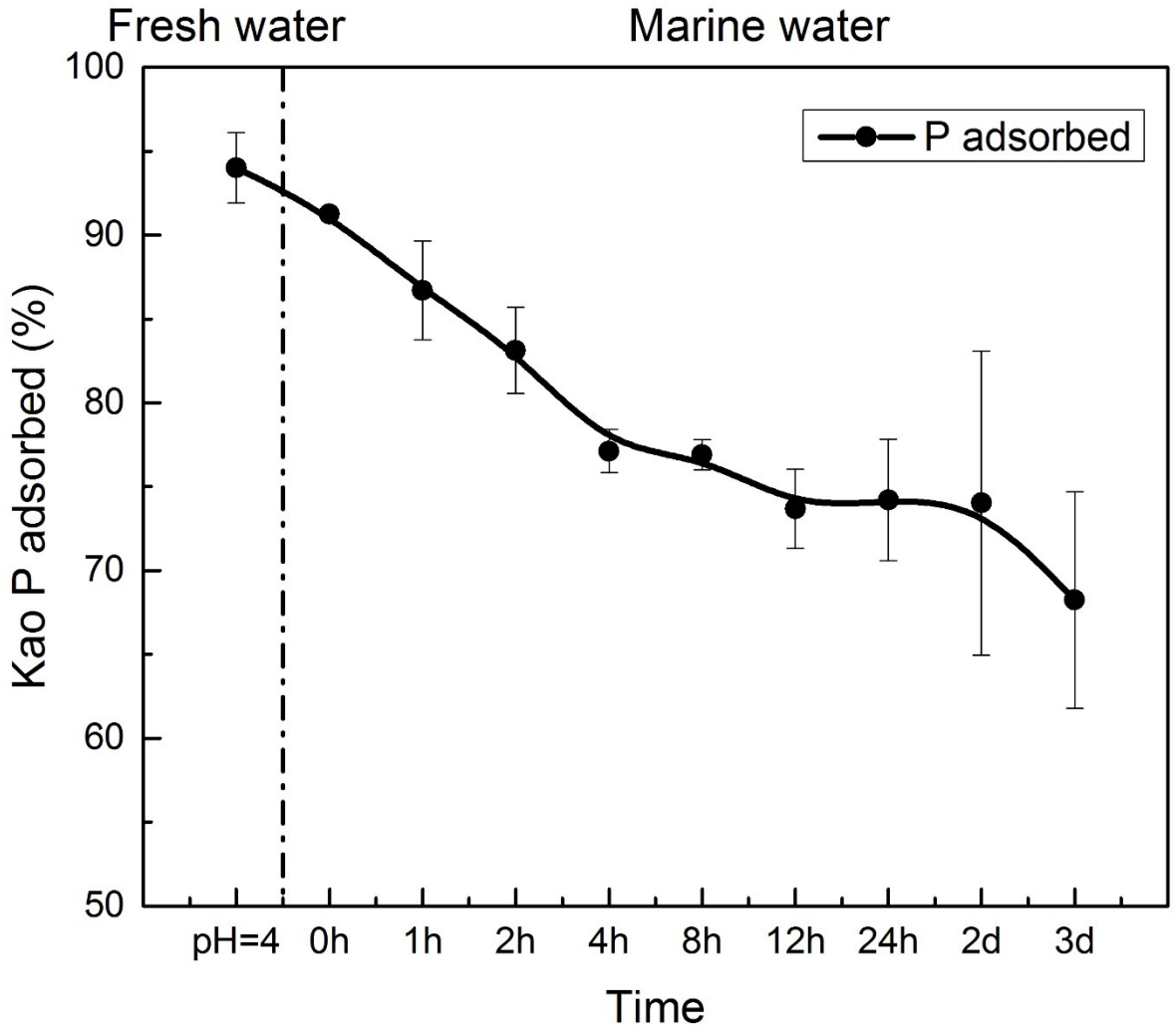

Figure 6.2 Desorption of P from kaolinite surfaces when transiting from freshwater conditions to marine conditions. Freshwater conditions are mimicked by a pH=4, ionic strength=0.01M solution, while marine conditions are simulated at pH=8 and ionic strength=0.56M.

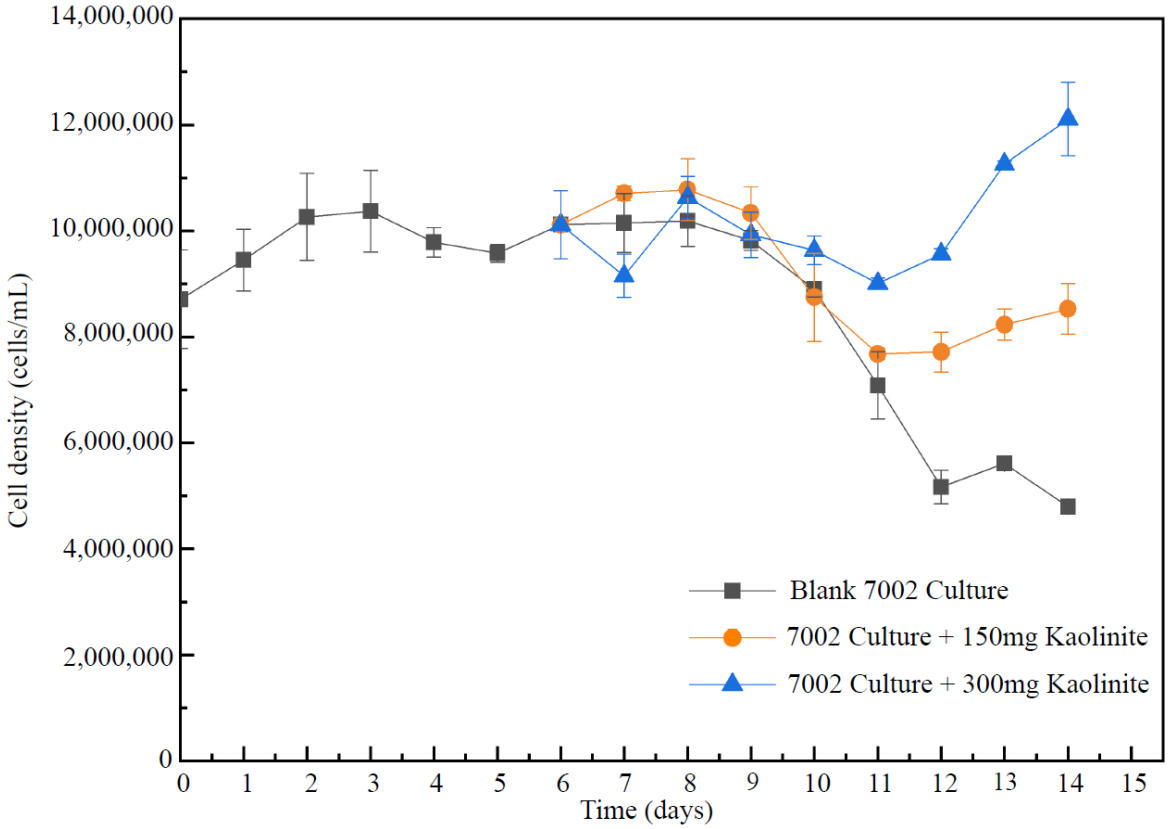

Figure 6.3 Growth curves of cyanobacterium Synechococcus PCC7002 cultures. The original culture was divided into three 150 mL subcultures after day 6. Black squares represent the control culture incubated in modified A+ growth media with only 5 μM potassium phosphate. The orange circles show the growth of a culture with addition of 150 mg of P-bearing kaolinite after day 6. The blue triangles stand for the culture in which 300mg of P-bearing kaolinite was added after day 6.

Chapter 7. Conclusions

Clay minerals are pervasive at the Earth's surface and their transport from rivers to the ocean carries trace elements as a consequence of their high surface charge and surface area. Once carried to an estuary, the clays experience flocculation, burial, diagenesis, and ultimately lithification into mudstone and shales. Since clays are enriched in trace elements, ancient shales are intensively studied in terms of trace elemental concentration to interpret conditions on the ancient Earth surface, such as redox evolution, crustal weathering and seawater composition (Tribovillard et al., 2006; Scott et al., 2008; Lyons et al., 2009; Scott et al., 2012; Partin et al., 2013; Reinhard et al., 2013; Reinhard et al., 2017). In the case of the latter, their utility as a paleo-marine proxy is predicated on the assumption that the accumulation of trace elements in shale directly relates to their concentrations in seawater.

The work in this thesis provides detailed and fundamental information on clay surface reactivity as a function of aqueous pH and IS (Chapter 1, 2, 3), and then demonstrates that the transport of clay minerals from rivers to the ocean is likely a significant source of trace elements, such as Cd and P, into estuaries (Chapter 4, 5). In turn, this suggests that shale composition is not necessarily a first order proxy for seawater composition, but for some elements it instead reflects continental weathering and the composition of the source terraine. Ultimately, I propose new transportation mechanisms of trace elements from continents to oceans, which is crucial to marine biosphere.

7.1 The shale record and its interpretation

Shales, mainly composed of clay minerals, have been extensively studied throughout geological time to understand the secular evolution of Earth's paleoenvironment, including the rise of oxygen in the atmosphere and changes in redox conditions in oceans (Tribovillard et al., 2006; Scott et al., 2008; Lyons et al., 2009; Scott et al., 2012; Partin et al., 2013; Reinhard et al., 2013; Reinhard et al., 2017). For example, the enrichment of Mo in black shales was used as an indicator of atmospheric oxygenation and wide spread sulfidic oceans during the Proterozoic (Scott et al., 2008). Similarly, based on Zn enrichment in black shales through time and a first order relationship between the concentration of dissolved Zn and Zn in sediments, limited ocean euxinia but highly ferruginous deep waters were instead proposed for much of the Proterozoic (Scott et al., 2012). Similarly, a study of coupled Cr and Mo enrichment in black shales constrained a pervasively anoxic Proterozoic ocean with a relatively small extent of euxinic seafloor (Reinhard et al., 2013). Proterozoic ocean conditions were also concluded through a Fe-S-Mo analysis of shales (Lyons et al., 2009), and a study of U enrichment in shales (Partin et al., 2013).

The enrichment mechanism of trace elements onto clay minerals in near-shore environments, where muds were deposited, is a crucial foundation for interpreting trace element concentrations in the shale record. Although the fundamental reactions of pore-water trace elemental redox and surface adsorption-desorption have been intensively explored (Crusius et al., 1996; Morford and Emerson, 1999; Morford et al., 2005; Algeo and Tribovillard, 2009), the role of clay delivery from continents to oceans via river transport is less well studied.

To address the above question, Chapter 1 of this work focused on resolving the question of clay surface charge properties as a function of IS and pH due to distinctly different conditions between rivers and the ocean. The experimental results indicated a decrease in surface charge with

increase in ionic strength, which can exert a significant impact to adsorbed trace element on clay surfaces when transported from rivers to the ocean. A mathematic relationship was built between surface proton charge and ionic strength to quantify the impact of IS to clay surface charge, which could then be applied to estimate clay surface reactivities.

The quantification and assessment of trace elemental adsorption onto clay minerals and modeling adsorption behavior under various aqueous conditions can be accomplished via a thermodynamics-based surface complexation modeling approach. To successfully apply this approach, the first step is to model protonation behavior on clay surfaces due to the fact that protons are competing ions with trace elements and cannot be ignored under aqueous environments. Chapter 2 of this work modeled the proton interaction constants (K_a values) of the three studied clay minerals and established a mathematic relationship between K_a values and solution IS. These results finally explained that the impact of IS to clay surface reactivities is through attenuation of the clay surface electrostatic field instead of competitive adsorption by solution electrolytes.

In addition to IS, solution pH is another important factor that effects clay surface reactivity. Chapter 3 evaluated how clay surface reactivity was impacted under extremely acidic environments; this has direct bearing on the hypothesis that the Protoerozoic Earth underwent conditions of acid rock drainage after the GOE because of the oxidation of crustal pyrite (Konhauser et al., 2011). The work in this chapter demonstrated that exposure of clay minerals to acidic aqueous environment can increase the surface area of clays but may mask clay surface adsorption sites due to secondary precipitation. However, clay morphology and crystal structure are not significantly affected under extremely acidic environments.

With the fundamental framework of clay surface reactivity influenced by solution pH and IS being established, Chapter 4 examined the Cd behavior on clay surfaces when transported from

rivers to the ocean. In contrast to previous studies, our collective experimental results were modeled using an SCM approach, informed by EXAFS spectroscopic data, and demonstrated that clay minerals can serve as a source of Cd to estuaries. This result highlights the trace elemental interaction with clays before deposition and diagenesis, leading to the conclusion that the accumulation of trace elements on clay surfaces is not limited to pore-water space but starts during river transportation.

Phosphorus, as a bio-limiting nutrient, was investigated in Chapter 5 for its adsorption-desorption behavior on kaolinite surfaces with the goal being to test whether acid rock weathering post-GOE was a source of nutrients to marine plankton. The experiments showed that kaolinite has a strong affinity for P under acidic conditions, but that upon changing aqueous composition to alkaline and saline seawater, the clays could release up to 20% of P into seawater, a source of P for stimulating ocean bio-productivity. This was supported by a cyanobacteria growth experiment suggesting that the supply of P by kaolinite can increase the bacterial population by more than 2 times as compared to control experiments without P-bearing kaolinite input. The dissolved P concentration and P adsorbed on river suspended sediment was compiled based on river suspended sediments studied previously to demonstrate that suspended sediments are indeed a major P carrier in river system.

7.2 Future work

Shales remain one of the few geological archives that can be exploited to infer paleo-ocean geochemistry, and they have provided a context with which to link Earth's surface composition to biological evolution. However, a better interpretation of the geological record requires more detailed investigations into the trace metal enrichment processes onto clay minerals. Since the

accumulation of trace elements on clay surfaces at river conditions contributes to trace elemental signature in shales, this work proposes a number of future research questions which are outlined briefly below:

(1) How do trace elements behave on clay surfaces when they are transported from rivers to the ocean? This may include such questions as:

(a) What is clays' role (source or sink) for untested trace elements (e.g. U, Mo, W, V, Ni, Co, Cu, Zn) when pH and IS are varied?

(b) What are the trace elemental local structures on clays during adsorption and how do such local structures vary as a result of environmental conditions change?

(2) Is there any trace elemental isotopic fractionation due to the adsorption of trace elements onto clay minerals?

(a) If there is isotopic fractionation during adsorption process, will isotopic fractionation change as a function of solution pH and ionic strength during adsorption?

(b) Can isotopic fractionation signature be predicted by ab initio first principle molecular dynamic and density functional theory calculations?

(3) What is the impact of bacteria-clay aggregate on trace elemental behavior? and can aggregation process leave a fingerprint to trace elemental concentration in shale formation?

(a) Can component additivity surface complexation modelling approach be applied to predict trace elemental behavior in multiple-adsorbent (clay and bacteria) system?

(b) Is bacteria-clay aggregate a precursor to black shales? If so, what is the impact of bacterial trace elemental composition to trace elemental enrichment in shale formation?

In summary, shales are and remain an important proxy record for exploration of ancient oceanic and atmospheric geochemical environment. Fundamental studies conducted in this thesis have provided new insights in interpreting trace elemental concentration in shales by investigating various trace elemental enrichment mechanisms.

7.3 References

Algeo, T.J., Tribovillard, N., 2009. Environmental analysis of paleoceanographic systems based on molybdenum–uranium covariation. Chemical Geology, 268(3): 211-225.

Crusius, J., Calvert, S., Pedersen, T., Sage, D., 1996. Rhenium and molybdenum enrichments in sediments as indicators of oxic, suboxic and sulfidic conditions of deposition. Earth and Planetary Science Letters, 145(1): 65-78.

Lyons, T.W., Anbar, A.D., Severmann, S., Scott, C., Gill, B.C., 2009. Tracking euxinia in the ancient ocean: a multiproxy perspective and Proterozoic case study. Annual Review of Earth and Planetary Sciences, 37: 507-534.

Morford, J.L., Emerson, S., 1999. The geochemistry of redox sensitive trace metals in sediments. Geochimica et Cosmochimica Acta, 63(11): 1735-1750.

Morford, J.L., Emerson, S.R., Breckel, E.J., Kim, S.H., 2005. Diagenesis of oxyanions (V, U, Re, and Mo) in pore waters and sediments from a continental margin. Geochimica et Cosmochimica Acta, 69(21): 5021-5032.

Partin, C.A. et al., 2013. Large-scale fluctuations in Precambrian atmospheric and oceanic oxygen

levels from the record of U in shales. Earth and Planetary Science Letters, 369-370: 284-293.

Reinhard, C.T. et al., 2013. Proterozoic ocean redox and biogeochemical stasis. Proceedings of the National Academy of Sciences, 110(14): 5357-5362.

Reinhard, C.T. et al., 2017. Evolution of the global phosphorus cycle. Nature, 541(7637): 386-389.

Scott, C. et al., 2008. Tracing the stepwise oxygenation of the Proterozoic ocean. Nature, 452(7186): 456-9.

Scott, C. et al., 2012. Bioavailability of zinc in marine systems through time. Nature Geoscience, 6(2): 125-128.

Tribovillard, N., Algeo, T.J., Lyons, T., Riboulleau, A., 2006. Trace metals as paleoredox and paleoproductivity proxies: an update. Chemical geology, 232(1-2): 12-32.

Bibliography

Adams, J.M., Davies, S.E., Graham, S.H., Thomas, J.M., 1982. Catalyzed reactions of organic molecules at clay surfaces: Ester breakdown, dimerizations, and lactonizations. Journal of Catalysis, 78(1): 197-208.

Agboola, O. et al., 2017. Characterization of Two Nanofiltration Membranes for the Separation of Ions from Acid Mine Water. Mine Water and the Environment, 36(3): 401-408.

Ahmady-Asbchin, S., Jafari, N., 2012. Physicochemical Studies of Copper (II) Biosorption from Wastewater by Marine Brown Algae Sargassum angustifolium C. Agardh (Fucales, Phaeophyceae). International Journal on Algae, 14(4): 367-379.

Alam, M.S. et al., 2018. Application of surface complexation modeling to trace metals uptake by biochar-amended agricultural soils. Applied Geochemistry, 88: 103-112.

Alessi, D.S., Fein, J.B., 2010. Cadmium adsorption to mixtures of soil components: Testing the component additivity approach. Chemical Geology, 270(1): 186-195.

Alessi, D.S., Henderson, J.M., Fein, J.B., 2010. Experimental Measurement of Monovalent Cation Adsorption onto Bacillus subtilis Cells. Geomicrobiology Journal, 27(5): 464-472.

Algeo, T.J., Tribovillard, N., 2009. Environmental analysis of paleoceanographic systems based on molybdenum–uranium covariation. Chemical Geology, 268(3): 211-225.

Anna, B., Kleopas, M., Constantine, S., Anestis, F., Maria, B., 2015. Adsorption of Cd(II), Cu(II), Ni(II) and Pb(II) onto natural bentonite: study in mono- and multi-metal systems. Environmental Earth Sciences, 73(9): 5435-5444.

Appel, C., Ma, L.Q., Dean, R.R., Kennelley, E., 2003. Point of zero charge determination in soils and minerals via traditional methods and detection of electroacoustic mobility. Geoderma, 113(1): 77-93.

Arda, D., Hizal, J., Apak, R., 2006. Surface complexation modelling of uranyl adsorption onto kaolinite based clay minerals using FITEQL 3.2. Radiochimica Acta, 94: 835- 844.

Avena, J.M., Pauli, P.D.C., 1998. Proton Adsorption and Electrokinetics of an Argentinean Montmorillonite. Journal of Colloid and Interface Science, 202: 195-204.

Bachmaf, S., Merkel, B.J., 2011. Sorption of uranium(VI) at the clay mineral-water interface. Environmental Earth Sciences, 63(5): 925-934.

Baes, C.F., Mesmer, R.S., 1977. The Hydrolysis of Cations. John Wiley & Sons, New York, London, Sydney, Toronto 1976. 489 Seiten. Berichte der Bunsengesellschaft für physikalische Chemie, 81(2): 245-246.

Baeyens, B., Bradbury, M.H., 1997. A mechanistic description of Ni and Zn sorption on Na-montmorillonite .1. Titration and sorption measurements. Journal of Contaminant Hydrology, 27(3-4): 199-222.

Bandopadhyay, P., Eriksson, P., Roberts, R., 2010. A vertic paleosol at the Archean-Proterozoic contact from the Singhbhum-Orissa craton, eastern India. Precambrian Research, 177(3-4): 277-290.

Barbier, F., Duc, G., Petit-Ramel, M., 2000. Adsorption of lead and cadmium ions from aqueous solution to the montmorillonite/water interface. Colloids and Surfaces A: Physicochemical and Engineering Aspects, 166(1–3): 153-159.

Barrios, M.S., Gonzalez, L.V.F., Rodriguez, M.A.V., Pozas, J.M.M., 1995. Acid Activation of a Palygorskite with Hcl - Development of Physicochemical, Textural and Surface-Properties. Applied Clay Science, 10(3): 247-258.

Bekker, A., Holland, H.D., 2012. Oxygen overshoot and recovery during the early Paleoproterozoic. Earth and Planetary Science Letters, 317: 295-304.

Bekker, A., Karhu, J.A., Eriksson, K.A., Kaufman, A.J., 2003. Chemostratigraphy of Paleoproterozoic carbonate successions of the Wyoming Craton: tectonic forcing of biogeochemical change? Precambrian Research, 120(3-4): 279-325.

Bergaya, F., Lagaly, G., 2006. General introduction: clays, clay minerals, and clay science. Developments in clay science, 1: 1-18.

Bhattacharyya, K.G., Gupta, S.S., 2008a. Adsorption of a few heavy metals on natural and modified kaolinite and montmorillonite: a review. Adv Colloid Interface Sci, 140(2): 114-31.

Bhattacharyya, K.G., Gupta, S.S., 2008b. Influence of acid activation on adsorption of Ni(II) and Cu(II) on kaolinite and montmorillonite: Kinetic and thermodynamic study. Chemical Engineering Journal, 136(1): 1-13.

Bhattacharyya, K.G., Sen Gupta, S., 2006. Adsorption of chromium (VI) from water by clays. Industrial & engineering chemistry research, 45(21): 7232-7240.

Bibi, I., Singh, B., Silvester, E., 2011. Dissolution of illite in saline-acidic solutions at 25 degrees C. Geochimica et Cosmochimica Acta, 75(11): 3237-3249.

Bibi, I., Singh, B., Silvester, E., 2014. Dissolution kinetics of soil clays in sulfuric acid solutions: Ionic strength and temperature effects. Applied Geochemistry, 51: 170-183.

Bohn, H.L., Myer, R.A., O'Connor, G.A., 2002. Soil chemistry. Chapter 8 Cation Retention (Exchange) in Soils. John Wiley & Sons.

Borrok, D.M., Fein, J.B., 2005. The impact of ionic strength on the adsorption of protons, Pb, Cd, and Sr onto the surfaces of Gram negative bacteria: testing non-electrostatic, diffuse, and triple-layer models. Journal of Colloid and Interface Science, 286(1): 110-126.

Brack, A., 2013. Chapter 10.4 - Clay Minerals and the Origin of Life. In: Bergaya, F., Lagaly, G.

(Eds.), Developments in Clay Science. Elsevier, pp. 507-521.

Bradbury, M.H., Baeyens, B., 2002. Sorption of Eu on Na- and Ca-montmorillonites: Experimental investigations and modelling with cation exchange and surface complexation. Geochimica et Cosmochimica Acta, 66(13): 2325-2334.

Bradbury, M.H., Baeyens, B., 2009. Sorption modelling on illite Part I: Titration measurements and the sorption of Ni, Co, Eu and Sn. Geochimica et Cosmochimica Acta, 73(4): 990-1003.

Bradl, H.B., 2004. Adsorption of heavy metal ions on soils and soils constituents. Journal of colloid and Interface Science, 277(1): 1-18.

Cao, X. et al., 2016. Study and modeling surface charge characteristics of montmorillonite. Functional Material, 4(47): 4152-4156 (in Chinese).

Catalano, J.G., Brown, G.E., 2005. Uranyl adsorption onto montmorillonite: Evaluation of binding sites and carbonate complexation. Geochimica et Cosmochimica Acta, 69(12): 2995-3005.

Chiffoleau, J.-F., Cossa, D., Auger, D., Truquet, I., 1994. Trace metal distribution, partition and fluxes in the Seine estuary (France) in low discharge regime. Marine Chemistry, 47(2): 145-158.

Chiou, C.T., Rutherford, D.W., 1997. Effects of exchanged cation and layer charge on the sorption of water and EGME vapors on montmorillonite clays. Clays and Clay Minerals, 45(6): 867-880.

Chitnis, S.R., Mohan Sharma, M., 1997. Industrial applications of acid-treated clays as catalysts. Reactive and Functional Polymers, 32(1): 93-115.

Choi, E.Y., Lee, S.H., Kim, Y., Han, Y.W., Seff, K., 2002. Crystal structure of a cadmium sorption complex of dehydrated fully Cd2+-exchanged zeolite X containing Cd2+, Cd+, and Cd0.

Journal of Physical Chemistry B, 106(30): 7569-7573.

Chorom, M., Rengasamy, P., 1995. Dispersion and zeta potential of pure clays as related to net particle charge under varying pH, electrolyte concentration and cation type. European Journal of Soil Science, 46(4): 657-665.

Christidis, G.E., Scott, P.W., Dunham, A.C., 1997. Acid activation and bleaching capacity of bentonites from the islands of Milos and Chios, Aegean, Greece. Applied Clay Science, 12(4): 329-347.

Conley, D.J., Smith, W.M., Cornwell, J.C., Fisher, T.R., 1995. Transformation of particle-bound phosphorus at the land-sea interface. Estuarine, Coastal and Shelf Science, 40(2): 161-176.

Coppin, F., Berger, G., Bauer, A., Castet, S., Loubet, M., 2002. Sorption of lanthanides on smectite and kaolinite. Chemical Geology, 182(1): 57-68.

Crusius, J., Calvert, S., Pedersen, T., Sage, D., 1996. Rhenium and molybdenum enrichments in sediments as indicators of oxic, suboxic and sulfidic conditions of deposition. Earth and Planetary Science Letters, 145(1): 65-78.

da Fonseca, M.G., de Oliveira, M.M., Arakaki, L.N., 2006. Removal of cadmium, zinc, manganese and chromium cations from aqueous solution by a clay mineral. Journal of Hazardous Materials, 137(1): 288-292.

Davis, J.A., James, R.O., Leckie, J.O., 1978. Surface ionization and complexation at the oxide/water interface: I. Computation of electrical double layer properties in simple electrolytes. Journal of Colloid and Interface Science, 63(3): 480-499.

Davis, J.A., Kent, D.B., 1990. Surface complexation modeling in aqueous geochemistry. Reviews in Mineralogy and Geochemistry, 23(1): 177-260.

de Wall, H., Pandit, M.K., Chauhan, N.K., 2012. Paleosol occurrences along the Archean–

Proterozoic contact in the Aravalli craton, NW India. Precambrian Research, 216: 120-131.

Dekany, I., Turi, L., Fonseca, A., Nagy, J.B., 1999. The structure of acid treated sepiolites: small-angle X-ray scattering and multi MAS-NMR investigations. Applied Clay Science, 14(1-3): 141-160.

Drever, J.I., 1997. The geochemistry of natural waters: surface and groundwater environments, Prentice-Hall, Inc., Upper Saddle River, NJ.

Du, H.H. et al., 2016. Cd(II) Sorption on Montmorillonite-Humic acid-Bacteria Composites. Scientific Reports, 6.

Dyer, J.A., Trivedi, P., Scrivner, N.C., Sparks, D.L., 2003. Lead sorption onto ferrihydrite. 2. Surface complexation modeling. Environmental Science and Technology, 37(5): 915-922.

Dzombak, D.A., Morel, F.M., 1990. Surface complexation modeling: hydrous ferric oxide. John Wiley & Sons.

Edwards, K.J., Bond, P.L., Gihring, T.M., Banfield, J.F., 2000. An archaeal iron-oxidizing extreme acidophile important in acid mine drainage. Science, 287(5459): 1796-1799.

Eisma, D., Van Der Gaast, S.J., Martin, J.M., Thomas, A.J., 1978. Suspended matter and bottom deposits of the Orinoco delta: Turbidity, mineralogy and elementary composition. Netherlands Journal of Sea Research, 12(2): 224-251.

El-Bayaa, A.A., Badawy, N.A., AlKhalik, E.A., 2009. Effect of ionic strength on the adsorption of copper and chromium ions by vermiculite pure clay mineral. Journal of Hazardous Materials, 170(2): 1204-1209.

El-Bouraie, M., El-Barbary, A., Yehia, M., Motawea, E., 2010. Heavy metal concentrations in surface river water and bed sediments at Nile Delta in Egypt. Suo, 61(1): 1-12.

Elshanawany, R., Ibrahim, M.I., Frihy, O., Abodia, M., 2018. Foraminiferal evidence of

anthropogenic pollution along the Nile Delta coast. Environmental earth sciences, 77(12): 444.

Espantaleon, A.G., Nieto, J.A., Fernandez, M., Marsal, A., 2003. Use of activated clays in the removal of dyes and surfactants from tannery waste waters. Applied Clay Science, 24(1-2): 105-110.

Fedo, C.M., Wayne Nesbitt, H., Young, G.M., 1995. Unraveling the effects of potassium metasomatism in sedimentary rocks and paleosols, with implications for paleoweathering conditions and provenance. Geology, 23(10): 921-924.

Fein, J.B., Boily, J.-F., Yee, N., Gorman-Lewis, D., Turner, B.F., 2005. Potentiometric titrations of Bacillus subtilis cells to low pH and a comparison of modeling approaches. Geochimica et Cosmochimica Acta, 69(5): 1123-1132.

Feng, H. et al., 2014. Distribution characteristic of clay minerals contents in Minjiang River and its environmental significance. Journal of Applied Oceanography, 33(3): 418-424.

Fournier, R.O., Rowe, J.J., 1977. The solubility of amorphous silica in water at high temperatures and high pressures. American Mineralogist, 62(9-10): 1052-1056.

Gall, Q., 1994. The Proterozoic Thelon paleosol, Northwest Territories, Canada. Precambrian Research, 68(1-2): 115-137.

Ghayaza, M., Le Forestier, L., Muller, F., Tournassat, C., Beny, J.M., 2011. Pb(II) and Zn(II) adsorption onto Na- and Ca-montmorillonites in acetic acid/acetate medium: Experimental approach and geochemical modeling. Journal of Colloid and Interface Science, 361(1): 238-246.

Gibbs, R.J., 1967. The geochemistry of the Amazon River system: Part I. The factors that control the salinity and the composition and concentration of the suspended solids. Geological

Society of America Bulletin, 78(10): 1203-1232.

Gingele, F.X., De Deckker, P., Hillenbrand, C.-D., 2001. Clay mineral distribution in surface sediments between Indonesia and NW Australia - source and transport by ocean currents. Marine Geology, 179(3–4): 135-146.

Goldberg, S., 2005. Inconsistency in the triple layer model description of ionic strength dependent boron adsorption. Journal of Colloid and Interface Science, 285(2): 509-517.

González Sánchez, F. et al., 2008. Self-diffusion of water and its dependence on temperature and ionic strength in highly compacted montmorillonite, illite and kaolinite. Applied Geochemistry, 23(12): 3840-3851.

Grafe, M., Singh, B., Balasubramanian, M., 2007. Surface speciation of Cd(II) and Pb(II) on kaolinite by XAFS spectroscopy. Journal of Colloid and Interface Science, 315(1): 21-32.

Griffin, J.J., Windom, H., Goldberg, D.E., 1968. The distribution of clay minerals in the World Ocean. Deep-Sea Research, 15: 433-459.

Griffioen, J., Klaver, G., Westerhoff, W., 2016. The mineralogy of suspended matter, fresh and Cenozoic sediments in the fluvio-deltaic Rhine–Meuse–Scheldt–Ems area, the Netherlands: An overview and review. Netherlands Journal of Geosciences, 95(1): 23-107.

Gu, X., Evans, L.J., 2007. Modelling the adsorption of Cd(II), Cu(II), Ni(II), Pb(II), and Zn(II) onto Fithian illite. Journal of colloid and interface science, 307(2): 317-25.

Gu, X., Evans, L.J., 2008. Surface complexation modelling of Cd(II), Cu(II), Ni(II), Pb(II) and Zn(II) adsorption onto kaolinite. Geochimica et Cosmochimica Acta, 72(2): 267-276.

Gu, X., Evans, L.J., Barabash, S.J., 2010. Modeling the adsorption of Cd (II), Cu (II), Ni (II), Pb (II) and Zn (II) onto montmorillonite. Geochimica et Cosmochimica Acta, 74(20): 5718-5728.

Gupta, S.S., Bhattacharyya, K.G., 2012. Adsorption of heavy metals on kaolinite and montmorillonite: a review. Physical Chemistry Chemical Physics, 14(19): 6698-6723.

Gutzmer, J., Beukes, N.J., 1998. Earliest laterites and possible evidence for terrestrial vegetation in the Early Proterozoic. Geology, 26(3): 263-266.

Hao, W., Flynn, S.L., Alessi, D.S., Konhauser, K.O., 2018a. Change of the point of zero net proton charge (pHPZNPC) of clay minerals with ionic strength. Chemical Geology, 493: 458-467.

Hao, W., Flynn, S.L., Alessi, D.S., Konhauser, K.O., 2018b. Change of the point of zero net proton charge (pHPZNPC) of clay minerals with ionic strength. Chemical Geology.

Hao, W. et al., 2019a. The impact of ionic strength on the proton reactivity of clay minerals. Chemical Geology: 119294.

Hao, W. et al., 2019b. The impact of ionic strength on the proton reactivity of clay minerals. Chemical Geology, 529: 119294.

Hao, W. et al., 2019c. Effect of acidic conditions on surface properties and metal binding capacity of clay minerals. ACS Earth and Space Chemistry.

Helmy, A.K., Ferreiro, E.A., Debussetti, S.G., 1994. Cation-exchange capacity and condition of zero charge of hydroxy-Al montmorillonite. Clays and Clay Minerals, 42(4): 444-450.

Hemmingsen, L. et al., 1999. Structure, chemical bonding, and nuclear quadrupole interactions of beta-Cd(OH)(2): Experiment and first principles calculations. Inorganic Chemistry, 38(12): 2860-2867.

Hizal, J., Apak, R., 2006. Modeling of copper(II) and lead(II) adsorption on kaolinite-based clay minerals individually and in the presence of humic acid. Journal of Colloid and Interface Science, 295(1): 1-13.

Hohl, H., Stumm, W., 1976. Interaction of Pb2+ with hydrous γ-Al2O3. Journal of Colloid and

Interface Science, 55(2): 281-288.

Hou, W., Song, S., 2004. Intrinsic surface reaction equilibrium constants of structurally charged amphoteric hydrotalcite-like compounds. Journal of Colloid and Interface Science, 269(2): 381-387.

Hower, J., Mowatt, C.T., 1966. The mineralogy of illite and mixed-layer illite/montmorillonites. The American Mineralogist, 51: 825-854.

Hu, G. et al., 2015. Distribution and assessment of heavy metals off the Changjiang River mouth and adjacent area during the past century and the relationship of the heavy metals with anthropogenic activity. Marine pollution bulletin, 96(1-2): 434-440.

Huang, W., Zhang, J., Zhou, Z., 1992. Particulate element inventory of the Huanghe (Yellow River): A large, high-turbidity river. Geochimica et Cosmochimica Acta, 56(10): 3669-3680.

Huertas, F.J., Chou, L., Wollast, R., 1998. Mechanism of kaolinite dissolution at room temperature and pressure: Part 1. Surface speciation. Geochimica Et Cosmochimica Acta, 62(3): 417-431.

Ijagbemi, C.O., Baek, M.H., Kim, D.S., 2009. Montmorillonite surface properties and sorption characteristics for heavy metal removal from aqueous solutions. Journal of Hazardous Materials, 166(1): 538-546.

Ikhsan, J., Wells, J.D., Johnson, B.B., Angove, M.J., 2005. Surface complexation modeling of the sorption of Zn(II) by montmorillonite. Colloids and Surfaces A: Physicochemical and Engineering Aspects, 252(1): 33-41.

Jackson, M., Tyler, S., Willis, A., Bourbeau, G., Pennington, R., 1948. Weathering sequence of clay-size minerals in soils and sediments. I. Fundamental generalizations. The Journal of Physical Chemistry, 52(7): 1237-1260.

Jiang, M., Jin, X., Lu, X., Chen, Z., 2010. Adsorption of Pb(II), Cd(II), Ni(II) and Cu(II) onto natural kaolinite clay. Desalination, 252(1): 33-39.

Johnson, C.R., Hopf, J., Shrout, J.D., Fein, J.B., 2019. Testing the component additivity approach to surface complexation modeling using a novel cadmium-specific fluorescent probe technique. Journal of Colloid and Interface Science, 534: 683-694.

Johnson, D.B., Hallberg, K.B., 2005. Acid mine drainage remediation options: a review. Science of the total environment, 338(1-2): 3-14.

Jozefaciuk, G., Bowanko, G., 2002. Effect of acid and alkali treatments on surface areas and adsorption energies of selected minerals. Clays and Clay Minerals, 50(6): 771-783.

Kafkafi, U., Bar-Yosef, B., Rosenberg, R., Sposito, G., 1988. Phosphorus adsorption by kaolinite and montmorillonite: II. Organic anion competition. Soil Science Society of America Journal, 52(6): 1585-1589.

Kallay, N., Kovačević, D., Žalac, S., 2006. Chapter 6 - Thermodynamics of the solid/liquid interface - its application to adsorption and colloid stability. In: Johannes, L. (Ed.), Interface Science and Technology. Elsevier, pp. 133-170.

Karhu, J.A., Holland, H.D., 1996. Carbon isotopes and the rise of atmospheric oxygen. Geology, 24(10): 867-870.

Kashiwabara, T. et al., 2014. Chemical processes for the extreme enrichment of tellurium into marine ferromanganese oxides. Geochimica et Cosmochimica Acta, 131: 150-163.

Kashiwabara, T. et al., 2013. Tungsten species in natural ferromanganese oxides related to its different behavior from molybdenum in oxic ocean. Geochimica et Cosmochimica Acta, 106: 364-378.

Kashiwabara, T., Takahashi, Y., Tanimizu, M., Usui, A., 2011. Molecular-scale mechanisms of

distribution and isotopic fractionation of molybdenum between seawater and ferromanganese oxides. Geochimica et Cosmochimica Acta, 75(19): 5762-5784.

Kaya, A., Yukselen, Y., 2005. Zeta potential of clay minerals and quartz contaminated by heavy metals. Canadian Geotechnical Journal, 42(5): 1280-1289.

Khawmee, K., Suddhiprakarn, A., Kheoruenromne, I., Bibi, I., Singh, B., 2013. Dissolution behaviour of soil kaolinites in acidic solutions. Clay Minerals, 48(3): 447-461.

Komárek, M., Koretsky, C.M., Stephen, K.J., Alessi, D.S., Chrastný, V., 2015. Competitive Adsorption of Cd(II), Cr(VI), and Pb(II) onto Nanomaghemite: A Spectroscopic and Modeling Approach. Environmental Science and Technology, 49(21): 12851-12859.

Konhauser, K.O., Fisher, Q.J., Fyfe, W.S., Longstaffe, F.J., Powell, M.A., 1998. Authigenic mineralization and detrital clay binding by freshwater biofilms: The Brahmani River, India. Geomicrobiology Journal, 15(3): 209-222.

Konhauser, K.O. et al., 2011. Aerobic bacterial pyrite oxidation and acid rock drainage during the Great Oxidation Event. Nature, 478(7369): 369-373.

Kosmulski, M., 2011. The pH-dependent surface charging and points of zero charge: V. Update. Journal of Colloid and Interface Science, 353(1): 1-15.

Kraepiel, A.M.L., Keller, K., Morel, F.M.M., 1998. On the acid-base chemistry of permanently charged minerals. Environmental Science and Technology, 32(19): 2829-2838.

Kriaa, A., Hamdi, N., Srasra, E., 2007. Acid-base chemistry of montmorillonitic and beidellitic-montmorillonitic smectite. Russian Journal of Electrochemistry, 43(2): 167-177.

Kriaa, A., Hamdi, N., Srasra, E., 2008. Determination of Point of Zero Charge of Tunisian Kaolinites by Potentiometric and Mass Titration Methods. Journal of the Chinese Chemical Society, 55(1): 53-61.

Kumar, P., Jasra, R.V., Bhat, T.S.G., 1995. Evolution of Porosity and Surface Acidity in Montmorillonite Clay on Acid Activation. Industrial & Engineering Chemistry Research, 34(4): 1440-1448.

Kuo, C., Hst, D., 1985. Adsorption of uranyl onto ferric oxyhydroxides: Application of the surface complexation site-binding model. Geochimica et Cosmochimica Acta, 49: 1931-1941.

Lackovic, K., Angove, M.J., Wells, J.D., Johnson, B.B., 2003. Modeling the adsorption of Cd(II) onto Muloorina illite and related clay minerals. Journal of Colloid and Interface Science, 257(1): 31-40.

Lalonde, S.V., Dafoe, L.T., Pemberton, S.G., Gingras, M.K., Konhauser, K.O., 2010. Investigating the geochemical impact of burrowing animals: Proton and cadmium adsorption onto the mucus lining of Terebellid polychaete worms. Chemical Geology, 271(1-2): 44-51.

Landry, C.J., Koretsky, C.M., Lund, T.J., Schaller, M., Das, S., 2009. Surface complexation modeling of Co(II) adsorption on mixtures of hydrous ferric oxide, quartz and kaolinite. Geochimica et Cosmochimica Acta, 73(13): 3723-3737.

Langmuir, D., 1997. Aqueous Environmental Geochemistry. Prentice-Hall, Inc.

Lanson, B., Beaufort, D., Berger, G., Baradat, J., Lacharpagne, J.C., 1996. Illitization of diagenetic kaolinite-to-dickite conversion series: Late-stage diagenesis of the Lower Permian Rotliegend sandstone reservoir, offshore of the Netherlands. Journal of Sedimentary Research, 66(3): 501-518.

Liu, Y. et al., 2018. Acid-base properties of kaolinite, montmorillonite and illite at marine ionic strength. Chemical Geology, 483: 191-200.

Liu, Y.X. et al., 2015. Cell surface reactivity of Synechococcus sp PCC 7002: Implications for metal sorption from seawater. Geochimica et Cosmochimica Acta, 169: 30-44.

Lützenkirchen, J., Preočanin, T., Bauer, A., Metz, V., Sjöberg, S., 2012a. Net surface proton excess of smectites obtained from a combination of potentiometric acid–base, mass and electrolyte titrations. Colloids and Surfaces A: Physicochemical and Engineering Aspects, 412(Supplement C): 11-19.

Lützenkirchen, J. et al., 2012b. Potentiometric Titrations as a Tool for Surface Charge Determination. Croatica Chemica Acta, 85(4): 391-417.

Lyons, T.W., Anbar, A.D., Severmann, S., Scott, C., Gill, B.C., 2009. Tracking euxinia in the ancient ocean: a multiproxy perspective and Proterozoic case study. Annual Review of Earth and Planetary Sciences, 37: 507-534.

Malferrari, D., Brigatti, M.F., Laurora, A., Pini, S., Medici, L., 2007. Sorption kinetics and chemical forms of Cd(II) sorbed by thiol-functionalized 2 : 1 clay minerals. Journal of Hazardous Materials, 143(1-2): 73-81.

Manning, B.A., Goldberg, S., 1996. Modeling arsenate competitive adsorption on kaolinite, montmorillonite and illite. Clays and clay minerals, 44(5): 609-623.

Manning, B.A., Goldberg, S., 1997. Adsorption and stability of arsenic (III) at the clay mineral−water interface. Environmental Science & Technology, 31(7): 2005-2011.

Marmo, J.S., 1992. The lower Proterozoic Hokkalampi paleosol in north Karelia, eastern Finland, Early Organic Evolution. Springer, pp. 41-66.

McBride, M., 1989. Reactions controlling heavy metal solubility in soils, Advances in soil science. Springer, pp. 1-56.

Melezhik, V.A., Fallick, A.E., Medvedev, P.V., Makarikhin, V.V., 1999. Extreme C-13(carb) enrichment in ca, 2.0 Ga magnesite-stromatolite-dolomite- 'red beds' association in a global context: a case for the world-wide signal enhanced by a local environment. Earth-Science

Reviews, 48(1-2): 71-120.

Missana, T., García-Gutiérrez, M., Fernńdez, V., 2003. Uranium (VI) sorption on colloidal magnetite under anoxic environment: experimental study and surface complexation modelling. Geochimica et Cosmochimica Acta, 67(14): 2543-2550.

Morford, J.L., Emerson, S., 1999. The geochemistry of redox sensitive trace metals in sediments. Geochimica et Cosmochimica Acta, 63(11): 1735-1750.

Morford, J.L., Emerson, S.R., Breckel, E.J., Kim, S.H., 2005. Diagenesis of oxyanions (V, U, Re, and Mo) in pore waters and sediments from a continental margin. Geochimica et Cosmochimica Acta, 69(21): 5021-5032.

Morton, J.D., Semrau, J.D., Hayes, K.F., 2001. An X-ray absorption spectroscopy study of the structure and reversibility of copper adsorbed to montmorillonite clay. Geochimica et Cosmochimica Acta, 65(16): 2709-2722.

Nedachi, Y., Nedachi, M., Bennett, G., Ohmoto, H., 2005. Geochemistry and mineralogy of the 2.45 Ga Pronto paleosols, Ontario, Canada. Chemical Geology, 214(1-2): 21-44.

Nery, J.G., Mascarenhas, Y.P., Cheetham, A.K., 2003. A study of the highly crystalline, low-silica, fully hydrated zeolite P ion exchanged with (Mn2+, Cd2+, Pb2+, Sr2+, Ba2+) cations. Microporous and Mesoporous Materials, 57(3): 229-248.

Ongley, E., Bynoe, M., Percival, J., 1981. Physical and geochemical characteristics of suspended solids, Wilton Creek, Ontario. Canadian Journal of Earth Sciences, 18(8): 1365-1379.

Osman, A.G., Kloas, W., 2010. Water quality and heavy metal monitoring in water, sediments, and tissues of the African Catfish Clarias gariepinus (Burchell, 1822) from the River Nile, Egypt. Journal of Environmental Protection, 1(4): 389-400.

Ozdes, D., Duran, C., Senturk, H.B., 2011. Adsorptive removal of Cd(II) and Pb(II) ions from

aqueous solutions by using Turkish illitic clay. Journal of Environmental Management, 92(12): 3082-3090.

Partin, C.A. et al., 2013. Large-scale fluctuations in Precambrian atmospheric and oceanic oxygen levels from the record of U in shales. Earth and Planetary Science Letters, 369-370: 284-293.

Partin, D.E., Okeeffe, M., 1991. The Structures and Crystal-Chemistry of Magnesium-Chloride and Cadmium Chloride. Journal of Solid State Chemistry, 95(1): 176-183.

Peacock, C.L., Sherman, D.M., 2004a. Copper(II) sorption onto goethite, hematite and lepidocrocite: a surface complexation model based on ab initio molecular geometries and EXAFS spectroscopy. Geochimica et Cosmochimica Acta, 68(12): 2623-2637.

Peacock, C.L., Sherman, D.M., 2004b. Vanadium(V) adsorption onto goethite (α-FeOOH) at pH 1.5 to 12: a surface complexation model based on ab initio molecular geometries and EXAFS spectroscopy. Geochimica et Cosmochimica Acta, 68(8): 1723-1733.

Peacock, C.L., Sherman, D.M., 2005. Surface complexation model for multisite adsorption of copper(II) onto kaolinite. Geochimica et Cosmochimica Acta, 69(15): 3733-3745.

Peng, X. et al., 2017a. Remediation of acid mine drainage using microbial fuel cell based on sludge anaerobic fermentation. Environmental Technology (United Kingdom), 38(19): 2400-2409.

Peng, X. et al., 2017b. Remediation of acid mine drainage using microbial fuel cell based on sludge anaerobic fermentation. Environmental technology, 38(19): 2400-2409.

Pentrak, M., Madejova, J., Komadel, P., 2010. Effect of chemical composition and swelling on acid dissolution of 2: 1 clay minerals. Philosophical Magazine, 90(17-18): 2387-2397.

Petersen, K., Kristensen, E., Bjerregaard, P., 1998. Influence of bioturbating animals on flux of cadmium into estuarine sediment. Marine Environmental Research, 45(4): 403-415.

Petrash, D.A., Lalonde, S.V., Raudsepp, M., Konhauser, K.O., 2011. Assessing the Importance of Organic Matrix Materials in Biofilm Chemical Reactivity: Insights from Proton and Cadmium Adsorption onto the Commercially Available Biopolymer Alginate. Geomicrobiology Journal, 28(3): 266-273.

Pivovarov, S., 2008. Adsorption of ions onto amorphous silica: ion exchange model. Journal of colloid and interface science, 319(1): 374-376.

Planavsky, N.J. et al., 2010. The evolution of the marine phosphate reservoir. Nature, 467(7319): 1088-1090.

Presley, B., Trefry, J., Shokes, R., 1980. Heavy metal inputs to Mississippi Delta sediments. Water, Air, and Soil Pollution, 13(4): 481-494.

Qin, H.-B. et al., 2019. Enrichment mechanisms of antimony and arsenic in marine ferromanganese oxides: Insights from the structural similarity. Geochimica et Cosmochimica Acta, 257: 110-130.

Rabung, T., Geckeis, H., Kim, J., Beck, P.H., 1998. Sorption of Eu(III) on a natural hematite application of a surface complexation model. Journal of Colloid and Interface Science, 208: 153-161.

Reich, T.J., Das, S., Koretsky, C.M., Lund, T.J., Landry, C.J., 2010. Surface complexation modeling of Pb(II) adsorption on mixtures of hydrous ferric oxide, quartz and kaolinite. Chemical Geology, 275(3): 262-271.

Reinhard, C.T. et al., 2017. Evolution of the global phosphorus cycle. Nature, 541(7637): 386-389.

Reinhard, C.T. et al., 2013. Proterozoic ocean redox and biogeochemical stasis. Proceedings of the National Academy of Sciences, 110(14): 5357-5362.

Retallack, G.J., Krinsley, D.H., 1993. Metamorphic alteration of a Precambrian (2.2 Ga) paleosol

from South Africa revealed by backscattered electron imaging. Precambrian Research, 63(1): 27-41.

Rozalén, M., Brady, P.V., Huertas, F.J., 2009. Surface chemistry of K-montmorillonite: Ionic strength, temperature dependence and dissolution kinetics. Journal of Colloid and Interface Science, 333(2): 474-484.

Ruiz-Agudo, E., Putnis, C.V., Rodriguez-Navarro, C., Putnis, A., 2012. Mechanism of leached layer formation during chemical weathering of silicate minerals. Geology, 40(10): 947-950.

Rye, R., Holland, H.D., 1998. Paleosols and the evolution of atmospheric oxygen: a critical review. American journal of science, 298(8): 621-672.

Appendix 1. Supplementary information for Chapter 2

SI Table 1.1: SSA, CEC and Ca/Na data for three clay minerals

	SSA (m^2/g)	CEC (meq/100g)	Ca/Na
Kaolinite	23.5	3.3	0
Illite	21.1	22.5	0
Montmorillonite	31.8	76.4	0.375

Note: Surface area of three clays was measured by BET liquid nitrogen adsorption. CEC of Kaolinite and montmorillonite are from the website of Clay Minerals Society (http://www.clays.org/sourceclays_data.html), while CEC of illite is from Missana et al. (2009). The Ca content in kaolinite and illite are negligible.

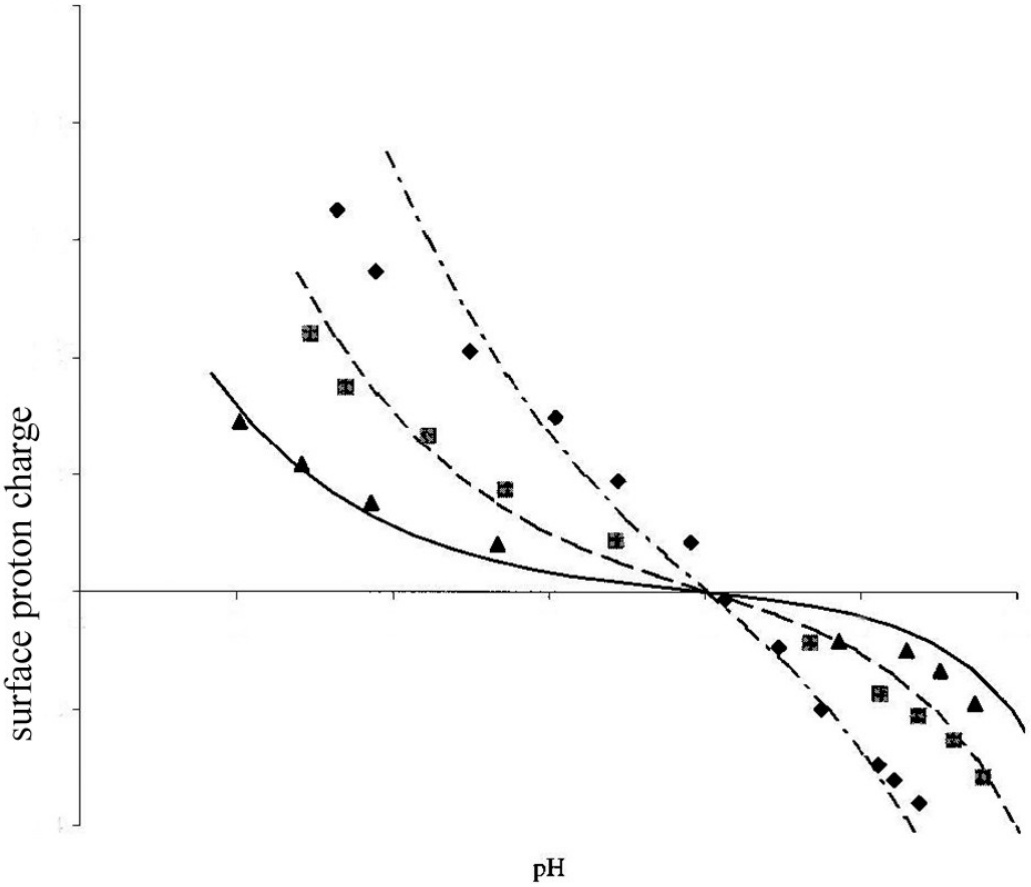

SI Figure 1.1 A theoretical model of titration curves for simple oxides at different ionic strength. Triangles: IS=0.001 M; squares: IS=0.01 M; diamonds: IS=0.1 M. Modified from Rabung et al. (1998).

Appendix 2. Supplementary information for Chapter 3

Description of clay mineral properties

The three clay minerals (KGa-2, Swy-2, and IMt-2) were obtained from the Clay Mineral Society, Source Clay Repository (Purdue University, West Lafayette, USA). Physical and chemical properties of the clays are listed in Table SI 2.1:

SI Table 2.1: Specific Surface Area (SSA), Cation Exchange Capacity (CEC), and Ca/Na data for three clay minerals.

	SSA (m^2/g)	CEC (meq/100g)	Ca/Na
Kaolinite	23.5	3.3	0
Illite	21.1	22.5	0
Montmorillonite	31.8	76.4	0.375

Note: Surface area of three clays was measured by BET liquid nitrogen adsorption. CEC of kaolinite and montmorillonite are from the website of Clay Minerals Society (http://www.clays.org/sourceclays_data.html), while CEC of illite is from Missana et al. (2009). The Ca content in kaolinite and illite are negligible.

Fits of titration and Cd adsorption data for the three clay minerals

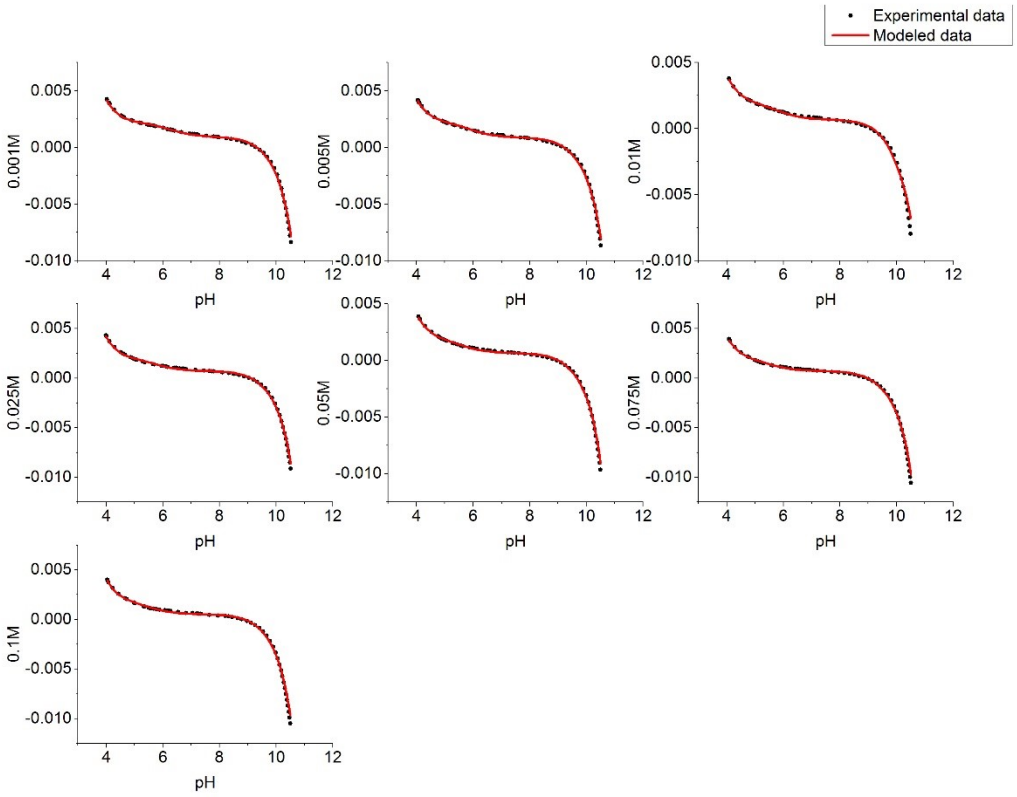

SI Figure 2.1 Fits of titration data for illite.

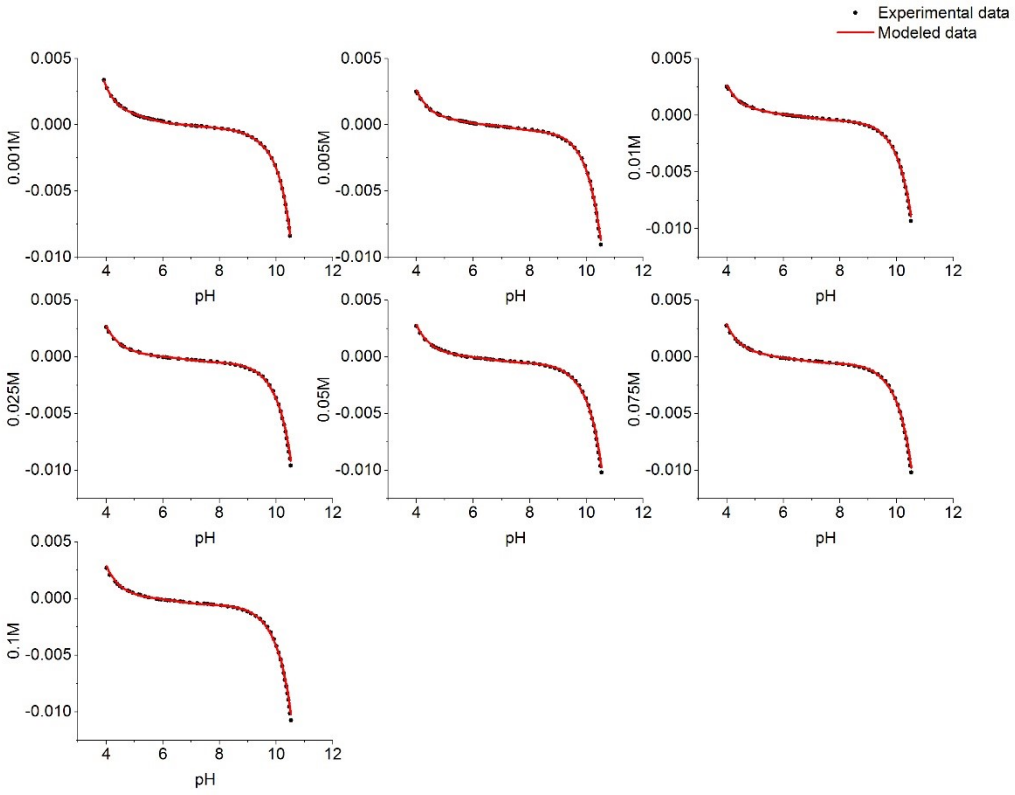

SI Figure 2.2 Fits of titration data for kaolinite.

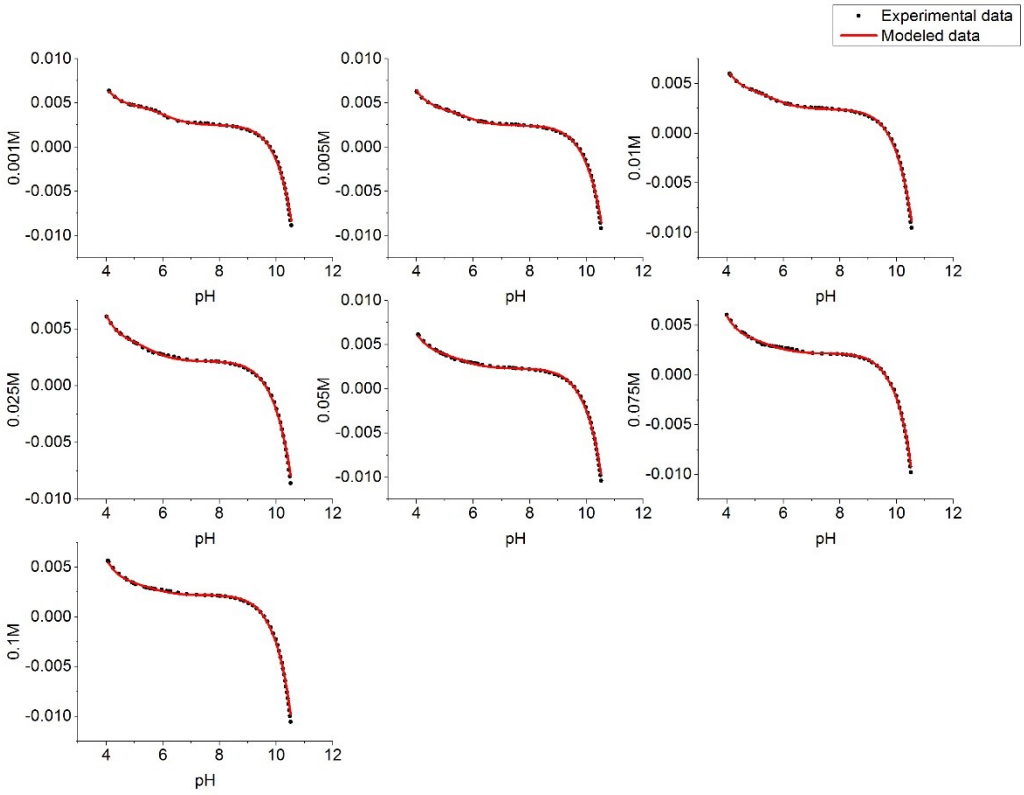

SI Figure 2.3 Fits of titration data for montmorillonite.

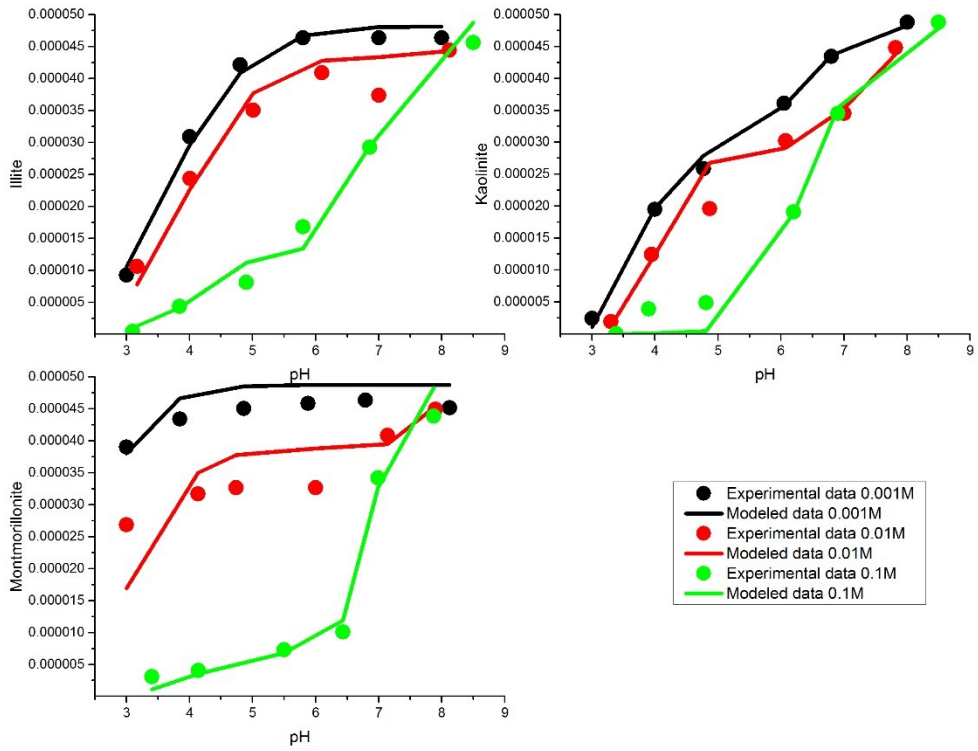

SI Figure 2.4 Fits of Cd adsorption data for all three clay minerals.

Summary of K values for three clay minerals

SI Table 2.2: Summary of FITEQL modeling parameters for kaolinite

0.001 M	K_L	K_{XO^-}	K_{XOH2^+}	Error
1	No Convergence			
2	-10.466	-7.786	5.708	0.076
3	-10.703	-7.745	5.657	0.086
Average	-10.584	-7.765	5.682	
STD	0.168	0.030	0.036	
0.005 M	K_L	K_{XO^-}	K_{XOH2^+}	Error
1	-8.979	-6.644	5.224	0.016
2	-10.233	-7.450	5.461	0.083
3	-10.142	-7.436	5.470	0.079
Average	-9.785	-7.177	5.385	
STD	0.699	0.462	0.139	
0.01 M	K_L	K_{XO^-}	K_{XOH2^+}	Error
1	-10.171	-7.576	5.391	0.089
2	-9.998	-7.167	5.295	0.112
3	-9.910	-7.079	5.354	0.112
Average	-10.027	-7.274	5.346	
STD	0.133	0.266	0.048	
0.025 M	K_L	K_{XO^-}	K_{XOH2^+}	Error
1	-9.118	-6.418	5.240	0.052
2	-9.777	-7.070	5.189	0.096
3	-9.971	-6.868	5.108	0.123
Average	-9.622	-6.785	5.179	

STD	0.447	0.334	0.067	
0.05 M	K_L	K_{XO-}	K_{XOH2+}	Error
1	-8.657	-6.305	5.130	0.065
2	-9.619	-6.699	4.934	0.133
3	-9.622	-6.542	4.735	0.138
Average	-9.299	-6.515	4.933	
STD	0.556	0.199	0.197	
0.075 M	K_L	K_{XO-}	K_{XOH2+}	Error
1	-9.647	-6.526	4.888	0.142
2	-9.648	-6.807	4.754	0.185
3	-9.191	-6.324	4.988	0.142
Average	-9.495	-6.552	4.877	
STD	0.263	0.242	0.118	
0.1 M	K_L	K_{XO-}	K_{XOH2+}	Error
1	-9.365	-6.389	4.730	0.146
2	-9.780	-6.635	4.698	0.161
3	-9.731	-6.594	4.693	0.165
Average	-9.625	-6.539	4.707	
STD	0.227	0.132	0.020	

Note: Number 1, 2, 3 indicates each of the triplicates for each titration run at the given IS.

SI Table 2.3: Summary of FITEQL modeling parameters for illite

0.001 M	K_L	K_{XO^-}	K_{XOH2^+}	Error
1	-6.275	-11.043	9.788	0.396
2	-6.283	-11.842	9.855	0.355
3	-6.307	-11.372	9.833	0.297
Average	-6.288	-11.419	9.825	
STD	0.017	0.401	0.034	
0.005 M	K_L	K_{XO^-}	K_{XOH2^+}	Error
1	-5.981	-11.030	9.640	0.308
2	-5.950	-11.608	9.715	0.348
3	-6.053	-10.716	9.790	0.311
Average	-5.995	-11.118	9.715	
STD	0.053	0.452	0.075	
0.01 M	K_L	K_{XO^-}	K_{XOH2^+}	Error
1	-5.860	-10.143	9.727	0.723
2	-5.970	-10.140	9.742	0.799
3	-5.920	-10.075	9.732	0.832
Average	-5.917	-10.119	9.734	
STD	0.055	0.038	0.008	
0.025 M	K_L	K_{XO^-}	K_{XOH2^+}	Error
1	-5.802	-11.060	9.606	0.299
2	-5.761	-11.127	9.632	0.317
3	-5.817	-11.310	9.650	0.318
Average	-5.793	-11.166	9.629	
STD	0.029	0.130	0.022	

0.05 M	K_L	K_{XO^-}	K_{XOH2^+}	Error
1	-5.630	-10.808	9.487	0.274
2	-5.720	-10.251	9.637	0.586
3	-5.660	-10.775	9.538	0.288
Average	-5.670	-10.611	9.554	
STD	0.045	0.312	0.077	
0.075 M	K_L	K_{XO^-}	K_{XOH2^+}	Error
1	-5.600	-10.711	9.450	0.301
2	-5.582	-10.510	9.457	0.371
3	-5.486	-10.793	9.511	0.324
Average	-5.556	-10.671	9.473	
STD	0.062	0.146	0.033	
0.1 M	K_L	K_{XO^-}	K_{XOH2^+}	Error
1	-5.582	-10.432	9.526	0.326
2	-5.565	-10.783	9.514	0.272
3	-5.318	-10.008	9.698	0.962
Average	-5.488	-10.408	9.579	
STD	0.148	0.388	0.103	

Note: Number 1, 2, 3 indicates each of the triplicates for each titration run at the given IS.

SI Table 2.4: Summary of FITEQL modeling parameters for montmorillonite

0.001 M	K_L	K_{XO^-}	K_{XOH2^+}	Error
1	-6.065	-11.358	10.214	0.375
2	-5.944	-11.620	10.155	0.493
3	-5.983	-10.400	10.029	0.834
Average	-5.997	-11.126	10.133	
STD	0.062	0.643	0.094	
0.005 M	K_L	K_{XO^-}	K_{XOH2^+}	Error
1	-5.758	-11.329	10.032	0.340
2	-5.811	-10.993	10.101	0.332
3	-5.708	-10.648	10.048	0.608
Average	-5.759	-10.990	10.060	
STD	0.051	0.341	0.036	
0.01 M	K_L	K_{XO^-}	K_{XOH2^+}	Error
1	-5.708	-11.334	10.021	0.314
2	-5.648	-10.359	10.012	0.736
3	-5.628	-10.856	9.930	0.457
Average	-5.661	-10.850	9.988	
STD	0.041	0.488	0.050	
0.025 M	K_L	K_{XO^-}	K_{XOH2^+}	Error
1	-5.490	-10.968	9.844	0.599
2	-5.594	-10.968	9.922	0.348
3	-5.596	-10.715	9.860	0.424
Average	-5.560	-10.884	9.875	
STD	0.061	0.146	0.041	

0.05 M	K_L	K_{XO^-}	K_{XOH2^+}	Error
1	-5.637	-10.983	9.926	0.413
2	-5.519	-10.731	9.711	0.338
3	-5.545	-10.741	9.975	0.574
Average	-5.567	-10.818	9.871	
STD	0.062	0.143	0.141	
0.075 M	K_L	K_{XO^-}	K_{XOH2^+}	Error
1	-5.526	-11.033	9.839	0.393
2	-5.420	-10.620	9.865	0.666
3	-5.487	-10.491	9.870	0.556
Average	-5.478	-10.715	9.858	
STD	0.054	0.283	0.017	
0.1 M	K_L	K_{XO^-}	K_{XOH2^+}	Error
1	-5.618	-10.738	9.880	0.346
2	-5.628	-10.474	9.957	0.510
3	-5.850	-10.487	9.661	1.749
Average	-5.699	-10.566	9.833	
STD	0.131	0.149	0.153	

Note: Number 1, 2, 3 indicates each of the triplicates for each titration run at the given IS.

Sodium ions release during ultrapure water titration

Since our clay minerals were washed in 0.1 M $NaNO_3$ solution prior to titration, some Na^+ ions will be initially present on the clay mineral surfaces. To test how the initially loaded Na^+ might influence the solution IS, the three pretreated clay minerals were placed in pH=4 ultrapure water at the same clay-to-solution ratio as in the titrations. After 30 mins, the suspension was centrifuged, and the supernatant was analyzed for Na^+ concentration by Inductively Coupled Plasma Mass Spectrometry (ICP-MS) on an Agilent 8800 MS/MS at the University of Alberta's Environmental Geochemistry lab. This process was repeated in triplicate and the initial Na^+ released from each of the three clays is presented in the below figure.

The amount of Na^+ released from clay minerals is generally less than 30 mg/kg for 50 mg of clay minerals, with montmorillonite having the highest amount of Na^+ released and kaolinite/illite being considerably lower. Relative to our experimental condition, where the lowest IS is 0.001 M, the 30 mg/kg of Na^+ released into solution effectively doubles the ionic strength. However, when plotting IS in logarithmic units, the difference is relatively small. To calculate the concentration of Na^+ in solution for montmorillonite, the 30 mg/kg of Na^+ released by montmorillonite was added, while for kaolinite and illite, the amount of Na^+ released was ignored for the calculation of solution Na^+ concentration.

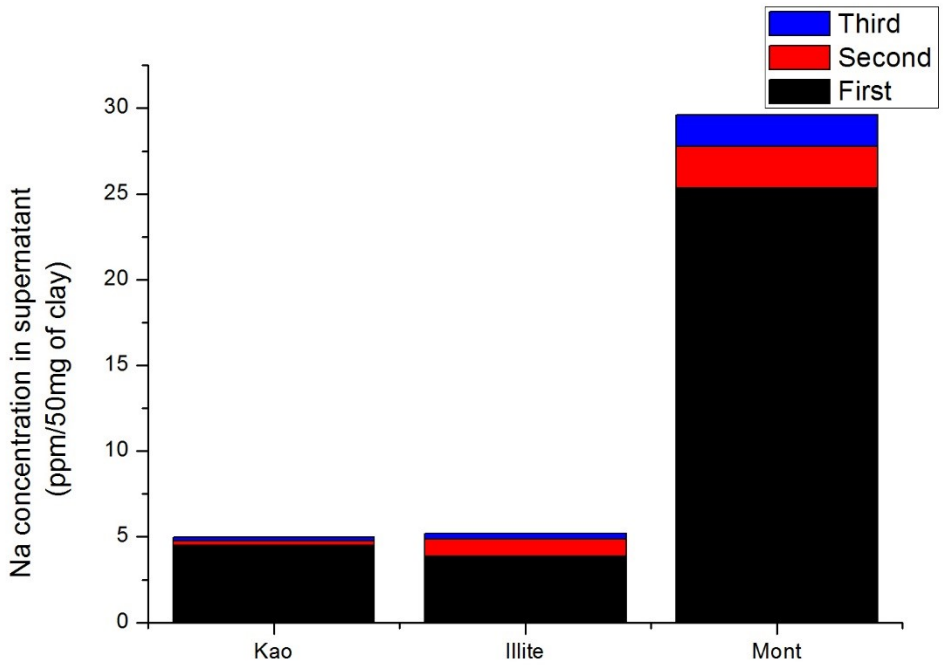

SI Figure 2.5 Sodium release from the Milli-Q water washing process

The incorporation of Na binding constant into SCM

The system equations for the SCM that incorporates Na binding constants are listed below:

$$\equiv LH \leftrightarrow H^+ + \equiv L^- \qquad \text{(R. SI 2.1)}$$

$$K_a = \frac{[\equiv L^-] \bullet \alpha_{H+}}{[\equiv LH]} \qquad \text{(eq. SI 2.1)}$$

$$\equiv XOH \leftrightarrow H^+ + \equiv XO^- \qquad \text{(R.SI 2.2)}$$

$$K_{a-} = \frac{[\equiv XO^-] \bullet \alpha_{H+}}{[\equiv XOH]} \qquad \text{(eq. SI 2.2)}$$

$$\equiv XOH + H^+ \leftrightarrow \equiv XOH_2^+ \qquad \text{(R. SI 2.3)}$$

$$K_{a+} = \frac{[\equiv XOH_2^+]}{[\equiv XOH] \bullet \alpha_{H+}} \qquad \text{(eq. SI 2.3)}$$

$$\equiv LH + Na^+ \leftrightarrow \equiv LNa + H^+ \qquad \text{(R. SI 2.4)}$$

$$K_{LNa} = \frac{[\equiv LNa] \bullet \alpha_{H+}}{[\equiv LH] \bullet \alpha_{Na+}} \qquad \text{(eq. SI 2.4)}$$

Once incorporated, Na binding and Cd adsorption data from literature were used to test if constant Cd binding capacity can be derived under varying IS condition.

SI Table 2.5: The modeling of Cd adsorption using literature data

Kao	Gu and Evans (2008)		
IS	0.001M	0.01M	0.1M
$\log(K_{LCd})$	-2.072	-3.054	-2.764
$\log(K_{XOCd})$	3.968	3.437	-0.794
Illite	Gu and Evans (2007)		

IS	0.001M	0.01M	0.1M
$\log(K_{LCd})$	0.805	0.453	-0.471
$\log(K_{XOCd})$	-163.0	-2.322	0.546
Mont		Gu et al. (2010)	
IS	0.001M	0.01M	0.1M
$\log(K_{LCd})$	1.668	0.784	-0.284
$\log(K_{XOCd})$	-160.0	-1.601	-0.303

Size fractionation titration and XRD

Size fractionation experiments were done for all three clay minerals. To separate the <2 μm and >2 μm size fractions of illite, kaolinite, and montmorillonite, the procedure of Arroyo et al. (2004) was followed. 25 g of each clay was measured and mixed with 500 mL of deionized water in separate 1 L beakers. In order to hydrate the clays, the mixtures were then stirred using a magnetic stir bar for 24 hr prior to centrifuging. For each clay, the resulting slurry was separated into three 500 mL polyethylene centrifuge bottles and centrifuged at 600 rpm for 6 min (Sorvall Lynx 4000). The supernatant containing the <2 μm size fraction was split further into twelve 50 mL polyethylene centrifuge tubes and centrifuged at 4500 rpm for 30 min. The pellet, representing the >2 μm size fraction, was transferred to 50 mL falcon tubes. The subsequent supernatant was then discarded. The top portion of the pellet, the portion clearly smallest in size, was then separated into new 50 mL polyethylene tubes. Both the <2 and >2 μm size fractions were frozen overnight at -4°C, freeze-dried (Thermo Savant MicroModulyo-115), and stored.

The mass of the <2μm size fractions was 0.3g, 0.4g, and 4.9g for kaolinite, illite, and montmorillonite, respectively, which accounted for 1.2%, 1.6%, and 19.6% of the total mass. The acid-base titrations of size fractionated clay were performed in a 0.1 M $NaNO_3$ electrolyte solution. The same experimental conditions were applied to the size-fractionated clay with raw clay samples, and triplicate experiments were performed for all three clays. The SCM modeling procedure was the same with raw samples in order to be able to make a direct comparison. The titration results are given in Table SI 5. And the XRD spectrum is shown in Fig. SI 6 a-c.

According to XRD spectra, the size fractionated clays still contain impurities, although at lower levels. Kaolinite mainly has anatase, while montmorillonite and illite have quartz, gibbsite,

and muscovite, among other minor contaminants. The spectra of the size fractionated clays were similar to that of the raw clay samples.

SI Table 2.6: The comparison of SCM modeling results for size fractionated clay samples and raw samples.

	$logK_a$		$logK_{a-}$		$logK_{a+}$	
	Mont size fractionated	Mont raw	Mont size fractionated	Mont raw	Mont size fractionated	Mont raw
average	-6.662	-5.699	-10.18	-10.57	9.338	9.833
STD	0.05307	0.1310	0.3035	0.1490	0.09077	0.1530
	Illite size fractionated	Illite raw	Illite size fractionated	Illite raw	Illite size fractionated	Illite raw
average	-6.486	-5.488	-10.23	-10.41	9.459	9.579
STD	0.1728	0.1476	0.2691	0.3879	0.06303	0.1031
	Kao size fractionated	Kao raw	Kao size fractionated	Kao raw	Kao size fractionated	Kao raw
average	No convergence	-9.625	No convergence	-6.539	No convergence	4.707
STD	No convergence	0.227	No convergence	0.132	No convergence	0.020

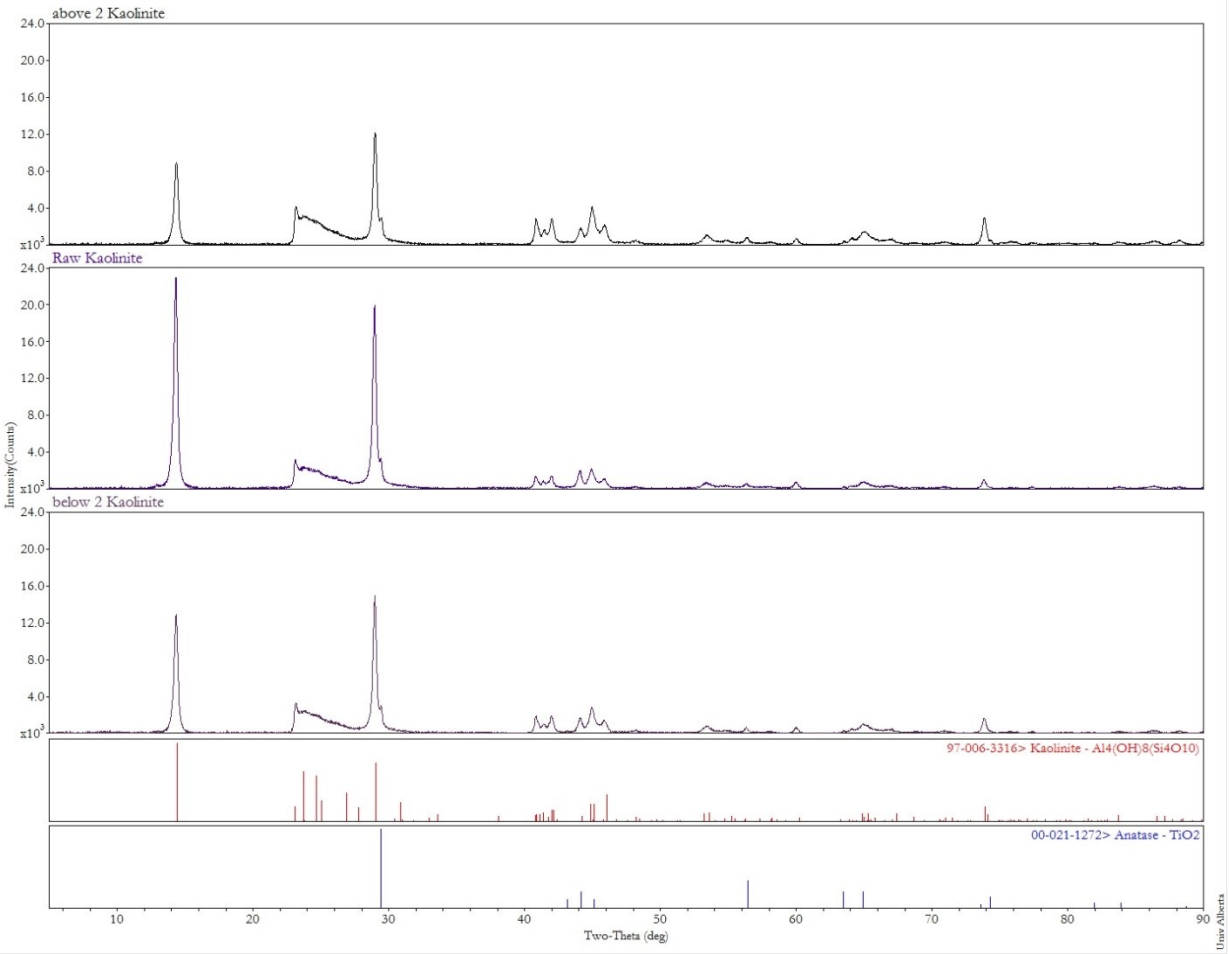

SI Figure 2.6 XRD spectrum of size fractionated kaolinite and the fitting by reference materials.

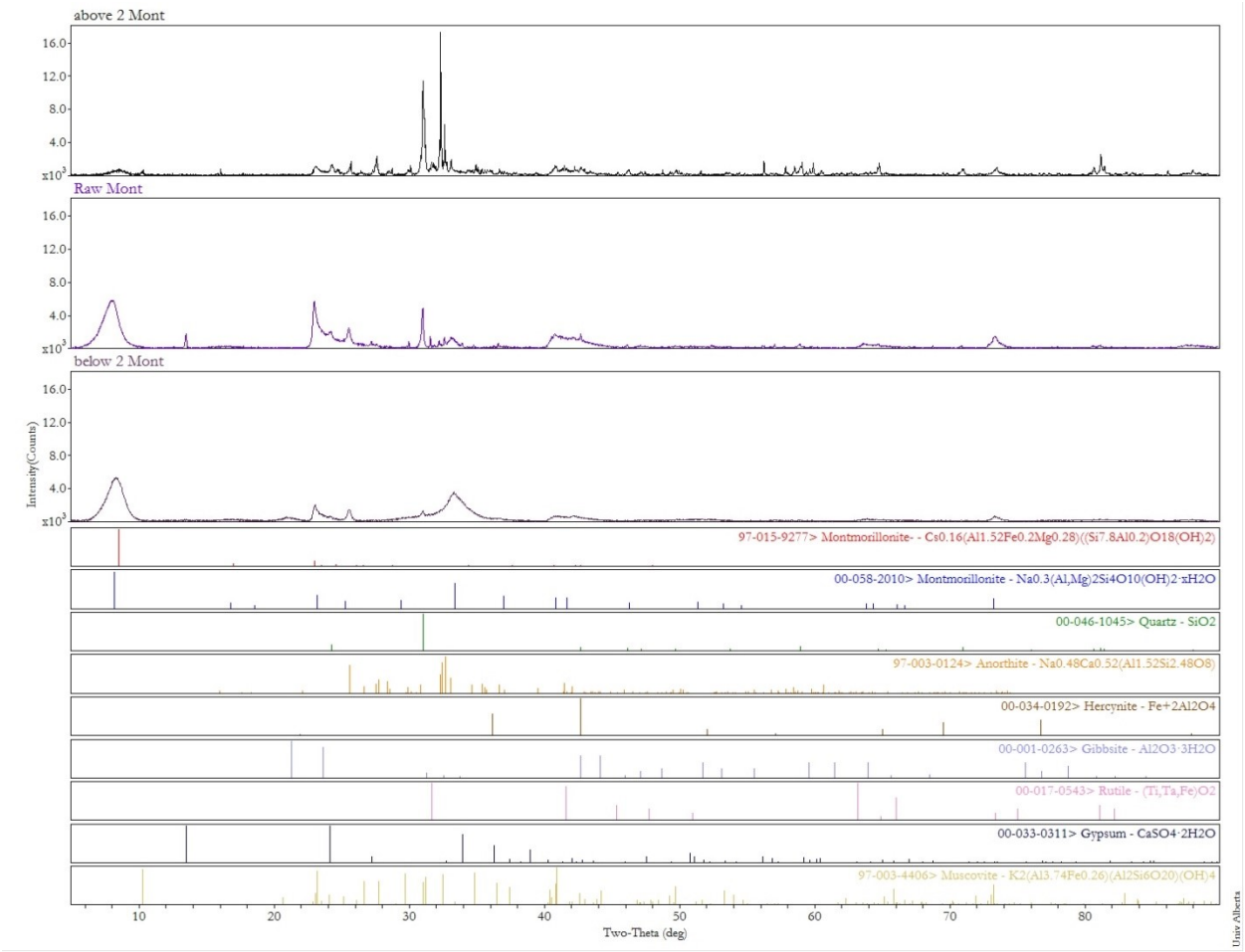

SI Figure 2.7 XRD spectrum of size fractionated montmorillonite and the fitting by reference materials.

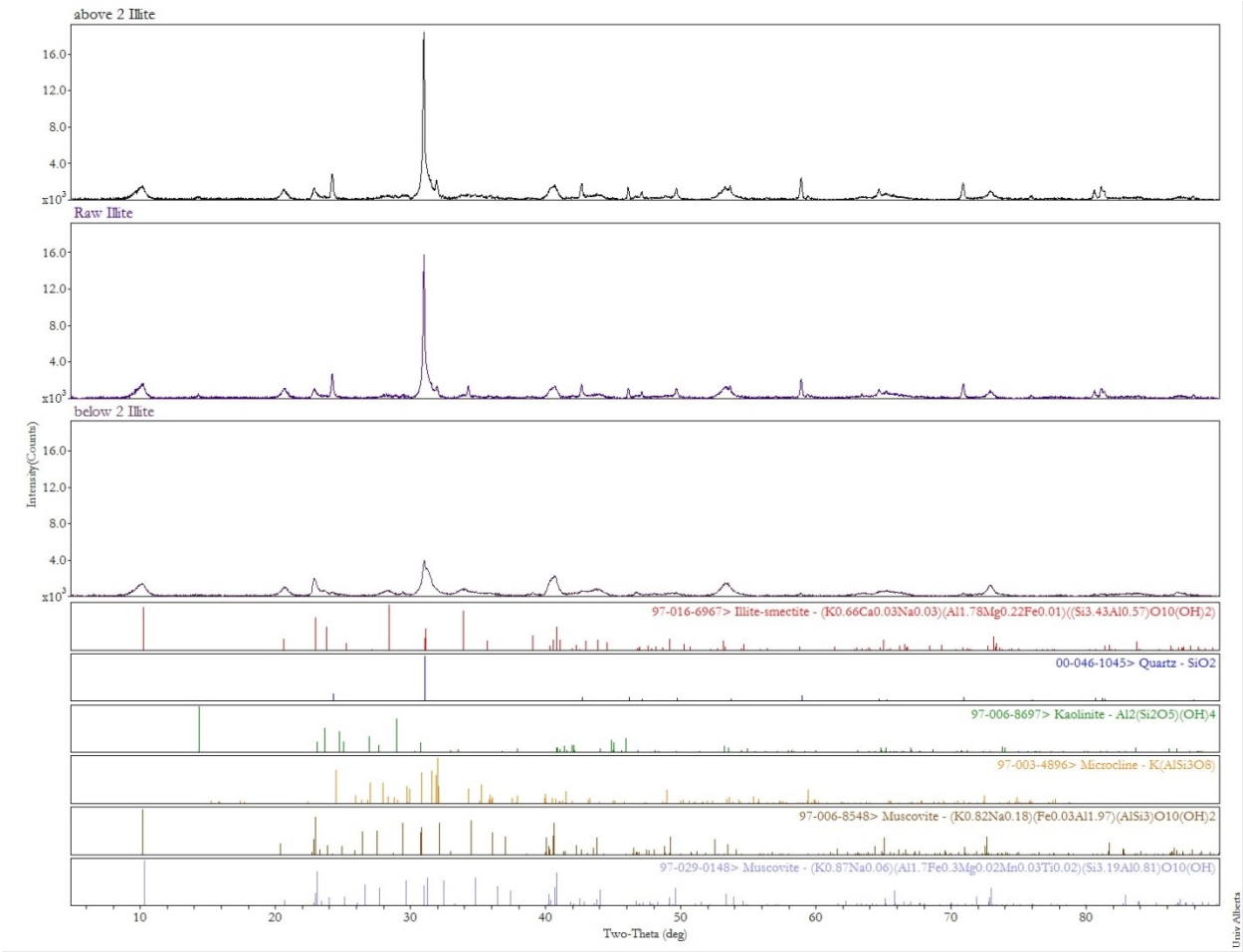

SI Figure 2.8 XRD spectrum of size fractionated illite and the fitting by reference materials.

Reference

Arroyo, L. J., Li, H., Teppen, B. J., Johnston, C. T., Boyd, S. A. (2004). Hydrolysis of Carbaryl by Carbonate Impurities in Reference Clay SWy-2. *Journal of Agricultural and Food Chemistry* 54: 8066-8073.

Modeling results by applying cation exchange reaction for ≡LH sites

SI Table 2.7: Summary of FITEQL modeling results

IS	0.001	0.005	0.01	0.025	0.05	0.075	0.1
Log(IS)	-3	-2.301	-2	-1.602	-1.301	-1.125	-1
				Kaolinite			
$LogK_{Na}$	-7.633	-7.678	-8.027	-7.932	-7.985	-8.522	-8.625
STD	0.196	0.367	0.133	0.362	0.578	0.001	0.227
$LogK_{a-}$	-7.763	-7.411	-7.274	-6.785	-6.507	-6.620	-6.539
STD	0.031	0.054	0.266	0.334	0.212	0.162	0.132
$LogK_{a+}$	5.687	5.426	5.347	5.179	4.934	4.843	4.707
STD	0.035	0.070	0.048	0.066	0.199	0.077	0.020
				Illite			
$LogK_{Na}$	-3.277	-3.691	-3.934	-4.191	-4.379	-4.432	-4.558
STD	0.017	0.053	0.049	0.029	0.062	0.063	0.029
$LogK_{a-}$	-11.413	-11.118	-10.627	-11.166	-10.899	-10.643	-10.575
STD	0.396	0.452	0.033	0.130	0.187	0.142	0.180
$LogK_{a+}$	9.831	9.716	9.643	9.629	9.538	9.481	9.514
STD	0.034	0.075	0.015	0.022	0.052	0.028	0.009
				Montmorillonite			
$LogK_{Na}$	-2.973	-3.454	-3.657	-3.956	-4.265	-4.331	-4.619
STD	0.064	0.052	0.041	0.061	0.065	0.059	0.009
$LogK_{a-}$	-11.166	-10.585	-10.440	-10.647	-10.425	-10.320	-10.132
STD	0.695	0.169	0.331	0.297	0.070	0.176	0.153
$LogK_{a+}$	10.137	10.045	9.996	9.880	9.880	9.884	10.024
STD	0.093	0.039	0.070	0.040	0.128	0.041	0.122

Appendix 3. Supplementary information for Chapter 5

SI Table 3.1: The input parameters for FITEQL modelling of Cd adsorption onto the three studied clay minerals.

Log K of protonation reactions			≡LH+Na^+↔H^++≡LNa	≡XOH↔H^++≡XO^-	≡XOH+H^+↔ ≡XOH_2^+
Kaolinite (NEM)	Ka	IS=0.01M	-8.027	-7.274	5.347
		IS=0.56M	-8.973	-5.971	4.437
	Site density	IS=0.01M	1.020E-04	2.322E-05	
		IS=0.56M	5.865E-05	2.166E-05	
Kaolinite (CCM)	Ka	IS=0.01M	-5.726	-9.271	8.442
		IS=0.56M	-5.247	-8.899	7.902
	Site density	IS=0.01M	3.490E-05	2.427E-05	
		IS=0.56M	3.427E-05	1.588E-05	
Montmorillonite (NEM)	Ka	IS=0.01M	-3.657	-10.440	9.996
		IS=0.56M	-5.083	-9.917	9.821
	Site density	IS=0.01M	9.286E-05	2.147E-04	
		IS=0.56M	4.844E-05	1.448E-04	
Montmorillonite (CCM)	Ka	IS=0.01M	-3.625	-10.353	11.229
		IS=0.56M	-5.046	-9.790	10.679
	Site density	IS=0.01M	9.050E-05	2.146E-04	
		IS=0.56M	4.597E-05	1.443E-04	
Illite (NEM)	Ka	IS=0.01M	-3.934	-10.627	9.643
		IS=0.56M	-5.030	-10.406	9.367
	Site density	IS=0.01M	5.243E-05	8.310E-05	
		IS=0.56M	4.343E-05	6.235E-05	
Illite (CCM)	Ka	IS=0.01M	-6.389	-10.243	9.761
		IS=0.56M	-5.517	-9.647	9.475
	Site density	IS=0.01M	5.655E-05	8.788E-05	
		IS=0.56M	5.055E-05	6.971E-05	

Parameters used in CCM	Surface area (m^2/g)	Suspension density (g/L)	Inner-layer capacitance (F/m^2)
kaolinite	18.15	1	16.0
montmorillonite	22.21	1	14
illite	21.06	1	8.0

Log K of hydrolysis reactions and chloride complex	River	Marine
$Cd^{2+}+H_2O=CdOH^{+}+H^{+}$	-10.010	-9.835
$Cd^{2+}+2H_2O=Cd(OH)_2$	-20.210	-20.035
$Cd^{2+}+3H_2O=Cd(OH)_3^{-}+3H^{+}$	-31.700	-31.700
$Cd^{2+}+4H_2O=Cd(OH)_4^{2-}+4H^{+}$	-47.480	-47.830
$2Cd^{2+}+H_2O=Cd_2(OH)_3^{+}+H^{+}$	-9.490	-9.665
$4Cd^{2+}+4H_2O=Cd_4(OH)_4^{4+}+4H^{+}$	-32.979	-32.330
$Cd^{2+}+Cl^{-}=CdCl^{+}$	2.18	2.53
$Cd^{2+}+2Cl^{-}=CdCl_2$	2.97	3.49
$Cd^{2+}+3Cl^{-}=CdCl_3^{-}$	2.37	2.89

Note, the protonation and site density data are from Hao et al. (2019a); Cd hydrolysis and chloride complex data are from Baes and Mesmer (1997) and Liu et al. (2018).

SI Table 3.2: Calculated binding constants for Cd adsorption onto three clay minerals.

		Freshwater			Marine		
		$Log(K_{LCd})$	$Log(K_{XOCd})$	V(Y)	$Log(K_{LCd})$	$Log(K_{XOCd})$	V(Y)
Kaolinite	NEM	-3.164	-1.664	0.142	-0.514	0.942	0.005
	CCM	-0.930	-1.516	0.012	1.331	-0.522	0.018
Illite	NEM	-1.209	0.199	0.179	1.388	-1.425	0.009
	CCM	-0.583	-0.104	0.118	1.495	-1.746	0.004
Montmorillonite	NEM	-0.687	-2.214	0.596	1.551	-1.173	0.015
	CCM	0.496	-1.021	0.573	2.137	-0.364	0.014

The modelled log K_{Cd} values for the NEM and CCM are similar for each clay at both marine and freshwater conditions. In almost all cases, log K_{Cd} adsorption constants vary from -3 to 3 (except for NEM of kaolinite under freshwater conditions, which has a log K_{LCd} of -3.164), within the same range reported in previous research (Gu and Evans, 2007; Gu and Evans, 2008; Gu et al., 2010; Liu et al., 2018), indicating that the calculated values are consistent with the intrinsic Cd binding constants for the clay surface functional groups.

Despite the similarity of the log K_{Cd} values, the log K values determined for marine conditions are slightly higher than those calculated for freshwater conditions. In fact, the intrinsic K value should not vary with solution ionic strength and is only a function of temperature, pressure and specific to adsorbent/adsorbate properties (Sverjensky and Sahai, 1996). Electronic SCM, by comparison with non-electrostatic SCM, has an advantage in deriving intrinsic K values through considering electrostatic interaction. However, previous research has concluded that the difficulty of deriving IS-independent K values even applying electrostatic SCM. especially for clay minerals (Goldberg, 2005; Landry et al., 2009; Reich et al., 2010; Hao et al., 2019a; Schaller et al., 2009) This is possibly due to the complexity of clay surface electrostatic field which consists of both

protonation-deprotonation induced and permanent-charge induced sites (Hao et al., 2019a). It is also possible that the modelling procedure was influenced by the high Cl concentration under marine conditions because it can strongly mobilize Cd from clay surfaces to form soluble Cd-Cl molecules, such as $CdCl^-$ and $CdCl_2$. Although it is hard to derive the intrinsic Cd adsorption K value, our results provide an acceptable range for intrinsic $logK_{Cd}$ which could cover most of natural ionic strength condition.

Appendix 4. Supplementary information for Chapter 6

Surface complexation modelling (SCM) of phosphate adsorption onto kaolinite surfaces

Kaolinite surface adsorption sites are highly protonated with a positive charge under low pH but are deprotonated with pH increasing. Specifically, under pH<4.7, kaolinite surfaces are dominated by $\equiv XOH_2^+$ (0.023 mmol/g) and ≡LH (0.068 mmol/g) group, while both of them are deprotonated with pH increasing (SI Figure 4.1). $\equiv XOH_2^+$ sites are firstly deprotonated as ≡XOH at pH=4.7, and then a secondly deprotonation occurs at pH=6.5 resulting in a $\equiv XO^-$ species. By contrast, ≡LH has a single deprotonation reaction which occurs at pH=9.6.

The P speciation diagram is shown in SI Fig. 2. At pH<2, P is highly protonated as H_3PO_4, which has three deprotonation reactions at pH=2, 7, 12, resulting in species of $H_2PO_4^-$, HPO_4^{2+}, and PO_4^{3+} respectively. At pH<4.7, while under this condition phosphate aqueous species is negatively charged ($H_2PO_4^-$, see SI Fig 2), which shows affinity to kaolinite positively charged surfaces ($\equiv XOH_2^+$). With pH increasing to 8, surface species are mainly dominated by $\equiv L^-$ and $\equiv XO^-$ group which is repulsive to negatively charged $H_2PO_4^-$ and HPO_4^{2-}.

A surface complexation modelling of P adsorption onto kaolinite generate the best fit by applying double site bidentate adsorption model. This indicates that both ≡XOH and ≡LH sites can adsorb P while ≡XOH sites bind P though bidentate complex and ≡LH sites form monodentate complex with P. The adsorption constants (K_{P1} and K_{P2} in SI Table 4.1) indicate that P is more preferentially adsorbed on $\equiv XOH_2^+$ sites (K_{P2}=37.46) than ≡LH sites (K_{P1}=16.06).

Modelling and experimental procedure

Acid-base titration experiments coupled with surface complexation modelling were performed to determine its surface proton/deprotonation behaviour (detailed information is listed in (Hao et al., 2018; Hao et al., 2019). Two surface functional groups were applied in the modelling and the surface protonation and deprotonation reactions are listed in SI Table 4.1 (detailed modelling procedure and discussion could refer to (Hao et al., 2019)):

Phosphate adsorption onto kaolinite as a function of pH batch experiments were performed under 10μmol of P and 1g/L kaolinite suspension. A 100ml of 10μmol phosphate solution was prepared in 150ml beaker by diluting 5 mmol of Na_2HPO_4 solution. The experimental procedure was similar to our previous study (Liu et al., 2018). The phosphate adsorption pH edge experiments were performed by duplicate to ensure the accuracy of results. All the adsorption pH edge results were modelled by applying a non-electrostatic model using Fiteql 4.0 (Westall, 1982). SI Table 4.1 listed all the P adsorption equations that are incorporated into the model.

Phosphate adsorption onto kaolinite as a function of pH is shown in SI Fig. 3. The experimental data were fitted by single site bidentate adsorption model, single site monodentate model, double site bidentate model, double site monodentate model (fitting results are listed in SI Fig. 3, the schematic models of the four models are shown in SI Fig. 4). Among these models, double site monodentate model has poor fitting result at low pH range, while both single site bidentate and single site monodentate underestimated P adsorption at high pH range. Based on our simulation results, double site bidentate model is the best model for P adsorption onto kaolinite surfaces. The adsorption equilibrium constants that derived were listed in SI Table 4.1.

SI Table 4.1: Surface complexation modelling results of P adsorption onto kaolinite

Reaction	Equilibrium constant	logK1	Site density 1 (mol/g)
Surface protonation reactions			
$\equiv LH \leftrightarrow H^+ + \equiv L^-$	$K_a = \frac{[\equiv L^-] \bullet \alpha_{H^+}}{[\equiv LH]}$	9.625*	6.789E-5*
$\equiv XOH \leftrightarrow H^+ + \equiv XO^-$	$K_{a-} = \frac{[\equiv XO^-] \bullet \alpha_{H^+}}{[\equiv XOH]}$	6.539*	2.305E-5*
$\equiv XOH + H^+ \leftrightarrow \equiv XOH_2^+$	$K_{a+} = \frac{[\equiv XOH_2{}^+]}{[\equiv XOH] \bullet \alpha_{H^+}}$	4.707*	
Phosphate adsorption reactions			
$\equiv LH + PO_4^{3-} + H^+ \leftrightarrow \equiv LH\text{–}HPO_4^{2-}$	$K_{P1} = \frac{[\equiv LH\text{–}HPO_4{}^{2-}]}{[\equiv LH] \bullet \alpha_{H^+} \bullet \alpha_{PO4^{3-}}}$	16.06**	
$2\equiv XOH_2^+ + HPO_4^{2-} \leftrightarrow (\equiv XOH_2^+)_2\text{–}HPO_4^{2-}$	$K_{P2} = \frac{[(\equiv XOH_2{}^+)_2\text{–}HPO_4{}^{2-}]}{[\equiv XOH_2{}^+]_2{}^2 \bullet \alpha_{HPO4^{2-}}}$	37.46**	
Hydrolysis reactions and sodium complexes			
$PO_4^{3-} + H^+ \leftrightarrow HPO_4^{2-}$	$K_1 = \frac{\alpha_{HPO4^{2-}}}{\alpha_{PO4^{3-}} \bullet \alpha_{H^+}}$	12.38***	
$PO_4^{3-} + 2H^+ \leftrightarrow H_2PO_4^-$	$K_2 = \frac{\alpha_{H2PO4^-}}{\alpha_{PO4^{3-}} \bullet \alpha_{H^+}{}^2}$	19.57***	
$PO_4^{3-} + 3H^+ \leftrightarrow H_3PO_4$	$K_3 = \frac{\alpha_{H3PO4}}{\alpha_{PO4^{3-}} \bullet \alpha_{H^+}{}^3}$	21.72***	
$PO_4^{3-} + H^+ + 2Na^+ \leftrightarrow Na_2HPO_4$	$K_4 = \frac{\alpha_{Na2HPO4}}{\alpha_{PO4^{3-}} \bullet \alpha_{H^+} \bullet \alpha_{Na^+}{}^2}$	13.32***	
$PO_4^{3-} + 2Na^+ \leftrightarrow Na_2PO_4^-$	$K_5 = \frac{\alpha_{Na2PO4^-}}{\alpha_{PO4^{3-}} \bullet \alpha_{Na^+}{}^2}$	2.59***	

$PO_4^{3-}+2H^++Na^+ \leftrightarrow NaH_2PO_4$	$K_6 = \frac{\alpha_{NaH2PO4}}{\alpha_{PO4^{3-}} \bullet \alpha_{Na^+} \bullet \alpha_{H^+}{}^2}$	19.87***
$PO4^{3-}+H^++Na^+ \leftrightarrow NaHPO_4^-$	$K_7 = \frac{\alpha_{NaHPO4^-}}{\alpha_{PO4^{3-}} \bullet \alpha_{H^+} \alpha_{Na^+}}$	13.45***
$PO4^{3-}+Na^+ \leftrightarrow NaPO_4^{2-}$	$K_8 = \frac{\alpha_{NaPO4^{2-}}}{\alpha_{PO4^{3-}} \bullet \alpha_{Na^+}}$	1.430***

Note: * are values from (Hao et al., 2019); ** are values derived from this study; *** are values from Visual MINTEQ version 3.1.

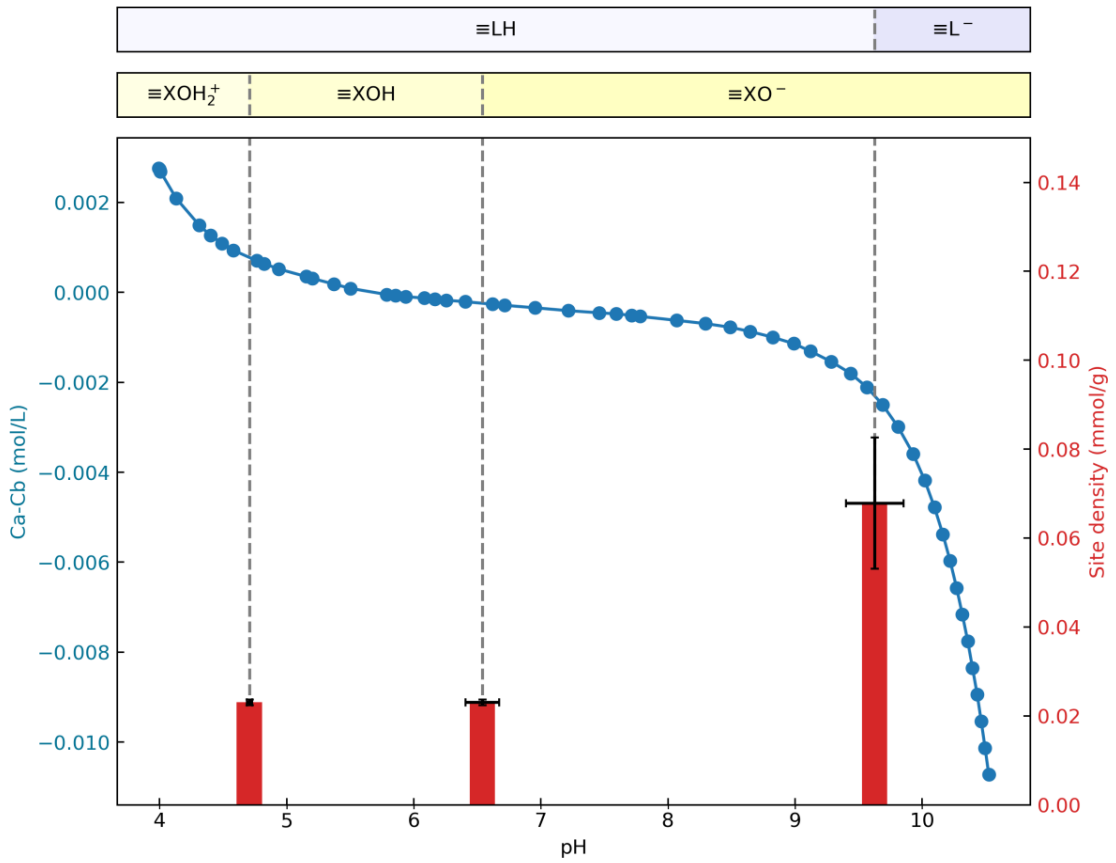

SI Figure 4.1 Titration and surface complexation modelling results of kaolinite. Blue dots and line are raw titration (C_a-C_b as a function of pH; C_a-C_b is the subtraction of added acid and base concentration, representing the net protons added); Red bars are the pK_a values of the two surface functional group plotted with the site concentration of two groups, to be specific, the left and middle red bars represent ≡XOH group (site concentration is 0.023mmol/g, left y axis) with protonation pH at 4.7, and deprotonation pH at 6.5; right red bar is ≡LH group (site concentration is 0.023mmol/g, left y axis) with deprotonation pH at 9.6. The blue and yellow bars on top of the figure represent dominated surface sites speciation at different pH range, specifically, $\equiv XOH_2^+$ dominated at pH<4.7, while ≡XOH is mostly existed from pH 4.7 to 6.5, and $\equiv XO^-$ is the main speciation at pH>6.5; The same is ≡LH group, which is dominated at pH<9.6, while it deprotonates as $\equiv L^-$ at pH>9.6.

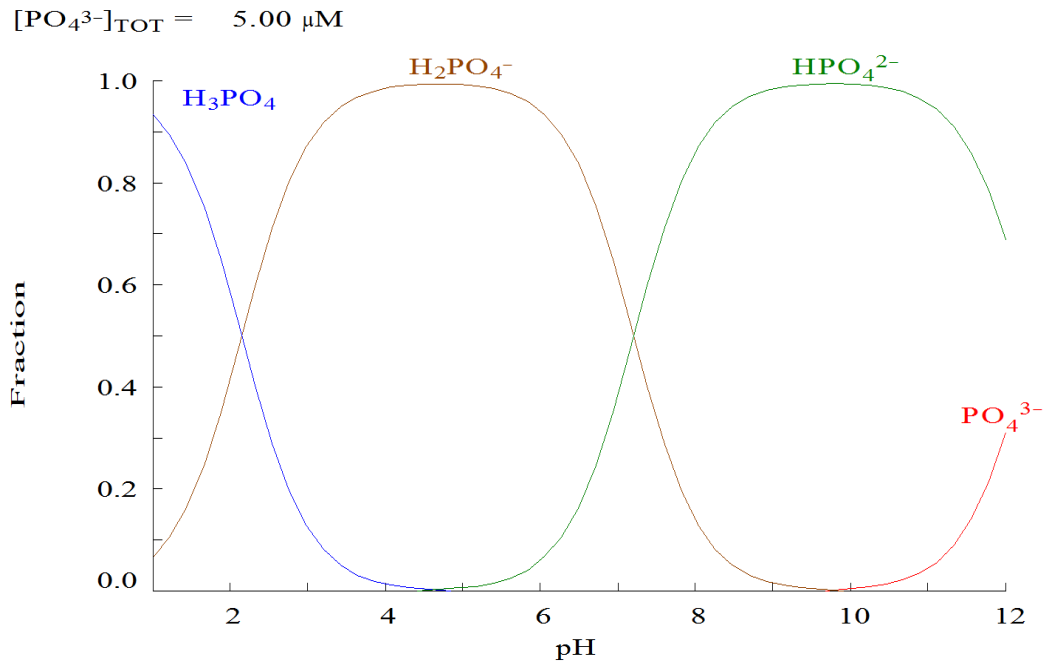

SI Figure 4.2 Phosphate aqueous speciation diagram

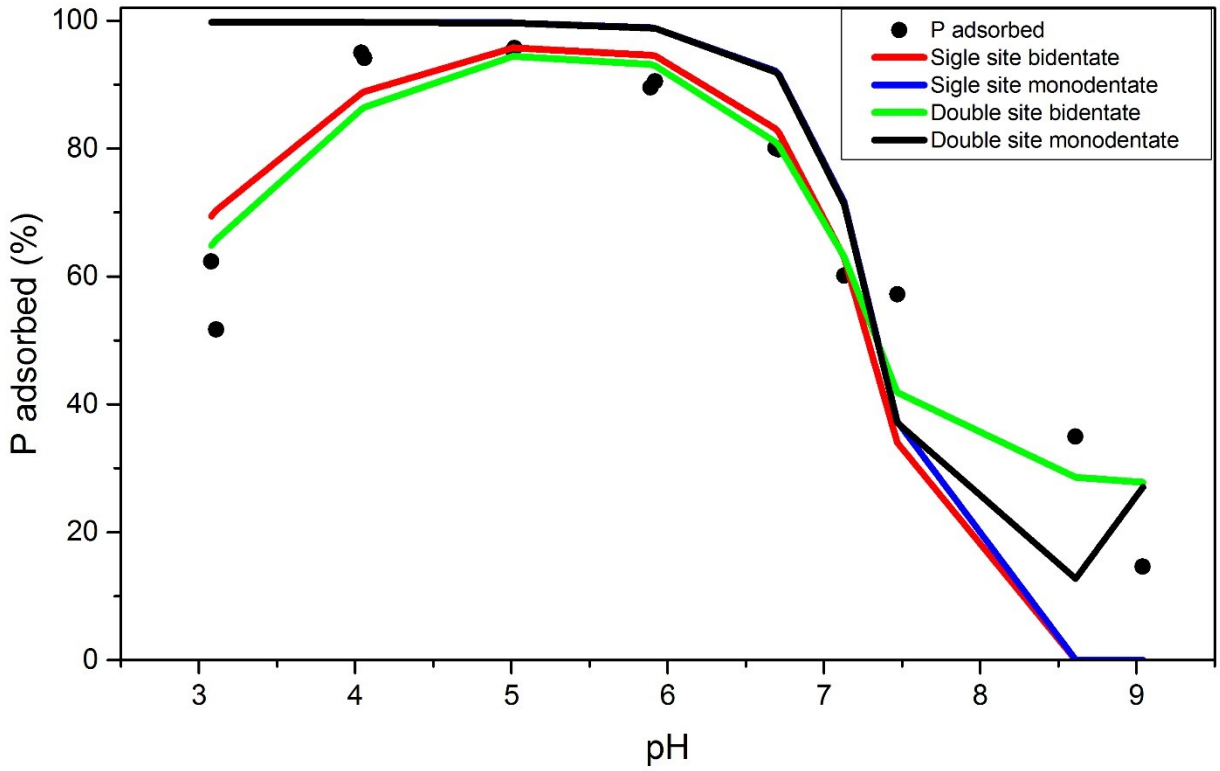

SI Figure 4.3 Fitting of phosphate adsorption pH edge data by SCM

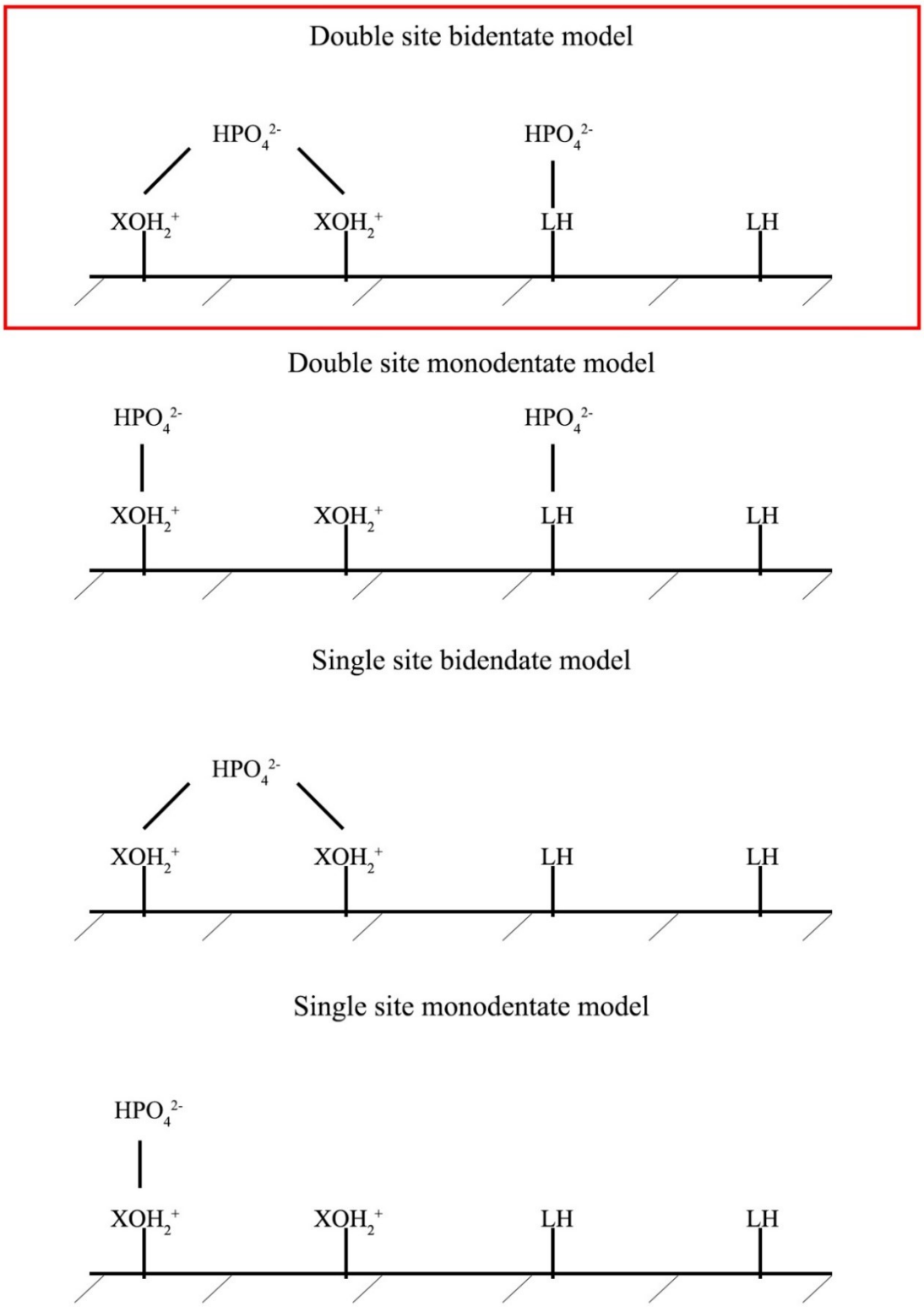

SI Figure 4.4 Schematic model of phosphate adsorption onto kaolinite surfaces

References

Hao, W., Flynn, S.L., Alessi, D.S., Konhauser, K.O., 2018. Change of the point of zero net proton charge (pHPZNPC) of clay minerals with ionic strength. Chemical Geology.

Hao, W. et al., 2019. The impact of ionic strength on the proton reactivity of clay minerals. Chemical Geology: 119294.

Liu, Y. et al., 2018. Acid-base properties of kaolinite, montmorillonite and illite at marine ionic strength. Chemical Geology, 483: 191-200.

Westall, J.C., 1982. FITEQL: A Computer Program for Determination of Chemical Equilibrium Constants from Experimental Data. Department of Chemistry, Oregon State University.

Supplementary information 2

Modern river P distribution in suspended sediments—A literature review

Compared to N and C with virtually unlimited atmospheric source, the supply of P derives almost entirely from continental weathering reaching oceans via riverine transport in various forms mainly as dissolved inorganic or organic P, and particulate P in river suspended sediments (SS). A large portion of P in river reservoir occurs in different phases of SS, including P absorbed onto Fe-mineral particles, carbonate, in clay minerals interlayers, and detrital P minerals. The concentration of dissolved free phosphorus in river is generally low, however, the fractions of phosphorus that existed as exchangeable or adsorbed phase on river SS can easily be released into water column once aqueous environmental condition changed. In this section, we reviewed phosphorus phases in modern rivers SS (especially bioavailable P) to cast light on ancient river shuttling phosphorus into ocean.

Sequential extraction has been widely applied to determine the modes of occurrences of elements in sediments. We particularly selected the literature applying sequential extraction to river suspended sediments to determine the portion of bioavailable P in river suspended sediments. Due to the inconsistence of literature sequential extraction techniques, there is different definition of bio-available P. For example, Dorich et al. (1984) determined bioavailable P by culturing *S. capricornutum*; Logan et al. (1979) applied NaOH extracted P as bioavailable P; a six-step extraction procedure was utilized by He et al. (2009) and the sum of exchangeable-P, organic-P and Fe-bound-P was used to represent bioavailable-P (Dorich et al., 1984; He et al., 2009; Logan et al., 1979). In our compilation of literature data, unless well-defined in their study, we use the subtraction between total-P and detrital-P to represent bioavailable P.

The inconsistence in unit for P concentration is another obstacle to summarize and make comparison between literature. Most researcher applied μM of P per gram of suspended sediments (μM/g) or μg of P per gram of SS (μg/g) to represent the fraction of different phases of P in river SS. In order to make comparison with dissolved reactive P and have an assessment of the composition of riverine P pool, we converted all the units into μg of P per liter of water (μg/L) by multiplying river SS concentration (g/L). For those literature that provided no information of SS concentration, we applied μg of P per gram of SS and % of total particulate P to represent the composition of bioavailable P.

Due to different degree of anthropogenic impact, the total P concentration varies from 56μg/L (subglacial rivers) (Hodson et al., 2004) to 28626.95μg/L (Yellow River) (Huijun et al., 2010). The amount of bioavailable P in SS composed a large portion of total P in SS and the concentration is significantly higher than dissolved P in river, indicating that dissolved P only contribute a small percentage of total P pool in river system, and most of P are existed as bioavailable form on suspended sediments and are transported by river SS. It should be noticed that the subglacial rivers in Svalbard shows lowest total P, bioavailable P and dissolved P (Hodson et al., 2004), which possibly because of the island is less weathered and P in SS mainly in the form of detrital P mineral which is hard to extract.

SI Table 4.2: Compilation of P concentration in river suspended sediment (SS) and dissolved phase

Bioavailable P in SS	Total P in SS	Dissolved P	% of dissolved P	Reference

Amazon River (Brazil)	133.2µg/L	216.9µg/L	9µg/L	3.98%	Chase and Sayles (1980)
Amazon River (Brazil)	119.6µg/L	141.2µg/L	12µg/L	7.83%	Berner and Rao (1994)
Yamuna River (India)	48.5-81.1µg/L	56.4-103.7µg/L	No data	No data	Chakrapani and Subramanian (1995)
Great lakes tributaries (US)	784.2µg/L	856.2µg/L	No data	No data	Depinto et al. (1981)
Black Creek Watershed (US)	900.5µg/g	2060µg/g	No data	No data	Dorich et al. (1984)
Changjiang River (China)	1096.2µg/L	3669.2µg/L	65.7µg/L	1.76%	He et al. (2009)
Subglacial rivers (Svalbard)	0.5µg/L	56µg/L	below detection limit	No data	Hodson et al. (2004)
Yellow River (China)	846.3-4654.7µg/L	5204.9-28627.0µg/L	4.9-22.7µg/L	0.079%-0.094%	He et al. 2010
Streams draining into Lake Erie (US)	234.1µg/L	757.3µg/L	135.8µg/L	15.20%	Logan et al. (1979)
Yarra River (Australia)	77-81% of total particulate P	No data	No data	No data	Sinclair et al. (1989)

Yellow river (China)	27.42% of total P	No data	0.11% of total P	0.11%	Yao et al. (2016)
Jiulong River (China)	100-113.2μg/L	114.3-141.8μg/L	54.8-47.2μg/L	27.11%-22.52%	Lin et al. (2013)
Two Lake Erie tributaries (US)	23-27% of total P	No data	No data	No data	Stone and English (1993)
Kleine Aa catchment (Switzerland)	43-66% of total particulate P	No data	No data	No data	Pacini and Gachter (1999)
Upper Brisbane River (Australia)	517μg/g	909μg/g	No data	No data	Kerr et al. (2011)
Patuxent River (US)	93.7-94% of total particulate P	No data	No data	No data	Jordan et al. (2008)
Black Creek Watershed (US)	94-111.7μg/L	470.7-477.7μg/L	46.7-54.5μg/L	9.03%-10.24%	Dorich et al. (1980)

References

Dorich, R.A., Nelson, D.W., Sommers, L.E., 1984. Algal Availability of Phosphorus in Suspended Stream Sediments of Varying Particle-Size. Journal of Environmental Quality, 13(1): 82-86.

He, H.J. et al., 2009. Behavior of different phosphorus species in suspended particulate matter in the Changjiang estuary. Chinese Journal of Oceanology and Limnology, 27(4): 859-868.

Hodson, A., Mumford, P., Lister, D., 2004. Suspended sediment and phosphorus in proglacial rivers: bioavailability and potential impacts upon the P status of ice-marginal receiving waters. Hydrological Processes, 18(13): 2409-2422.

Huijun, H., Zhigang, Y., Qingzheng, Y., Hongtao, C., Tiezhu, M., 2010. The hydrological regime

and particulate size control phosphorus form in the suspended solid fraction in the dammed Huanghe (Yellow River). Hydrobiologia, 638(1): 203-211.

Logan, T.J., Oloya, T.O., Yaksich, S.M., 1979. Phosphate characteristics and bioavailability of suspended sediments from streams draining into Lake Erie. Journal of Great Lakes Research, 5(2): 112-123.

Molybdenum adsorption/desorption on kaolinite surfaces

The adsorption of Mo onto kaolinite surface was performed under 0.01M $NaNO_3$ electrolyte solution. A 100 mL of 1ppm Mo solution was made by diluting 1000ppm of Mo stock solution, and then a 10 mL aliquot was pipetted to measure initial concentration of Mo. Then, 100mg of acidic treated kaolinite was added into solution to make a 1g/L kaolinite suspension. Once stirred by magnetic stir bar for 10 minutes at 240 rpm, the solution was aliquoted to 7 different tubes for pH adjustment. The pH of each tube was manipulated by 0.1M HNO_3 and 0.1M NaOH solution to make a pH range from 3 to 9 with 1 pH interval. After 24 h, the suspension was filtered by 0.2 μm filter, and then the supernatant was prepared to measure Mo concentration by ICP-MS.

Molybdenum desorption experiments were performed under transitional environment from freshwater to marine water condition. A 400ml of 0.01M NaCl solution was prepared to simulate freshwater condition. The Mo concentration was set as 50 ppb by diluting 1000ppm Mo stock solution. After that, a 5 ml aliquot was taken to measure initial Mo concentration. Then, 395 mg of acidic treated kaolinite was added into suspension to make a 1 g/L suspension. The pH of suspension was adjusted to 4 to mimic paleo-river pH. After 24 h, 5 mL of aliquot was pipetted and filtered to measure Mo concentration representing river water adsorption. Then, the solution pH was adjusted to 8 by 0.1M NaOH solution and 12.87g of NaCl solid particle was added into beaker at the same time to change ionic strength to 0.56M, representing marine water condition. Once pH is stable, 5mL of aliquot was pipetted out for phosphate concentration analysis at t=0. The whole marine condition adsorption process took 3 days and time interval of sample collecting was t=0, t=1h, t=2h, t=4h, t=8h, t=12h, t=1d, t=2d, t=3d. During the whole process, reaction beaker was covered by parafilm to prevent possible solution evaporation. The phosphate concentration in these samples were then acidified and analysed by ICP-MS.

Kaolinite has highest affinity to Mo at pH 4, with around 50% of Mo adsorbed (SI Fig. 5). From pH=3 to pH=4, the amount of Mo adsorbed onto kaolinite surface increased and then decrease sharply with pH increasing. At neutral and basic pH (pH above 6), the amount of Mo adsorbed is lower than 20%. This pH dependent adsorption was also reflected in SI Fig.5 when transport Mo-bearing kaolinite from freshwater condition to marine water condition. At pH=4, ionic strength (IS) =0.01M, approximately 100% of Mo is adsorbed on kaolinite surface. The differences in percentage of adsorption between SI Fig. 5 and 6 is because SI Fig. 6 applied lower concentration of Mo (50 ppb). Once aqueous environment changes into marine condition, the amount of Mo adsorbed steadily decrease. After 3 days' desorption, only 21% of Mo remains in kaolinite surface.

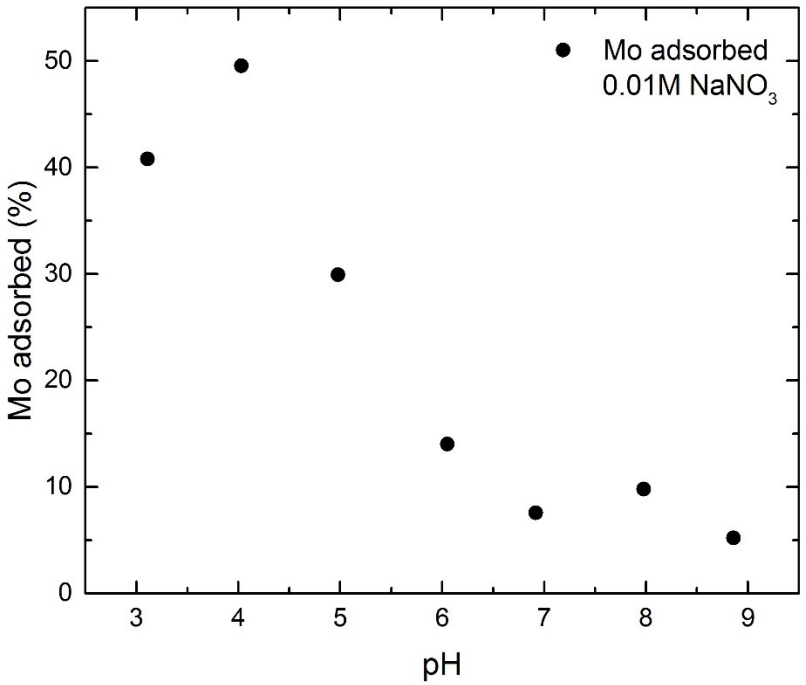

SI Figure 4.5 Molybdenum adsorption onto kaolinite as a function of pH

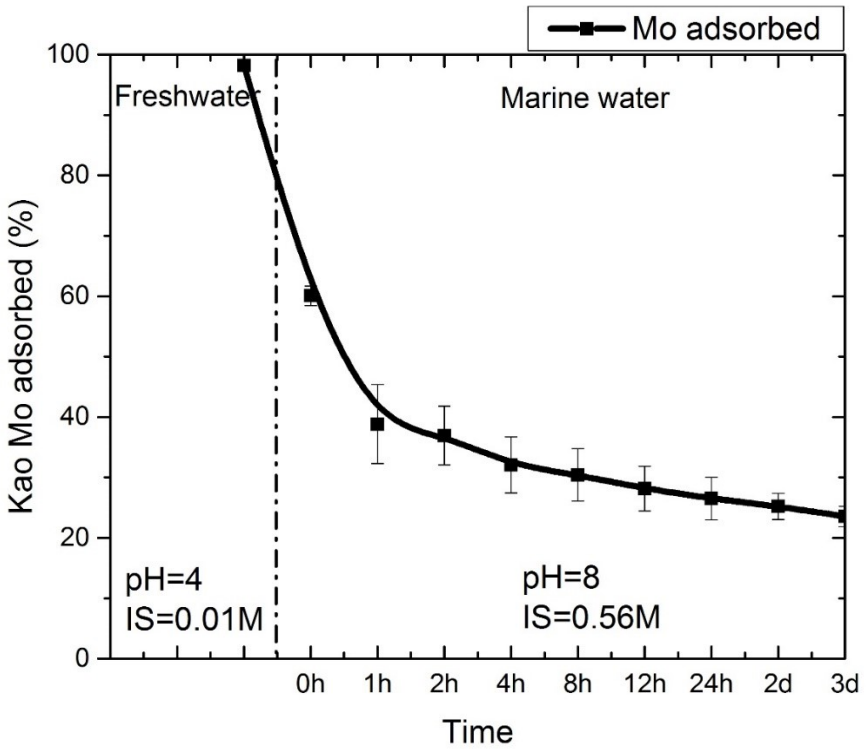

SI Figure 4.6 The desorption of Mo from kaolinite surface from freshwater water to marine water

P adsorption capacity of montmorillonite and illite

Phosphate adsorption onto montmorillonite and illite was performed as a function of P concentration. The experimental procedure is the same with kaolinite adsorption isotherm (specific experimental procedure in main text, Method section). The adsorption isotherm of P onto montmorillonite and illite was shown in SI Fig. 7. The adsorption of P onto illite surfaces shows insignificant difference at low initial P concentration for the three conditions. However, with initial P concentration increase, freshwater water condition (pH=4, ionic strength (IS)=0.01M) shows higher adsorption capacity compared to the other two conditions. Marine condition has the lowest P adsorption capacity among all three conditions. Montmorillonite displays differences in P adsorption capacity even at low initial P concentration, with the highest P adsorption at pH=6, IS=0.01 condition. Throughout the whole P initial concentration range, pH=6, IS=0.01 condition shows more P adsorption capacity compared to the other two conditions, while marine water condition has the lowest P adsorption capacity.

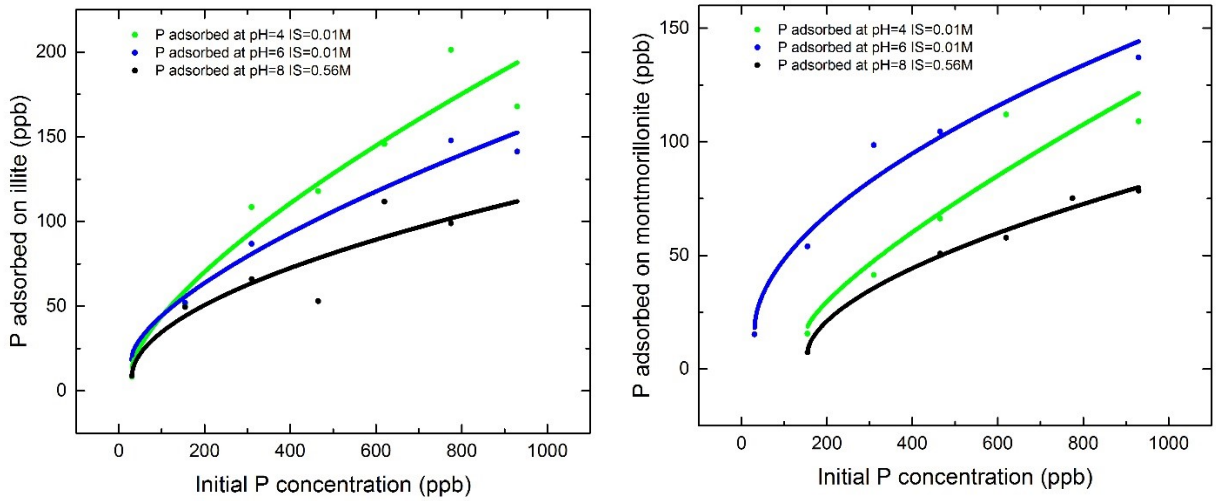

SI Figure 4.7 Phosphate adsorption isotherm of illite and montmorillonite.